Etude et modélisation de l'effet des séquences de sollicitations thermomécanique sur le comportement, l'endommagement et la rupture des matériaux composites des réservoirs à hydrogène.

Imen Feki

ECOLE DOCTORALE SCIENCES ET METIERS DE L'INGENIEUR

Laboratoire des Procédés et Ingénierie en Mécanique et Matériaux (PIMM)

Campus de Paris

THÈSE

Présentée par : **Imen FEKI**

Soutenue le : 22 Janvier 2025

Pour obtenir le : **Doctorat** délivré par

L'Ecole Nationale Supérieure d'Arts et Métiers

Spécialité : Mécanique des matériaux

Étude et modélisation de l'effet des séquences de sollicitations thermomécanique sur le comportement, l'endommagement et la rupture des matériaux composites des réservoirs à hydrogène

Thèse co-dirigée par :

Dr. Joseph FITOUSSI, MCF, HDR

Dr. Mohammadali SHIRINBAYAN, HDR

Jury

M. Emmanuel RICHAUD	**Professeur, Arts et Métiers ParisTech**	**Président**
Mme. Isabelle BRUANT	**MCF, HDR, Université de Paris-Nanterre**	**Rapportrice**
M. Patrick ROZYCKI	**Professeur, Ecole Centrale de Nantes**	**Rapporteur**
M. Laurent GORNET	**Professeur, Ecole Centrale de Nantes**	**Examinateur**
M. Fodil MERAGHNI	**Professeur, Arts et Métiers ParisTech**	**Examinateur**
M. Jihed ZGHAL	**MCF, Université de Paris-Nanterre**	**Examinateur**
M. Joseph FITOUSSI	**MCF, HDR Arts et Métiers ParisTech**	**Co-directeur**
M. Mohammadali SHIRINBAYAN	**Docteur, HDR, Arts et Métiers ParisTech**	**Co-directeur**
Mme. Samia NOUIRA	**Docteur, Arts et Métiers ParisTech**	**Invitée**
M. Robert TIE BI	**Ingénieur Expert Calcul, FORVIA**	**Invité**

T H È S E

À mes adorables jumelles, Aline et Acile...

Remerciements

Ce travail est réalisé pour et en collaboration avec Forvia, acteur du transport automobile en tant qu'équipementier automobile pour différents constructeurs dans le monde entier. Il a été réalisé au sein du PIMM du Campus ENSAM de Paris.

Après avoir obtenu mon grade de docteur, c'est le temps d'adresser mes vifs remerciements aux personnes que j'ai pu rencontrer tout au long de cette thèses. J'exprime ma gratitude et ma grande reconnaissance à mes directeurs de thèse, Monsieur Joseph FITOUSSI, Maître de conférences aux Arts et Métiers ParisTech-Paris et Monsieur Mohammadali SHIRINBAYAN, Ingénieur de recherche au laboratoire PIMM, ainsi qu'à mon co-encadrant Ingénieur de recherche Forvia , leur implication, leur excellent encadrement, leurs conseils et surtout leur soutien moral et encouragement toutau long de cette thèse.

Aux membres du jury Madame Isabelle BRUANT, Monsieur Patrick ROZYCKI, Monsieur . Laurent GORNET, Monsieur Jihed ZGHAL et Monsieur Ali ZGHAL pour avoir fait l'honneur d'assister à ma soutenance et évaluer mon travail. Je tiens bien évidemment à remercier mes amis et mes collègues qui ont toujours été là pour moi et qui m'ont aidé lors des périodes difficiles. Je pense à Sawsan, Samia, Mariem, Halima, Sabrine, Nader, MohammadHossein, Hamza, Rahim, et Clara.

A mes très chers parents, Abdelrrazek et Soulef. Cette thèse est pour vous. C'est le fruit des sacrifices et de patience malgré les moments difficiles qu'on a vécu. Mes remerciements et ma reconnaissance la plus sincère de m'avoir toujours encourager tout au long mon cursus, rien ne vaut les efforts fournis pour moi. Je suis également très reconnaissant envers ma sœur Ameni, mon frère Rami et sa femme Eya, mes beaux parents Najib et Samia et mon beau frére Mohammed boubaker avec qui j'ai passé d'excellents moments en famille toutes ces années.

Enfin, c'est à ma petite famille que sont dédiées ces dernières lignes. Mon mari Ahmed, Je témoigne toute ma gratitude pour m'avoir soutenu lors des moments difficiles. Que mon mari sache que son support, sa patience, sa complicité m'ont été très précieux. À mes adorables jumelles, Aline et Acile, Vous êtes ma plus grande source d'inspiration. Que cette thèse vous rappelle que la persévérance et le travail mènent toujours à de belles réalisations. Vous remplissez ma vie de joie et de motivation chaque jour.

Table des matières

Table des figures

Table des tableaux

Table des équations

1. Introduction générale

Le développement de matériaux plastiques dotés de propriétés spécifiques leur permettant de remplacer des matériaux traditionnels comme l'acier ou le bois a massivement contribué à la croissance de la consommation de ces matériaux. En fait, les innovations recherchées sont celles qui préservent les avantages de la réduction des coûts, de la légèreté et de la facilité de traitement. Les composites peuvent être considérés comme un type de matériaux supérieur qui a un large éventail d'applications dans plusieurs industries telles que l'aéronautique, la marine, le militaire, l'automobile et le médical. Une caractéristique importante des composites est la possibilité de modifier l'ordre d'empilement des plis ou des lamelles pour obtenir des structures présentant les propriétés mécaniques souhaitées.

Il est important de noter que l'hydrogène est un gaz léger et qu'il possède la densité énergétique volumétrique la plus faible de tous les carburants à température et pression normales. En ce qui concerne ses caractéristiques énergétiques, la densité énergétique gravimétrique de l'hydrogène est environ trois fois supérieure à celle de l'essence et du méthane. Le projet européen intégré sur l'hydrogène (EIHP) est le fer de lance de l'expansion des normes réglementaires mondiales pour l'essai de l'hydrogène et la certification des composants et systèmes de l'infrastructure de ravitaillement en hydrogène, y compris les réservoirs de stockage de l'hydrogène sous forme de gaz comprimé. Ces réservoirs peuvent être divisés en cinq types différents. Le système de stockage léger le plus innovant pour le gaz comprimé est une cuve composée d'un réservoir composite avancé avec un revêtement métallique (type III) ou plastique (type IV) non porteur. Ce document de recherche s'est concentré sur l'étude des propriétés mécaniques de la résine époxy renforcée par des fibres de carbone (type IV) pour la fabrication de réservoirs sous pression légers pour le stockage de l'hydrogène [1].

Le processus de fabrication des réservoirs sous pression par enroulement filamentaire est largement utilisé, notamment pour le stockage d'hydrogène. Ces réservoirs sont dotés d'un revêtement qui prévient la perméation de l'hydrogène et d'une structure composite qui garantit leur résistance mécanique. Les recherches en cours visent à accroître la fiabilité et la sécurité des réservoirs en optimisant leur forme complexe et les matériaux utilisés. L'efficacité du processus d'enroulement filamentaire dépend du schéma d'enroulement et

des propriétés mécaniques de la matrice, notamment d'un module de traction élevé et d'une bonne résistance à la fissuration. Cependant, la présence de vides dans les composites époxy-fibres de carbone peut affaiblir le matériau et réduire la pression d'éclatement du réservoir. Des techniques de réduction des vides, telles que l'application précise de fibres et le compactage à haute pression, sont nécessaires pour améliorer les performances.

Les mécanismes d'endommagement des récipients sous pression en matériaux composites sont complexes et présentent de multiples facettes, principalement en raison de la structure en couches de ces récipients. Les modes de défaillance typiques de ces systèmes comprennent la fissuration de la matrice, la délamination, la rupture des fibres et la défaillance interfaciale entre les fibres et la matrice (décollement). Ces défaillances sont souvent dues aux effets combinés des charges mécaniques, des facteurs environnementaux, des vides et des faiblesses inhérentes aux matériaux composites utilisés [2].

Bien que les réservoirs d'hydrogène en composites présentent de nombreux avantages, ils restent sensibles à divers types d’endommagements mécaniques sous des charges variées. Il est essentiel de comprendre leur comportement sous différentes sollicitations, notamment les impacts quasi-statiques, dynamiques et fatigue, pour garantir leur sécurité et leur fiabilité. En raison de leur composition hétérogène, les composites montrent des mécanismes de défaillance complexes, et la répartition des dommages peut varier considérablement selon les conditions de charge. Des études approfondies sont donc nécessaires pour mieux anticiper et maîtriser ces mécanismes sous diverses situations de chargement.

Les essais quasi-statiques, où la charge est appliquée lentement, offrent la possibilité d'examiner en détail les dommages progressifs et les mécanismes de défaillance des matériaux composites. Ces essais peuvent causer divers types de dommages tels que la formation de fissures dans la matrice, la rupture des fibres et la séparation des couches du composite (délamination). Les fissures dans la matrice surviennent sous contrainte de traction ou de cisaillement, tandis que la rupture des fibres, due à une charge excessive, compromet la résistance du matériau. La délamination, qui consiste en la séparation des couches du composite, est particulièrement critique car elle peut conduire à une défaillance catastrophique. Des études, notamment celle de Berthelot, ont montré que les essais quasi-statiques permettent de détecter ces défaillances précoces, mettant

en évidence l'importance d'intégrer ces mécanismes dans la conception et l'évaluation des réservoirs d'hydrogène en composites [2].

Les essais cycliques, également appelés essais de fatigue, mettent en évidence la dégradation progressive d'un matériau soumis à des charges répétées. Dans le cas des composites polymères renforcés de fibres de carbone (CFRP), le processus de rupture par fatigue est particulièrement complexe en raison de l'hétérogénéité du matériau. Même lorsque la contrainte appliquée est inférieure à la limite d'élasticité, des dommages apparaissent sous des charges cycliques continues. Ce processus se divise en trois phases : l'apparition de fissures, la propagation de microfissures et, finalement, la formation de microfissures entraînant la défaillance du matériau. Les niveaux de contrainte influencent le type de fatigue observé : la fatigue Oligo cyclique, à haute contrainte, cause des dommages irréversibles, tandis que la fatigue à cycle élevé, à faible contrainte, permet au matériau de rester dans sa limite d'élasticité, entraînant une dégradation plus lente. Si les contraintes sont suffisamment basses, on peut atteindre une quasi-absence de dommages, assurant ainsi une durée de vie en fatigue quasi infinie [3].

Les essais impliquant des charges dynamiques à impact rapide présentent des défis spécifiques pour les matériaux composites. Les niveaux élevés de déformation associés à ces essais peuvent entraîner des dommages plus importants que lors de chargements quasi-statiques. Il s'agit notamment d'une augmentation de l'absorption d'énergie, de la rupture des fibres, de la formation de fissures dans la matrice, voire même de la pénétration complète de l'élément impactant. Ces dommages, souvent localisés et difficiles à détecter immédiatement, peuvent occasionner une diminution critique de la résistance de la structure. Des recherches, telles que celles menées par Gower et Shaw, ont mis en évidence l'ampleur des dommages internes causés par les impacts à grande vitesse, lesquels influent fortement sur les modes de défaillance. Comprendre ces mécanismes est essentiel pour assurer l'intégrité structurelle des réservoirs d'hydrogène en matériaux composites [4].

Cette thèse porte sur l'étude approfondie des mécanismes d'endommagement dans les matériaux composites, en particulier les composites époxy renforcés de fibres de carbone utilisés dans les réservoirs de stockage d'hydrogène de type IV. Elle vise à analyser l'influence des orientations des fibres, de la porosité et des conditions de chargement sur les propriétés mécaniques sous sollicitations quasi-statiques, dynamiques, et

en fatigue. L'étude débute par une caractérisation des propriétés physico-chimiques et de la microstructure des composites, suivie par une analyse détaillée de leurs réponses thermomécaniques. Une attention particulière sera accordée à l'impact de la porosité et des orientations des fibres (±15°, ±30° ainsi que des configurations multicouches) sur les propriétés mécaniques. Des essais quasi-statiques de traction et des essais de chargement/déchargement seront menés pour identifier les mécanismes d'endommagement à plusieurs échelles, en lien avec l'initiation et la propagation des fissures incluant la décohésion des interfaces et la fissuration induite par la porosité.

Les résultats obtenus permettront de mieux appréhender les impacts des sollicitations sur l'intégrité structurelle des réservoirs en matériaux composites, et de proposer des solutions pour optimiser leur durabilité et sécurité en service.

Ce travail est réalisé pour et en collaboration avec Forvia, acteur du transport automobile en tant qu'équipementier automobile pour différents constructeurs dans le monde entier. Il a été réalisé au sein du PIMM du Campus ENSAM de Paris.

Le présent manuscrit est structuré en deux parties : la première partie (Partie I) est consacrée à un résumé étendu en français, tandis que la seconde (Partie II) regroupe les articles publiés ou en cours de publication dans des revues internationales de rang A en anglais. L'organisation du résumé étendu suit une démarche méthodique :

- Une description détaillée des matériaux composites époxy/fibres de carbone ±θ, ainsi que des méthodes de caractérisation employées ;

-Une analyse expérimentale approfondie de l'état de santé des matériaux, avec une attention particulière portée à l'impact de la porosité et de l'orientation des fibres (±15°, ±30° et configurations multicouches) sur leurs propriétés mécaniques.

-L'examen des mécanismes d'endommagement sous diverses conditions de chargement (quasi-statique, fatigue et dynamique) permet d'appréhender les processus d'endommagement multi-échelles, incluant la décohésion des interfaces et la fissuration induite par la porosité.

Les articles publiés dans le cadre de cette étude ou en cours de publication sont listés ci-après et sont référencés dans le texte sous la forme « Article N°-- ».

- **Article N°1 :** Imen Feki , Mohammadali Shirinbayan , Samia Nouira , Robert Tie Bi , Jean-Baptiste Maeso , Cedric Thomas , Joseph Fitoussi , Composites in high-pressure hydrogen storage: a review of multiscale characterization and mechanical behavior, Composites Part C: Open Access (2024), doi: https://doi.org/10.1016/j.jcomc.2024.100555.

- **Article N°2 :** Feki I, Shirinbayan M,Nouira S, et al. Multi-scale experimental investigation of porosity-induced damage effects in filament-wound carbon fiber reinforced epoxy composites used in hydrogen storage tanks. Polym Compos. 2024;1-13. doi:10.1002/pc.29121

- **Article N°3 :** Imen Feki, Mohammadali Shirinbayan, Samia Nouira, Robert Tie Bi, Jean-Baptiste Maeso, Cedric Thomas, Joseph Fitoussi, Multi-scale fatigue damage analysis in filament-wound carbon fiber reinforced epoxy composites for hydrogen storage tanks,Composites Part C: Open Access,Volume 15, 2024,100537,ISSN 2666-6820, https://doi.org/10.1016/j.jcomc.2024.100537.

- **Article n°4 :** Shirinbayan M, Feki I, Nouira S, et al. Multi-scale damage analysis of filament-wound carbon fiber-reinforced epoxy composites for hydrogen storage tanks under high strain rates. Polym Compos. 2024;1-12. doi:10.1002/pc.29273

Ces articles apportent une contribution significative à la compréhension des matériaux composites utilisés pour le stockage d'hydrogène sous haute pression et sont cités tout au long du manuscrit.

2. Matériaux composites des réservoirs à hydrogène

2.1. Généralité sur le stockage d'hydrogène

2.2.1. Les différentes méthodes de stockage d'hydrogène

L'hydrogène, ou plus exactement le dihydrogène (H2), présente une source d'énergie prometteuse pour remplacer les combustibles fossiles en raison de la pollution de l'environnement et de la crise énergétique. Il offre plusieurs caractéristiques intéressantes tels que l'absence d' émission de gaz à effet de serre , une efficacité élevée et des ressources abondantes. Afin de faire de l'hydrogène une ressource alternative viable, il est essentiel de traiter diverses questions techniques, telles que la génération , le stockage, le transport et la combustion d' hydrogène . Le stockage de l'hydrogène reste un enjeu important pour son utilisation à grande échelle. De manière générale l'hydrogène peut être stocké sous trois formes :

- **Le stockage liquide à basse température**, où l'hydrogène est stocké à 20K (-253°C) et à faible pression (10 bars). Il s'agit d'une technologie intéressante du point de vue de la capacité de stockage (grandes densités massiques et volumiques) et des coûts de fabrication de ces réservoirs de stockage. Néanmoins, les coûts de liquéfaction de l'hydrogène rendent sa mise en œuvre et son utilisation moins compétitives que pour les autres technologies.
- **Le stockage sous forme solide**, technologie qui utilise les propriétés réversibles d'adsorption ou d'absorption de l'hydrogène par un matériau (généralement des hydrures). Les avantages principaux de cette technologie sont les capacités de stockage volumique très importantes des hydrures et les faibles pressions de mise en œuvre. En revanche, plusieurs verrous restent actuellement à lever : cinétiques d'adsorption ou d'absorption de l'hydrogène, températures de désorption élevées, coûts prohibitifs des matériaux utilisés (hydrures), et matériaux à caractère pyrophorique nécessitant des manipulations délicates.
- **Le stockage gazeux sous pression**, procédé où l'hydrogène est stocké sous forme gazeuse à très haute pression (700 bars) pour obtenir des densités volumiques et massiques intéressantes c.-à-d. suffisamment importantes pour obtenir des autonomies analogues à celles des véhicules actuels. Pour cette technologie, les coûts sont essentiellement dus à la fabrication des réservoirs, généralement en matériaux composites pour satisfaire de telles pressions à faible masse et volume de matière, et aux coûts de compression de l'hydrogène.

Actuellement, le stockage d'hydrogène à haute pression est la méthode la plus populaire en raison de son faible coût, de sa maturité et de sa facilité d'utilisation. Les réservoirs haute pression se divisent en quatre sous-familles (Figure1):

- **Type I :** Il s'agit d'un réservoir en acier qui remplit les deux objectifs de tenue mécanique du réservoir ainsi que celle d'étanchéité. Les inconvénients de ce type de réservoirs sont : une faible densité de stockage1 (ici 1,2 %) et des pressions de stockage limitées à 30MPa.
- **Type II :** Il s'agit également d'un réservoir acier qui est renforcé sur la partie cylindrique (virole) par un matériau composite dépose par enroulement filamentaire. Le composite aide à la tenue mécanique, la bouteille acier assure une grande partie de la tenue mécanique et garantit l'étanchéité du réservoir. Comme pour les réservoirs de type 1, densité et pression de stockage restent faibles (1,3% et 35MPa).
- **Type III :** Il est constitué d'une bouteille métallique et d'une coque en composite déposée par enroulement filamentaire sur toute la surface de la bouteille. Le rôle de la bouteille métallique est uniquement de garantir l'étanchéité du réservoir. Le terme " liner " est alors utilise pour parler de cette enveloppe étanche qui sert également de support pour la dépose du composite. La tenue mécanique est assurée par la coque composite. L'inconvénient de ce type de réservoirs est que le liner métallique présente des faiblesses en fatigue et contribue a une partie non négligeable de la masse du réservoir. Cependant, les capacités de ces réservoirs sont nettement améliorées par rapport aux précédents. Ces réservoirs permettent des pressions de services de 70MPa.
- **Type IV :** Il s'agit d'un réservoir ou l'étanchéité est assurée par un liner polymère et la tenue mécanique par une coque en composite. Contrairement aux réservoirs de type 3, ils ne présentent pas de faiblesse en fatigue, mais les liners polymères sont plus perméables que les métalliques. Les pressions de service peuvent également atteindre 70MPa et l'amélioration par rapport aux réservoirs de type 3 réside dans le gain de masse.
- **Type V :** Il est entièrement constitué de matériaux composites et dépourvu de revêtement, représentant la pointe de la technologie en matière de stockage de l'hydrogène. Cette solution offre l'option la plus légère et la plus performante, mais elle est encore en cours de développement et confrontée à des problèmes de perméation de l'hydrogène ainsi qu'à des coûts de fabrication élevés.

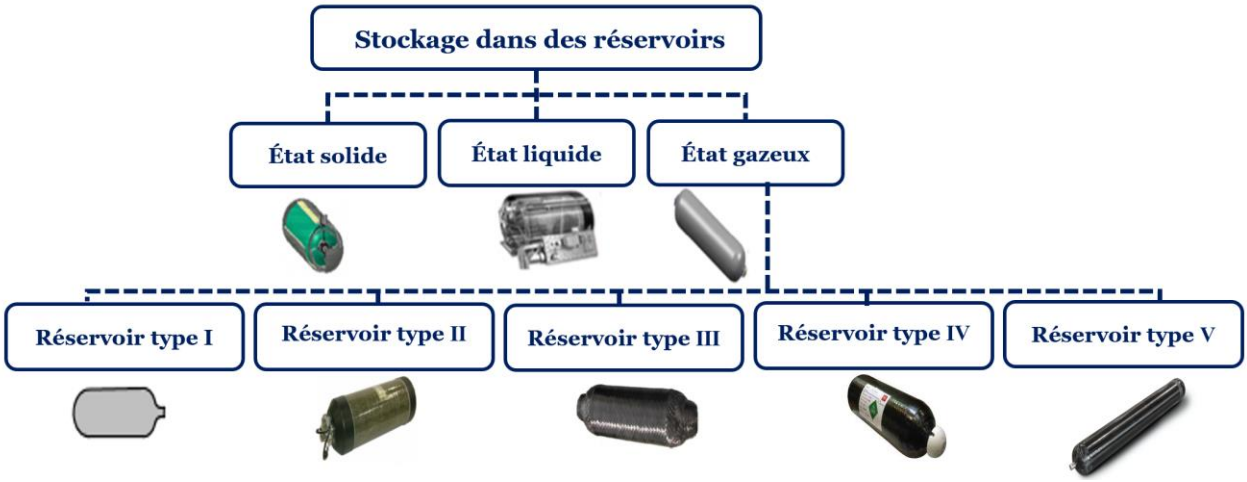

Figure 1. Les differents méthodes de stockage d'hydrogène [5] [6]].

2.2.2. Stockage d'hydrogène automobile : réservoirs de type III et IV

Les recherches sur le véhicule à hydrogène s'inscrivent dans le contexte de l'épuisement progressif des ressources fossiles et surtout du réchauffement climatique, qui imposent de trouver une alternative aux énergies fossiles. Avec le développement des véhicules à pile à combustible à hydrogène , la technologie de stockage d'hydrogène embarqué avec sécurité, efficacité et économie est devenue un élément fondamental. Des autonomies plus élevées nécessitent plus de stockage d'hydrogène. Actuellement, les réservoirs hyperbares s'agissent de la solution la plus mature et la plus couramment adoptée pour le stockage de l'hydrogène dans les véhicules [7][8]. En général, les bouteilles d'hydrogène peuvent être pressurisées jusqu'à 25 MPa, 35 MPa ou 70 MPa. Compte tenu de l'autonomie et de l'espace limité l'espace limité du véhicule, 70 MPa est la pression la plus économique pour la pression la plus économique pour le stockage à bord [9]. En comparant les quatre types ci-dessus, on constate que les types I et II ne peuvent pas être utilisés dans les véhicules en raison de la faible densité de stockage de l'hydrogène et des graves problèmes de fragilisation de l'hydrogène.

Dans l'industrie des véhicules à pile à combustible (FCV), les types III et IV sont largement utilisés pour minimiser le poids [10,7,8]. Cependant, les types III et IV ont un comportement différent en ce qui concerne l'augmentation de la température en raison des différences de matériaux. En Chine, le développement technologique du Type III est relativement avancé. Parmi elles, la cuve de 35 MPa a été largement utilisée

dans les véhicules à pile à combustible ces dernières années et la cuve de 70 MPa est proche du marché. Cependant, la pénurie de fibres de carbone et de résine, ainsi que les performances de ces matériaux, bloquent le développement des cuves à hydrogène. Le réservoir de type IV n'a été développé que récemment [9]. Par exemple, plusieurs constructeurs automobiles ont introduit des systèmes de stockage avancés afin d'améliorer les performances et l'autonomie de leurs véhicules. La Honda FCX, équipée de deux réservoirs de 35 MPa, atteint une capacité de stockage d'hydrogène de 156,6 L. De son côté, la Toyota FCHV-adv utilise quatre réservoirs de type IV à 70 MPa, permettant une autonomie d'au moins 500 km dans des conditions réelles, avec un temps de ravitaillement de 10 minutes [12,13]. La Toyota Mirai pousse encore plus loin la technologie de stockage avec deux réservoirs de plus grand diamètre (60 L et 62,4 L), capables de stocker près de 5 kg d'hydrogène en seulement 3 minutes, offrant ainsi une autonomie de 500 km. De manière similaire, la Hyundai NEXO est équipée de trois réservoirs haute capacité (pour un volume total de 156 L), permettant une autonomie de 800 km selon le cycle d'essai NEDC, avec un temps de ravitaillement de 5 minutes. En outre, Stellantis, en collaboration avec STELIA Aerospace Composites et Faurecia, a développé des réservoirs à 700 bars destinés aux véhicules utilitaires. Ces réservoirs offrent une autonomie de plus de 400 km en zéro émission, avec une capacité totale de 120 [14].

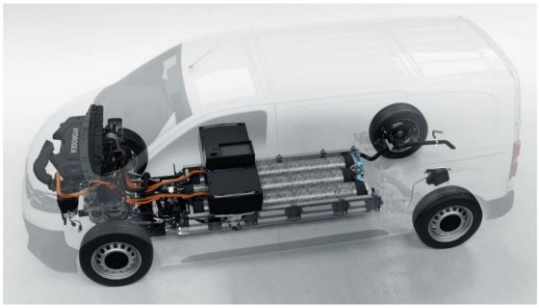

Figure 2. Utilitaire léger Zéro Émission développé par Stellantis [15].

2.2.3. Présentation du réservoir hydrogène type IV

Les réservoirs hydrogène de type IV sont constitués de trois éléments et de leurs interfaces (voir Figure 3.a) : Le liner polymère, l'embase métallique et le composite.

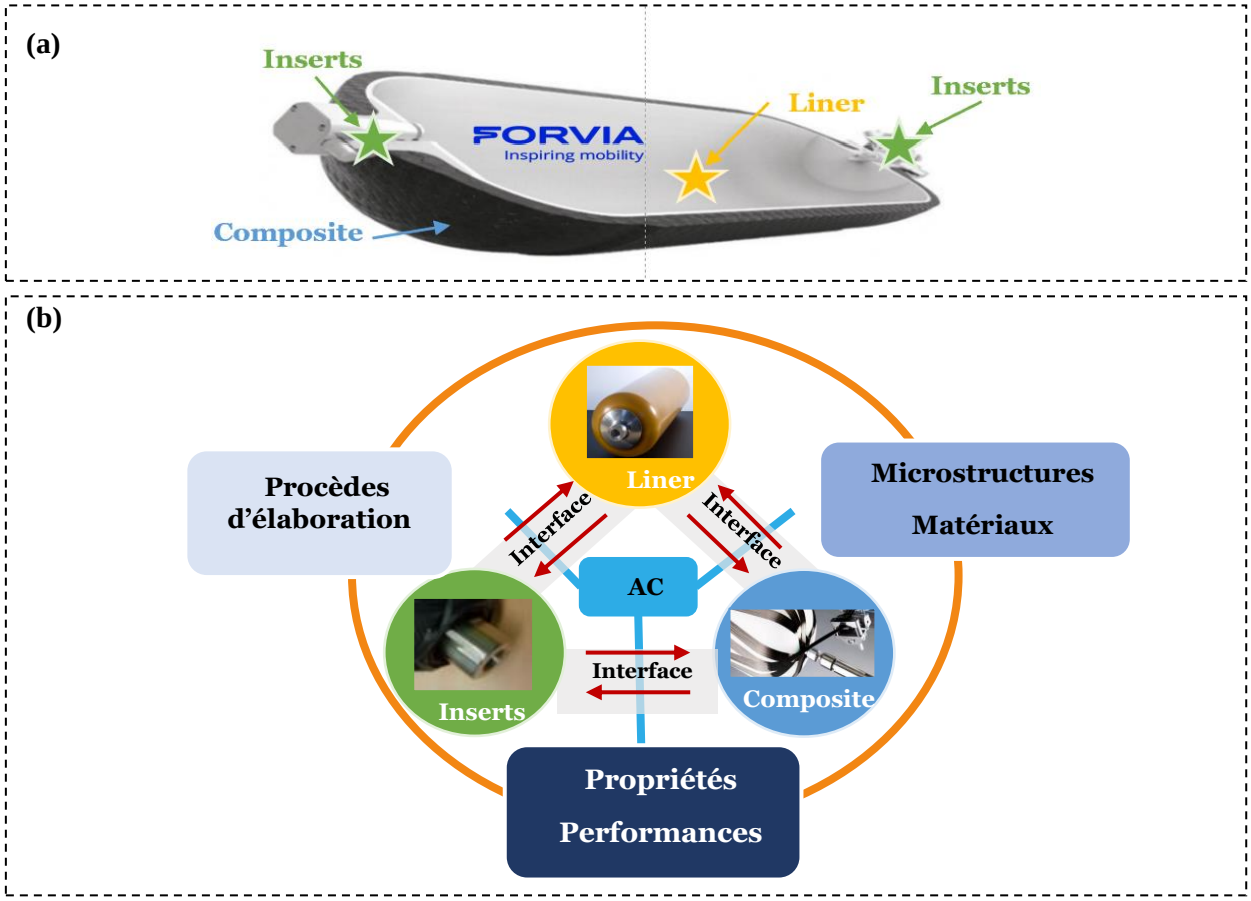

Figure 3. a) Schéma et coupe d'un réservoir hydrogène de type IV **b)** Le réservoir hydrogène : Une structure assemblée complexe[16].

- **Le liner polymère** ayant pour fonction d'assurer l'étanchéité du réservoir. L'étanchéification est difficile à assurer d'une part du fait de la pression élevée qui favorise l'infiltration de l'hydrogène au niveau des interfaces, mais également par le fait de la perméation de l'hydrogène, la plus petite des molécules, à travers la matière. Ce dernier aspect requière un choix approprié de la matière de liner pouvant limiter le plus possible la perméation à l'hydrogène. Plusieurs matériaux sont étudiés aujourd'hui pour la conception du liner : le PEA, le PEB et le PA11. Aujourd'hui fabriqué par un procédé de rotomoulage, d'autres procédés sont à l'étude pour tenir une cadence de production en série, comme l'injection-soudage ou encore l'extrusion-soufflage. Nous distinguons trois parties sur les liners : deux dômes aux extrémités et la virole, partie purement cylindrique.

- **Des embases en aluminium** sont fixées aux deux extrémités du réservoir pour fixer le réservoir au châssis, remplir le réservoir et assurer l'une des fonctions principales du réservoir qui est de fournir de

l'hydrogène à la pile à combustible. Certains petits réservoirs n'ont qu'une seule base. Ce dernier se dilate lors du remplissage, le réservoir doit donc pouvoir se déformer axialement. Par conséquent, les deux bases n'ont pas la même taille. L'un est complètement bloqué et l'autre peut glisser sur des paliers lisses. Il existe d'autres façons d'intégrer le réservoir autour. Il s'agit notamment du système de harnais connu en anglais sous le nom de "strap mounting". Ceux-ci sont généralement placés directement sur la partie cylindrique de la coque composite.

- **Une coque en composite**, composé de plusieurs couches de composite à base de fibre de carbone et de résine époxy, dont le rôle principal est de contrer les contraintes mécaniques exercées sur le réservoir notamment aux pressions internes élevées imposées au réservoir : pression nominale : 700 bars et pression d'éclatement : 1750 bars. Ces couches de composite sont enroulées autour du liner à l'aide d'un enrouleur filamentaire. La bande, composée de plusieurs mèches (selon le diamètre du réservoir), passe d'abord dans une rainure pour les mettre sous tension afin d'assurer leur maintien sur le patin. Elles sont ensuite trempées dans un bain d'eau plastique pour être imprégnées, puis passées à une extrémité du rouleau avant d'être enroulées autour de la doublure. L'enroulement est réalisé selon un programme défini, pour obtenir le nombre de couches souhaité et différents angles. La séquence est relativement longue : environ 1h30 de bobinage, puis environ 8h de cuisson pour polymériser la résine.

Enfin, une fine couche de fibre de verre peut être déposée par-dessus le composite, afin d'identifier les zones endommagées en cas de choc sur le réservoir ou chute de ce dernier, et de le protéger de l'humidité. D'ailleurs, des dômes protecteurs en mousse sont souvent ajoutés au réservoir afin de lui procurer une protection supplémentaire aux chocs.

L'analyse et la prédiction des défaillances des systèmes de stockage d'hydrogène de type IV à travers l'établissement de modèles prédictifs représentent un défi important et sont au cœur des préoccupations industrielles.

2.2 Composition des Composites CFRP : Matrice, Renforts et Additifs

Les composites CFRP sont constitués de plusieurs composants fondamentaux : une matrice polymère, des renforts en fibres de carbone et divers additifs permettant d'optimiser leurs propriétés mécaniques et leur mise en œuvre [17].

2.2.1. La Matrice

Les matrices utilisées dans les composites CFRP sont principalement des **résines thermodurcissables**, notamment des résines époxy et, dans certains cas, des polymères thermoplastiques tels que le polyétheréthercétone (PEEK). Ces résines présentent une excellente résistance mécanique, thermique et chimique, ce qui est essentiel pour garantir l'intégrité structurelle des réservoirs d'hydrogène sous haute pression [18]. La matrice joue plusieurs rôles clés :

- Assurer la **cohésion** entre les fibres de carbone et transférer les charges mécaniques appliquées au composite.
- Protéger les fibres contre l'**oxydation** et les agressions chimiques externes.
- Améliorer la **résistance aux chocs** et aux sollicitations dynamiques [19].

2.2.2. Le Renfort en Fibres de Carbone

Les propriétés mécaniques des composites CFRP sont largement déterminées par les fibres de carbone qui les renforcent. Ces fibres, disposées sous forme de fils continus ou de nappes, offrent une résistance spécifique extrêmement élevée [20]. Les principales caractéristiques des fibres de carbone utilisées sont :

- **Diamètre** : Environ 5 à 7 µm, permettant une densité de renfort élevée.
- **Module d'élasticité** : Variant de 230 à 600 GPa selon la nature des fibres (fibres de carbone standards, intermédiaires ou à haut module).
- **Orientation** : Déterminée par le procédé d'enroulement filamentaire, influençant directement la résistance aux contraintes mécaniques [21].

Les composites CFRP utilisés pour les réservoirs de type IV sont généralement renforcés par des fibres **haute résistance** ou **haut module**, afin d'optimiser la tenue mécanique et la durabilité en fatigue sous cycles de pression [19].

2.2.3. Les Charges, Adjuvants et Additifs

L'ajout de charges et d'adjuvants dans la matrice permet d'améliorer certaines propriétés mécaniques et fonctionnelles des composites CFRP. Les principaux additifs utilisés sont :

- **Nanoparticules et nanotubes de carbone** : Améliorent la conductivité thermique et électrique tout en renforçant la résistance mécanique.
- **Agents anti-oxydation et stabilisants UV** : Prolongent la durée de vie des réservoirs en limitant la dégradation sous exposition aux rayons UV et aux températures élevées.
- **Plastifiants et modificateurs de viscosité** : Facilitent l'imprégnation des fibres lors du procédé d'enroulement filamentaire.
- **Agents anti-retrait et lubrifiants** : Permettent d'améliorer la qualité de surface et de réduire les contraintes résiduelles dans la matrice [21].

L'optimisation de ces composants est essentielle pour garantir une homogénéité structurelle du composite et une tenue mécanique adaptée aux exigences des applications de stockage d'hydrogène.

2.3. Procédés de fabrication des réservoirs composites

Les réservoirs de type IV sont principalement fabriqués par enroulement filamentaire, une technique de fabrication avancée qui permet un contrôle précis de l'orientation des fibres et garantit des performances mécaniques optimales en termes de résistance, de rigidité et de tenue en fatigue [22]. Cette technologie est particulièrement adaptée aux applications nécessitant une résistance à haute pression, comme le stockage d'hydrogène à 700 bars.

Le procédé d'enroulement filamentaire suit plusieurs étapes clés :

1. **Préparation des fibres** : Les fibres de carbone, choisies pour leur rapport résistance/poids exceptionnel, sont imprégnées d'une résine polymère (généralement une résine époxy, parfois thermoplastique) afin d'assurer une cohésion optimale avec la matrice [23]. L'imprégnation est réalisée via un bain de résine ou un procédé de pré imprégnation contrôlé, garantissant une répartition homogène de la résine sur les fibres [24].
2. **Enroulement sur le mandrin** : Les fibres imprégnées sont déposées sous tension contrôlée sur un mandrin rotatif selon des angles optimisés (généralement ±θ, 0° et 90°**),** permettant d'ajuster les propriétés mécaniques du réservoir [25]. L'orientation des fibres influence directement la résistance à la traction, à la compression et aux charges cycliques [26].
3. **Polymérisation et post-traitement** : Une fois le bobinage terminé, le réservoir subit un durcissement thermique sous pression et température contrôlées dans un four ou un autoclave. Cette étape est essentielle pour assurer une bonne réticulation de la résine et une consolidation optimale de la structure composite [27].
4. **Inspection et contrôle qualité** : La détection de défauts tels que les porosités, délaminations et inclusions est réalisée par des techniques avancées telles que la tomographie aux rayons X, la thermographie infrarouge et les ultrasons [28]. Ces contrôles garantissent la conformité aux normes de sécurité strictes requises pour le stockage d'hydrogène sous haute pression [29].

Grâce à cette méthode, les réservoirs de type IV combinent légèreté, résistance mécanique élevée et durabilité**,** répondant ainsi aux exigences croissantes de la mobilité durable et des applications hydrogène [30].

2.4 Comportement mécanique et endommagement des composites stratifiés

2.4.1. Les échelles usuelles de travail

Généralement, on définit trois échelles de travail (Figure 4) :

- L'échelle microscopique qui distingue les fibres de la matrice et voit les hétérogénéités les plus fines au sein du matériau ;

- L'échelle mésoscopique qui ne distingue plus les fibres de la matrice mais voit chacun des plis comme étant constitué d'un matériau homogène ;
- L'échelle macroscopique qui ne distingue pas les couches de la séquence d'empilement et voit la stratification dans sa globalité comme une entité homogène [31].

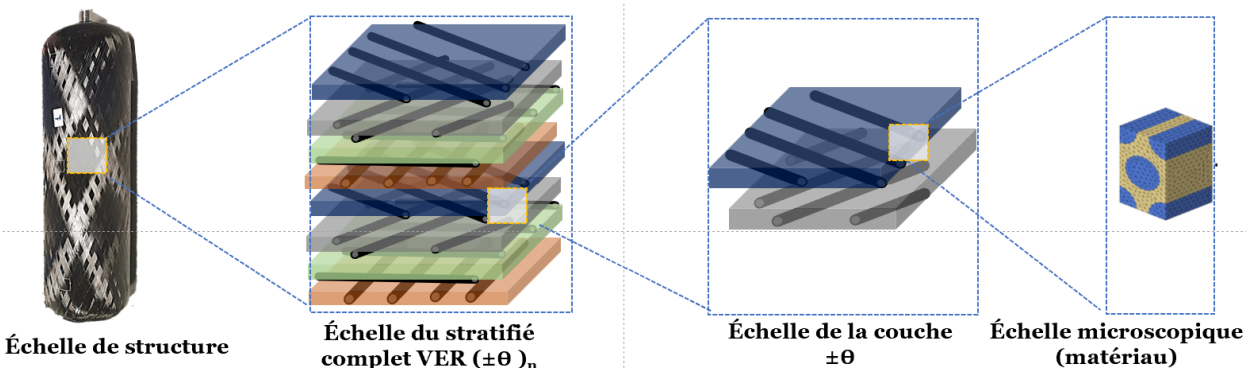

Figure 4. Echelle de travail d'un composite stratifié.

2.4.2. Mécanismes d'endommagement

Par définition, l'endommagement mécanique d'un matériau correspond à un défaut irréversible qui altère ses propriétés structurales. Dans un stratifié composite, ce processus débute lorsque certaines zones du matériau deviennent localement moins résistantes que d'autres. Sous l'effet d'une charge appliquée, ces zones fragilisées subissent une dégradation progressive, entraînant un transfert de charge vers une surface de plus en plus réduite. Cette redistribution des efforts conduit à une augmentation locale des contraintes, favorisant ainsi la propagation des dommages initiaux et menant progressivement à la rupture du matériau.

L'endommagement suit un schéma de ruine bien défini comme le montre la Figure 5. Il commence à l'échelle microscopique par une décohésion fibre-matrice, où l'adhésion entre les fibres et la matrice est localement compromise. Ensuite, des fissurations transverses apparaissent dans la matrice, créant des chemins de rupture préférentiels. Ces micro-endommagements évoluent vers un délaminage localisé entre les plis du stratifié, affaiblissant les interfaces inter laminaires et réduisant la cohésion globale de la structure. Enfin, lorsque les fibres elles-mêmes se rompent sous l'effet des contraintes maximales, la structure subit une perte complète de rigidité, aboutissant à sa ruine totale [32,33].

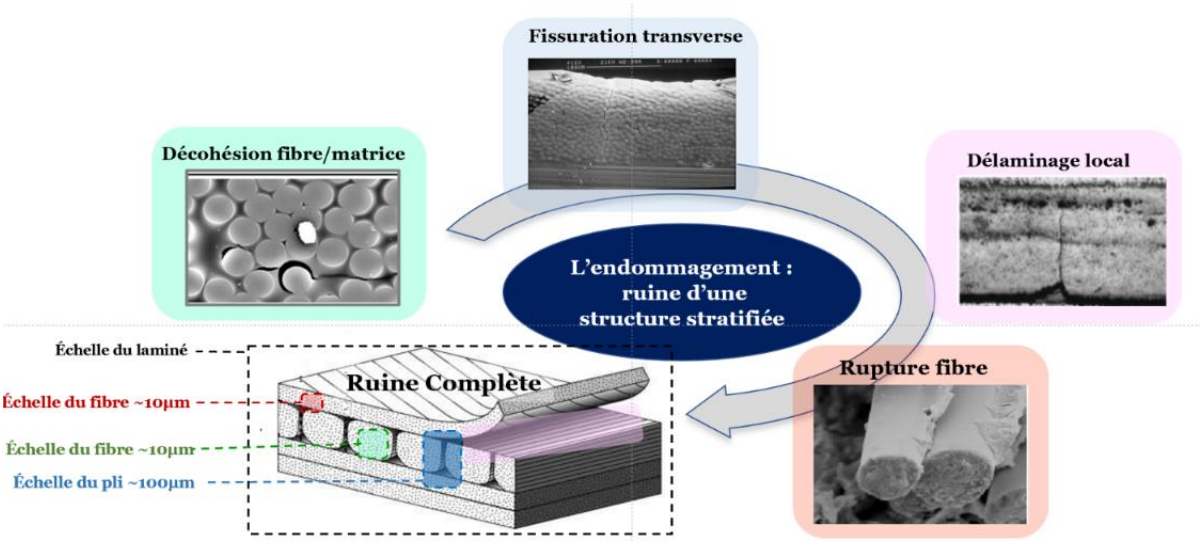

Figure 5. Les mécanismes clés d'endommagement des stratifiés composites.

Pour les composites stratifiés et pour les composites bobinés en particulier, les phénomènes d'endommagement prennent naissance à l'échelle microscopique (microfissuration matricielle, apparition de micro-vides) et conduisent à des mécanismes macroscopiques (délaminage, macro-fissures matricielles, décohésion fibre/matrice, rupture des fibres) [1]. Ces mécanismes d'endommagement, qui interagissent à différentes échelles (fibre, pli, stratifié), sont cruciaux à comprendre pour améliorer la conception et la fiabilité des structures composites, notamment en optimisant leur résistance aux charges mécaniques et en retardant l'apparition de la rupture.

De nombreux facteurs exercent une influence sur l'apparition puis l'évolution des différents mécanismes d'endommagement. Ces facteurs peuvent être le type de sollicitation (statique/fatigue) [34], la direction du chargement [35], le type d'empilement, la température, l'humidité, le processus de fabrication [36]. Dans ce présent rapport on s'intéresse à l'étude du comportement mécanique des composites stratifiés sous différents types de chargement (monotone et cyclique).

2.4.3. Caractérisation multi-échelle sous chargement monotone (de quasi-statique à dynamique rapide)

Sous des conditions de chargement quasi-statique, l'endommagement des matériaux composites se développe progressivement, en commençant par l'apparition de fissures dans la matrice. À mesure que la charge augmente, la densité de ces fissures s'intensifie, entraînant un décollement entre les fibres et la matrice,

puis une délamination. Lorsque l'endommagement se propage à travers les couches et atteint l'interface, la délamination se produit, provoquant la rupture des fibres et le transfert de charge vers les fibres adjacentes. Lorsque ces dernières ne peuvent plus supporter la contrainte, le matériau finit par se rompre. Ce phénomène est particulièrement observable lorsque la sollicitation est appliquée parallèlement aux fibres, où le comportement demeure linéaire et élastique jusqu'à la rupture des fibres. À l'inverse, une contrainte de traction perpendiculaire à l'orientation des fibres entraîne des dommages dans la matrice et la formation de microfissures aux endroits présentant des défauts. Le mode de rupture dépend alors de la qualité de l'adhésion entre les fibres et la matrice. L'orientation des fibres par rapport à l'axe de contrainte influe sur le niveau de sollicitation subi par la matrice et les fibres, entraînant l'apparition de différents modes d'endommagement. Par exemple, des essais de traction quasi-statique sur des composites carbone/époxy montrent que le comportement est linéaire et fragile dans l'axe des fibres, tandis qu'une sollicitation transversale induit une réponse non linéaire, en raison de la viscoélasticité de la matrice et du glissement des fibres. L'accumulation progressive de fissures dans la matrice et du décollement fibre-matrice dégrade les propriétés élastiques du matériau, notamment en cisaillement, où la non-linéarité est marquée [37,38]. Plusieurs études ont montré que la rupture des fibres se produit généralement en fin d'essai [39 :42]. Lorsque le composite est soumis à une traction perpendiculaire aux fibres, seuls la matrice et les interfaces du matériau sont endommagés, entraînant la formation de microfissures aux défauts. L'adhésion fibre-matrice détermine alors le type de fissure qui se propage et conduit à la rupture du composant. En revanche, sous une contrainte inclinée par rapport aux fibres, la matrice et les fibres subissent simultanément des sollicitations. Le mode d'endommagement dépend alors de l'orientation des fibres par rapport à l'axe de contrainte.

D'un point de vue macroscopique, le comportement des stratifiés unidirectionnels est hautement anisotrope. Il varie en fonction de la direction de chargement par rapport aux fibres et n'est pas nécessairement linéaire. Des essais réalisés sur des composites carbone/époxy ont mis en évidence le comportement du matériau pour des orientations de fibres à 0°, 45° et 90°. Lorsque le chargement est appliqué dans l'axe des fibres, le comportement est linéaire et élastique, caractéristique du comportement des fibres, et la rupture est fragile. En revanche, sous chargement transverse, le comportement devient moins linéaire en raison de la

viscoélasticité de la matrice et du glissement des fibres. La fissuration de la matrice et la décohésion fibre-matrice entraînent une dégradation importante des propriétés élastiques, notamment en cisaillement, où la non-linéarité est particulièrement prononcée (Figure 6).

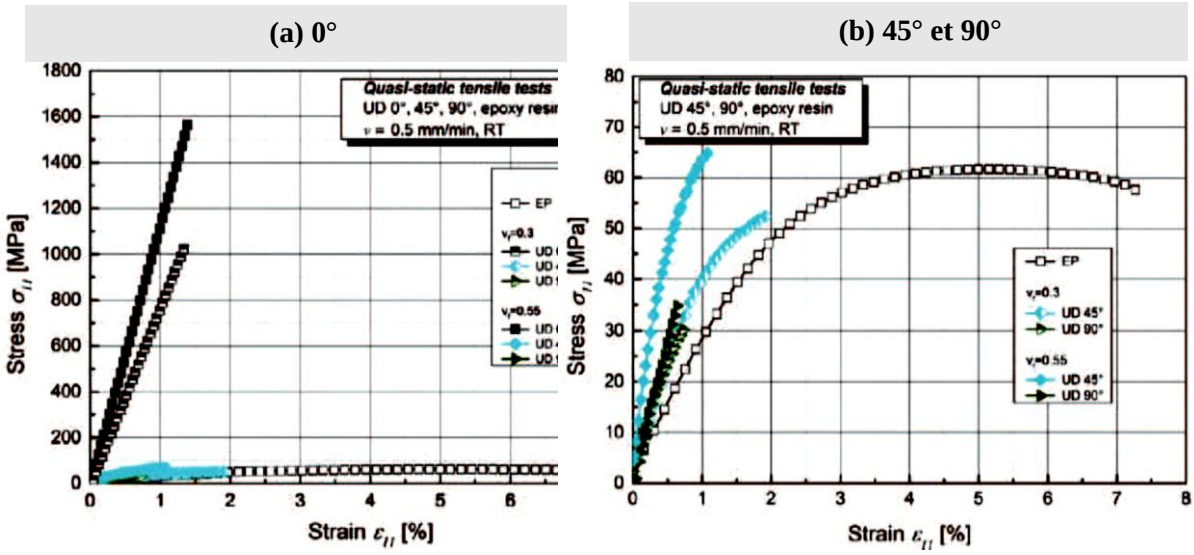

Figure 6.Courbes de contrainte-déformation axiales pour un stratifié carbone/époxyde sollicité suivant 3 directions de fibres [43].

Sous des conditions de chargement dynamique ou d'impact, le comportement du stratifié peut différer considérablement de celui observé en quasi-statique. Ce phénomène est particulièrement important dans des domaines comme l'aéronautique et l'automobile, où les matériaux sont soumis à des charges soudaines telles que des chocs ou des explosions. Lorsqu'un composite est soumis à un chargement dynamique, les effets inertiels empêchent la redistribution des contraintes au sein du stratifié, entraînant une concentration locale des dommages. Dans le même temps, la matrice devient plus fragile, ce qui accélère l'initiation des fissures.

Les principaux mécanismes d'endommagement incluent la fissuration de la matrice, la rupture des fibres, le décollement fibre-matrice, la délamination et la rupture interlaminaire en cisaillement. Les fissures de la matrice apparaissent généralement aux endroits où les contraintes sont concentrées et se propagent rapidement, perturbant le transfert des charges entre les fibres. Ensuite, la rupture des fibres résulte des contraintes locales élevées, tandis que le décollement fibre-matrice, causé par la différence de taux de déformation entre les fibres et la matrice, affaiblit encore davantage la structure.

La délamination réduit la rigidité du composite et favorise l'apparition d'autres formes de défaillance, telles que la rupture des fibres et la fissuration de la matrice. Enfin, la rupture inter laminaire en cisaillement, induite par des contraintes de cisaillement aux interfaces des plis, conduit à la délamination et à la séparation des couches, notamment lors d'impacts. L'évolution des dommages suit plusieurs étapes : initiation des fissures, propagation, rupture des fibres et, en dernier lieu, défaillance catastrophique lorsque la délamination et la rupture en cisaillement s'étendent.

Le taux de déformation joue un rôle crucial dans ces mécanismes : plus il est élevé, plus la rupture devient fragile. Des études montrent que les composites stratifiés soumis à un chargement dynamique ont une capacité d'absorption d'énergie réduite et que l'initiation des dommages se produit bien plus tôt qu'en quasi-statique. La sensibilité de la matrice au taux de déformation est donc un facteur déterminant dans la défaillance globale du stratifié.

Des méthodes expérimentales, telles que les essais d'impact à poids tombant et les barres de Hopkinson, ainsi que des approches numériques basées sur l'analyse par éléments finis et les modèles de zones cohésives, permettent d'évaluer la progression des dommages et d'optimiser la conception de structures composites résistantes aux impacts. Cependant, transposer ces résultats à des applications réelles reste un défi, notamment pour prédire la durabilité sous des charges dynamiques répétées et dans des conditions environnementales variées.

Une compréhension approfondie de ces mécanismes d'endommagement est essentielle pour concevoir des matériaux composites plus résistants et adaptés aux applications exigeantes.

2.4.4. Caractérisation sous sollicitation cyclique

Les composites stratifiés, tels que les polymères renforcés de fibres de carbone (CFRP), subissent des processus d'endommagement complexes lorsqu'ils sont soumis à un chargement cyclique. Une contrainte ou une déformation prolongée entraîne une accumulation progressive des dommages, principalement par la fissuration de la matrice, qui débute aux concentrations de contraintes comme les vides, les inclusions ou les

interfaces fibre/matrice dès les premières phases de fatigue. À mesure que le chargement cyclique se poursuit, ces fissures se propagent, compromettant la capacité de la matrice à transférer les charges entre les fibres, ce qui conduit finalement à la rupture des fibres, en particulier dans les plis alignés avec la direction de chargement. Un autre mécanisme critique est la décohésion fibre/matrice, qui affaiblit l'adhésion entre les fibres et la matrice, accélérant ainsi l'accumulation des dommages et aggravant la fissuration de la matrice ainsi que la rupture des fibres. La délamination, qui correspond à la séparation entre les couches du stratifié, est l'un des modes de défaillance les plus critiques sous chargement cyclique, car elle réduit significativement la rigidité et la résistance du composite. Ces mécanismes d'endommagement interagissent et évoluent avec le temps, entraînant une dégradation progressive de la rigidité, un indicateur clé de la durée de vie en fatigue (Figure 7).

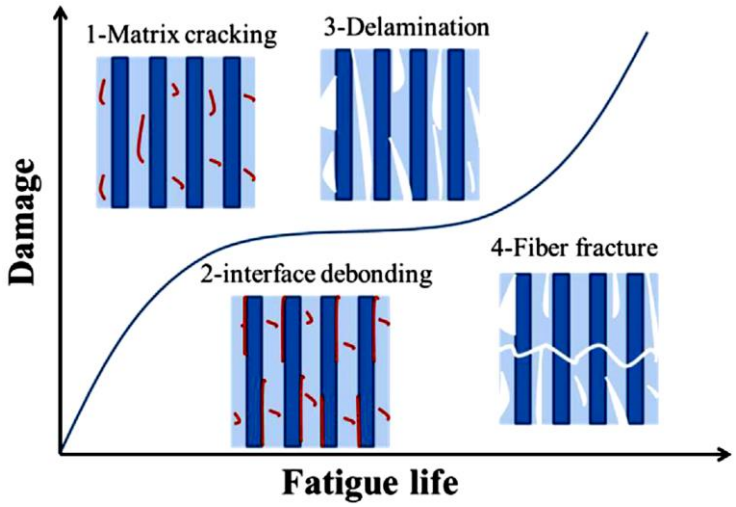

Figure 7. Processus général d'endommagement d'un stratifié sous chargement en fatigue traction-traction quasi-statique [48].

Le taux de dégradation est influencé par plusieurs facteurs, notamment l'orientation des fibres, la séquence d'empilement des plis, l'amplitude de la charge et les conditions environnementales comme la température et l'humidité. Par exemple, les stratifiés croisés sont plus sensibles à la délamination, tandis que les stratifiés unidirectionnels sont plus susceptibles de subir une rupture des fibres. Des conditions environnementales défavorables, telles qu'un taux d'humidité élevé, peuvent encore accélérer la fissuration de la matrice et la délamination [44 :46].

L'étude expérimentale s'est concentrée sur l'endommagement en fatigue des stratifiés. La Figure. 7 [47,48] illustre les étapes séquentielles de ce processus : fissuration de la matrice, décohésion fibre/matrice et rupture des fibres. Le schéma montre l'évolution des dommages en fonction de la durée de vie en fatigue d'un composite unidirectionnel stratifié soumis à un chargement périodique. Ce processus peut être divisé en trois phases :

1. Une phase d'accumulation rapide des dommages,
2. Une phase de propagation lente et stable,
3. Une phase finale d'accélération des dommages.

Au début du processus de fatigue, des microfissures apparaissent dans la matrice et s'étendent pour former des fissures le long des fibres hors axe sous chargement en traction. À mesure que le chargement cyclique se poursuit, des fissures apparaissent dans d'autres couches, augmentant progressivement en densité. Ce phénomène se poursuit jusqu'à ce que l'espacement ou la taille des fissures atteigne un niveau d'équilibre, appelé État de Dommage Caractéristique (*Characteristic Damage State - CDS*). À ce stade, la redistribution des contraintes limite l'initiation de nouvelles fissures.

Au fur et à mesure du processus de fatigue, la délamination se déclenche sous l'effet des fortes contraintes interlaminaires causées par l'effet de bord libre ainsi que par les fissures de la matrice et la rupture des fibres dans le stratifié. Par la suite, la délamination s'étend progressivement avec la poursuite du chargement cyclique.

Lors du chargement cyclique, la rupture prématurée des fibres est principalement due à la formation de fissures dans la matrice et de décohésions interfaciales, qui engendrent des concentrations de contraintes. Dans la phase initiale, la fissuration de la matrice est le phénomène dominant, suivie de la délamination lors de la phase intermédiaire. Finalement, l'accumulation progressive de multiples modes d'endommagement conduit à la rupture complète du stratifié. Cette séquence d'événements est similaire aux mécanismes d'endommagement observés sous chargement quasi-statique, bien que le processus de fatigue se déroule à un rythme plus lent.

Les résultats des analyses par imagerie aux rayons X indiquent qu'à mesure que la charge augmente, les fissures dans la matrice apparaissent plus tôt lors des essais de fatigue. Les travaux de Brunbauer et al. [43] montrent que les composites carbone/époxy atteignent une limite d'endurance en fatigue correspondant à 60 % de leur résistance à la traction après 5 millions de cycles lorsqu'ils sont chargés à 0°**.** De plus, les contraintes appliquées hors axe accélèrent l'accumulation des dommages, mettant en évidence la complexité des modes d'endommagement dans les matériaux composites, dont beaucoup se manifestent à l'échelle microscopique et ne sont pas visibles à l'œil nu.

Des modèles numériques tels que **l'**Analyse par Éléments Finis (*Finite Element Analysis - FEA*) et les Modèles de Zone Cohésive (*Cohesive Zone Models - CZM*) permettent de simuler la progression des dommages en fatigue et montrent une bonne corrélation avec les résultats expérimentaux. Toutefois, la transposition des résultats obtenus en laboratoire aux applications réelles reste un défi, en particulier dans des environnements soumis à des conditions de chargement complexes.

Les recherches en cours visent à optimiser la conception des matériaux composites et à améliorer leur résistance à la fatigue dans des applications de haute performance telles que l'aérospatiale, l'automobile et les énergies renouvelables.

3. Préparation des matériaux et méthodes

3.1. Composite époxy/fibres de carbone ± θ

Trois échantillons cylindriques de résine époxy renforcée par des fibres de carbone ont été préparés par Forvia, chacun avec différentes orientations angulaires des fibres. Ces échantillons comprenaient des stratifiés antisymétriques avec des orientations de ±15° et ±30°, ainsi qu'un stratifié multicouche comprenant des orientations de ±15°/±30°/±45°/±86°. Le Tableau 1 présente des photographies macroscopiques des différents tubes. Pour l'analyse des échantillons, les échantillons cylindriques ont été découpés en tranches courbes à l'aide d'une machine à découper munie d'une lame rotative.

Tableau 1. Vue et illustration du composite de résine époxy cylindrique renforcé de fibres de carbone

N° tubes	Orientation	Illustration
1	±15°	
2	±30°	
3	Multicouches	

3.2. Méthodes de caractérisation

3.2.1. Caractérisations physico-chimiques

La calorimétrie différentielle à balayage (DSC) est utilisée non seulement pour déterminer la capacité thermique spécifique des matériaux, mais aussi pour analyser le comportement de durcissement des résines époxy. L'analyse a été effectuée à l'aide d'un instrument DSC (Q1000 V9.0 Build 275, TA Instruments). Les échantillons ont été pressés dans des moules en aluminium non hermétiques, scellés et chauffés à une vitesse de 10°C/min jusqu'à 220°C. Les échantillons ont ensuite été refroidis à 30°C à une vitesse de 10°C/min.

L'analyse mécanique dynamique (DMA) a été utilisée pour déterminer les températures de transition vitreuse de la matrice époxy. Les expériences ont été réalisées à l'aide d'un instrument DMA Q800 TA Instruments sur des échantillons de 25×4 mm². Les conditions d'essai comprenaient un mode de chargement en flexion 3 points à une fréquence de 1 Hz sur une plage de température de 25°C à 150°C avec un taux de rampe de 2°C par minute.

3.2.2. Observations microscopiques

Le microscope électronique à balayage (MEB) HITACHI S-4800 a été utilisé pour examiner qualitativement la microstructure du matériau, les surfaces de rupture des éprouvettes de traction et en particulier la propagation des fissures pendant les essais quasi statiques. Il a également été utilisé pour mesurer quantitativement la porosité au sein de la microstructure. La porosité, ou fraction de vide, est le volume de vides dans un matériau par rapport à son volume total. Après l'analyse de la microstructure, la première étape du processus expérimental consiste à mesurer la porosité du matériau, qui peut être déterminée selon la méthode suivante : calcul du pourcentage massique de fibres (M_f %) ou d'époxy (M_e %). Pour quantifier la

teneur en fibres du composite, tous les échantillons ont été soumis à une pyrolyse, au cours de laquelle ils sont chauffés à 550°C pendant 5,5 heures. Ce processus conduit à la dégradation de la matrice, ne laissant que la fibre de carbone intacte. La formule utilisée pour calculer la teneur en fibres est la suivante :

$$M_f = \left(\frac{M_0 - M_p}{M_0}\right) * 100 \qquad \textbf{Équation 1}$$

Où M_0 est la masse initiale et M_p la masse après pyrolyse. En outre, la densité de la fibre de carbone (1,8 g/cm³) et la densité de l'époxy utilisé (1,2 g/cm³) sont utilisées pour déterminer le taux de porosité.

3.2.3. Essai de traction quasi-statique

Les essais de traction quasi-statique ont été réalisés à l'aide d'une machine Instron 5966 à une vitesse de 10 mm/min (~0,001 s^{-1}) et à une température de 20°C. La mesure de la déformation dans la longueur de la jauge a été facilitée par un extensomètre vidéo sans contact. Cet instrument de pointe utilise des techniques de mesure optique sans contact, avec une caméra numérique et un traitement d'image en temps réel pour mesurer avec précision la déformation dans les directions axiale et latérale pendant l'essai de traction. Pour éviter que les échantillons ne glissent, des pinces auto-serrantes ont été utilisées pour les maintenir en place. Les dimensions des échantillons sont indiquées à la Figure 8.

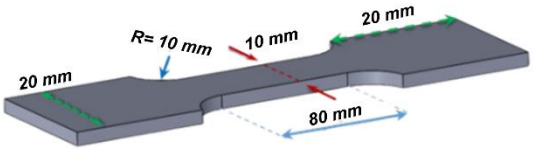

Figure 8. Dimensions des échantillons d'époxy renforcé de fibres de carbone

3.3. Méthodologie de l'analyse de l'endommagement

Pour démontrer les phénomènes d'endommagement particuliers des composites en CFRP, il est essentiel de créer un point de référence pour comparer différents états et scénarios d'endommagement dans diverses microstructures. Cette référence permet de comprendre comment l'endommagement affecte le comportement des composites CFRP. Les changements de rigidité sont un indicateur important de la progression des dommages. La surveillance des changements de rigidité permet de suivre les mécanismes de dommages microscopiques et la rigidité résiduelle à différents niveaux de contrainte, fournissant ainsi une vue d'ensemble complète et détaillée de l'évolution des dommages.

La méthodologie consiste à effectuer des essais de chargement et de déchargement quasi-statiques, au cours desquels le module d'Young est quantifié à chaque niveau de contrainte. À chaque étape de l'essai, les zones endommagées font l'objet de balayages MEB à haute résolution afin de saisir les changements microstructuraux et la propagation des fissures. Ces analyses détaillées sont essentielles pour comprendre l'origine et la progression des dommages dans le matériau composite. Le processus se poursuit avec des mesures et des analyses répétées jusqu'à la rupture de l'échantillon. Cette approche permet un suivi complet de la progression des dommages, depuis la formation initiale des fissures jusqu'à la rupture complète. En corrélant les changements mesurés du module d'Young avec les mécanismes d'endommagement microscopiques observés, il est possible d'établir une relation quantitative entre les propriétés macroscopiques et les phénomènes d'endommagement sous-jacents. Cette relation est d'une importance cruciale pour comprendre comment les différents niveaux de contrainte et les configurations microstructurales affectent l'intégrité et la fonctionnalité globales des composites en polymère renforcé de fibres de carbone (CFRP). La valeur de cette méthodologie réside dans sa capacité à fournir un lien clair et quantifiable entre les dommages au niveau microscopique et les changements qui en résultent dans les propriétés mécaniques du matériau. Ces informations sont cruciales pour le développement de matériaux composites plus durables et plus fiables, car elles permettent d'envisager l'atténuation des dommages et l'amélioration de la résistance du matériau à la rupture. La Figure 9 illustre la méthodologie détaillée utilisée pour identifier et comprendre les mécanismes d'endommagement spécifiques des composites en polymère renforcé de fibres de carbone (CFRP).

La Figure 9 fournit une représentation visuelle du processus étape par étape, commençant par l'établissement de la base de référence et se terminant par la capture d'images MEB et l'analyse de l'évolution des dommages. Cette approche globale permet de bien comprendre la relation complexe entre les dommages microstructuraux et le comportement mécanique macroscopique des composites en CFRP.

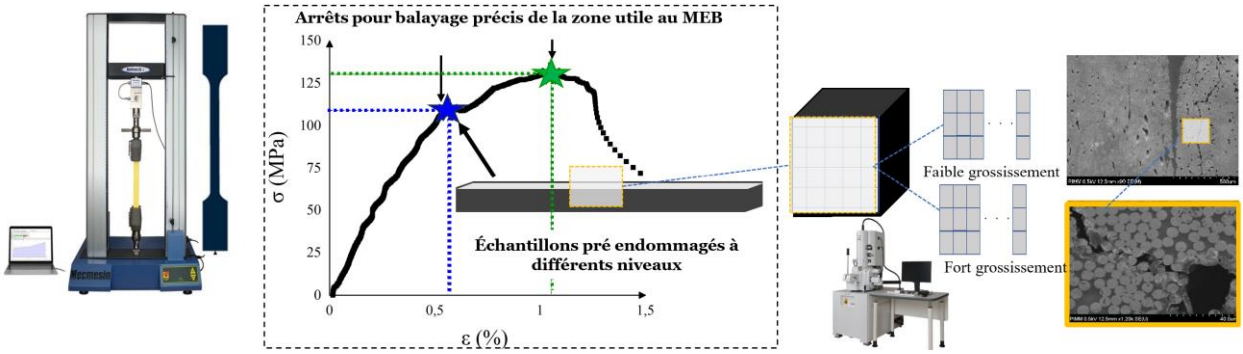

Figure 9. Méthodologie utilisée pour démontrer les phénomènes d'endommagement spécifiques

3.4. Essais de traction à basse et grande vitesse de déformation

Des essais de traction à basse vitesse ont été réalisés à différents niveaux de contrainte maximale prédéfinis à l'aide d'une machine Instron 5966 à une vitesse de 10 mm/min et à une température de 20°C.

En outre, une machine servo-hydraulique (Schenk Hydropuls VHS 5020) a été utilisée pour effectuer des essais de traction à différentes vitesses de déformation, allant de quasi-statique à $100s^{-1}$. L'échantillon composite a été positionné entre la cellule de charge (extrémité supérieure) et le dispositif mobile (extrémité inférieure), comme illustré à la Figure 10. (a). Afin de garantir une vitesse de déformation constante dès le début de l'essai de traction à grande vitesse, un dispositif à piston tubulaire a été utilisé pour appliquer un déplacement au dispositif mobile sans charge pendant la phase d'accélération.

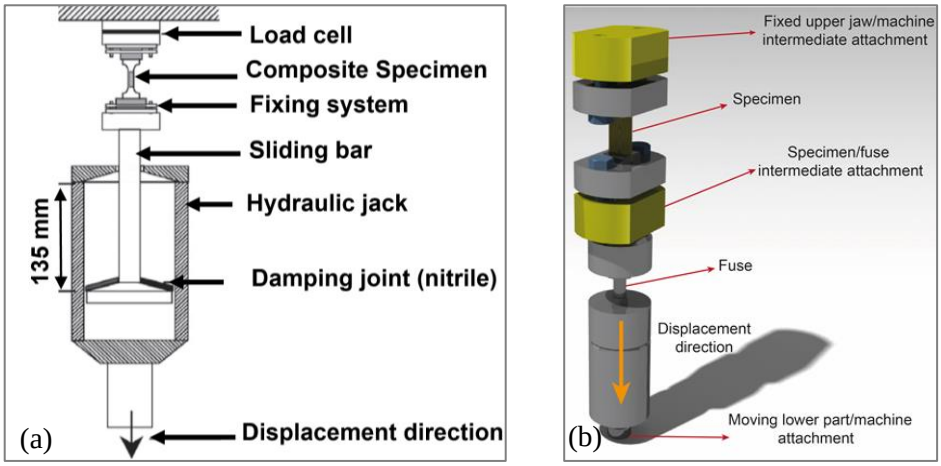

Figure 10. (a) Appareil de traction à taux de déformation élevé ; dispositif d'essai de traction dynamique interrompu, et (b) essai de traction à grande vitesse interrompu

3.5. Essai de traction dynamique interrompu (IDTT)

Le concept d'essai de traction interrompu à taux de déformation élevé a été initialement proposé par Lataillade et al pour les stratifiés verre-époxy, puis appliqué par Fitoussi et al aux composites SMC standard, aux stratifiés carbone-époxy et au polypropylène renforcé par des fibres de verre courtes. L'essai de traction dynamique interrompu (IDTT) a deux objectifs distincts : premièrement, identifier les mécanismes d'endommagement progressif se produisant au niveau microscopique et deuxièmement, déterminer la perte progressive de rigidité due à l'endommagement. En analysant à la fois le seuil et la cinétique des dommages, ces tests permettent de corréler les résultats obtenus aux niveaux microscopique et macroscopique. Dans cette étude, l'IDTT a été adapté pour être utilisé avec des composites en résine époxy renforcée de fibres de carbone. L'IDTT est un essai dynamique de charge/décharge qui génère des états successifs de dommages dans l'échantillon à différents niveaux de force au cours d'une charge à grande vitesse. Le même échantillon est soumis à des cycles de chargement répétés à des niveaux de force appliqués progressivement croissants. Avant chaque étape de rechargement, des observations au MEB ont été effectuées sur les surfaces polies afin de quantifier les effets de la vitesse de déformation sur les mécanismes d'endommagement microscopiques. Cette approche a permis une évaluation complète des dommages dans les composites en résine époxy renforcée par des fibres de carbone aux niveaux micro et macro. Le dispositif IDTT, illustré à la Figure 10(b), se heurte à un problème important lors d'une charge dynamique en raison de l'inertie du cylindre hydraulique. Une fois que l'essai a commencé, cette inertie empêche d'arrêter l'essai à des niveaux de contrainte prédéterminés, contrairement aux essais de charge/décharge quasi-statiques. Par conséquent, la charge se poursuit jusqu'à ce que l'échantillon subisse une défaillance macroscopique. Pour résoudre ce problème, un fusible élastique fragile est intégré en série à l'échantillon composite. Dans cette étude, un dispositif sur mesure a été développé et adapté pour accueillir des fusibles cylindriques en acier à encoche. La longueur du ligament du fusible est calibrée avec précision pour correspondre à la force maximale requise.

3.5.1. Caractérisation du fusible

Des essais de traction ont été effectués sur le fusible en acier afin de déterminer l'ordre de grandeur de la contrainte maximale pour différentes longueurs de ligament. La Figure 11 illustre la force ultime en fonction

de la longueur du ligament du fusible. On peut observer que la force définie pendant un taux de déformation élevé interrompu peut être obtenue en faisant varier la longueur du ligament. Il est à noter que la contrainte ultime peut varier pour des taux de déformation élevés. Cependant, aucune variation significative n'a été observée pendant l'IDTT.

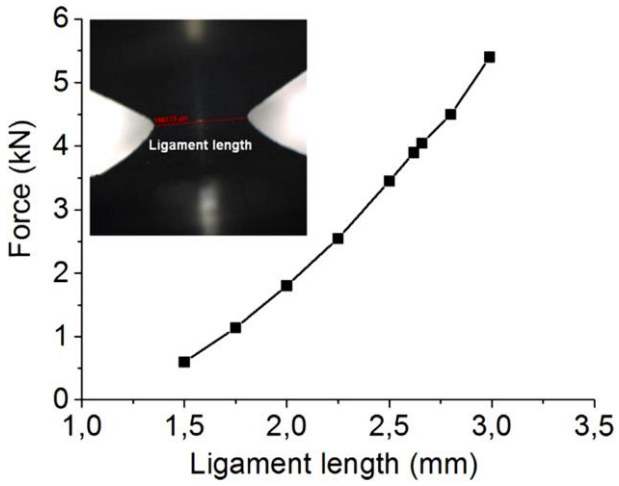

Figure 11. Force ultime requise en fonction du diamètre du fusible

3.5.2. Mesures de la déformation et de la vitesse de déformation

Une technique sans contact est employée pour quantifier la déformation locale à l'aide d'une caméra à grande vitesse (FASTCAM-APX RS). La méthodologie de mesure des vitesses de déformation a déjà été décrite dans une publication séparée. Elle implique l'analyse des images capturées pendant la déformation de la surface filmée.

Afin de mieux comprendre les mécanismes d'endommagement qui se produisent lors d'une charge dynamique, il est essentiel de mener des études expérimentales aux niveaux macroscopique et microscopique.

4. Résultats expérimentaux et discussion

4.1. Analyse physico-chimique

Trois orientations de composites époxy renforcés de fibres de carbone, à savoir ±15°, ±30° et multicouches, ont été soumises à la calorimétrie différentielle à balayage (DSC) afin d'évaluer leur réponse thermique aux variations de température. Les résultats de la DSC ont montré une pente caractéristique correspondant au changement de phase associé à la température de transition vitreuse (Tg), qui s'est avérée

être d'environ 124°C pour toutes les orientations testées. Cette observation suggère une réticulation efficace de l'époxy dans la structure du composite. En outre, aucun autre pic ou indication de vieillissement physique n'a été observé dans la plage de température de 30°C à 220°C, comme le montre la Figure 12. Cette absence de pics indique que les composites ont conservé leur stabilité thermique et n'ont pas subi de modifications significatives de leur structure moléculaire ou de leurs propriétés thermiques dans la plage de températures testée. En conclusion, l'analyse DSC confirme que les composites époxy renforcés de fibres de carbone avec les orientations ±15°, ±30°, ainsi que la configuration multicouche, ont des matrices de résine stables et bien réticulées avec un comportement thermique cohérent et une résistance au vieillissement physique sur la plage de température spécifiée.

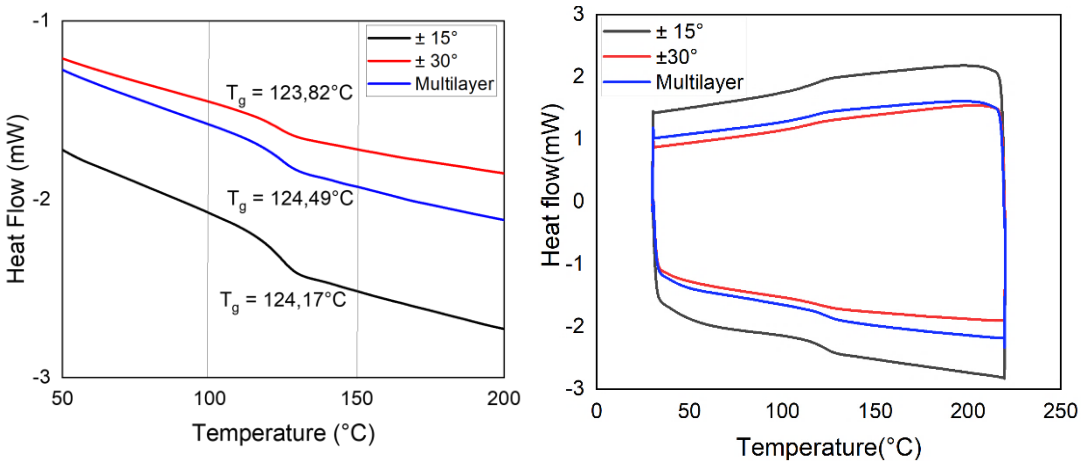

Figure 12. Courbe DSC et stabilité des composites CFRP

Les résultats de la DMA ont montré que le module de stockage présente une variation minimale avec l'augmentation de la température dans la zone vitreuse jusqu'à 100°C. Cependant, au-delà de cette température, on observe une diminution significative du module. Les valeurs de la température de transition vitreuse (Tg) déterminées par DMA pour chaque échantillon se situent systématiquement autour de 124°C. Cette constatation corrobore les valeurs de Tg obtenues à partir de l'analyse DSC. Ces résultats indiquent que les composites époxy renforcés de fibres de carbone conservent leur intégrité structurelle et leur rigidité à l'état vitreux jusqu'à environ 100°C, après quoi une diminution significative du module se produit. La concordance entre les résultats de la DSC et de la DMA confirme la réticulation efficace et la stabilité thermique de la matrice époxy dans les composites [2].

4.2. Analyse microstructurale

La compréhension de la distribution et de l'impact de ces caractéristiques microstructurales, en particulier en relation avec les différentes orientations des fibres, est essentielle pour optimiser les processus de fabrication et améliorer les performances mécaniques globales et la durabilité des composites époxy renforcés par des fibres de carbone.

L'analyse microstructurale par microscopie optique (Figure 13) confirme la structure stratifiée du composite et valide l'architecture produite par le processus industriel, y compris les différentes orientations des fibres telles que ±15°, ±30° et les configurations multicouches (±30°/±45°/±88°/±30°/±45°/±45°/±30°).

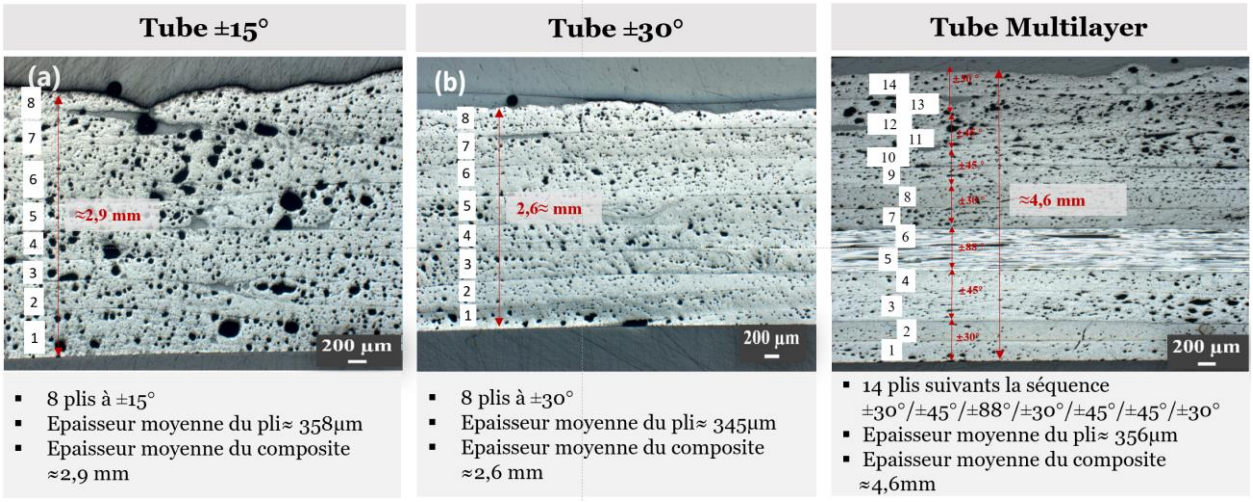

Figure 13. Micrographie optique : (a) configurations ±15°, (b) ±30° et (c) Multicouches

Chaque micrographie montre des porosités résultant du processus de fabrication, qui peuvent agir comme des sites d'initiation de fissures.

Les observations ultérieures au microscope électronique à balayage (Figure 14) corroborent les résultats de la microscopie optique. Ces observations confirment non seulement la structure en couches du composite, mais mettent également en évidence l'hétérogénéité et l'état de l'interface fibre/matrice, en particulier dans les régions adjacentes aux porosités observées. Des signes de décohésion fibre/matrice sont évidents, indiquant des faiblesses potentielles dans le matériau [2].

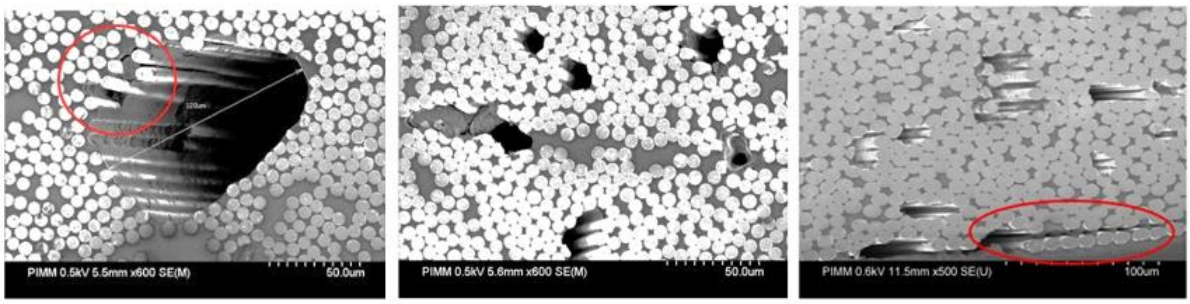

Figure 14. Micrographie MEB : (a) configurations ±15°, (b) ±30° et (c) multicouches

4.3. Impact de l'orientation des fibres sur la porosité

Le Tableau 2 montre le pourcentage de volume de porosité dans les tubes avec différentes orientations de fibres et montre des variations significatives de 4,7 % à 7,8 %. Ces résultats mettent en évidence l'influence significative de l'orientation des fibres sur les niveaux de porosité dans les composites.

Pour l'orientation ±15°, la densité du composite est de 1,39 g/cm³, les fibres représentant 69,8 % de la masse (54,20 % en volume) et l'époxy 30,21 % de la masse (37,9 % en volume). La porosité est de 7,8 %. Dans l'orientation ±30°, la densité du composite est de 1,45 g/cm³, les fibres représentant 70,94% de la masse (57,28% en volume) et la résine époxy 29,06% de la masse (3,00% en volume). La porosité est de 4,7 %. Dans la configuration multicouche, la densité du composite est de 1,46 g/cm³, les fibres représentant 72,92% de la masse (59,17% en volume) et l'époxy 27,08% de la masse (35,6% en volume). La porosité est de 5,2 %.

Globalement, sur l'ensemble des tubes testés, la densité moyenne est de 1,44 g/cm³. Les fibres constituent 71,1 % de la masse (56,9 % en volume), tandis que la résine époxy représente 28,8 % de la masse (37,5 % en volume). La porosité moyenne de tous les échantillons est de 5,4 %. Ces résultats soulignent le rôle critique de l'optimisation de l'orientation des fibres lors de la fabrication des composites afin de minimiser la porosité et d'améliorer l'intégrité globale du matériau et les performances mécaniques [2].

Tableau 2. Pourcentage de porosité en volume dans les tubes avec différentes orientations des fibres pourcentage de porosité en volume dans les tubes avec différentes orientations des fibres

Tube	Densité du composite	Fibre [% massique]	Fibre [% volumique]	Matrice [% massique]	Matrice [%volumique]	Porosité [% volumique]
±15°	1,39	69,79%	54,20%	30,21%	37,99%	7,8%
±30°	1,45	70,94%	57,28%	29,06%	38,00%	4,7%
Multicouches	1,46	72,92%	59,17%	27,08%	35,65%	5,2%
Moyenne	1,44	71,15%	56,99%	28,85%	37,49%	5,4%

4.4. Comportement en traction

Les propriétés mécaniques des composites époxy renforcés de fibres de carbone, comme le montrent la Figure 15 et le Tableau 3, présentent des variations significatives influencées par l'orientation des fibres.

Figure 15 et le Tableau 3, montrent des variations significatives influencées par l'orientation des fibres. Pour chaque orientation testée ±15°, ±30° et configurations multicouches, environ cinq échantillons ont été analysés pour garantir la fiabilité et la répétabilité des courbes contrainte-déformation. Ces résultats mettent en évidence la cohérence du comportement en traction sur plusieurs essais.

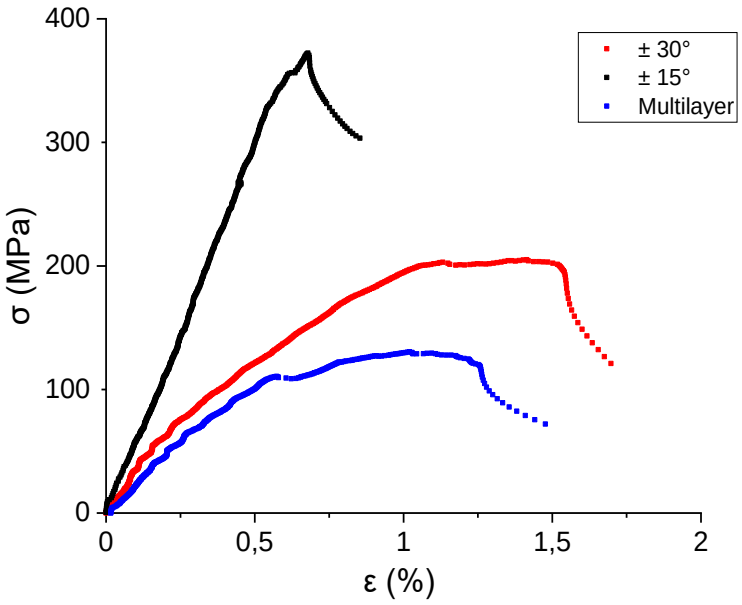

Figure 15. Courbes représentatives des essais de traction quasi-statiques à 20°C ($d\varepsilon/dt = 0{,}001\ s^{-1}$)

Tableau 3 .Résumé des propriétés mécaniques de traction pour différents tubes

Tube	E (GPa)	σ_{seuil} (MPa)	ε_{seuil} (%)	σ_{max} (MPa)	ε_{max} (%)
±15°	$60^{\pm 2,7}$	$331^{\pm 5,2}$	$0,56^{\pm 0,02}$	$361,4^{\pm 8}$	$0,66^{\pm 0,08}$
±30°	$36,8^{\pm 2,20}$	$55^{\pm 2,3}$	$0,17^{\pm 0,06}$	$206,6^{\pm 4,2}$	$1,3^{\pm 0,10}$
Multicouches	$21,1^{\pm 0,75}$	$111,8^{\pm 3,4}$	$0,538^{\pm 0,10}$	$157,1^{\pm 6,4}$	$0,94^{\pm 0,08}$

Les résultats montrent que l'orientation des fibres joue un rôle critique dans la détermination du comportement mécanique. Les échantillons alignés plus étroitement sur la force appliquée, tels que ceux orientés à ±15°, présentent une résistance à la traction et un module plus élevé, reflétant un transfert de charge efficace le long des fibres. Inversement, les configurations ±30° et multicouches présentent une plus grande ductilité, caractérisée par un allongement plus important à la rupture.

Plus précisément, les échantillons orientés à ±15° présentent des performances supérieures en raison d'une répartition optimale des contraintes le long des fibres, ce qui se traduit par une plus grande rigidité et une meilleure résistance à la déformation. En revanche, les échantillons orientés à ±30° et les configurations multicouches, où les fibres sont moins bien orientées par rapport à la direction de chargement, présentent une rigidité plus faible mais une meilleure capacité à se déformer avant la rupture. Ce comportement est attribué aux dommages et à la déformation plastique dans la matrice époxy et reflète l'influence des interactions fibre-matrice sous charge.

Les échantillons provenant de différentes orientations présentent des caractéristiques de rupture différentes. Les échantillons orientés à ±15° présentent des surfaces de rupture propres et droites, indiquant un comportement de rupture fragile cohérent avec leur rigidité élevée et leur faible déformation à la rupture. En revanche, les échantillons orientés à ±30° et les configurations multicouches présentent des surfaces de rupture plus irrégulières et rugueuses. Ces observations sont cohérentes avec les propriétés mécaniques résumées dans le Tableau 3 et renforcent le rôle critique de l'orientation des fibres dans la détermination du comportement à la rupture et des performances mécaniques globales des composites époxy renforcés de fibres de carbone.

La transition entre les modes de rupture ductile et fragile sous différentes conditions de chargement est étudiée par analyse microscopique, comme le montre la Figure 16. Les micrographies orientées à ±15° des

échantillons présentent des caractéristiques indiquant une rupture fragile. Les surfaces de rupture semblent plates, lisses et sans caractéristiques, dépourvues des caractéristiques ductiles typiques. Le passage observé de modes de rupture fragiles à des modes de rupture ductiles de ±15° à ±30° et à des configurations multicouches met en évidence la sensibilité du comportement de rupture du matériau à l'orientation des fibres [2].

Tube	Fractographie	
±15°	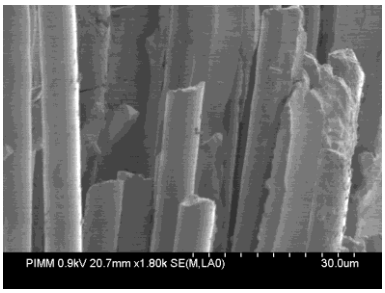	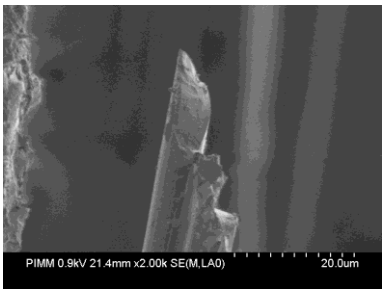
±30°	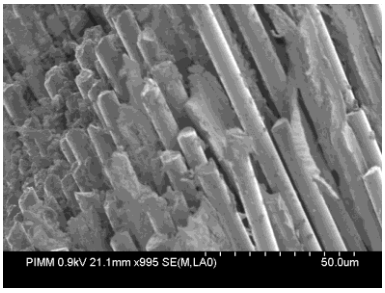	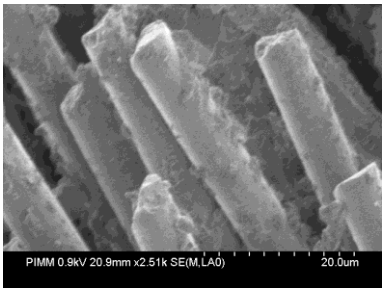
Multicouche	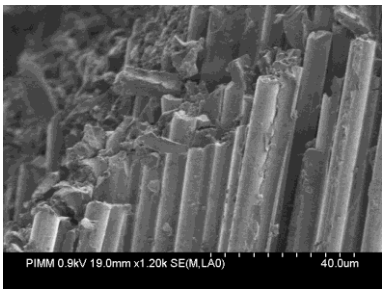	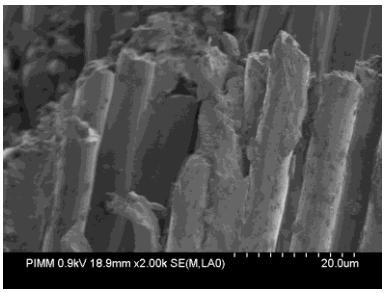

Figure 16. Analyse microscopique des surfaces de rupture

4.5. Analyse des mécanismes d'endommagement

4.5.1. Analyse quantitative de l'endommagement macroscopique

L'évolution du comportement mécanique d'un matériau, de son état initial à sa rupture, est décrite par la théorie de l'endommagement macroscopique suivante :

$$D_{macro} = 1 - \frac{E^D}{E^0} \qquad \textbf{Équation 2}$$

Où E^0 et E^D sont respectivement les modules du matériau non endommagé et endommagé. L'analyse de la Figure 16 couplée à la Figure 17 montre l'évolution de la rigidité relative (E/E^0) pour les différentes orientations du tube étudiées. Quelle que soit l'orientation, deux phases distinctes sont observées :

Dans cette première phase, le matériau présente un comportement linéaire sans plasticité ni endommagement.

Dans la seconde phase, le matériau présente une réponse anélastique due aux effets combinés de l'endommagement et de la plasticité de la matrice.

La Figure 17 illustre l'évolution macroscopique de l'endommagement pour les différentes orientations du tube, mettant en évidence l'influence de l'orientation des fibres sur la vitesse et l'étendue de l'endommagement et de la plasticité. L'effet de l'orientation des fibres sur la cinétique d'endommagement est significatif. Les orientations ±30° et mixte des tubes présentent une cinétique d'endommagement plus rapide que l'orientation ±15°. Plus précisément, les tubes à ±15° présentent les niveaux de dommages et de plasticité les plus faibles, ce qui indique que cette orientation offre une plus grande résistance à la progression des dommages. Cette représentation visuelle souligne le rôle critique de l'orientation des fibres dans la détermination du comportement mécanique et de la durabilité des composites CFRP sous charge [2].

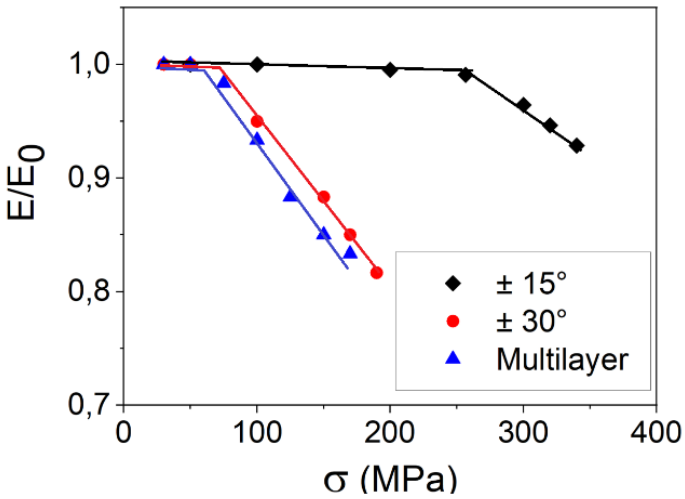

Figure 17. Évolution macroscopique de l'endommagement pour différents tubes

4.5.2. Analyse microscopique qualitative de l'endommagement

Pour identifier les mécanismes d'endommagement survenant lors d'un chargement quasi-statique, il est nécessaire de mener des investigations expérimentales à la fois à l'échelle macroscopique et microscopique. A cette fin, des échantillons rectangulaires avec des surfaces polies permettant des observations microscopiques à l'aide du MEB ont été préparés. La Figure 18 montre le comportement mécanique du composite orienté à ±15° sous charge. Le matériau ne présente aucun signe d'endommagement jusqu'à 300 MPa et conserve un comportement élastique linéaire. Au-delà de ce point, le matériau commence à accumuler des dommages conduisant à un comportement non linéaire et finalement à la rupture. Le premier mécanisme d'endommagement observé est la décohésion à l'interface fibre-matrice, comme l'ont démontré NOUIRA et al.

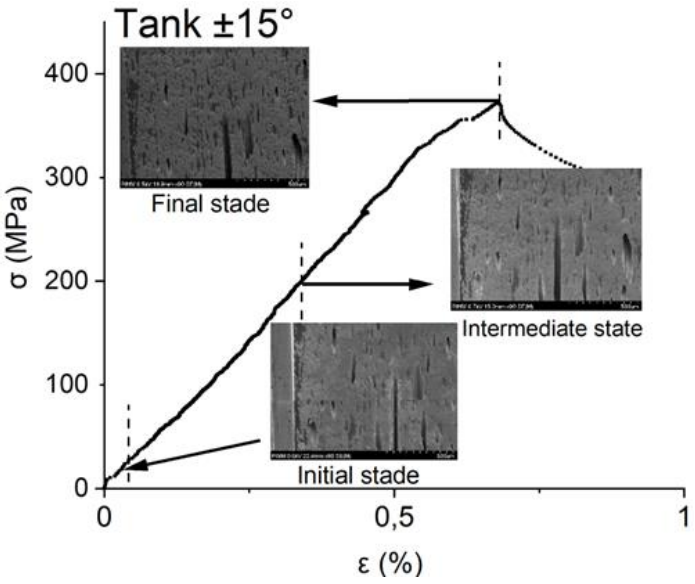

Figure 18. Mécanismes d'endommagement microscopiques : configuration ±15°

La Figure 19 montre le comportement mécanique du composite multicouche orienté à ±30° sous charge. Initialement, le matériau présente un comportement élastique linéaire jusqu'à 80 MPa sans dommage. Une fois encore, le premier mécanisme d'endommagement observé est la décohésion à l'interface fibre-matrice.

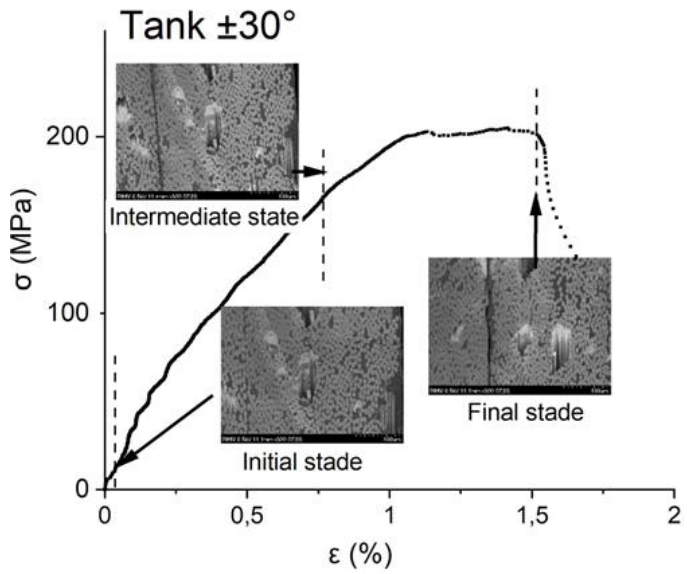

Figure 19. Mécanismes d'endommagement microscopiques : configuration ±30°

La Figure 20 montre une courbe contrainte-déformation (σ-ε) pour un composite multicouche, accompagnée d'images MEB à différents stades de déformation : initial, intermédiaire et final. Au stade initial, le matériau présente un comportement élastique linéaire sans dommage ni déformation plastique visible, comme le montre l'image MEB intitulée « Initial Stade ». Une fois encore, le premier mécanisme d'endommagement observé est la décohésion à l'interface fibre-matrice à environ 60 MPa. Lorsque la déformation augmente jusqu'à environ 1 %, la contrainte continue d'augmenter, mais à un rythme décroissant, pour atteindre son maximum à environ 120 MPa. Au cours de cette phase intermédiaire, le matériau commence à montrer des signes d'endommagement et de plasticité, comme en témoigne l'image MEB montrant le début de la décohésion à l'interface fibre/matrice et la microfissuration, suivie de la fracture de la matrice.

Au-delà de 1 % de déformation, après que la contrainte maximale a été atteinte, la courbe montre un déclin, indiquant une défaillance ou des dommages importants. À ce stade final, le matériau présente un comportement anélastique dû à des dommages importants et à une déformation plastique. L'image MEB intitulée ‘Final stade’ montre de grandes fissures et des dommages importants conduisant à une délamination, en particulier sur les couches à ±86°, et par conséquent à la défaillance finale du matériau.

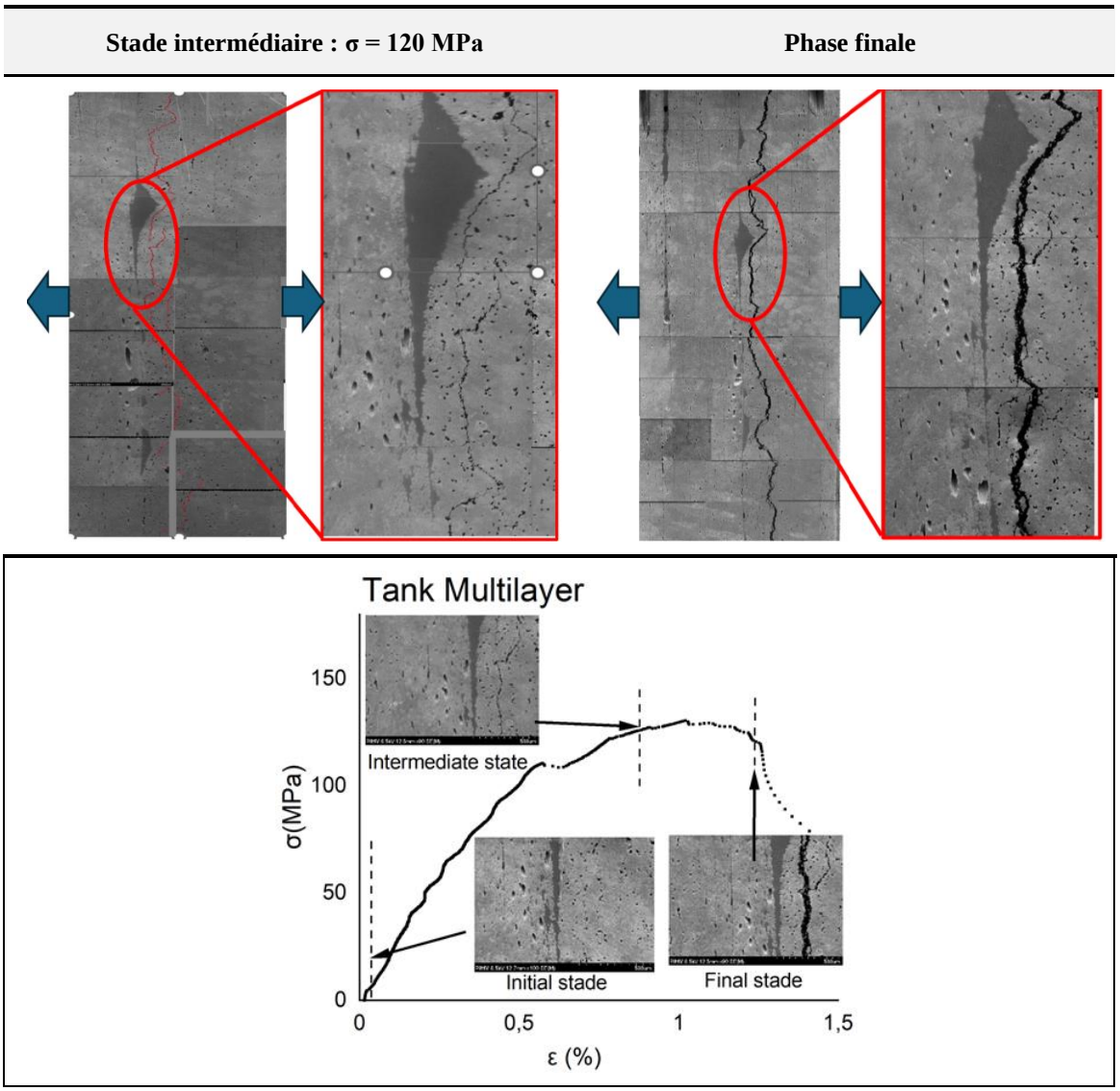

Figure 20. Mécanismes d'endommagement microscopiques : configuration multicouche

Dans la microstructure des configurations ±15°, ±30° et multicouches (Figure 20), les composites à l'état initial contiennent des pores ou des vides résultant du processus de fabrication. Ces pores peuvent être répartis de manière aléatoire dans le matériau, les fibres s'étendant souvent à la surface des parois des pores. Lors des essais de traction, les contraintes sont inégalement réparties en raison de l'orientation différente des fibres dans les différentes couches. Autour des pores, les contraintes de traction sont amplifiées en raison de la disparité de rigidité entre la matrice et les régions poreuses, ce qui entraîne des concentrations locales de contraintes (voir Figure 21).

Tube	±15°	±30°	Multicouches
Stade initial	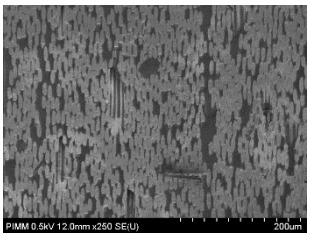	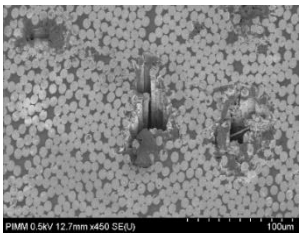	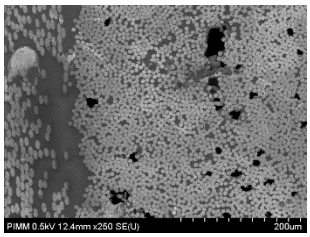
Initiation des dommages par la **porosité**	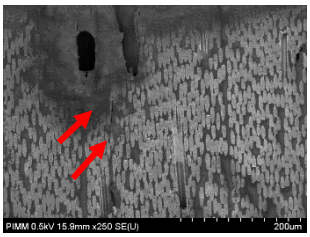	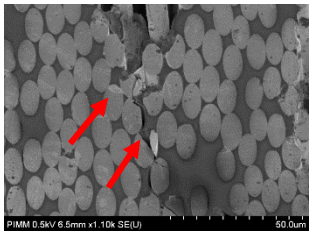	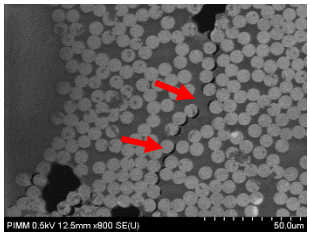
Propagation des dommages	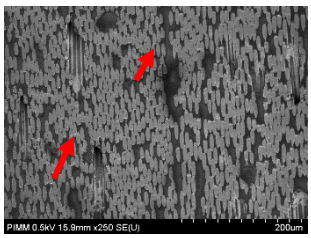	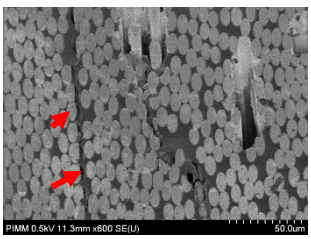	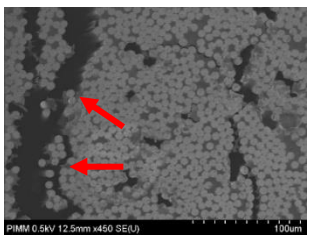
Rupture final	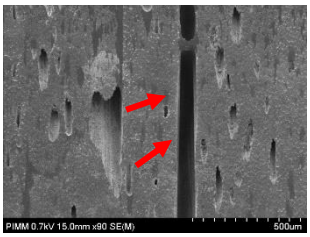	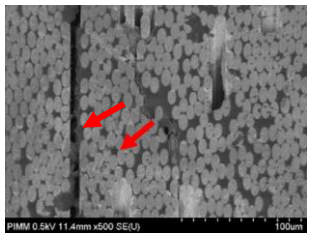	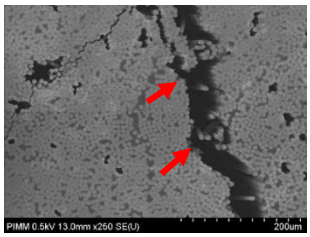

Figure 21. Évolution de la microstructure et mécanismes d'endommagement pour différents tubes

Ces contraintes concentrées près des pores peuvent dépasser la résistance du matériau et provoquer des fissures. Ces fissures prennent généralement naissance sur les bords des pores et se propagent dans le matériau en suivant les chemins de moindre résistance. On observe que le phénomène d'endommagement initial coïncide avec la première non-linéarité de la courbe contrainte-déformation, qui correspond à la décohésion fibre/matrice aux interfaces des pores. Il en résulte la propagation de microfissures entre les pores dans la direction de la contrainte appliquée, ce résultat a été confirmé par SHIRINBAYAN et al. pour un composite stratifié.

Au fur et à mesure que la contrainte appliquée augmente, ce mécanisme d'endommagement se propage de manière diffuse dans toute la zone d'observation, en prenant naissance à plusieurs endroits des pores. Dans le même temps, les microfissures existantes continuent de se développer. Au niveau de contrainte maximale,

la déformation locale par cisaillement autour des faisceaux de fibres devient significative. Cela entraîne une déformation des fibres autour des faisceaux, ce qui se traduit par un pseudo-délaminage à proximité de la rupture.

Les seuils et la cinétique des mécanismes d'endommagement dans les composites ±θ dépendent de plusieurs facteurs : l'orientation spécifique des fibres dans chaque couche, l'état de contrainte subi par chaque couche (fonction de la séquence d'empilement et de la charge macroscopique), la variation statistique de la distribution spatiale des pores (qui diffère selon l'orientation des fibres) et la vitesse à laquelle la contrainte est appliquée (les seuils de contrainte augmentant avec la vitesse de la contrainte). Lors d'un essai de traction, l'endommagement des structures composites à fibres longues se caractérise par différents comportements à différentes échelles. À l'échelle microscopique, l'initiation des fissures dans les porosités contribue de manière significative à l'endommagement du matériau, y compris la décohésion fibre/matrice aux interfaces et la rupture des fibres conduisant à la formation de nouvelles porosités (Figure 22).

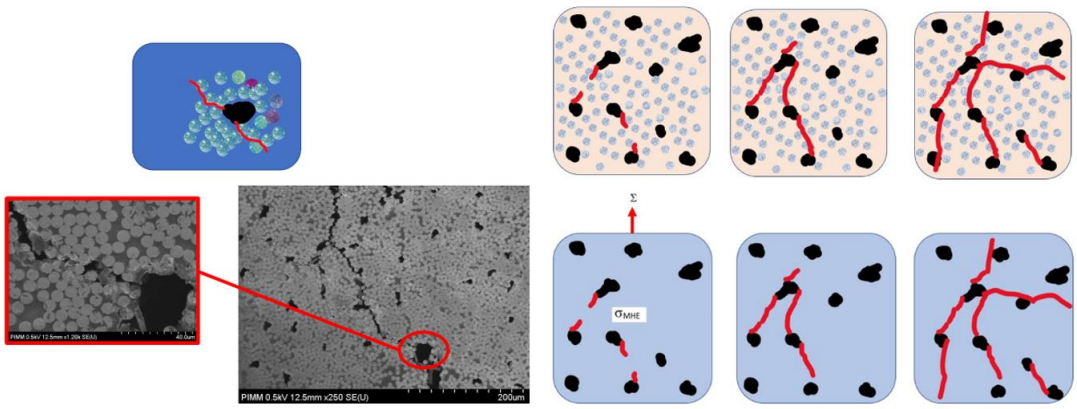

Figure 22. Schéma du scénario d'endommagement d'un composite époxy renforcé de fibres de carbone

À l'échelle mésoscopique, la coalescence de ces décohésions microscopiques forme des fissures transversales qui s'étendent sur toute l'épaisseur du pli, les extrémités de ces fissures agissant comme des sites de micro-délamination, conduisant à la délamination entre les plis. Cette interaction complexe de multiples mécanismes d'endommagement dans les composites épais et hétérogènes met en évidence le besoin de modèles robustes pour prédire leur performance sous charge [2].

4.5. Analyse du comportement en fatigue : effet de la distribution de l'orientation des fibres

La Figure 23 montre les courbes de Wöhler dérivées des essais de fatigue en traction-tension à une fréquence de 10 Hz pour des échantillons avec des orientations de fibres de ±15°, ±30° et des configurations multicouches. Ces courbes montrent l'influence significative de la distribution de l'orientation des fibres sur le comportement en fatigue. La configuration ±15° présente une résistance à la fatigue supérieure à celle des autres configurations. Les configurations ±30° et multicouche présentent des points de données qui se chevauchent, ce qui indique un comportement à la fatigue similaire.

Les données montrent qu'une contrainte appliquée d'environ 120 MPa entraîne une durée de vie en fatigue d'environ 103 cycles pour les échantillons à ±30° et à orientation mixte. Inversement, une contrainte appliquée d'environ 90 MPa prolonge la durée de vie en fatigue à environ 105 cycles. Cela indique qu'une réduction de 33 % de la contrainte appliquée peut se traduire par une durée de vie en fatigue 100 fois plus longue. Les résultats mettent en évidence le rôle critique de l'orientation des fibres dans la détermination de la résistance à la fatigue. En particulier, l'orientation des fibres peut être optimisée pour améliorer la résistance à la fatigue du matériau. Pour des applications pratiques telles que les réservoirs d'hydrogène, cela signifie que l'ajustement de l'orientation des fibres peut améliorer de manière significative la résistance à la fatigue sans compromettre de manière significative les propriétés transversales du matériau. En conclusion, la résistance à la fatigue des composites renforcés de fibres est très sensible à la distribution de l'orientation des fibres. En modifiant stratégiquement l'orientation des fibres, il est possible d'optimiser la conception de la fatigue et d'améliorer la durabilité des structures soumises à des charges cycliques [3].

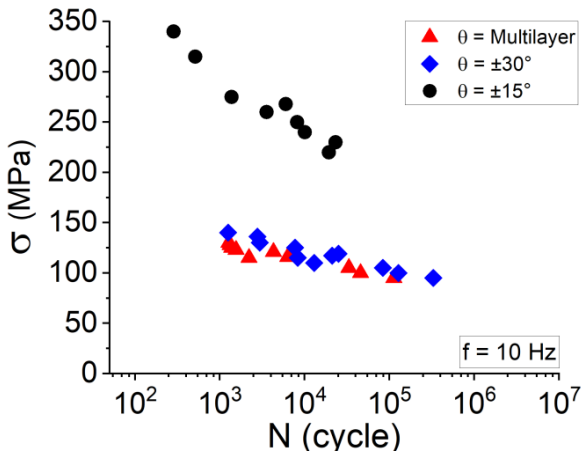

Figure 23. Courbes de Wöhler pour les échantillons chargés à 10 Hz

4.6. Analyse multi-échelle des dommages dus à la fatigue

4.6.1. Évolution macroscopique de l'endommagement

Les mécanismes d'endommagement dans les éprouvettes avec différentes orientations angulaires des fibres sont illustrés dans la Figure 24. Les courbes montrent l'existence de différentes cinétiques d'endommagement pour différentes orientations des fibres. Bien que les modèles d'endommagement macroscopiques restent cohérents pour une orientation de fibre donnée à différents niveaux de contrainte, le nombre de cycles jusqu'à la rupture diminue à mesure que l'amplitude de la contrainte augmente. Cette observation est importante dans le contexte de la compréhension du comportement en fatigue des composites.

Pour toutes les orientations testées, les courbes montrent trois stades distincts d'évolution des dommages. Le premier stade est caractérisé par une constance linéaire de l'endommagement. Le deuxième stade est caractérisé par une augmentation lente de l'endommagement. Le troisième stade est caractérisé par une augmentation rapide de l'endommagement. Une forte diminution de la rigidité conduit finalement à la rupture. Ces étapes servent à élucider la cinétique de la progression des dommages, permettant ainsi d'affiner les modèles micromécaniques dans le but de prédire la durée de vie et le comportement en fatigue des matériaux composites. La Figure 24 illustre l'évolution du module d'élasticité relatif (E/E_0) au cours d'essais de fatigue en traction-tension à 10 Hz.

Dans le cas d'une charge de grande amplitude, le E/E_0 diminue rapidement dans un régime logarithmique linéaire jusqu'au point de rupture. Ce processus s'accompagne d'une quantité importante de dommages précoces dans le stratifié, en particulier aux interfaces entre les différentes couches. Ces défaillances sont principalement de nature interfaciale et se manifestent par une délamination et un décollement des fibres et de la matrice. En revanche, le module diminue plus graduellement lorsque l'amplitude de la charge est plus faible. Cela se caractérise par une diminution initiale rapide due à l'accumulation précoce de dommages, une diminution progressive plus lente et une diminution finale brutale avant la rupture catastrophique. Cette diminution progressive est principalement contrôlée par les interactions matrice-fibre, y compris la fissuration de la matrice [3].

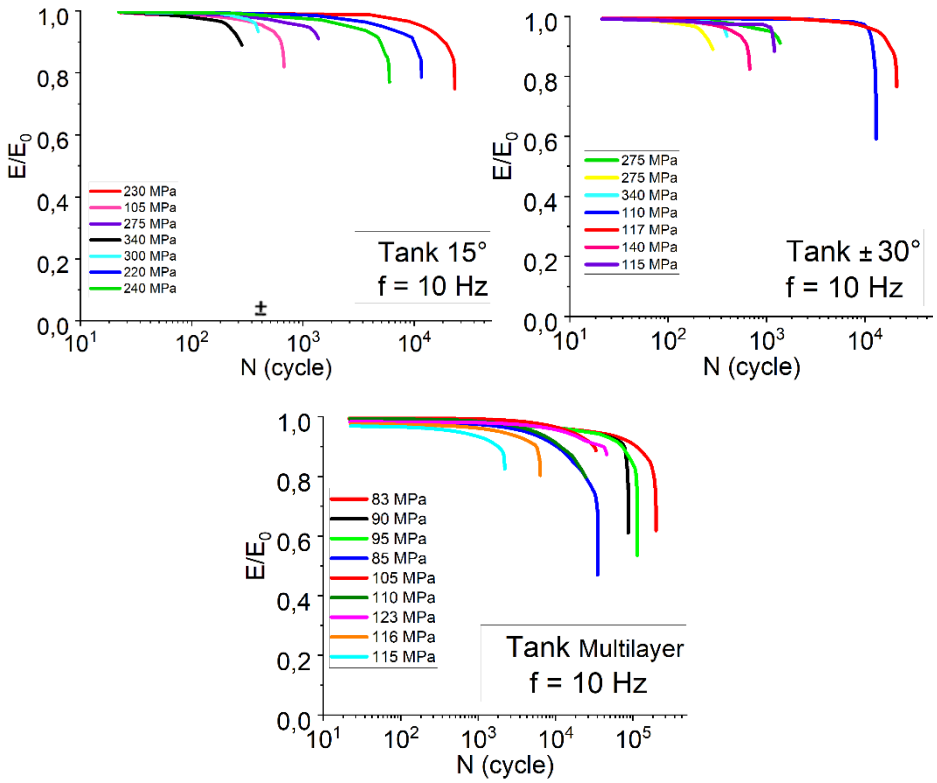

Figure 24. Évolution du module d'Young relatif (E/E_0) au cours des essais de fatigue :

(a) Réservoir ±15°, (b) Réservoir ±30° et (c) Réservoir multicouche.

L'orientation des fibres dans le stratifié a un effet significatif sur le comportement en fatigue, l'orientation ±15° conduisant à une quantité importante de dommages précoces et à une diminution rapide du module, tandis que les orientations ±30° et multicouches montrent un taux de dégradation plus lent et une gamme de comportements de rupture (Figure 25). Il est donc très important de comprendre ces évolutions si nous voulons développer et valider des modèles micromécaniques qui nous permettront de prédire la durée de vie en fatigue et l'évolution des dommages dans les composites stratifiés. Ces connaissances permettront d'optimiser la conception des stratifiés en ajustant l'orientation des fibres et en améliorant les propriétés interfaciales, améliorant ainsi la résistance à la fatigue, les performances mécaniques, la durabilité et la fiabilité des structures composites dans les applications à forte charge [3].

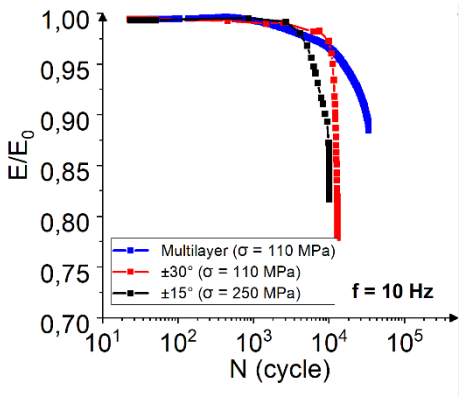

Figure 25. Évolution du module d'Young relatif (E/E0) au cours des essais de fatigue

4.6.2. Évolution de l'endommagement au niveau microscopique

Pour suivre la progression de l'endommagement au niveau microstructural pendant les essais de fatigue, des essais de fatigue interrompus ont été menés conjointement avec des observations de la microstructure pour différentes orientations angulaires. L'analyse microscopique a été effectuée sur une zone d'observation de 5×10 mm², chaque cycle étant examiné individuellement au fur et à mesure que le nombre de cycles augmentait. La Figure 26 montre les résultats pour les échantillons soumis à une amplitude de contrainte appliquée de 250 MPa pour l'orientation ±15° à une fréquence de 10 Hz.

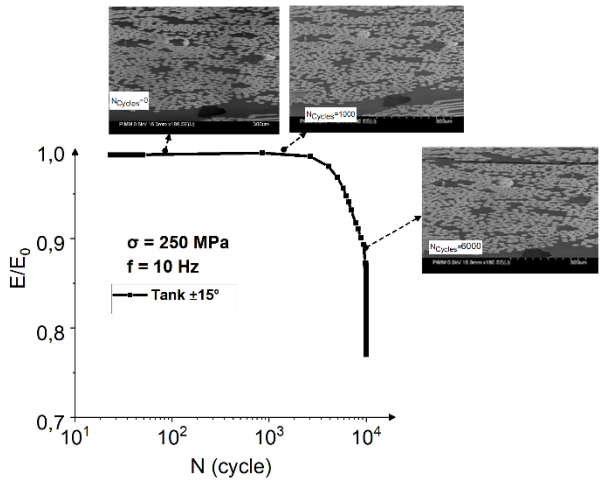

Figure 26. Essai de fatigue interrompu couplé à des observations de la microstructure pour l'orientation ±15°

La Figure 27 montre l'évolution de l'endommagement par fatigue microscopique du composite orienté à ±15° sous charge. La configuration ±15° présente un comportement élastique linéaire sans aucune indication

d'endommagement jusqu'à 300 MPa (voir Figure 18). Une fois ce seuil dépassé, l'accumulation des dommages commence, ce qui entraîne un comportement non linéaire et finalement la rupture. La phase initiale est définie par une augmentation linéaire de l'endommagement. Il convient de noter que la formation initiale de dommages, qui se manifeste par une fissuration de la matrice et un décollement des fibres de la matrice, était évidente dans les échantillons orientés à ±15°. Ce dommage est apparu très tôt, en particulier dans ces échantillons. Au fur et à mesure que le nombre de cycles augmentait, l'endommagement de la matrice et de l'interface fibre-matrice s'aggravait, conduisant à la délamination (voir Figure 27).

Dans les microstructures des configurations ±15°, ±30° et multicouches, les composites présentent initialement des pores ou des vides, qui peuvent être attribués au processus de fabrication. Les pores susmentionnés sont répartis de manière aléatoire dans le matériau et présentent souvent des fibres qui s'étendent à leur surface. La distribution hétérogène de l'orientation des fibres à travers les couches entraîne une répartition inégale des contraintes lors des essais de fatigue. La présence de pores dans le matériau entraîne une amplification des contraintes de fatigue en raison de la disparité de rigidité entre la matrice et les régions poreuses, ce qui donne lieu à des concentrations de contraintes localisées. Au fur et à mesure que la contrainte appliquée augmente, les mécanismes d'endommagement se propagent dans toute la zone d'observation, en prenant naissance à plusieurs endroits des pores. Parallèlement, les microfissures existantes continuent de s'étendre. Aux niveaux de contrainte les plus élevés, une déformation locale importante se produit par cisaillement autour des faisceaux de fibres, ce qui entraîne une pseudo-délamination à proximité des zones de rupture.

Tube ±15°	
Stade initial : $N_{Cycle} = 0$, $\sigma = 250$ MPa	**Mécanismes d'endommagement**
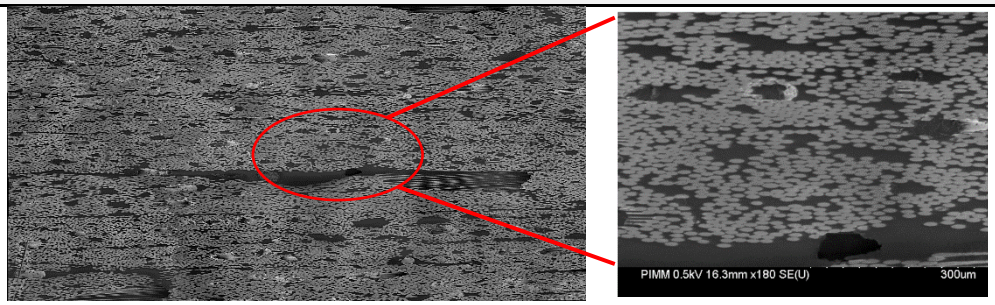	Pas d'endommagement

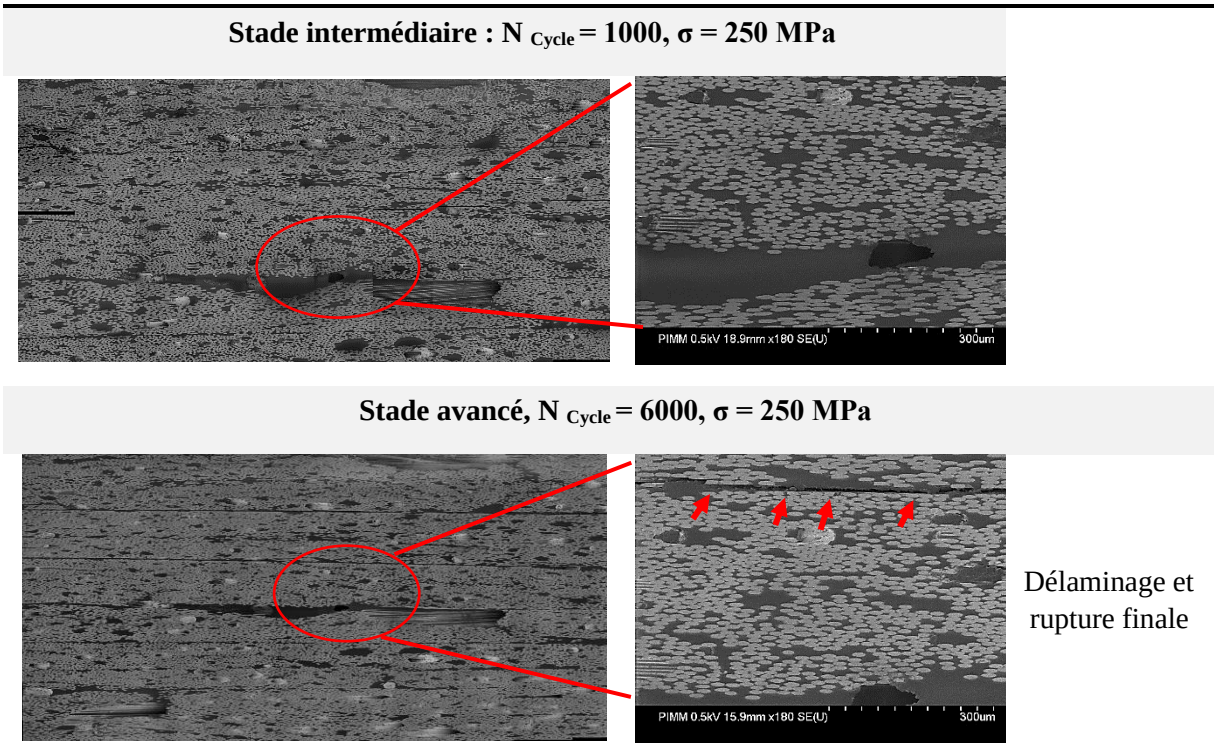

Figure 27. Essai de fatigue interrompu et mécanismes d'endommagement : configuration ±15°

Les Figures 28 et 29 présentent des essais de fatigue expérimentaux couplés à des observations de la microstructure pour la configuration ±30°, analysés à différents stades du cycle : initial, intermédiaire et final. Au stade initial, le matériau présente un comportement élastique linéaire sans dommage visible, comme le montre l'image MEB intitulée ‘Stade initial’ (Figure 29).

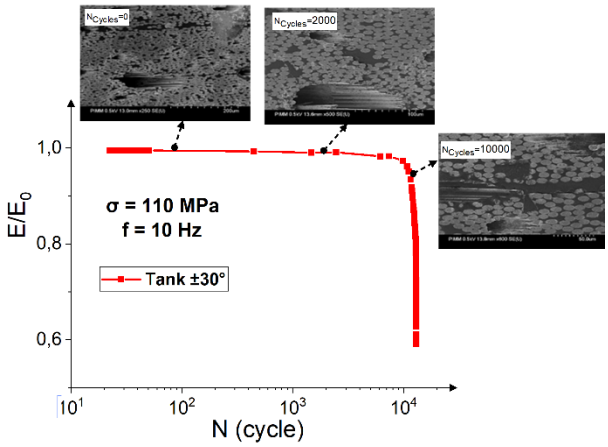

Figure 28. Essai de fatigue interrompu couplé à des observations de la microstructure pour un angle de ±30°

Le mécanisme d'endommagement initial observé est la décohésion à l'interface fibre-matrice. Au fur et à mesure que le nombre de cycles augmente jusqu'à environ 2×10^3 cycles, les dommages continuent à s'accumuler à un rythme modéré. Au cours de cette phase intermédiaire, le matériau présente des signes d'endommagement, comme le montre l'image MEB montrant le début de la décohésion à l'interface fibre-matrice, la microfissuration et la fracture ultérieure de la matrice. L'image MEB désignée ‘Stade final’ (environ 10^4 cycles) illustre la présence de fissures étendues et de dommages importants, qui conduisent finalement à la délamination et à la rupture complète du matériau. Les phénomènes responsables de ces dommages comprennent la décohésion initiale à l'interface fibre-matrice, la microfissuration dans la matrice, la progression vers la fracture de la matrice et le développement de grandes fissures entraînant la délamination. Cette progression des dommages permet de mettre en évidence les étapes critiques de la rupture par fatigue dans les composites renforcés de fibres et de souligner l'importance de comprendre ces mécanismes afin d'améliorer la conception des matériaux et leur résistance à la fatigue [3].

Tube ±30°	
Stage initial: $N_{Cycle} = 0$, $\sigma = 110$ MPa	**Mécanisme d'endommagement**
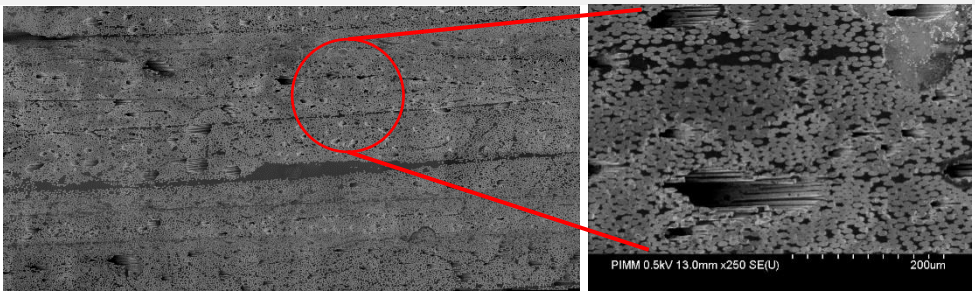	Pas d’endommagement
Stade intermédiaire : $N_{Cycle} = 2000$, $\sigma = 110$ MPa	
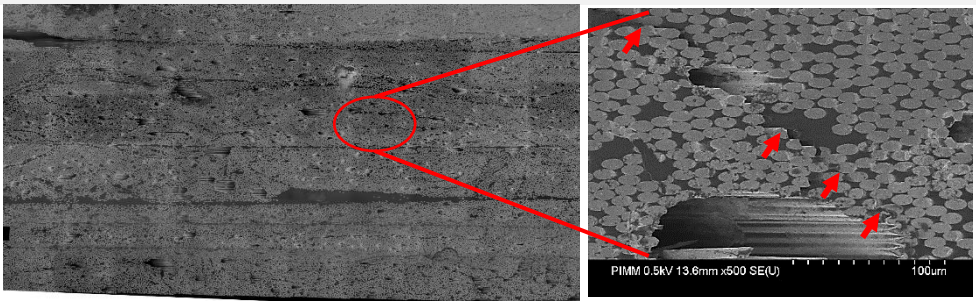	Décohésion à l'interface fibre-matrice, Endommagement de la matrice
Stade avancé, $N_{Cycle} = 10000$, $\sigma = 110$ MPa	

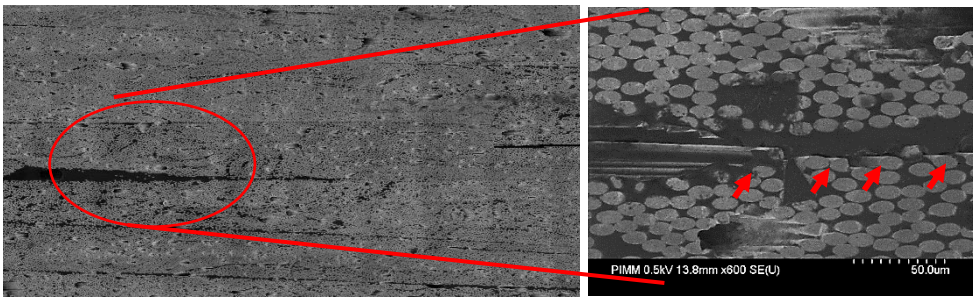

Délaminage et rupture finale

Figure 29. Mécanismes d'endommagement microscopiques : configuration ±30

Les figures 30 et 31 présentent les résultats pour une configuration multicouche. Le même scénario d'endommagement est observé pour cette configuration composite, à savoir que les mécanismes d'endommagement se propagent à partir de plusieurs emplacements de pores. On peut noter que la propagation de l'endommagement se produit au niveau des couches à ±86° du composite multicouche (Figure 31).

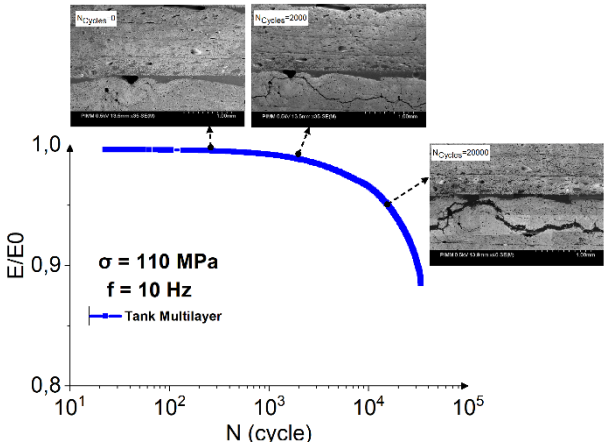

Figure 30. Essai de fatigue interrompu couplé aux observations de la microstructure pour la configuration multicouche

En effet, les seuils et la cinétique des mécanismes d'endommagement dans les composites ±θ dépendent d'un certain nombre de facteurs, notamment l'orientation spécifique des fibres dans chaque couche, l'état de contrainte subi par chaque couche (qui est influencé par la séquence d'empilement et la charge macroscopique), la variation statistique de la distribution spatiale des pores (qui varie avec l'orientation des fibres) et la vitesse à laquelle la contrainte est appliquée (les seuils de contrainte augmentant avec la vitesse de la contrainte). Au cours des essais de fatigue, l'endommagement des structures composites à fibres longues se manifeste d'une manière qui varie en fonction de l'échelle considérée. Au niveau microscopique, l'initiation de fissures dans

les porosités joue un rôle important dans l'endommagement du matériau, y compris la séparation des fibres et des matrices aux interfaces et la rupture des fibres, qui entraîne à son tour la formation de nouvelles porosités.

Il est essentiel de comprendre l'importance de ces dommages microscopiques afin de mieux appréhender les premières étapes de la rupture des composites. Ils servent à établir les conditions qui facilitent la propagation des dommages, ce qui est un facteur clé dans l'évaluation globale de la résilience du matériau. À l'échelle mésoscopique, la coalescence de ces décohésions microscopiques entraîne la formation de fissures transversales qui s'étendent sur toute l'épaisseur du pli (voir les Figures 27, 29 et 31).

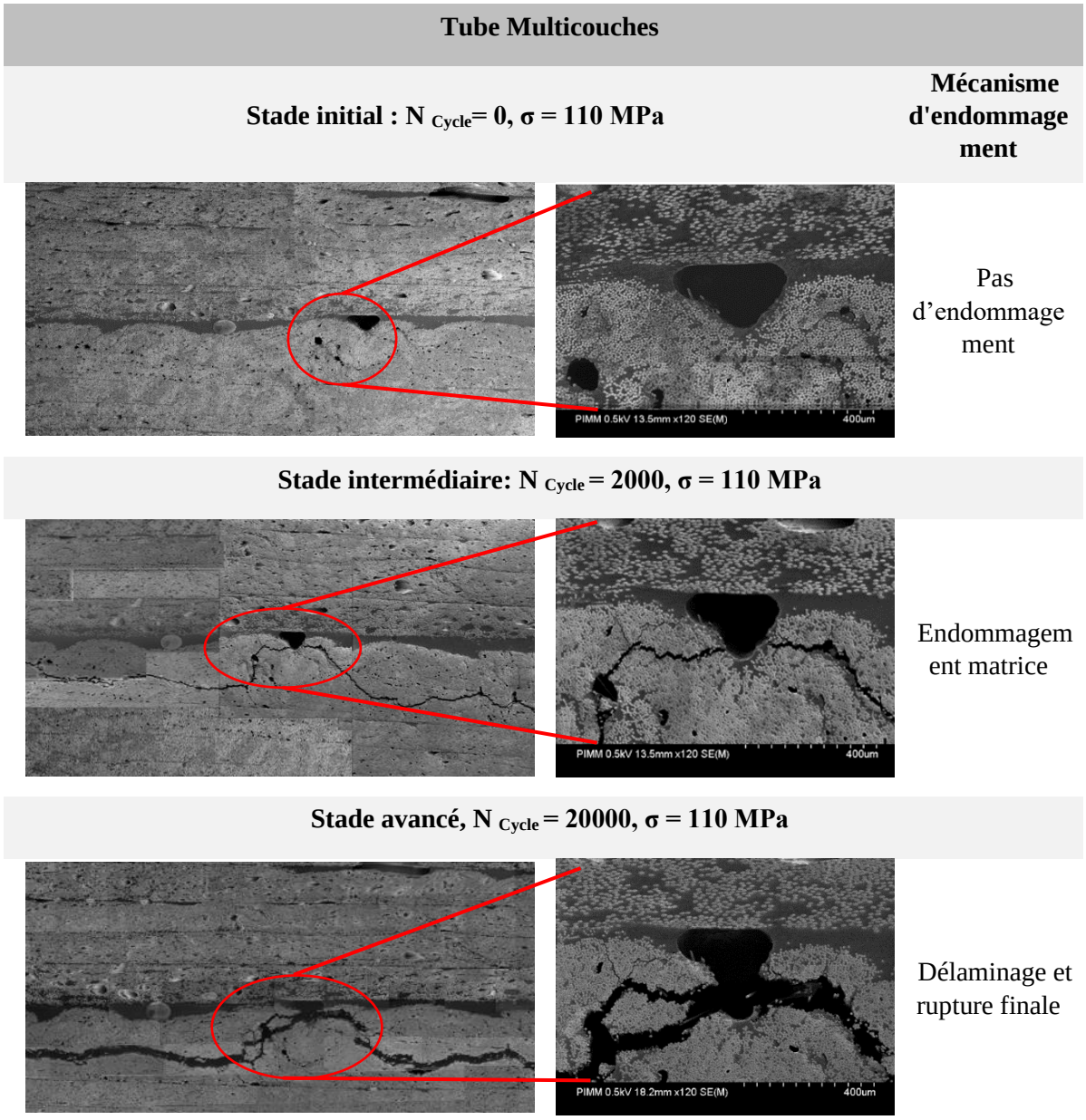

Figure 31. Mécanismes d'endommagement microscopiques : configuration multicouche

Les extrémités de ces fissures transversales deviennent des sites de micro-délamination, qui peuvent ensuite évoluer vers une délamination entre les plis. Il est donc clair que ce dommage mésoscopique représente un facteur critique dans l'intégrité structurelle globale du composite, car il a un impact direct sur la capacité de charge et la durabilité du matériau. L'interaction complexe de multiples mécanismes d'endommagement dans les composites épais et hétérogènes nécessite le développement de modèles robustes pour prédire avec précision leur performance sous charge. Il est essentiel que ces modèles prennent en compte les différentes échelles d'endommagement, de l'initiation microscopique des fissures à la propagation mésoscopique des fissures et à la délamination. Il est essentiel de comprendre ces interactions pour pouvoir concevoir des composites plus durables et plus résistants à la rupture dans des conditions de charge cyclique. En conclusion, l'orientation spécifique des fibres, l'état de contrainte, la distribution des pores et le taux de contrainte ont tous un impact significatif sur les mécanismes d'endommagement des composites $\pm\theta$. Au niveau microscopique, les principaux mécanismes d'endommagement sont l'initiation de fissures dans les porosités et la décohésion fibre/matrice. Au niveau mésoscopique, la coalescence des dommages microscopiques conduit à la fissuration transversale et à la délamination. Ces résultats soulignent l'importance de l'analyse multi-échelle pour comprendre et anticiper le comportement des composites époxy renforcés par des fibres de carbone sous charge cyclique [3].

4.6.3. Fractographique

La Figure 32 présente l'analyse fractographique d'échantillons de tubes ayant subi des essais de fatigue. Comme indiqué précédemment, le dommage initial observé dans ces échantillons est la séparation des fibres de la matrice. Au fur et à mesure que le processus de fatigue se poursuit, il peut en résulter une rupture des fibres.

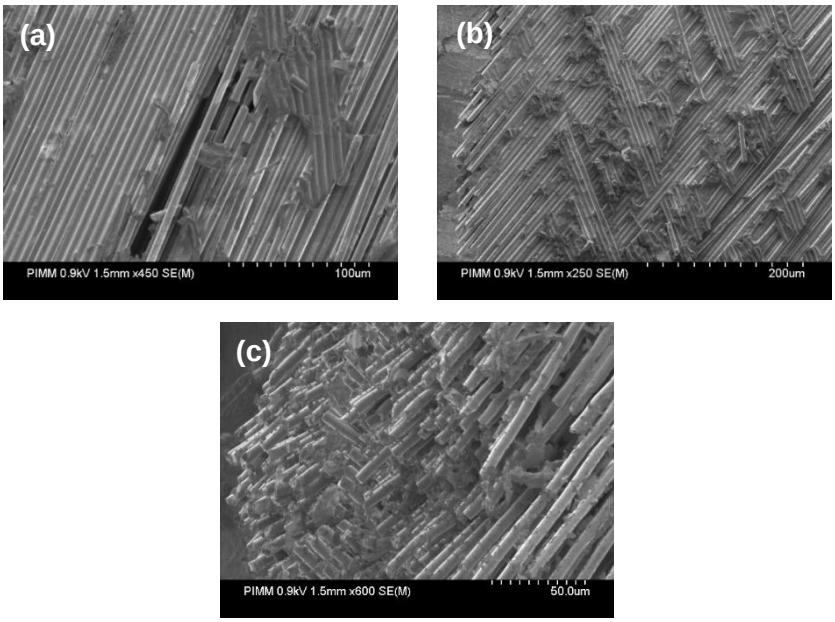

Figure 32. Micrographie de la surface de rupture par fatigue :

(a) Réservoir ±15°, (b), Réservoir ±30° et (c) Réservoir multicouche

La fractographie du composite multicouche fibre de carbone-époxy révèle des caractéristiques de rupture typiques, notamment la rupture des fibres, la fissuration de la matrice, l'arrachement des fibres et la délamination potentielle. Ces caractéristiques démontrent l'importance critique de l'adhésion fibre-matrice et le rôle des vides dans l'intégrité structurelle du matériau composite [3].

4.7. Comportement en traction à vitesse de déformation élevée

La Figure 33 illustre les courbes contrainte-déformation d'éprouvettes d'époxy renforcé de fibres de carbone soumises à des essais de traction à vitesse de déformation élevée jusqu'à la rupture. Les échantillons ont été orientés selon différents angles, notamment ±15°, ±30° et des configurations multicouches. Les essais ont été réalisés à différents taux de déformation, à savoir 100 s^{-1}, 1s^{-1}, 0,1s^{-1} et quasi-statique. Les essais de traction à taux de déformation élevé sur des échantillons d'époxy renforcé de fibres de carbone orientés à ±15°, ±30° et en configurations multicouches fournissent des informations cruciales sur le comportement du matériau dans des conditions de charge dynamique. Les essais, réalisés à différentes vitesses de déformation (100 s^{-1}, 1 s^{-1}, 0,1 s^{-1} et quasi-statique), démontrent une sensibilité notable à la vitesse de déformation. Il a été observé que des vitesses de déformation plus élevées entraînaient systématiquement une augmentation des niveaux de contrainte et une réduction de la ductilité dans toutes les orientations. Par exemple, les échantillons

à ±15° présentent les niveaux de contrainte les plus élevés, atteignant environ 480 MPa à 100 s-1, avec des niveaux de contrainte notables à des taux plus faibles (environ 430 MPa à 1 s^{-1} et 400 MPa à 0,1 s^{-1}), tandis que les essais quasi-statiques atteignent environ 350 MPa. De même, l'orientation ±30° présente des valeurs de contrainte maximales d'environ 300 MPa à 100 s^{-1}, qui diminuent à 235 MPa et 225 MPa à 1 s^{-1} et 0,1 s^{-1}, respectivement. Les essais quasi-statiques atteignent un pic d'environ 200 MPa. La configuration multicouche, bien que présentant des valeurs de contraintes globales plus faibles, montre une tendance similaire, avec des pics de contraintes de 210 MPa pour 100 s^{-1}, 175 MPa pour 1 s^{-1} et 140 MPa pour 0,1 s^{-1}, les essais quasi-statiques atteignant environ 130 MPa.

Ces résultats soulignent l'amélioration de la résilience du matériau en réponse à une charge rapide, qui peut être attribuée aux caractéristiques viscoélastiques de la matrice époxy, qui offre une résistance accrue à des taux de déformation plus élevés. Cependant, on observe que la ductilité diminue avec l'augmentation de la vitesse de déformation, comme l'indique la réduction de la durée de déformation jusqu'à la rupture. L'écart entre les comportements de contrainte et de déformation selon les différentes orientations indique la présence de mécanismes d'endommagement disparates. À des taux de déformation élevés, des ruptures de la matrice et de l'interface fibre-matrice sont probables, alors qu'à des taux plus faibles, la rupture des fibres et la fissuration de la matrice sont plus probables. L'orientation des fibres exerce également une influence déterminante, les orientations ±15° et ±30° ayant démontré des performances supérieures à celles de la structure multicouche, en raison d'un meilleur transfert des charges et de la réduction des faiblesses entre les couches. Ces résultats sont essentiels pour l'optimisation des conceptions de composites pour les applications qui nécessitent des performances élevées dans des conditions dynamiques et soulignent la nécessité d'une prise en compte méticuleuse des effets de la vitesse de déformation et de l'orientation des fibres dans les applications d'ingénierie. La Figure 33 présente une analyse complète du comportement en traction et des surfaces de rupture des composites époxy renforcés de fibres de carbone avec différentes orientations de fibres (c'est-à-dire ±15°, ±30° et multicouches) dans des conditions de chargement quasi-statiques (QS) et à taux de déformation élevé (100 s^{-1}). Les courbes contrainte-déformation montrent que les valeurs de contrainte les plus élevées sont observées au taux de déformation le plus élevé (100 s^{-1}), avec des augmentations de 37 %, 50 % et 62 % pour les configurations ±15°, ±30° et multicouche, respectivement, par rapport à la charge quasi-

statique. Les courbes de taux de déformation élevé présentent un déclin précipité après le pic, ce qui indique un comportement de rupture fragile. Une analyse microscopique des surfaces de rupture indique que sous une charge quasi-statique, les surfaces de rupture pour toutes les orientations présentent une combinaison d'arrachement de fibres et de fissuration de la matrice, suggérant une rupture à mode mixte. À $100s^{-1}$, les surfaces de rupture sont caractérisées par une rupture importante des fibres et moins d'arrachement de fibres, ce qui indique un mode de rupture plus fragile. L'orientation ±15° présente la résistance la plus élevée, suivie par l'orientation ±30°, la configuration multicouche présentant la résistance la plus faible mais une ductilité plus élevée sous charge QS. La transition du mode de rupture ductile au mode de rupture fragile est plus prononcée à des taux de déformation plus élevés dans toutes les orientations, en raison des conditions de chargement rapide. Ces observations mettent en évidence la sensibilité significative à la vitesse de déformation et l'influence de l'orientation des fibres sur les propriétés de traction et les mécanismes de rupture, des vitesses de déformation plus élevées entraînant une augmentation de la résistance mais une réduction de la ductilité.

Cette analyse est cruciale pour la conception et l'optimisation des matériaux composites pour les applications de chargement dynamique, assurant un équilibre entre la résistance, la rigidité et la ténacité à la rupture sur la base d'exigences de performance spécifiques [4].

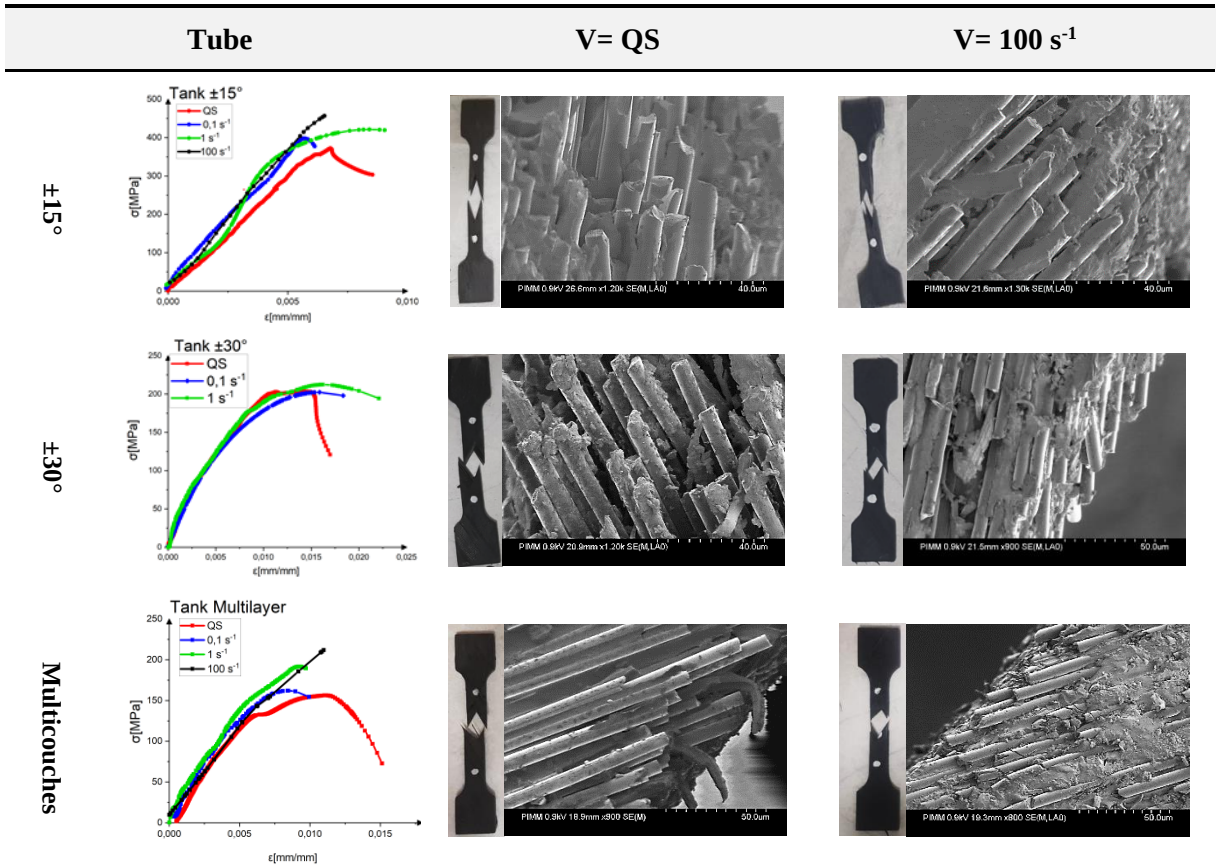

Figure 33. Courbes de traction à taux de déformation élevé : impact de l'orientation et du taux de déformation sur les surfaces de rupture

4.8. Effets de la vitesse de déformation sur la réponse globale à la traction

Les figures 34 et 35 montrent l'impact de la vitesse de déformation sur la réponse à la traction des composites époxy renforcés de fibres de carbone avec différentes orientations de fibres, à savoir ±15°, ±30° et multicouches. Les données, présentées à travers une variété de mesures, y compris le module de Young, la contrainte de seuil, la contrainte ultime, la déformation de seuil et la déformation ultime, offrent des indications significatives. La variation du module d'Young en fonction de la vitesse de déformation dépend de l'orientation de la fibre. L'orientation ±15° présente généralement les valeurs les plus élevées, ce qui indique une plus grande rigidité, tandis que la configuration multicouche présente des valeurs de module plus faibles, ce qui suggère une moins grande rigidité. À des taux de déformation plus élevés ($\geq$0,1s^{-1}), une augmentation du module est observée pour toutes les orientations, indiquant un raidissement dépendant du taux de déformation. La contrainte de seuil augmente avec la vitesse de déformation pour toutes les orientations, les orientations ±15° et ±30° présentant des valeurs plus élevées que la configuration multicouche. En outre, la contrainte ultime

augmente avec la vitesse de déformation, l'orientation ±15° présentant les valeurs les plus élevées, suivie par l'orientation ±30°, et la configuration multicouche présentant les valeurs les plus faibles. La déformation au seuil présente une variation moins importante avec la vitesse de déformation, l'orientation ±30° affichant des valeurs légèrement plus élevées à des vitesses plus faibles, ce qui indique un début d'endommagement plus précoce. La vitesse de déformation ultime diminue avec l'augmentation de la vitesse de déformation pour toutes les orientations, la configuration multicouche affichant les valeurs les plus élevées, ce qui indique une plus grande ductilité par rapport aux orientations ±15° et ±30°. La réduction de la déformation ultime à des taux plus élevés indique une augmentation de la fragilité. Ces résultats soulignent la sensibilité considérable des propriétés de traction à la vitesse de déformation, les vitesses élevées entraînant une augmentation de la rigidité et de la résistance, mais une diminution de la ductilité. L'orientation ±15° présente des propriétés toujours supérieures à celles de l'orientation ±30° et des configurations multicouches qui, malgré une diminution de la résistance et de la rigidité, présentent une ductilité accrue. La variation du seuil et des déformations ultimes suggère des mécanismes d'endommagement disparates selon les orientations et les taux de déformation, les taux élevés conduisant probablement à la fissuration de la matrice et au décollement des fibres de la matrice [4].

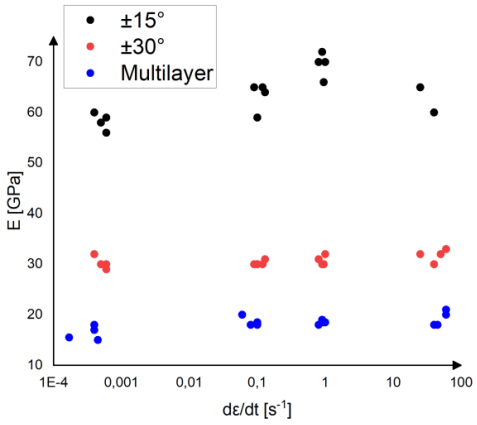

Figure 34. Évolution du module d'Young en fonction de la vitesse de déformation

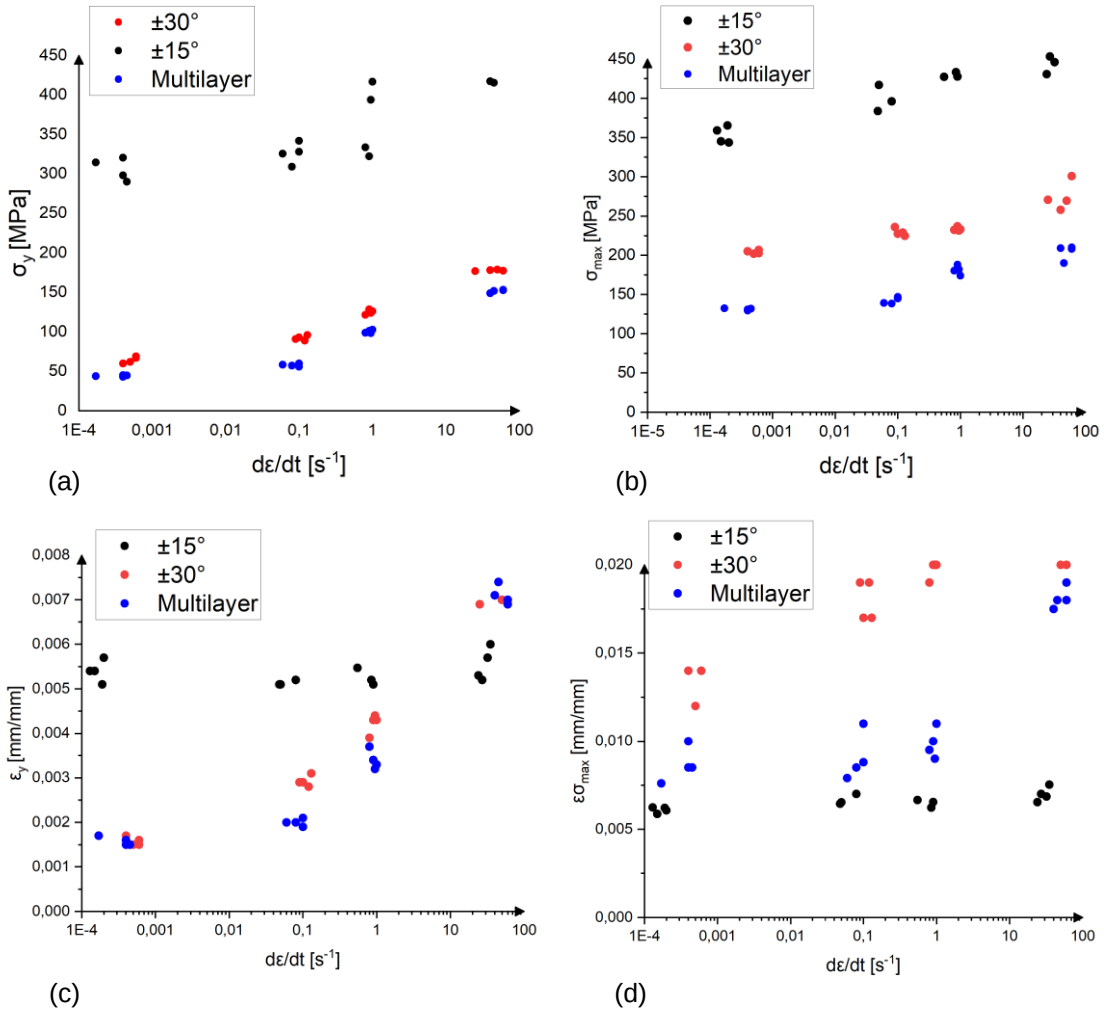

Figure 35. Influence de la vitesse de déformation sur : (a) la contrainte de seuil, (b) la contrainte de rupture, (c) la déformation au seuil et (d) la déformation à la limite.

4.9. Étude qualitative des mécanismes d'endommagement

La figure 36 illustre les résultats d'un essai de traction dynamique interrompu (IDTT) sur un composite époxy multicouche renforcé de fibres de carbone, démontrant les mécanismes d'endommagement progressifs à un niveau microscopique et la perte de rigidité correspondante due à l'endommagement, avec une vitesse de déformation de 1s-1. La courbe contrainte-déformation présente initialement une région élastique linéaire, indiquant une augmentation constante de la contrainte avec la déformation. Cependant, au fur et à mesure que la déformation progresse, la courbe s'écarte de la linéarité, mettant ainsi en évidence l'apparition de mécanismes d'endommagement. La micrographie de l'étape initiale montre l'émergence d'un endommagement précoce de la matrice, caractérisé par la formation de microfissures et de vides. Cependant, la courbe reste linéaire, ce qui indique que l'impact sur la rigidité est minime. Au stade intermédiaire (σ = 90 MPa), la

micrographie illustre une progression de l'endommagement de la matrice et l'apparition d'un délaminage, ce qui entraîne une déviation de la courbe contrainte-déformation et indique une réduction de la rigidité .

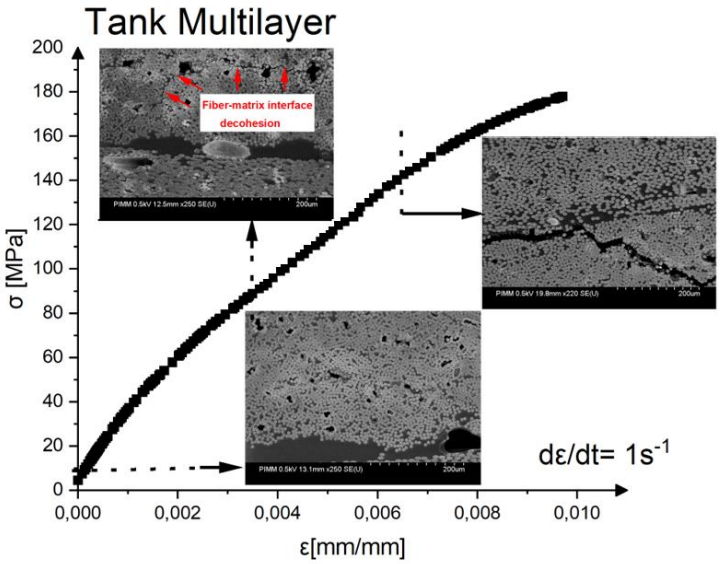

Figure 36. Mécanismes d'endommagement microscopiques : configuration multicouche

Au stade avancé de l'endommagement (σ = 140 MPa), la micrographie montre un endommagement important de la matrice et une délamination notable, avec des fissures plus grandes compromettant l'interface fibre/matrice. Il en résulte une réduction considérable de la pente de la courbe contrainte-déformation et une perte significative de rigidité. Les principaux mécanismes d'endommagement comprennent la fissuration de la matrice, la délamination et le décollement fibre/matrice, qui commencent à de faibles déformations et s'aggravent progressivement, entraînant une dégradation cumulative de la rigidité et une perte d'intégrité structurelle. Au fur et à mesure que les dommages s'accumulent, le comportement élastique initial du composite se transforme en une réponse non linéaire, ce qui met en évidence la sensibilité de ces mécanismes à la vitesse de déformation. Cette IDTT démontre efficacement comment les dommages initiaux de la matrice conduisent à la délamination et à la fissuration ultérieure, ce qui réduit de manière significative la capacité de charge du composite. Cela souligne l'importance de comprendre la cinétique de l'endommagement pour prédire la performance et la défaillance des composites dans des conditions de charge dynamique.

Les images fournies (Figure 30) illustrent la progression des dommages dans un réservoir en composite époxy multicouche renforcé de fibres de carbone à différents stades de la charge de traction. Les images sont

utilisées pour identifier et analyser les mécanismes d'endommagement qualitatifs à différents stades : initial, intermédiaire et final.

Dans la phase initiale (F = 0 N, $d\varepsilon/dt = 1s^{-1}$), le composite présente son état vierge en l'absence de force appliquée, affichant une surface largement intacte avec quelques défauts de surface mineurs ou porosités typiques du processus de fabrication. Ces porosités mineures indiquent des sites potentiels d'initiation de fissures lorsque le matériau est soumis à une charge, bien que la structure globale reste intacte, fournissant ainsi une base de comparaison pour les étapes ultérieures.

Tube Multicouches
Stade initial : F = 0 N, $d\varepsilon/dt = 1s^{-1}$
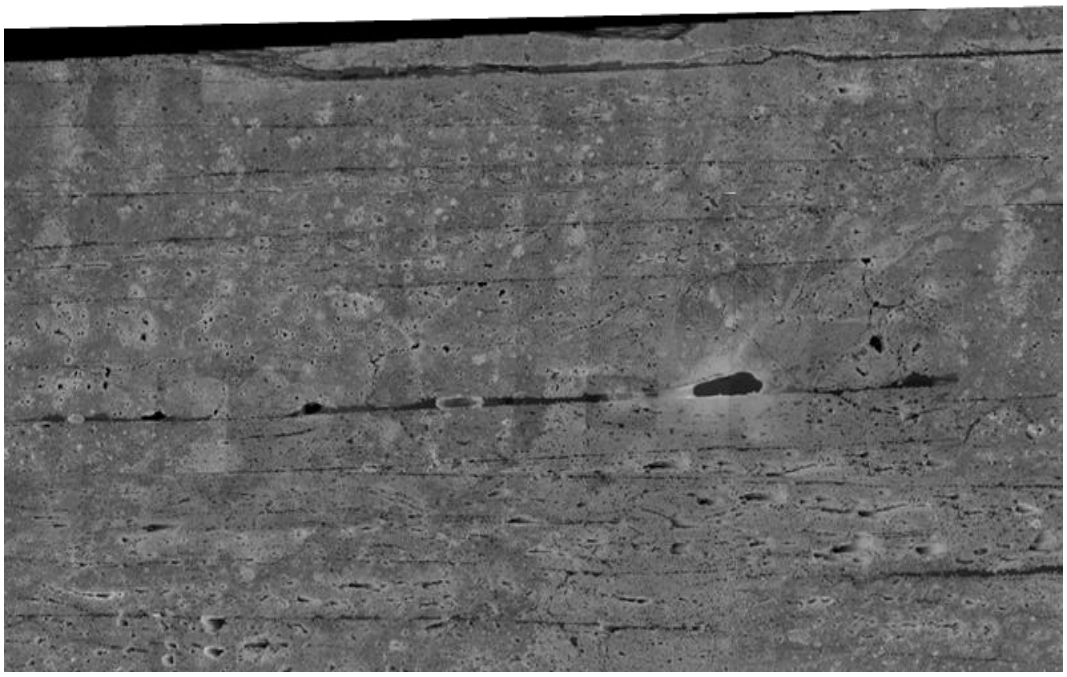
Stade intermédiaire : F = 4000 N , $d\varepsilon/dt = 1s^{-1}$

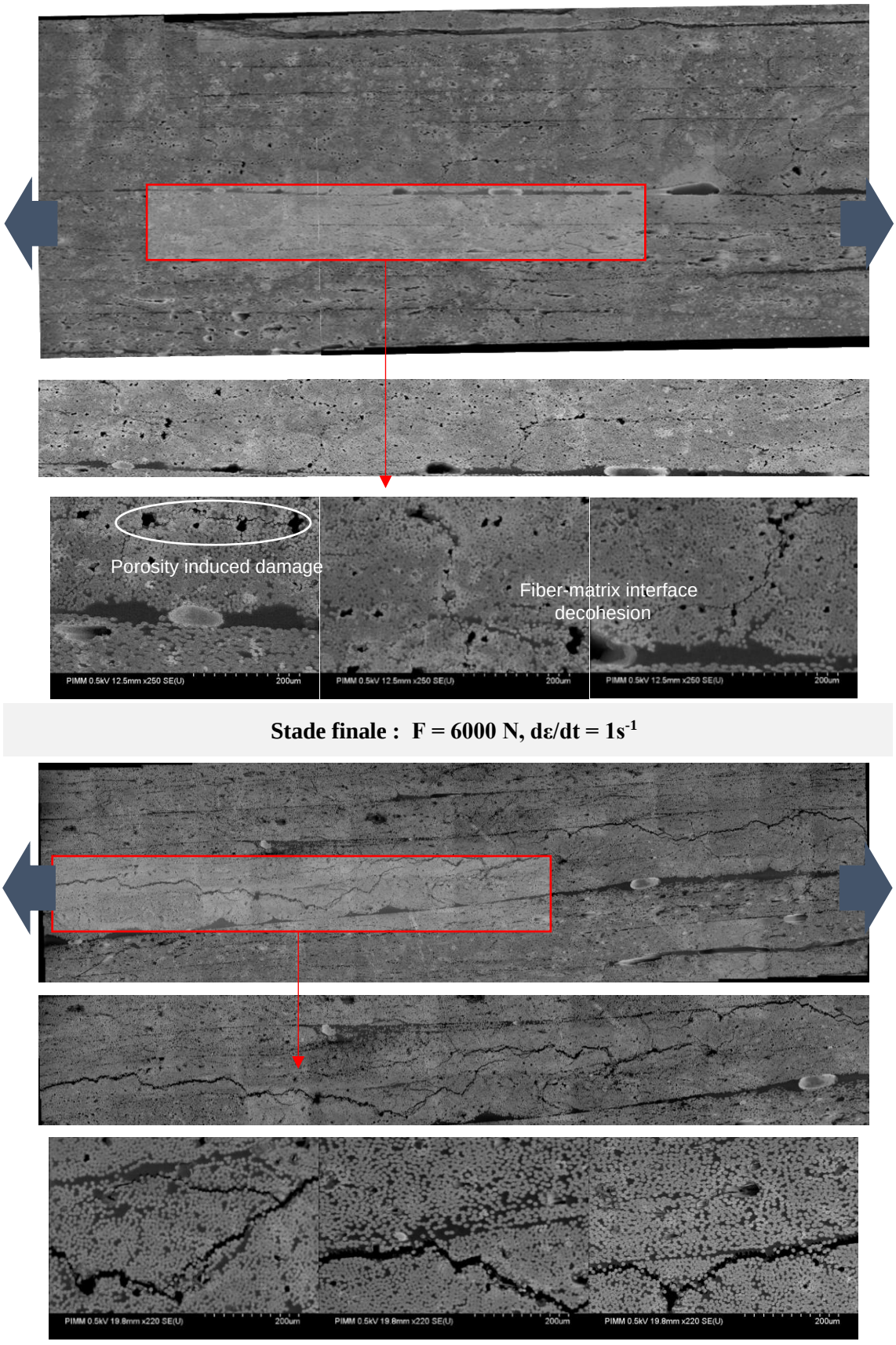

Stade finale : F = 6000 N, dε/dt = 1s^{-1}

Figure 37. Évolution de la microstructure et mécanismes d'endommagement pour la configuration multicouche

Au stade intermédiaire (F = 4000 N ou σ = 90 MPa), des fissures initiales (décohésion à l'interface fibre/matrice) apparaissent et se propagent à partir des porosités de surface à travers le matériau de la matrice, indiquant la présence de concentrations de contraintes internes autour des porosités et marquant le début de l'accumulation de dommages dans la structure composite. Les motifs linéaires et ramifiés des fissures indiquent la présence de composantes de contrainte de traction et de cisaillement, mettant ainsi en évidence l'existence de zones de liaison matrice-fibre plus faibles. Cette propagation entraîne une dégradation de la rigidité, observable dans la courbe contrainte-déformation sous la forme d'un écart par rapport à la linéarité. En outre, elle nuit à l'efficacité du transfert de charge entre les fibres et la matrice, créant des concentrations de contraintes localisées qui accélèrent l'endommagement. Au stade final (F = 6000 N ou σ = 140 MPa), des fissures étendues sont visibles dans l'ensemble du composite, les fissures augmentant de manière significative, se croisant et formant un réseau qui compromet l'intégrité du matériau, ce qui indique un degré élevé d'endommagement interne. Les fissures interconnectées indiquent une réduction de la capacité de charge, entraînant une défaillance macroscopique. Les mécanismes d'endommagement observés, notamment la fissuration de la matrice, le décollement fibre/matrice et la rupture potentielle des fibres, contribuent collectivement à la défaillance finale du matériau sous forte contrainte.

L'étude démontre que les dommages commencent au niveau des défauts ou des porosités préexistants et se propagent à travers la matrice. Les porosités agissent comme des concentrateurs de contraintes, facilitant l'apparition de fissures. Les principaux mécanismes de rupture observés sont le décollement fibre/matrice et la fissuration de la matrice, qui nuisent à l'efficacité avec laquelle les charges sont transférées entre les fibres et la matrice, réduisant ainsi la résistance globale du matériau et conduisant finalement à sa rupture. La vitesse de déformation constante ($d\varepsilon/dt = 1s^{-1}$) à tous les stades donne un aperçu de la réponse du matériau à la charge dynamique, soulignant ainsi l'importance de la vitesse de déformation dans la détermination des propriétés mécaniques des composites. L'étude qualitative des mécanismes d'endommagement du réservoir composite époxy multicouche renforcé de fibres de carbone sous charge de traction révèle des informations essentielles sur le comportement du matériau, soulignant l'importance de comprendre ces mécanismes pour améliorer les processus de fabrication des composites et accroître les performances et la durabilité du matériau dans les applications pratiques [4].

5. Conclusion générale et Perspectives

La sécurité dans l'industrie automobile est devenue un enjeu majeur pour les fabricants et les utilisateurs, surtout dans le secteur de la mobilité à hydrogène. Il est essentiel de bien comprendre les effets structurels et les propriétés des matériaux composites, ainsi que leur comportement sous fatigue et contrainte dynamique rapide, afin de garantir l'intégrité des réservoirs et la protection des usagers. Ces éléments sont cruciaux pour prévenir les défaillances potentielles et assurer la durabilité et la sécurité des réservoirs soumis répondant à des exigences strictes, notamment supporter des pressions élevées pouvant atteindre 700 bars et des sollicitations thermomécaniques complexes, telles que les cycles de fatigue lors du remplissage et du vidage, les chocs, le fluage, ainsi que les variations de température.

Cette étude a identifié les défis et les opportunités associés à l'utilisation des matériaux composites dans les réservoirs de stockage d'hydrogène à haute pression, en mettant particulièrement l'accent sur les composites époxy renforcés de fibres de carbone de type IV. En utilisant une approche multi-échelle, comprenant des études aux niveaux microscopique, mésoscopique et macroscopique, la recherche a examiné en détail les interactions entre la microstructure des composites (comme l'orientation des fibres, la porosité) et leur comportement mécanique dans différentes conditions de chargement. L'incidence de ces facteurs sur les performances mécaniques des réservoirs, leur durabilité et leur capacité à résister à la fatigue et aux charges dynamiques a été clairement démontrée.

Cette thèse a permis d’étudier en profondeur les mécanismes d’endommagement des matériaux composites époxy renforcés de fibres de carbone, utilisés dans les réservoirs de stockage d’hydrogène, sous des sollicitations quasi-statiques, cycliques et dynamiques. L’analyse des différentes orientations des fibres (±15°, ±30° et configurations multicouches) a révélé des impacts significatifs sur les propriétés mécaniques, la durée de vie en fatigue, ainsi que les critères d’endommagement et de rupture à l’échelle des couches unidirectionnelles.

Les essais mécaniques ont montré que l'orientation des fibres, couplée à la porosité inhérente au processus de fabrication, joue un rôle crucial dans la répartition des contraintes et dans les mécanismes d'endommagement, tels que la décohésion des interfaces, la fissuration de la matrice et la délamination. Les essais in situ et les analyses multi-échelles ont permis de mieux comprendre l'évolution des dommages, allant de l'initiation à la rupture, sous différents régimes de sollicitations.

Les essais de fatigue ont mis en évidence que la configuration ±15° présente une meilleure résistance à la fatigue, tandis que les autres configurations montrent des performances plus homogènes. L'effet de la réduction de la contrainte appliquée sur la durée de vie en fatigue a également été souligné, pointant l'importance de l'optimisation des orientations de fibres pour maximiser la durabilité sous charge cyclique.

Enfin, les essais sous sollicitations dynamiques rapides ont démontré une augmentation notable des propriétés mécaniques avec l'augmentation des taux de déformation, mettant en avant la sensibilité des composites à ces conditions extrêmes. Les résultats fractographiques ont confirmé la présence de phénomènes tels que la fracture des fibres, la fissuration de la matrice et la délamination, renforçant la nécessité de prendre en compte ces mécanismes dans la conception et l'évaluation des réservoirs d'hydrogène.

En conclusion, cette étude souligne la complexité des mécanismes d'endommagement des composites sous différentes sollicitations et l'importance de comprendre ces phénomènes à différentes échelles pour améliorer la conception, la fiabilité et la sécurité des réservoirs de stockage d'hydrogène. Ces résultats fournissent des pistes importantes pour la modélisation prédictive et la simulation numérique, essentielles pour garantir la robustesse de ces systèmes face aux sollicitations extrêmes.

L'étude et la modélisation de l'effet des séquences de sollicitations thermomécaniques sur le comportement, l'endommagement et la rupture des matériaux composites des réservoirs d'hydrogène ouvrent plusieurs axes de recherche et d'amélioration. Ces travaux offrent des perspectives prometteuses visant à optimiser la durabilité et la sécurité de ces structures critiques, tout en facilitant leur adoption plus large dans le cadre de la transition énergétique.

L'optimisation de la microstructure et de l'architecture des composites est un axe de recherche majeur. Une analyse approfondie des interactions fibre-matrice sous sollicitations complexes permettrait de mieux comprendre l'évolution des contraintes résiduelles et leur impact sur la propagation des fissures. L'optimisation

des orientations et de l'empilement des plis, en prenant en compte l'anisotropie des matériaux, ainsi que l'analyse des effets de l'épaisseur et des hétérogénéités microstructurales, sont essentielles pour limiter les concentrations de contraintes et améliorer la tenue mécanique des réservoirs. De plus, une meilleure gestion de la porosité, notamment par l'optimisation des procédés de fabrication tels que l'enroulement filamentaire, est cruciale pour assurer la durabilité des structures. L'intégration de capteurs en ligne et de techniques de contrôle non destructif avancées pourrait permettre une surveillance en temps réel de la formation des défauts et un ajustement adaptatif des paramètres de fabrication.

Le développement et la validation de modèles de prédiction du comportement et de la durée de vie des composites constituent un autre enjeu essentiel. L'élaboration de modèles multi-échelles tenant compte des effets couplés de la dilatation thermique, des contraintes mécaniques et du vieillissement chimique permettrait de prédire plus précisément la dégradation des réservoirs en service. Ces modèles pourraient être enrichis par des approches basées sur la mécanique de l'endommagement et des critères de rupture, ainsi que par l'intégration de l'intelligence artificielle et de l'apprentissage automatique pour anticiper les défaillances et proposer des stratégies de maintenance prédictive. La validation expérimentale de ces modèles, en couplant simulations éléments finis et essais de validation sur structures complètes, améliorerait leur prédictibilité et leur applicabilité à l'industrie.

L'optimisation des procédés de fabrication est également une priorité pour garantir une meilleure tenue mécanique. La réduction des défauts de fabrication, tels que les porosités, fissures interlaminaires et variations d'épaisseur, passe par une meilleure maîtrise des paramètres de moulage, de polymérisation et de post-traitement. De plus, l'impact des gradients thermiques et des contraintes internes lors de la fabrication devra être étudié pour limiter l'apparition de contraintes résiduelles délétères. L'optimisation des cycles de cuisson et des traitements post-polymérisation contribuera également à améliorer les propriétés mécaniques et la résistance au fluage sous charge.

Enfin, le développement de méthodes avancées de caractérisation et de surveillance de l'intégrité structurelle représente une perspective incontournable. L'utilisation de techniques expérimentales de pointe, telles que la tomographie à rayons X, la microscopie électronique à balayage et la spectroscopie Raman, permettra une meilleure visualisation des mécanismes de fissuration et de délaminage à l'échelle

microstructurale. Parallèlement, l’intégration de capteurs à fibres optiques et de systèmes de suivi par émission acoustique facilitera la détection précoce des défauts et l’évaluation en temps réel de l’état de santé des réservoirs en service. L’exploitation de méthodes d’apprentissage automatique appliquées aux données de surveillance ouvrira la voie à des stratégies de maintenance préventive plus efficaces.

Les résultats obtenus au cours de cette thèse ont permis d'établir un dialogue entre expériences et simulations sous LS-Dyna. À l'échelle de l'échantillon, la validation des lois MAT 54 et 58 a été réalisée en quasi-statique, en tenant compte de l'effet de vitesse. Une approche combinant fatigue et couplage dynamique-fatigue a été mise en place pour prédire la durée de vie des structures en conditions réelles. L’extension de ces validations à des structures de grande taille, représentatives des conditions industrielles, constituera une étape décisive vers l'application de ces modèles.

En définitive, ces avancées contribueront à renforcer la compréhension des interactions complexes entre les phénomènes thermiques, mécaniques et chimiques dans les composites de stockage d’hydrogène. Elles permettront d’améliorer la performance, la fiabilité et la sécurité des réservoirs, tout en facilitant leur industrialisation et leur adoption massive dans le cadre d’une transition énergétique durable. L'application de ces résultats pourrait également s'étendre à d'autres domaines où les matériaux composites sont soumis à des environnements extrêmes, renforçant ainsi leur résistance et leur durabilité.

6. Références

[1] Imen Feki , Mohammadali Shirinbayan , Samia Nouira , Robert Tie Bi , Jean-Baptiste Maeso , Cedric Thomas , Joseph Fitoussi , Composites in high-pressure hydrogen storage: a review of multiscale characterization and mechanical behavior, Composites Part C: Open Access (2024), doi: https://doi.org/10.1016/j.jcomc.2024.100555.

[2] Feki I, Shirinbayan M,Nouira S, et al. Multi-scale experimental investigation of porosity-induced damage effects in filament-wound carbon fiber reinforced epoxy composites used in hydrogen storage tanks. Polym Compos. 2024;1-13. doi:10.1002/pc.29121

[3] Imen Feki, Mohammadali Shirinbayan, Samia Nouira, Robert Tie Bi, Jean-Baptiste Maeso, Cedric Thomas, Joseph Fitoussi, Multi-scale fatigue damage analysis in filament-wound carbon fiber reinforced epoxy composites for hydrogen storage tanks,Composites Part C: Open Access,Volume 15, 2024,100537,ISSN 2666-6820, https://doi.org/10.1016/j.jcomc.2024.100537.

[4] Shirinbayan M, Feki I, Nouira S, et al. Multi-scale damage analysis of filament-wound carbon fiber-reinforced epoxy composites for hydrogen storage tanks under high strain rates. Polym Compos. 2024;1-12. doi:10.1002/pc.29273

[5] G. Gondor, «Pour le stockage de l'hydrogène : Analyse thermodynamique de la formation d'hydrures métalliques et optimisation du remplissage d'un réservoir.,» HAL Id: tel-00782271, Besançon, 29 jan 2013.

[6] K. H. D. Mori*, «Recent challenges of hydrogen storage technologies for fuel cell vehicles,» *i n t e r n a t i o n a l j o u rna l o f hydrogen energy 3 4,* p. doi:10.1016/j.ijhydene.2008.07.115, 2 0 0 9.

[7] J. Zheng, J. Guo, J. Yang, Y. Zhao, L. Zhao, X. Pan, J. Ma et L. Zhang, «EXPERIMENTAL AND NUMERICAL STUDY ON TEMPERATURE RISE WITHIN A 70 MPA TYPE III CYLINDER DURING FAST REFUELING.,» 13th China Hydrogen Energy Conference (CHEC) , p. DOI, 2013.

[8] N. M. CebollaB.AcostaP.MorettoF.HarskampC.Bonato, «Compressed hydrogen tanks for on-board application: Thermal behaviour during cycling,» International Journal of Hydrogen Energy, 2015.03.035, 2015.

[9] S. C. K. C. K. H. L. B. Y. B. Yoon, «Thermal characteristics during hydrogen fueling process of type IV cylinder,» International Journal of Hydrogen Energy 35, p. DOI: 10.1016/j.ijhydene.2010.03.130, 2010.

[10] Y. J. Z. Y. P. X. Z. L. Z. L. e. a. Guo J, «Investigations on temperature variation within a type III cylinder during the hydrogen gas cycling test.,» Hydrogen Energy, 2014.03.097, 2014.

[11] T. MORIYA, «DEVELOPMENT OF THE FCX FUEL CELL VEHICLE AT HONDA,» Wako Research Center, Honda R&D, 2003.

[12] M. K. H. M. Y. N. T. T. T. M. a. N. K. Tetsuya Bono, «Development of New TOYOTA FCHV-adv Fuel Cell System,» Journal of Engines, p. https://www.jstor.org/stable/26308444, 2009.

[13] M. K. S. G. a. N. O. Akira Yamashita, «Development of High-Pressure Hydrogen Storage System for the Toyota"Mirai",» SAE Technical Paper, pp. doi:10.4271/2015-01-1169., 2015.

[14] «Faurecia,» 31 mars 2021. [En ligne]. Available: https://www.faurecia.com/newsroom/faurecia-accompagne-stellantis-pour-des-vehicules-utilitaires-hydrogene.

[15] D. chalon, «le journal des flottes,» 18 octobre 2021. [En ligne]. Available: https://journalauto.com/journal-des-flottes/stellantis-vise-2-000-utilitaires-a-hydrogene/.

[16] DoE, Physical Hydrogen Storage, U.S. Department of Energy, America, 2023.

[17] Gibson, R. F. (2016). *Principles of composite material mechanics* (4th ed.). CRC Press.

[18] Callister, W. D., & Rethwisch, D. G. (2018). *Materials science and engineering: An introduction* (10th ed.). Wiley.

[19] Figueiredo, R. A., & Silva, F. (2017). *Mechanical performance of CFRP composites in hydrogen storage applications*. *Journal of Composite Materials, 51*(7), 957-970. https://doi.org/10.1177/0021998316657476

[20] Czigány, T., & László, A. (2019). *Carbon fiber reinforced polymer composites: A review of the properties and applications in hydrogen storage*. *Materials Science and Engineering: A, 752*, 111-126. https://doi.org/10.1016/j.msea.2019.03.029

[21] Zhang, Y., & Liu, X. (2015). *Polymer matrices in CFRP composites*. In P. G. Shodja & R. C. R. de Barros (Eds.), *Composite materials: Science and engineering* (pp. 241-263). Elsevier.

[22] T. Altayeb et al., "Filament Winding Process and Optimization for High-Pressure Hydrogen Storage," *Journal of Composite Materials*, vol. 54, no. 3, pp. 345-360, 2021.

[23] J. Smith et al., "Epoxy-Based CFRP Composites for Hydrogen Storage: Performance and Challenges," *Advanced Materials*, vol. 32, no. 45, 2020.

[24] P. Zhang et al., "Influence of Resin Impregnation on CFRP Mechanical Properties," *Composites Science and Technology*, vol. 185, pp. 107-123, 2019.

[25] K. Nakamura et al., "Optimization of Fiber Orientation in Filament Wound Composite Pressure Vessels," *Composite Structures*, vol. 250, 2022.

[26] B. Roux et al., "Effect of Winding Angles on Fatigue Resistance of Composite Cylinders," *Materials and Design*, vol. 180, pp. 107925, 2020.

[27] F. Lee et al., "Thermal Curing of CFRP and its Influence on Mechanical Properties," *Journal of Polymer Science*, vol. 58, no. 6, pp. 1203-1218, 2021.

[28] M. Dubois et al., "X-ray Tomography for Defect Analysis in Composite Pressure Vessels," *NDT & E International*, vol. 120, 2021.

[29] European Standards Committee, "Regulations for Composite Pressure Vessels in Hydrogen Storage," *EN 12245*, 2023.

[30] Hydrogen Council, *The Future of Hydrogen in Transport Applications*, 2022.

[31] Baramee Patamaprohm. Conception et durabilité de réservoirs en composites destinés au stockage de l'hydrogène. Mécanique des matériaux [physics.class-ph]. Ecole Nationale Supérieure des Mines de Paris, 2014. Français. NNT : 2014ENMP0021. tel-02018105

[32] Lise Angrand. Mécanique [physics]. Université Paris Saclay (COmUE), 2016. Français. NNT : 2016SACLN005. tel-01300513

[33] Federica Daghia, Pierre Ladevèze, Philippe Bordeu, Caroline Petiot.. JNC 16, Jun 2009, Toulouse, France. 10 p. hal-00386065

[34] P. PROMBUT, «Caractérisation de la propagation de délaminage des stratifiés composites multidirectionnels,» Université Toulouse, Toulouse, 2007.

[35] Y. D. e. J. QIAN, «Analysis of microdamage evolution histories in composites.,» *International Journal of Solids and Structures*, p. 1831–1854, 2001.

[36] F. LEBEL, «Contrôle de la fabrication des composites par injection sur renforts.,» Université de Montréal,, Miontréal, 2012.

[37]] S.HUGUET, «Application de classification aux données d'émission acoustique :identification de la signature acoustique des mécanismes d'endommagement dans lescomposites à matrice polymère.,» Institut National des SciencesAppliquées de Lyon, lyon, 2002.

[38] R.TALREJA, «Assessment of the fundamentals of failure theories for compositematerials.,» Composites Science and Technology, p. 105:190–201, 2014.

[39] Y. A. B. G. M. J.C.ABRY, «In-situ monitoring of damage in CFRP laminates by means of ACand DC measurements.,» Composites Science and Technology, p. 855–864, 2001.

[40] Feki I , Shirinbayan M , Nouira S , et al. Étude expérimentale multi-échelle des effets de dommages induits par la porosité dans les composites époxy renforcés de fibres de carbone à enroulement filamentaire utilisés dans les réservoirs de stockage d'hydrogène . *Polym Compos* . 2024 ; 1 - 13 . doi: 10.1002/pc.29121

[41] Shirinbayan, M., Nouira, S., Imaddahen, M. A., & Fitoussi, J. (2024). Microstructure-sensitive investigation on the plastic deformation and damage initiation of fiber-reinforced polypropylene composite. *Composites Part B: Engineering*, *286*, 111790.

[42] Nouira, S., Shirinbayan, M., Peixinho, J., Benfriha, K., Hassine, T., & Fitoussi, J. (2024). Effect of processing conditions on morphology and mechanical damage in glass-reinforced polypropylene composite. *Polymer Composites*.

[43] H. G. J.BRUNBAUER, «Mechanical properties, fatigue damage and microstructure of carbon/epoxy laminates depending on fibre volumecontent,» International Journal of Fatigue,, p. 85–92, 2015..
[44] Zhou, G., Zhao, L., & Adams, R. D. (2015). The influence of matrix cracking on the fatigue life of carbon fiber-reinforced polymer composites. Composite Structures, 123, 345-354.
[45] Shokrieh, M. M., & Lessard, L. B. (2000). Progressive fatigue damage modeling of composite materials. Composite Structures, 48(4), 453-461.
[46] Sendeckyj, G. P. (1990). Life prediction for resin matrix composite materials. International Journal of Fracture, 42(1), 1-31.
[47] K. S. K. R. e. W. S. R.D. JAMISON, «Characterization and analysis of damage mechanisms in tension-tension fatigue of graphite/epoxy laminates.,» Effects of Defects in Composite Materials, p. 21–55, 1984.
[48] Juliette Payan. Etude du comportement de composites stratifiés sous chargement statique et de fatigue. Mécanique [physics.med-ph]. Université de la Méditerranée - Aix-Marseille II, 2004 Français.

Article N°1 :

Imen Feki, Mohammadali Shirinbayan, Samia Nouira, Robert Tie Bi, Jean-Baptiste Maeso, Cedric Thomas, Joseph Fitoussi, Composites in high-pressure hydrogen storage: a review of multiscale characterization and mechanical behavior, Composites Part C: Open Access (2024), doi: https://doi.org/10.1016/j.jcomc.2024.100555.

Composites in high-pressure hydrogen storage: a review of multiscale characterization and mechanical behavior

Imen Feki[1], Mohammadali Shirinbayan[1,*], Samia Nouira[1], Robert Tie Bi[2], Jean-Baptiste Maeso[2], Cedric Thomas[2], Joseph Fitoussi[1]

[1]Arts et Metiers Institute of Technology, CNAM, PIMM, HESAM University, F-75013 Paris, France

[2]Zero Emission, FORVIA Clean Mobility, Bois Sur Prés, 25550 Bavans, France

E-mails: Mohammadali.Shirinbayan@ensam.eu (corresponding author), Imen.Feki@ensam.eu, Samia.Nouira@ensam.eu, Robert.tbr.tiebi@forvia.com, Jean-Baptiste.Maeso@forvia.com, Cedric.Thomas@forvia.com, Joseph.Fitoussi@ensam.eu.

Abstract

Environmental protection and sustainable development remain key concerns for all stakeholders. In this context, hydrogen has emerged as a particularly promising energy vector for electricity and heat generation, contributing to the transition toward clean energy solutions. However, the refueling of high-pressure hydrogen tanks can lead to a rapid increase in the internal temperature of the storage cylinder, potentially causing a decrease in the state of charge, damage to tank walls, and, ultimately, safety concerns. This paper provides a detailed review of hydrogen storage technologies, with a particular focus on Type IV tanks for automotive applications. These tanks, characterized by a polymer liner fully wrapped in carbon fiber composites, are pivotal for achieving high-pressure containment while maintaining lightweight properties. To understand and address critical challenges, the study conducts an in-depth examination of the mechanical behavior and failure mechanisms of laminated composites across multiple scales. Through advanced multiscale characterization methods, including infrared thermography, X-ray tomography, acoustic emission, and digital image correlation, the research investigates how these materials respond under impact and cyclic loading conditions. Key failure mechanisms, such as matrix cracking, fiber breakage, and delamination, are explored to elucidate their progressive development and impact on the structural integrity of composites. The study also examines residual properties following dynamic loading to provide a comprehensive understanding of long-term performance under real-world conditions. Findings emphasize the importance of multiscale coupling from macro to microstructure to achieve accurate modeling and prediction of composite behavior. Insights from this research aim to optimize the design and durability of hydrogen storage systems, enabling safer and more efficient implementation in the automotive sector. This review concludes by summarizing the implications of these findings for enhancing the performance and safety of high-pressure hydrogen storage technologies.

Highlights

- This paper provides a comprehensive analysis of the various hydrogen storage technologies, with a particular emphasis on the role of composite materials in high-pressure containment for the automotive sector, particularly Type IV tanks.
- The study examines the mechanical behavior and damage mechanisms of laminated composites under impact and cyclic loading, utilizing advanced techniques such as infrared thermography, X-ray tomography, and digital image correlation.
- The review highlights the significance of multiscale coupling for precise modelling and optimization of composite materials in high-pressure hydrogen storage systems, offering invaluable insights for future design enhancements.

Keywords: Hydrogen; storage; mechanical behavior; impact; cyclic; damage.

Table of contents

1. Introduction

Over the last three decades, our environment is generally confronted with the combined effects of the depletion of fossil resources (oil, natural gas, coal) and global warming linked to the sharp rise in the concentration of carbon dioxide (CO_2), which is a greenhouse gas. Green energies, those with low emissions, are required to compensate for traditional energy systems. In this respect, hydrogen is one of the promising candidates to meet society's demand in terms of sustainable development, not only because it appears as a particularly interesting energy vector but also because it is inexhaustible, non-polluting and can be produced from water [1]; [2]; [3].

The hydrogen sector includes different key stages: production, distribution, storage and exploitation. Today, the storage of this vector is still a major technological and scientific obstacle. There are different storage strategies: solid storage (hydrogen atoms stored in the form of simple hydrides [4] or complex hydrides, such as borohydrides, alanates or Li amides in a metallic crystal lattice or in carbon nanostructures); liquid or cryogenic storage [5] (volume of hydrogen maintained at a temperature of /250°C); gaseous storage (or compressed storage of a maximum quantity of hydrogen in a given volume). Among these three solutions, compressed gas storage appears to be the most mature solution, presenting the best compromise in terms of mass density (ratio of the mass of hydrogen stored to the mass of the whole) and volumetric density (ratio of the volume of hydrogen stored to the total volume).

Progress has been made in terms of storage mode and pressure, going from 200 bars to 350 bars in the case of cylinders distributed in industry. At present, developments are turning towards tanks that can withstand pressures of 700 bar. In this context, type IV tanks are made up of a polymer liner ensuring the watertightness, two metal bases allowing the introduction and distribution of hydrogen and the composite deposited all around the liner by filament winding to ensure mechanical strength while minimizing the total mass. However, the complex environment and the complex thermo-mechanical stresses undergone by the structure make it difficult to analyze the damage and failure of the composite and consequently to establish predictive models to control the design of hydrogen tanks. Thus, predicting the burst pressure, the state of damage or the fatigue life related to the filling/emptying cycles is a real challenge, especially from a safety point of view.

In this context, this paper presents a comprehensive analysis of the state-of-the-art in hydrogen storage, with a particular emphasis on various storage methods and types of hyperbaric tanks, especially Type IV tanks for automotive applications. High-pressure hydrogen storage systems, and particularly Type IV composite tanks, are required to withstand extreme mechanical demands, including impact and cyclic loading over

extended operational periods. To achieve this, it is critical to understand their mechanical behavior and the associated damage mechanisms to ensure structural integrity, safety, and efficiency.

Laminated composites, which are the primary materials used in these tanks, exhibit complex damage mechanisms such as matrix cracking, fiber breakage, and delamination, which interact across multiple scales under diverse loading conditions. Advanced multiscale characterization methods, including infrared thermography, X-ray tomography, and digital image correlation, are pivotal for capturing these interactions. These methods facilitate the detailed investigation of progressive damage accumulation and the residual strength of the material, offering essential insights for optimizing composite designs used in high-pressure hydrogen storage. By integrating these experimental techniques with fracture mechanics principles, engineers can develop predictive models to enhance safety and performance, addressing critical challenges like crack propagation and delamination.

While this study primarily focuses on laminated composites for high-pressure hydrogen storage, it also draws on broader advances in composite mechanics to provide valuable context. A review of relevant literature, including fracture mechanics applications in composite design and recent advancements in characterization techniques, underscores the engineering significance. For example, research on energy release rates during crack propagation offers direct implications for tank design and long-term durability under operational stresses (e.g., [6,7]). Similarly, studies on delamination and interfacial damage mechanisms provide essential perspectives on failure prevention and structural optimization [8,9,10]. The integration of these insights supports the development of safer and more efficient hydrogen storage systems.

This paper systematically reviews the mechanical behavior and damage mechanisms of laminated composites, beginning with multiscale characterization under monotonic loading, progressing to cyclic loading behavior, and concluding with impact response analysis. Additionally, the study investigates the dynamic residual properties of composites following cyclic loading and examines the influence of impact on the residual behavior of tank materials. A detailed classification of classical modeling approaches, such as those implemented in Abaqus and LS-Dyna, is also provided, focusing on progressive damage modeling, failure criteria, and associated numerical methods. Recognizing the importance of scale in composite material analysis, this work details the various scales to which modeling approaches can be applied. Finally, while the primary focus is on composite damage and failure, the study acknowledges that structural failures in these systems often originate from the liner, further highlighting the need for a holistic approach to tank design.

2. Composite materials for hydrogen tanks

2.1. General information on hydrogen storage

Hydrogen, or more precisely dihydrogen (H_2), presents a promising source of energy to replace fossil fuels due to environmental pollution and the energy crisis. It offers several interesting characteristics such as no greenhouse gas emissions, high efficiency and abundant resources. In order to make hydrogen a viable alternative resource, it is essential to address various technical issues, such as hydrogen generation, storage, transportation and combustion. The storage of hydrogen remains an important issue for its large-scale use. Generally speaking, hydrogen can be stored in three forms:

- **Low temperature liquid storage**, where hydrogen is stored at 20K (-253°C) and at low pressure (10 bars). This is an interesting technology from the point of view of storage capacity (high mass and volume densities) and the manufacturing costs of these storage tanks. Nevertheless, the costs of liquefying hydrogen make its implementation and use less competitive than for other technologies.
- **Solid state storage**, a technology that uses the reversible properties of adsorption or absorption of hydrogen by a material (generally hydrides). The main advantages of this technology are the very large volume storage capacity of hydrides and the low implementation pressures. On the other hand, several obstacles remain to be overcome: hydrogen adsorption or absorption kinetics, high desorption temperatures, prohibitive costs of the materials used (hydrides), and pyrophoric materials requiring delicate handling.
- **Pressurized gas storage**, a process where hydrogen is stored in gaseous form at very high pressure (700 bars) to obtain interesting volume and mass densities, i.e. sufficiently large to obtain autonomies similar to those of current vehicles. For this technology, the costs are essentially due to the manufacturing of the tanks, generally in composite materials to satisfy such pressures with low mass and volume of material, and to the costs of hydrogen compression.

Currently, high-pressure hydrogen storage is the most popular method due to its low cost, maturity and ease of use. High pressure tanks are divided into five subfamilies (Fig. 1):

- **Type I tanks**, made entirely of metal (usually steel or aluminum), are robust and affordable but extremely heavy, limiting their use in mobile applications. The disadvantages of this type of tanks are: low storage density1 (here 1.2%) and storage pressures limited to 30MPa.

▪ **Type II tanks** consist of a metal liner partially wrapped with composite material, providing some weight reduction compared to Type I, but they remain relatively heavy and more expensive. As for type 1 tanks, density and storage pressure remain low (1.3% and 35MPa).

▪ **Type III tanks** consist of a metal cylinder and a composite shell deposited by filament winding on the entire surface of the cylinder. The role of the metal cylinder is only to guarantee the tightness of the tank. The term "liner" is then used to refer to this watertight envelope which also serves as a support for the composite deposit. The mechanical strength is provided by the composite shell. The disadvantage of this type of tank is that the metal liner is weak in fatigue and contributes to a significant part of the tank's mass. However, the capacities of these tanks are significantly improved compared to the previous ones. These tanks allow service pressures of 70MPa.

▪ **Type IV tanks**, with a plastic liner fully wrapped in carbon fiber, are the lightest and most popular for automotive applications, offering significant weight savings and high-pressure resistance, though they are costly and can face long-term durability challenges such as hydrogen embrittlement.

▪ **Type V tanks**, made entirely of composite material with no liner, represent the cutting edge of hydrogen storage technology, offering the lightest and highest-performing option, but they are still in development and face challenges related to hydrogen permeation and high manufacturing costs.

Fig. 1. Different method of hydrogen storage.

2.2. Automotive hydrogen storage type III and IV tanks

Research on hydrogen vehicles is taking place in the context of the progressive depletion of fossil fuels and, above all, of global warming, which makes it necessary to find an alternative to fossil fuels. With the development of hydrogen fuel cell vehicles, the technology of safe, efficient and economical on-board hydrogen storage has become a fundamental element. Higher autonomies require more hydrogen storage. Currently, hyperbaric tanks are the most mature and commonly adopted solution for hydrogen storage in

vehicles [11] [12]. In general, hydrogen cylinders can be pressurized to 25 MPa, 35 MPa or 70 MPa. Considering the range and limited space the limited space of the vehicle, 70 MPa is the most economical pressure for the most economical pressure for onboard storage [13]. Comparing the above four types, it can be seen that Type I and Type II cannot be used in vehicles due to the low hydrogen storage density and severe hydrogen embrittlement issues.

In the fuel cell vehicle (FCV) industry, types III and IV are widely used to minimize weight [14], [11] [12]. However, Type III and Type IV have different behavior in terms of temperature rise due to the differences in materials. The evolution of hydrogen storage systems has seen notable contributions globally, with countries like China advancing Type III tank technology to achieve commercial readiness [13]. Meanwhile, companies such as Toyota and Hyundai have introduced innovative Type IV tanks, emphasizing larger storage capacities and shorter refueling times, aligning with market demands for longer driving ranges and zero-emission capabilities. Currently, most developed fuel cell vehicles utilize high-pressure cylinders for onboard hydrogen storage. For instance, various automotive manufacturers have introduced advanced storage systems to enhance performance and range. Honda's FCX, equipped with two 35 MPa tanks, achieves a hydrogen capacity of 156.6 L, while Toyota's FCHV-adv employs four 70 MPa Type IV tanks, enabling a range of at least 500 km under practical conditions with a refueling time of 10 minutes [16,17]. The Toyota Mirai further advances storage technology with two larger-diameter tanks (60 L and 62.4 L), capable of storing nearly 5 kg of hydrogen in 3 minutes and providing a 500 km range. Similarly, Hyundai's NEXO incorporates three high-capacity tanks (156 L total), enabling a driving range of 800 km in the NEDC test cycle with a refueling time of 5 minutes. Additionally, Stellantis, in collaboration with STELIA Aerospace Composites and Faurecia, has developed 700 bar tanks for commercial vehicles, offering a zero-emission range of over 400 km with a total capacity of 120 L [18].

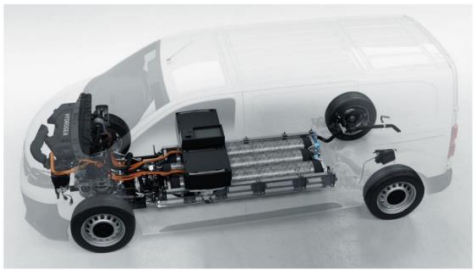

Fig. 2. Zero-emission light commercial vehicle developed by Stellantis [19].

2.3. Presentation of the hydrogen tank type IV

Type IV hydrogen tanks are made up of three components and their interfaces (see Fig. 3): The polymer liner, the metal base and the composite.

- **The liner:** a polymer used to seal the tank. Sealing is difficult to achieve, partly because of the high pressure, which favors hydrogen infiltration at the interfaces, but also because of the permeation of hydrogen, the smallest of molecules, through the material. This latter aspect requires an appropriate choice of liner material to limit hydrogen permeation as much as possible. Several materials are currently being studied for liner design: PEA, PEB and PA11. Currently manufactured using a rotational molding process, other processes such as injection-welding or extrusion-blow molding are being studied to achieve mass production rates. We distinguish three parts on the liners: two domes at the ends and the shell, a purely cylindrical part.
- **Aluminum bases:** are attached to both ends of the tank to secure the tank to the chassis, fill the tank and perform one of the tank's main functions, which is to supply hydrogen to the fuel cell. Some small tanks have only one base. As this expands during filling, the tank must be able to deform axially. As a result, the two bases are not the same size. One is completely locked and the other can slide on plain bearings. There are other ways of integrating the reservoir around it. These include the harness system known in English as "strap mounting". These are generally placed directly on the cylindrical part of the composite hull.
- **A composite shell:** made up of several layers of carbon-fiber and epoxy resin-based composite, whose main role is to counteract the mechanical stresses exerted on the tank, particularly at the high internal pressures imposed on the tank: nominal pressure: 700 bar and burst pressure: 1750 bar. These composite layers are wound around the liner using a filament winder. The band, made up of several rovings (depending on the diameter of the reservoir), first passes through a groove to put them under tension to ensure they stay in place on the skid. They are then soaked in a plastic water bath to impregnate them, then passed to one end of the roller before being wound around the liner. Winding is carried out according to a defined program, to obtain the desired number of layers and different angles. The sequence is relatively long: about 1h30 of winding, then about 8h of curing to polymerize the resin. Recent advancements in composite materials for hydrogen storage tanks have focused on addressing challenges like hydrogen embrittlement and thermal damage. Enhanced barrier layers [20], such as advanced polymer liners and coatings, have been developed to minimize hydrogen permeation and embrittlement.

The integration of nanostructured additives [21], including carbon nanotubes, improves mechanical strength and thermal stability. Thermal protective coatings and high-temperature-resistant resin systems [22] have also been introduced to mitigate thermal damage risks. Furthermore, advanced manufacturing techniques [23], such as filament winding and automatic fiber placement, ensure precise control over fiber orientation and resin distribution, enhancing the structural integrity and durability of storage tanks. These innovations collectively represent significant progress toward safer and more efficient hydrogen storage systems. Finally, a thin layer of fiberglass can be applied on top of the composite, to identify damaged areas in the event of the tank being knocked or dropped, and to protect it from moisture. Protective foam domes are often added to the tank to provide additional impact protection.

The analysis and prediction of Type IV hydrogen storage system failures through the establishment of predictive models represent a major challenge and are at the heart of industrial concerns.

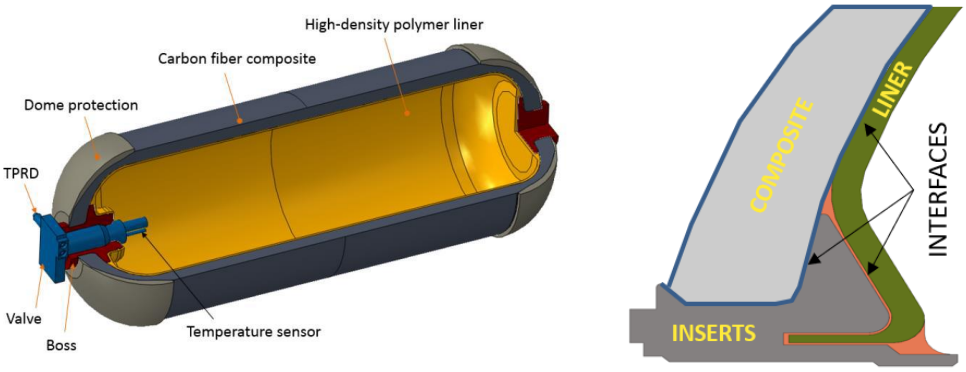

Fig. 3. Cross-section of a type IV hydrogen tank [24].

3. Mechanical behavior and damage of laminated composites

Laminated composites, especially those strengthened with fibers like carbon or glass, are extensively utilized in high-performance scenarios because of their outstanding mechanical characteristics, such as high strength-to-weight ratios, resistance to corrosion, and adaptability to specific needs. These composites comprise numerous layers (or plies) of unidirectional or woven fiber-reinforced materials stacked together, frequently at different angles, to enhance their mechanical performance in various loading situations. It is essential to comprehend their mechanical properties and the related damage mechanisms in order to develop dependable composite structures in industries like aerospace, automotive, energy, and marine engineering.

3.1. Fundamental mechanical behavior

Laminated composites have different mechanical properties depending on the direction of the applied load relative to the fiber orientation. These materials can be characterized by their responses to tension, compression, shear, and bending loads.

- **Tensile loading:** Tensile behavior in laminated composites is mainly influenced by the fiber orientation. When loaded along the fiber direction, laminates show high stiffness and strength due to the superior tensile properties of the fibers. Conversely, when loaded transversely (perpendicular to the fibers), the response is governed by the matrix, resulting in lower tensile strength and stiffness [25].
- **Compressive loading:** Compressive behavior is complex due to the susceptibility of the fibers to buckling. Under compressive loads, laminated composites may experience micro buckling of fibers, leading to matrix cracking, fiber kinking, and eventual delamination [26]. Compression strength is usually lower than tensile strength, as compressive failures can start from fiber-matrix debonding or misaligned fibers.
- **Shear loading:** The shear response of laminated composites is primarily driven by the matrix properties, as the fibers offer less resistance to shear deformation. Shear failure is often linked to matrix cracking and interlaminar shear failure, especially at the interfaces between plies. Fiber orientation significantly impacts the shear response of the laminate [27].
- **Bending and flexural loading:** During bending, the outer layers of the laminate experience tensile and compressive stresses, while the inner layers undergo shear. The fiber orientation is crucial for the laminate's bending stiffness, with 0° and ±45° oriented fibers contributing to higher flexural strength. Delamination is a common failure mode under bending, particularly in the presence of flaws or stress concentrations [28].

3.2. Failure mechanisms in laminated Composites

The breakdown of laminated composites often occurs gradually, starting at the microstructural level and spreading throughout the structure. The main mechanisms of damage observed in laminated composites include matrix cracking, fiber breakage, fiber/matrix debonding, delamination, and interlaminar shear failure. These mechanisms are interconnected and often happen together, impacting the overall structural integrity. A qualitative understanding of these mechanisms highlights their interdependence and the broader implications for composite behavior and design.

- **Matrix Cracking:** Matrix cracking usually begins early in the loading process, especially in off-axis plies where the matrix faces high transverse stresses. These cracks generally form perpendicular to the fiber direction and can spread through the thickness of the laminate. As precursors to delamination, matrix cracks decrease the load-carrying capacity of the composite by creating stress concentrations that accelerate the initiation of secondary damage mechanisms like fiber/matrix debonding and interlaminar shear failure (see Fig. 4) [29,30].

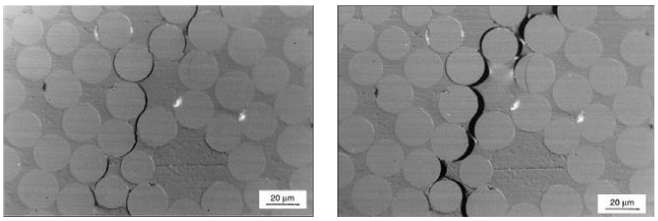

Fig. 4. Propagation of matrix cracking at the microscopic scale [31].

- **Fiber Breakage:** Fiber breakage occurs when the applied stress surpasses the tensile strength of the fibers. This mechanism is more likely to happen in the load-bearing plies (0° fibers) when they are subjected to tensile or compressive loads along the fiber direction. Fiber breakage is a crucial type of damage, as it directly reduces the strength and stiffness of the composite [32,33]. The failure of load-bearing fibers can induce cascading damage, such as matrix cracking or delamination, further compromising the composite's structural performance. This highlights the importance of optimizing fiber orientation and distribution in laminate design. The broken fibers have the following appearance (Fig. 5):

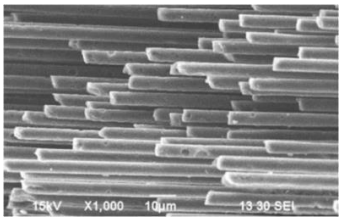

Fig. 5. Visualization of fibers with a scanning electron microscope [29].

- **Fiber/Matrix Debonding:** Fiber/matrix debonding involves the separation of the fibers from the surrounding matrix. This damage mechanism is often initiated by matrix cracks or interfacial stresses caused by differential thermal expansion between the fibers and matrix. Debonding reduces the efficiency of load transfer between the matrix and fibers, leading to a decrease in the composite's mechanical properties (see Fig. 6.) [34,35]. Fiber/matrix debonding creates localized regions of stress

concentration, accelerating other damage mechanisms such as delamination. Understanding this behavior is critical for improving fiber-matrix adhesion and optimizing composite durability.

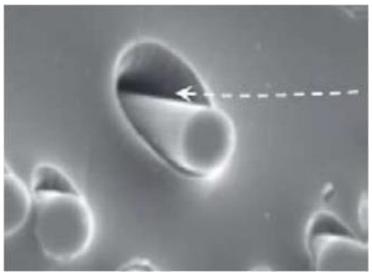

Fig. 6. Decohesion of the fiber-matrix interface observed via Scanning Electron Microscopy [35].

- **Delamination:** Delamination is the separation between adjacent plies, often caused by out-of-plane loads or stress concentrations at ply interfaces. Delamination significantly compromises the structural integrity of laminated composites, resulting in stiffness degradation and premature failure. Delamination is frequently observed in composites subjected to cyclic loading or impact. We can distinguish different modes of delamination propagation depending on the mode of stress of the sub-laminates on both sides of the crack:
    - Opening mode or mode I (Fig. 7.a): It is characterized by the spacing of each sub-laminate. Locally, the crack propagates under the effect of a tensile loading at the crack tip.
    - Straight slip mode or mode II (Fig. 7.b): For this configuration, the two sub-laminates slip relative to each other in the direction of propagation. Thus, the crack propagates by 1-3 shear of the interface.
    - Screw sliding mode or mode III (Fig. 7.c): For this last mode, the sliding of the sub-layers is

done in the direction normal to the propagation. It is therefore a tearing of the interface.

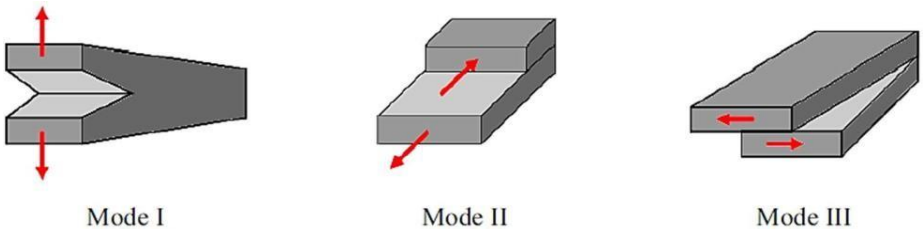

Fig. 7. Delamination opening modes [36].

Delamination alters the laminate's ability to resist out-of-plane stresses, propagating under repeated loading. The interplay between delamination and other mechanisms, like matrix cracking, reinforces the need for multiscale modeling to predict and mitigate damage.

Many factors influence the appearance and evolution of the different damage mechanisms. These factors can be the type of stress (static/fatigue) [37], the direction of loading [38], the type of stacking, the temperature, the humidity, the manufacturing process [39]. The objective of this study is to analyze the mechanical behavior of laminated composites under different loading types (monotonic, cyclic) and also under impact.

- **Interlaminar shear failure:** Interlaminar shear failure occurs due to shear stresses between layers, particularly in regions near stress concentrations, such as edges or holes. This mode of failure is worsened by matrix cracking and fiber/matrix debonding, leading to delamination between plies [40].

3.3. Multiscale characterization under monotonic loading (from quasi-static to fast dynamic)

Under quasi-static loading conditions, the damage in composite materials develops gradually, beginning with the formation of matrix cracking. As the load magnitude increases, the density of matrix cracks intensifies, resulting in fiber-matrix debonding and ultimately, delamination. When damage propagates across layers and reaches the interface, delamination occurs, and fibers begin to break, thereby transferring the load to adjacent fibers. When the fibers are unable to support the load, the material will ultimately fail. This phenomenon is particularly evident in components subjected to loading parallel to the fiber axis, where the behavior is predominantly linear elastic until the point of fiber rupture. In contrast, tensile stresses applied perpendicular to the fiber direction result in damage to the matrix and the formation of micro-fissures at the site of defects. The failure mode is determined by the strength of the bond between the fiber and the matrix. The degree of stress experienced by the matrix and fibers depends on their orientation relative to the stress axis, resulting in the emergence of different damage modes. For instance, quasi-static tensile tests on carbon/epoxy composites

demonstrate that the behavior along the fiber axis is linear and brittle, whereas transverse loading induces nonlinear behavior due to matrix viscoelasticity and fiber slippage. The gradual accumulation of matrix fissuration and fiber-matrix decohesion results in a degradation of the material's elastic properties, particularly in shear loading, where the behavior is highly nonlinear [41,42]. Several authors have demonstrated that fiber rupture occurs at the conclusion of the test [43:46]. When subjected to tension perpendicular to the fibers (in the transverse direction), only the matrix and material interfaces are damaged, leading to the development of micro-fissures at the defects. The strength of the fiber-matrix bond then determines the type of fissure that propagates and causes the component to fail. When under tension with stress deviating from the fibers, both the matrix and the fibers are consistently stressed. The occurrence of damage modes then relies on the orientation of the fibers relative to the stress axis. From a macroscopic perspective, the behavior of unidirectional laminates is highly anisotropic. The behavior varies depending on the loading direction in relation to the fibers, and is not necessarily linear [47]. Brunbauer et al [48] conducted quasi-static tensile tests on a carbon/epoxy composite, exhibiting the behavior at 0°, 45°, and 90° for the unidirectional laminate as depicted in Fig. 8(a) and Fig 8 (b). The behavior of a composite loaded along the fiber axis is linear and elastic, representative of the fiber behavior, and the failure is considered brittle. In the transverse direction, the behavior is less linear due to the viscoelasticity of the matrix and fiber slippage. Matrix fissuring and fiber-matrix decohesion significantly degrade the elastic properties. Under shear loading, the behavior is highly nonlinear [47].

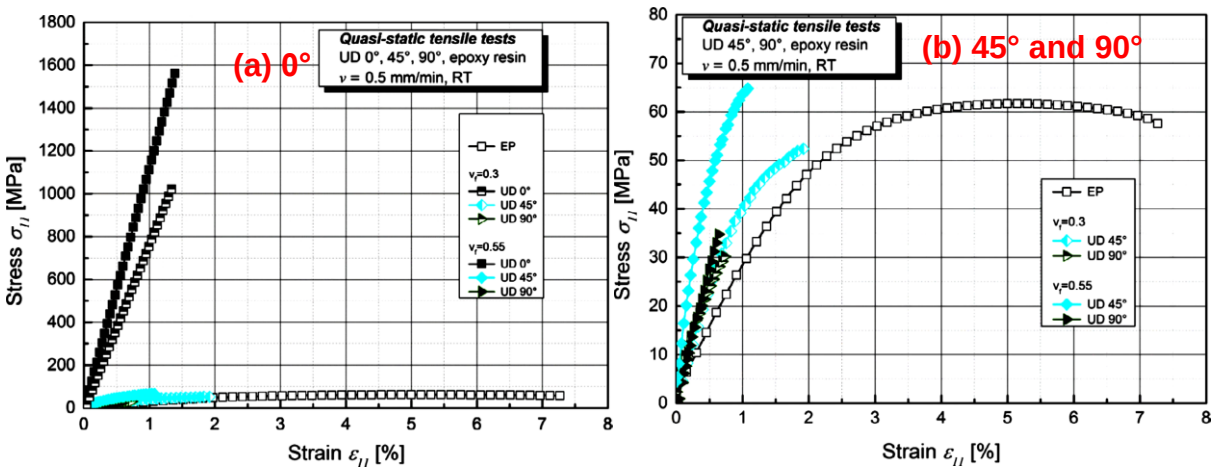

Fig. 8. Axial stress-strain curves for a carbon/epoxy laminate loaded along 3 fiber directions [48].

Under dynamic or impact loading conditions, the behavior of the laminate can differ significantly from its behavior under quasi-static conditions. The behavior described is crucial in industries like aerospace and

automotive, where materials are exposed to sudden forces such as impacts or explosions. When these materials are subjected to dynamic loading, the inertial effects hinder the redistribution of stress within the laminate, leading to localized damage. At the same time, the matrix becomes brittle, accelerating the initiation of damage [49,50,51]. The main damage mechanisms include matrix cracking, fiber breakage, fiber/matrix debonding, delamination, and interlaminar shear failure. Matrix cracks typically start at stress concentrations and spread quickly, compromising the transfer of loads between fibers. This is followed by fiber breakage due to high local stresses, as well as debonding caused by the mismatch in strain rate between fibers and the matrix, further weakening the structural integrity. Delamination weakens the composite by reducing stiffness and promoting further failures like fiber breakage and matrix cracking. Interlaminar shear failure, resulting from shear stresses at ply interfaces, leads to delamination and ply separation, especially during impact events. The damage progresses through stages, starting with crack initiation, followed by propagation, fiber failure, and ultimately catastrophic failure as delamination and shear failure spread. The strain rate significantly affects these mechanisms, with higher rates leading to more brittle failure. According to Zhu and Choi's research in 2010, laminated composites subjected to dynamic loading have lower energy absorption capacity and damage initiation occurs much earlier compared to quasi-static loading. Their study also suggests that the matrix's strain rate sensitivity is crucial in determining the overall failure of the laminate [52].

Experimental methods such as drop-weight impact tests and split-Hopkinson pressure bars, along with numerical models like Finite Element Analysis (FEA) and Cohesive Zone Models (CZM), help in predicting damage progression and offer valuable insights for designing impact-resistant composite structures. However, translating laboratory results to real-world applications remains challenging, especially in predicting long-term performance under repeated dynamic loads and varying environmental conditions. Understanding these damage mechanisms is crucial for developing resilient composite structures for high-performance applications.

3.4. Multiscale characterization under cyclic loading

Laminated composites, such as carbon fiber-reinforced polymers (CFRPs), undergo intricate damage processes when subjected to cyclic loading. Prolonged stress or strain leads to progressive damage accumulation, primarily through matrix cracking initiated at stress concentrations like voids, inclusions, or fiber/matrix interfaces early in the fatigue process. As cyclic loading persists, these cracks propagate, compromising the matrix's ability to transfer loads between fibers, ultimately leading to fiber breakage, especially in plies aligned with the loading direction. Another critical mechanism is fiber/matrix debonding, which weakens the bond between fibers and the matrix, accelerating damage accumulation and exacerbating

matrix cracking and fiber failure. Delamination, the separation between layers of the laminate, is a particularly damaging failure mode under cyclic loading, significantly reducing the composite's stiffness and strength. These damage mechanisms interact and evolve over time, resulting in progressive stiffness degradation, a key indicator of fatigue life. Degradation rate is influenced by factors such as fiber orientation, ply stacking sequence, load amplitude, and environmental conditions like temperature and humidity. For example, cross-ply laminates are more prone to delamination, while unidirectional laminates are more susceptible to fiber breakage. Environmental conditions, such as high humidity, can further accelerate matrix cracking and delamination [53:55].

The experimental investigation focused on the fatigue-induced damage of laminates. Fig. 9 [56,57] illustrates the sequential stages of this process: matrix cracking, fiber/matrix detachment, and fiber failure. The diagram depicts the evolution of damage relative to the fatigue life of the periodically loaded UD cross-laminated composite. This process can be categorized into three phases: rapid damage accumulation, followed by a phase of steady and slow damage accumulation, and ultimately a phase of accelerated damage accumulation. During the early stages of fatigue, microcracks in the matrix begin to emerge and extend into matrix cracks along the off-axis fibers under tensile loading. As cyclic loading continues, matrix cracks develop in other layers, gradually increasing in density. The cracking process persists until the spacing or size between cracks in each ply reaches an equilibrium or saturation level, known as the Characteristic Damage State (CDS). At this point, stress redistribution limits the initiation of new cracks. As the fatigue process continues, delamination initiation occurs due to high interlaminar stresses caused by the free edge effect and by matrix cracks and fiber failure within the laminate. Subsequently, delamination gradually spreads with continued cyclic loading.

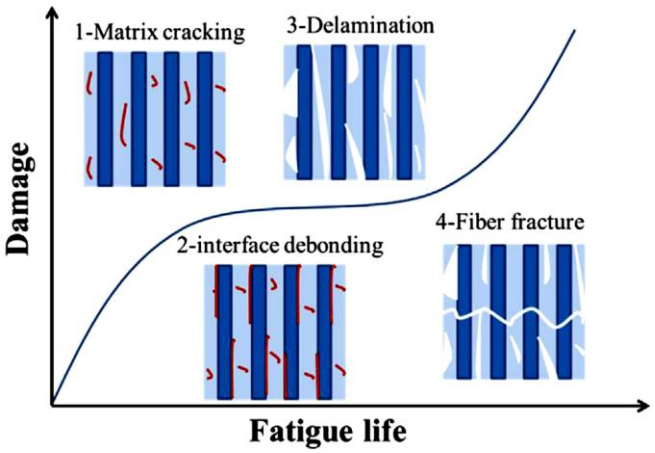

Fig. 9. General damage process of a laminate under quasi-static, tensile-tensile fatigue loading [57].

During cyclic loading, the occurrence of premature fiber failure can be attributed to the formation of matrix cracks and interfacial disbands, which in turn give rise to the development of stress concentrations. In the initial phase, matrix cracking is the primary phenomenon, followed by delamination in the intermediate phase. Ultimately, multiple damage modes accumulate until the laminate fails. This sequence of events bears resemblance to the damage mechanisms observed in quasi-static loading, though the process occurs at a slower pace in fatigue. The results of the X-ray imaging indicate that as the load increases, the number of matrix cracks appears earlier in fatigue tests [58,59]. The findings of Brunbauer et al. [48] indicate that carbon/epoxy composites reach a fatigue endurance limit at 60% of their tensile strength at 5 million cycles when loaded at 0°. Additionally, off-axis fiber stresses have been observed to cause accelerated damage accumulation. This underscores the intricate and multifaceted nature of damage modes in composite materials, many of which occur at the microscopic level and are not discernible to the unaided eye.

Numerical models like Finite Element Analysis (FEA) and Cohesive Zone Models (CZM) simulate fatigue damage progression, showing good agreement between experimental results and model predictions. However, translating laboratory findings to real-world applications remains challenging, especially in environments with complex loading conditions. Ongoing research aims to optimize composite material designs and improve fatigue resistance in high-performance applications such as aerospace, automotive, and renewable energy.

4. Characterization of dynamic residual properties under cyclic loading

Carbon fiber-reinforced polymer (CFRP) pressure vessels are widely utilized in high-pressure applications, such as hydrogen storage in the automotive and aerospace sectors. These vessels boast an outstanding strength-to-weight ratio, exceptional durability, and resistance to environmental degradation. Yet, throughout their operational lifespan, these pressure vessels experience dynamic and cyclic loading conditions, such as impact events or repeated pressurization and depressurization cycles. It is crucial to comprehend the post-dynamic residual fatigue behavior of these vessels in order to guarantee their long-term safety, reliability, and performance. The behavior of carbon fiber composite pressure vessels under dynamic loading has been extensively researched, with a focus on the impact of high-strain events on their structural integrity. However, when subjected to cyclic loading following a dynamic event (e.g., an impact or blast), the vessel's fatigue behavior and residual strength can degrade significantly, leading to a reduction in its overall fatigue life.

4.1. Post-dynamic residual fatigue behavior

Following a dynamic event, the residual fatigue performance of CFRP pressure vessels commonly deteriorates, resulting in decreased residual strength, stiffness, and fatigue life. Key factors influencing post-dynamic residual fatigue behavior include:

- Damage Accumulation, which refers to the continued propagation of damage incurred during the dynamic event (such as matrix cracking, fiber breakage, and delamination) under cyclic loading, leading to reduced stiffness and load-bearing capacity.
- Stiffness Degradation, where the vessel's stiffness decreases as cyclic loading progresses due to the progressive propagation of cracks and delamination, serving as an indicator of the extent of damage accumulated during dynamic and cyclic events.
- Residual Strength, which denotes the vessel's strength after experiencing dynamic loading followed by cyclic loading, and demonstrates the vessel's reduced ability to withstand subsequent loads as damage mechanisms continue to evolve.

The fatigue behavior of impacted specimens is relatively less studied in the literature. Atpresent, the service loading level remains below the material fatigue threshold. Nevertheless, knowledge of the fatigue behavior of impacted specimens will be more relevant when we wishto raise the value of these allowances. In the context of damage tolerance, the question iswhether damage can lead to failure under cyclic loading.

Gerharz and colleagues [60] conducted a study on the progression of impact-induced damage under fatigue loading. They distinguished two stages of progression. The first stage is characterized by a minimal increase in the magnitude of the blistering deflection, keeping delamination propagation within the damage envelope. The second stage occurs in the final 10% of the specimen's service life, during which delamination rapidly spreads perpendicular to the loading direction. Melin et al [61] observed buckling on both sides of the specimen during FAI tests, confirming some of Gerharz et al.'s findings. Additionally, they demonstrated that altering the tensile stress had minimal impact on the service life, while the compressive stress promoted delamination propagation. The interfaces on the non-impacted face were the most affected. Mitrovic and colleagues [62] conducted fatigue tests on AS4/3501-6 carbon/epoxy specimens that were initially impacted with BVID (Barely Visible Impact Damage). The progression of damage was monitored using X-ray radiography (Fig. 10). During tension-compression (R = -1) testing, no propagation of impact damage was observed up to 50% of the CAI stress. The failure of these specimens is caused by the spread of edge-initiated damage. In compression-compression tests, no propagation was observed up to 60% CAI load.

However, at higher loads (70% and 80%), significant propagation of impact delamination was observed, beginning after 100 cycles at 70% and reaching the specimen edges at around 10,000 cycles. This propagation occurs only at the first or second non-impacted face interface, driven by the buckling of this group of folds in the loading direction. Aboissière [63] also noted propagation of impact damage in FAI tests, where 4 mm thick HTA/EH25 carbon/epoxy material specimens of 100 x 100 mm^2 were subjected to a 25 J impact and then stressed to around 50% of their breaking load in CAI with an R=1 ratio. Ultrasound and X-ray damage monitoring revealed propagation of matrix cracking and delamination, predominantly at folds ± 45° to the stress direction. As failure approaches, cracks are present throughout the specimen, leading to fracture after several thousand cycles (250,000 to 500,000 cycles) when delamination cover the entire free surface of the specimen.

Aboissière [63] also documented the spread of impact-induced damage in FAI tests. The tests were conducted on 4 mm thick specimens measuring 100 x 100 mm^2 of the HTA/EH25 carbon/epoxy material. Following a 25 J impact, the specimens were exposed to a stress equivalent to around 50% of their ultimate load in CAI with an R=1 ratio. Damage is monitored using ultrasound and X-ray techniques, revealing the propagation of matrix cracking and delamination. Initially, matrix cracking occurs primarily at ± 45° folds with respect to the direction of stress. If the 0° folds are near the surface, delamination spreads from their interface due to local buckling. As failure approaches, cracks are observed throughout the specimen, even at the 0° folds. Fracture occurs after several thousand cycles (250,000 to 500,000 cycles) when delamination covers the entire free surface of the specimen.

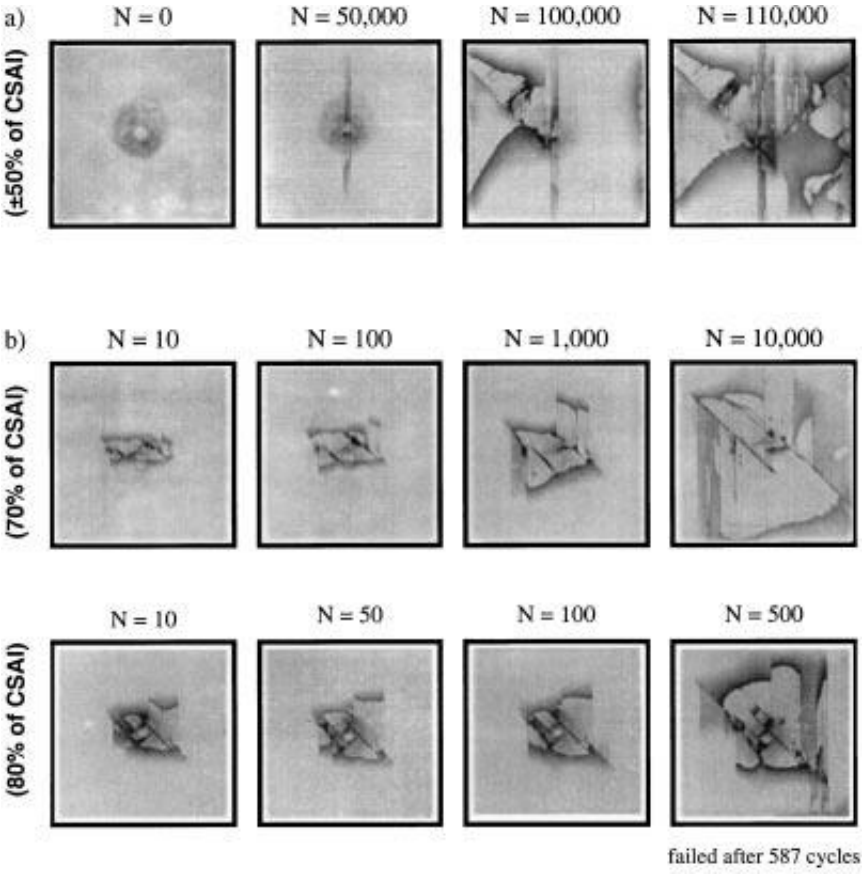

Fig. 10. Fatigue impact damage propagation (a) tension/compression, (b) compression/compression (draping [62]).

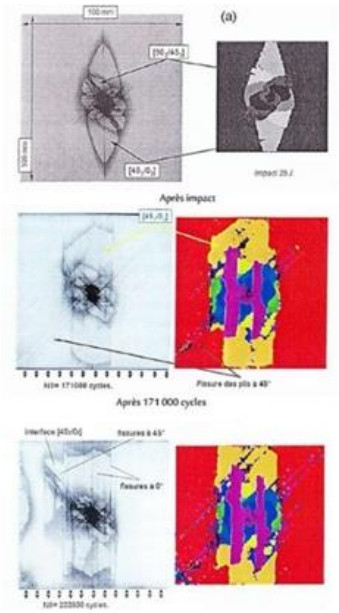

Fig. 11. Impact damage monitoring under fatigue loading (R= -1) [63].

4.2. Experimental methods to characterize post-dynamic residual fatigue

Impact damage tolerance is a crucial concern in the realm of composite structures. Initially, researchers focus on evaluating the damage and determining the remaining mechanical properties post-impact. The assessment can be carried out through quasi-static Compression After Impact (CAI) tests or dynamic biaxial fatigue tests. Numerous studies in both academia and the industrial sector have delved into the static behavior of monolithic composite structures in the presence of impact damage. These investigations have highlighted a substantial decrease in residual strength, particularly under compression. Delamination leads to the creation of multiple sub-laminates, significantly reducing the buckling limit stress. However, the loss of residual strength is less pronounced under tension since fiber breakage remains localized during impact. Additionally, Fig. 12 contrasts the residual tensile and compressive strengths of impacted composite plates.

CAI testing (Fig. 13) is carried out to evaluate the reduction in compressive strength of impacted samples. As per ASTM D7137/D7137M [65], it is noted that the test outcomes cannot be directly applied to an actual structure. The residual strength is heavily influenced by the size and boundary conditions of the impacted plates. Nonetheless, the results can be utilized for comparing the strength of different materials or for investigating failure mechanisms in laboratory settings. When it comes to boundary conditions, the sample is inserted into a device designed to restrict its overall buckling.

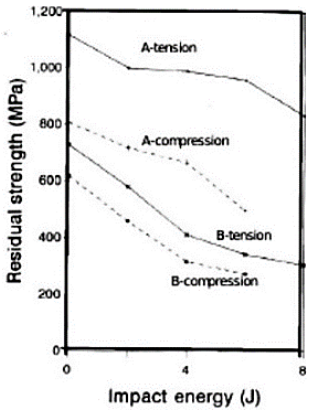

FIG. 12. COMPARISON OF RESIDUAL TENSILE AND COMPRESSIVE STRENGTH FOR AN IMPACTED LAMINATED COMPOSITE [64].

The arrangement is also specified by standards AITM 1-0010 [66] for Airbus and BSS 726 for Boeing. As for the dimensions, the specimen is supported on the longitudinal edges by knife-edge supports positioned 4

mm from the edges to prevent any out-of-plane movement, while allowing rotation. Moreover, the specimen's transverse edges are more or less recessed. The contacting face of the support is flat, introducing a certain degree of rotational rigidity at the edge, rather than embedding. Given that the loading force is applied on the flanks of the transverse sides, it is crucial that these two sides are perfectly parallel to limit parasitic forces that could affect the uniformity of the loading. Furthermore, proper alignment of the transverse supports is essential to avoid bending caused by misalignment of the loading plane with the specimen's mean plane.

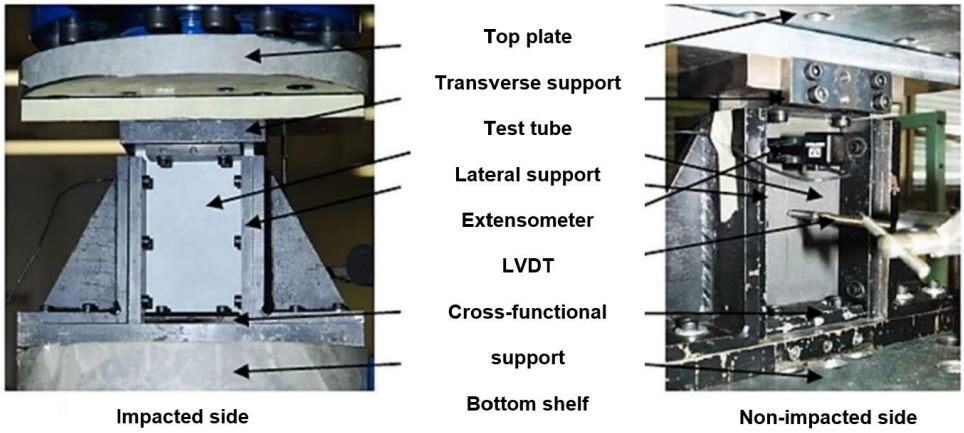

Fig. 13. Set-up for a CAI test [67].

In the literature, two trends have been recognized as explanations for failure mechanisms. The first one links the failure of specimens to buckling phenomena, while the second one associates it with the unstable propagation of impact damage. Buckling is caused by the delamination of the surface during impact. When the delamination created during impact involves large surface areas, the laminate is split into several independent "sub-laminates". The flexural strength of each "sub-laminate" is consequently lower than that of the intact laminate.

Hence, delamination reduces the buckling limit stress of the laminate. Reis and Freitas focus on the propagation of impact damage during CAI testing. They present impact and CAI test results for two materials, T800/5245C and IM7/977-2. In most cases, specimen failure is connected to global buckling. For low impact energies, blistering representing local buckling occurs, with each face flexing outwards. Other authors link failure to the propagation of delamination and fiber breakage caused during impact. During compression, micro-buckling of the fibers leads to local propagation of the delamination created during impact.

The delamination region around the point of impact expands laterally towards the edges of the specimen. This local delamination progresses in stages, slowly at the start of loading and rapidly as the ultimate load is approached. These phenomena were observed by Starnes et al. with post-mortem photographs of T300/5208

quasi-isotropic laminated composites. According to the author, delamination propagation leads to a loss of compressive stiffness, resulting in global buckling. Delamination is therefore the mechanism that controls the residual strength of impacted composite structures subjected to compressive loading.

This scenario was observed on carbon/epoxy specimens by [67]. The evolution of compressive stress as a function of imposed displacement is shown in Fig. 14. A linear compressive loading is observed, accompanied by a slight increase in plate thickness due to the opening of delamination. Failure of the specimen is linked to global buckling. The concentration of deformation at the point of impact extends towards the free edges, as illustrated in image correlation 1 to 7 in Fig. 12. When this strain reaches the compression strain at failure, a crack propagates leading to specimen failure, as shown in the lower photographs 4 to 7 in Fig. 14.

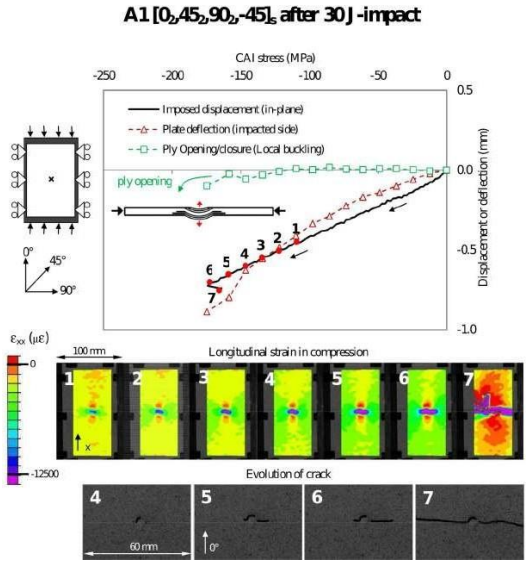

Fig. 14. Imposed stress-displacement curve and strain images during a CAI test on aquasi-isotropic laminate [67].

4.3. Damage state measurement techniques

In the realm of laminated composites, especially those utilized in high-pressure hydrogen storage tanks, it is essential to comprehend the progression of damage over time under different loading conditions. The methods for identifying and describing damage have a crucial impact on anticipating the mechanical behavior, resilience, and breakdown of these materials. This article delves into the sophisticated techniques used to measure damage states in composites research, such as infrared thermography, X-ray tomography, acoustic emission, and digital image correlation.

4.3.1. Infrared thermography

Infrared Thermography (IRT) is a non-destructive evaluation (NDE) technique used to detect variations in heat within composite materials in order to identify damage. When composites undergo mechanical stress, localized heat is produced due to matrix cracking, fiber-matrix debonding, or frictional sliding. IRT captures this thermal response in real-time, enabling researchers to monitor damage initiation and progression. One advantage of IRT is its high sensitivity to thermal changes, allowing for swift inspection of large areas. For instance, Alves et al. (2014) [68] utilized IRT to monitor fatigue damage in carbon fiber-reinforced polymers (CFRPs) and established a correlation between heat generation and damage development. Nonetheless, IRT has limited depth penetration, which diminishes its effectiveness in detecting subsurface damage in thicker laminates. Thermography works by capturing thermal images using specialized equipment within a specific spectral range, often in the infrared spectrum. In numerous non-destructive testing applications, the components being inspected do not naturally emit heat. To tackle this issue, active infrared thermography involves introducing heat into the sample and analyzing its thermal response to identify defects. This is achieved by exposing the component to a heat source using either halogen or flash lamps, depending on the requirements (as depicted in Fig. 15) [69]. Anomalies in the recorded heat distribution can reveal defects such as delamination, cracks, and porosity. Processing algorithms are then employed to highlight these defects, taking into account factors like excitation source, material properties, and defect size. While effective, active IRT requires precise calibration to align with the physical and thermal characteristics of the part for accurate defect detection.

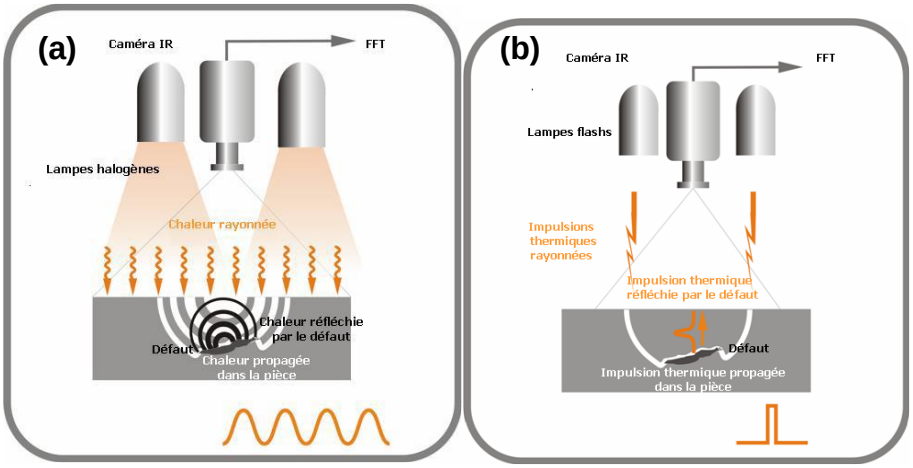

Fig. 15. Types of thermal excitation for active thermography: (a) Halogen lamp excitation device, (b) Flash lamp excitation device [69].

4.3.2. X-ray tomography

X-ray computed tomography (X-ray CT) is a sophisticated non-destructive evaluation method widely used to capture detailed internal images of composite materials. This technique produces three-dimensional reconstructions of the composite's internal structure, making it easier to identify important damage mechanisms like matrix cracking, fiber breakage, and delamination. High-resolution X-ray CT enables a detailed visualization of microstructural damage, measurement of void content, and monitoring of crack propagation within laminated composites. In applications such as composite pressure vessels, X-ray CT has been essential in evaluating damage caused by impacts and fatigue loading. Its non-invasive nature allows for repeated inspections of the same specimen, thus supporting the analysis of damage progression over time. For example, Zhang et al. (2019) [70] effectively used X-ray CT to identify delamination and matrix cracking in carbon fiber composites, showcasing the technique's effectiveness in assessing the damage state. The operational principle of tomography involves analyzing the interaction of X-ray beams with matter from multiple angles, enabling 3D reconstruction based on radiographic data (Fig. 16). During this process, X-rays are emitted from a source and pass through the object, while detectors on the opposite side capture the transmitted radiation. The object is rotated incrementally, resulting in the acquisition of hundreds to thousands of radiographs in varying gray scales. These 2D projections are then processed using advanced algorithms to reconstruct the object's internal volume and identify defects. Despite its precision and comprehensive imaging capability, X-ray CT is inherently time-consuming and necessitates extensive data processing, limiting its utility for rapid inspection in industrial environments. Additionally, like infrared thermography, X-ray CT requires complex image processing techniques to accurately characterize internal defects.

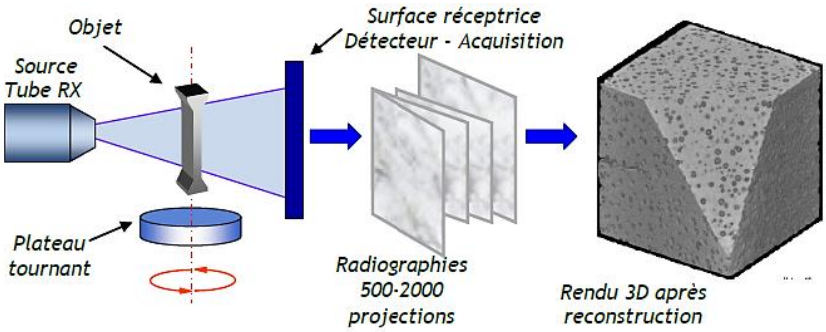

Fig. 16. Principle of X-ray tomography [71].

4.3.3. Acoustic Emission (AE)

Acoustic Emission stands as another widely utilized technique for real-time damage monitoring. It detects elastic waves produced by the sudden release of energy during damage events, such as matrix cracking, fiber

breakage, or delamination. AE sensors positioned on the surface of the composite capture these waves, enabling the identification and localization of damage within the material. AE proves to be sensitive to a broad spectrum of damage mechanisms, and its application in composites has been extensive. For instance, Lopresto et al. (2010) employed AE to analyze the damage progression in glass fiber-reinforced composites under tensile and fatigue loading [72]. This technique offers the advantage of real-time monitoring but necessitates skilled interpretation of the acoustic signals and lacks the direct visualization of damage provided by X-ray CT.

4.3.4. Digital Image Correlation (DIC)

Digital Image Correlation (DIC) is an optical measurement method utilized for analyzing the surface strain field of composites subjected to mechanical loading. This technique entails capturing high-resolution images of the composite's surface before and during deformation, allowing researchers to determine the strain distribution and pinpoint regions of localized deformation, often indicative of damage initiation sites. DIC is particularly valuable for detecting the emergence of matrix cracks and delamination. Sikarwar et al. (2016) utilized DIC to assess the strain field in CFRPs, demonstrating its effectiveness in identifying surface crack development [73]. However, DIC is limited to observing surface damage and does not offer insights into internal damage, such as matrix cracks deep within the laminate.

4.3.5. Ultrasonic Testing

Ultrasonic testing is the process of sending high-frequency sound waves into composite material to identify internal flaws. Variations in the reflected ultrasonic waves can indicate the presence of damage, such as delamination or voids. By producing detailed images of the internal structure of the composite material, ultrasonic C-scans are effective for locating delamination and assessing their size. The reliability and relatively straightforward application of ultrasonic testing make it widely used in various industries. For instance, Garcia et al. (2018) utilized ultrasonic testing to evaluate delamination in impact-damaged composite panels, confirming its effectiveness in detecting damage [74]. However, the accuracy of ultrasonic measurements is dependent on the material's thickness and the resolution of the equipment. Each approach to evaluating damage states in laminated composites has its own strengths and weaknesses. Infrared thermography and digital image correlation enable real-time monitoring and strain analysis, while X-ray computed tomography and ultrasonic testing offer insights into the internal structure and damage mechanisms of composites. Acoustic emission, with its sensitivity to various damage modes, proves to be a valuable tool for real-time monitoring, particularly during dynamic loading scenarios. Combining these techniques is often necessary to

develop dependable and damage-resistant hydrogen storage systems, in order to gain a comprehensive understanding of damage mechanisms at various scales. Future research in this field may focus on integrating these techniques for multi-modal damage characterization, ultimately enhancing the predictability and safety of composite structures in critical applications.

4.4. Post-residual impact approaches

Numerical techniques have been extensively investigated for their ability to predict impact damage tolerance in composite materials. In the early stages, prior to the development of advanced impact models, researchers estimated residual compressive strength by observing the behavior of delaminated laminates. These initial approaches focused on computing the critical buckling loads in the presence of delamination. For instance, Dost et al. [75] utilized analytical methods to determine the critical load, while Shivakumar and Withcomb [76] used similar techniques in conjunction with finite element analysis to calculate buckling eigenmodes. Subsequently, fracture mechanics emerged as a crucial tool for forecasting the initiation of impact damage propagation. Soutis and Curtis [77] adapted a model originally intended for predicting fiber failure at hole edges to investigate bending strip failure in compression following impact scenarios [78]. Similarly, De Moura et al. [79] and Suemasu et al. [80] utilized interface elements to examine the influence of impact-induced delamination on residual compressive strength. Their research revealed that delamination propagation directly resulted in a decrease in compressive strength, ultimately leading to the ultimate failure of the specimen (Fig. 17).

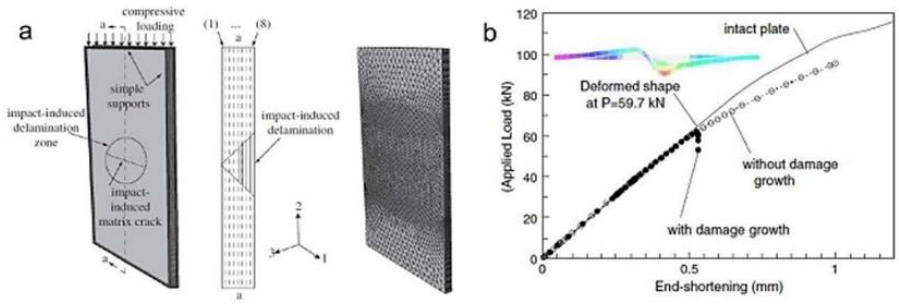

Fig. 17. Modeling CAI with artificial damage [80] [81].

Several methods exist for estimating the residual Compressive After Impact (CAI) strength, each with varying levels of accuracy. However, they cannot be categorized as "predictive models" because they rely on prior knowledge of the impact damage extent. Furthermore, due to the imprecise representation of impact damage and the exclusion of certain potential damage modes, our comprehension of the failure mechanisms in impacted specimens is still incomplete within these models. Despite the development of impact models by

various researchers, a fully integrated modeling of impact followed by CAI is still not well established. It is important to note that only a handful of studies, such as those carried out by Gonzalez et al. (Fig. 18) [82] and Rivallant et al. (Fig. 19) [83], have tackled low-speed impact. Both groups employed comprehensive models capable of simulating matrix cracking, delamination, and fiber breakage. While Gonzalez et al.'s model produced results that closely aligned with experimental data, their focus was mainly on overall comparisons rather than the specifics of failure mechanisms. In contrast, Rivallant et al.'s study emphasized the importance of fiber breakage propagation in determining residual strength, offering deeper insights into the underlying failure processes.

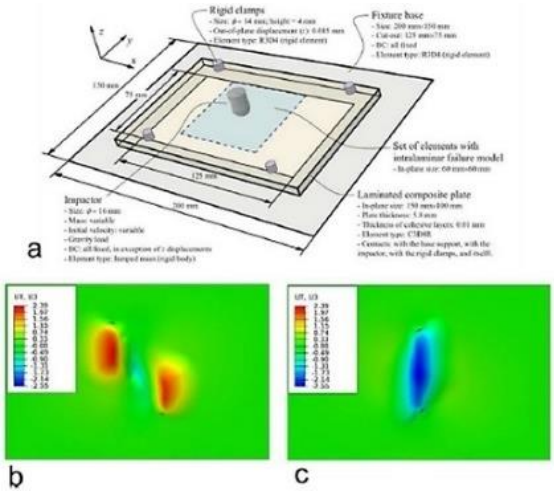

Fig. 18. Impact and CAI model [82]: a) impact model, b) out-of-plane displacement field onimpacted face and c) non-impacted.

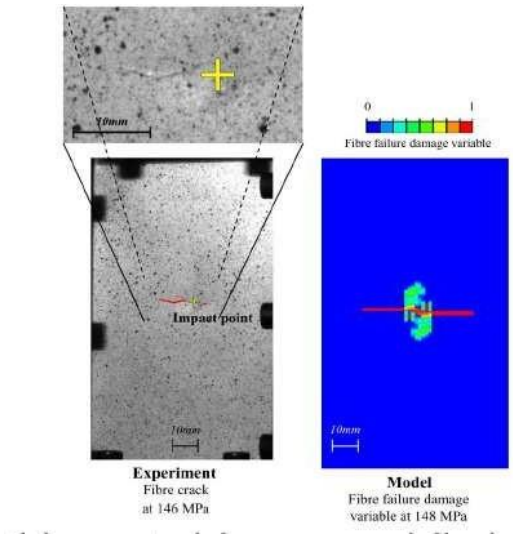

Fig. 19. Monitoring crack propagation by fiber breakage during CAI [83].

5. Different scales in the composite ±θ

In the analysis and modeling of composite materials, particularly those produced through filament winding processes, it is essential to recognize the various scales at which mechanical behavior, deformation, and damage take place [84]. This multi-scale approach is crucial for accurately capturing the material response under different loading conditions and guiding the selection of suitable modeling tools, behavior laws, and boundary criteria. When dealing with composites consisting of ±θ layers, four primary scales can be distinguished [85] (as depicted in Fig. 20).

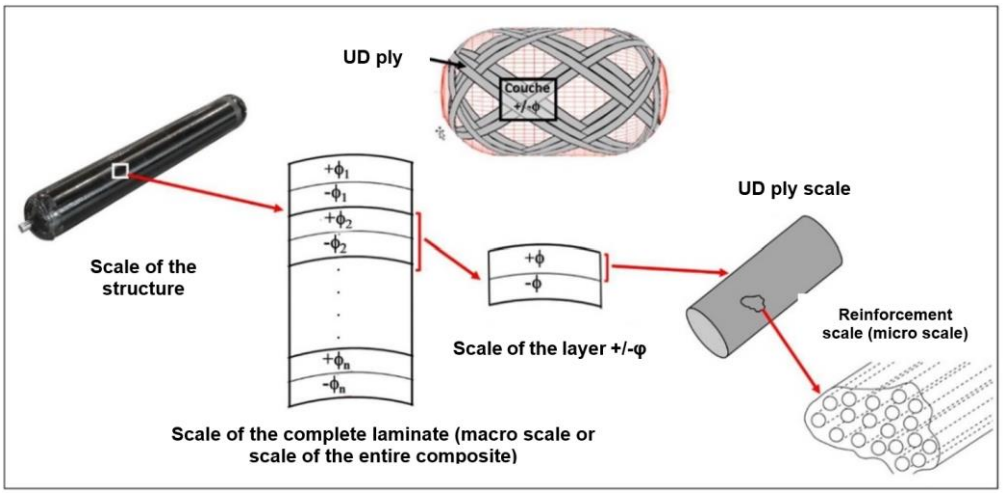

Fig. 20. Different scales of the composite.

5.1. The Entire Composite Structure (Macro Scale)

At the macro scale, the entire composite structure, with all the ±θ laminated layers, is considered as a unified entity in order to anticipate its overall response to external forces. This level of modeling is crucial for comprehending the overall behavior of the composite material, encompassing stress, strain, and deformation when exposed to various operational conditions like pressure, impact, and fatigue. Finite Element Analysis (FEA) or Finite Element Methods (FEM) are widely utilized tools at this level to replicate stress-strain behavior and pinpoint failure modes [86] The stacking sequence and fiber orientation embedded in the composite have a significant impact on its mechanical properties, such as stiffness and strength [91]. Furthermore, the arrangement of the ±θ layers and the boundary conditions imposed on the structure are pivotal in determining the composite's overall performance. Sophisticated progressive damage models, such as Hashin's failure theory, can be incorporated into FEA software to predict the initiation and propagation of damage within these

composites [88]. This comprehensive approach enables engineers to simulate and evaluate the performance of composite materials under realistic loading scenarios.

5.2. ±θ Layer (Meso Scale)

The meso scale analysis focuses on the individual ±θ layers of the composite, addressing the unique characteristics and interactions specific to each fiber orientation. This level of examination considers the impact of factors such as fiber direction, fiber/matrix interactions, and inter-laminar interfaces on the mechanical behavior of each layer [87]. Modeling at the meso scale is indispensable for understanding the response of individual layers to mechanical loading and the effects of inter-layer interactions.

The Key Aspects of Meso-Scale Modeling:

- **Layer-Specific Properties:** The modeling incorporates the specific elastic properties of each layer, which depend on the fiber orientation and matrix characteristics. Variations in stiffness and strength between layers oriented at +θ and -θ must be included in the model to accurately predict their mechanical behavior.
- **Inter-Layer Interactions:** Delamination modeling is essential at this scale to simulate the separation between layers with different fiber orientations. Cohesive Zone Models (CZMs) are often used to represent these interfaces, enabling the prediction of delamination initiation and propagation based on stress and strain conditions [88]. Effectively addressing inter-layer interactions is crucial to capture the failure mechanisms in composites.
- **Damage Mechanics:** Damage mechanisms such as matrix cracking, fiber-matrix debonding, and fiber breakage are depicted using damage evolution laws. Constitutive models at the meso scale help illustrate changes in stiffness and strength as damage accumulates, offering insight into the progressive degradation of the composite material.

By focusing on these aspects, meso-scale modeling assists in capturing the anisotropic properties of the composite and the implications of inter-layer interactions, which are critical for predicting its mechanical performance under various loading conditions.

5.3. Unidirectional Tape (UD) Scale

At the unidirectional (UD) tape scale, we examine the behavior of a single ply or layer of fibers aligned in one direction within the matrix. This scale is essential for understanding the mechanical properties of the composite material, as it isolates the influence of fiber orientation on the load-bearing capacity. By focusing on the UD tape, the elastic properties, such as the Young's modulus in both the fiber direction and transverse direction,

can be defined. Additionally, this scale aids in characterizing failure mechanisms, including fiber breakage and fiber/matrix interface decohesion [89].

Closely related to the UD tape scale is the micro-scale modeling, which delves into the material's fundamental constituents—individual fibers, the matrix, and their interfaces. This micro-scale analysis is critical for understanding how fiber/matrix interactions affect the composite's overall behavior. Micromechanical models, including the Mori-Tanaka method and Representative Volume Elements (RVEs), are used at this scale to simulate micro-cracks, fiber pull-out, and void formation [94]. The fiber/matrix interface plays a pivotal role in load transfer within the composite, and cohesive elements are often employed to simulate debonding, providing further insight into the composite's mechanical response. Together, both the UD tape and micro-scale modeling offer a comprehensive understanding of how internal microstructural features influence the overall mechanical behavior of composite materials.

5.4. Microstructure Scale (Micro Scale)

At the microstructure scale, the focus shifts to the fundamental constituents of the composite, including individual fibers, the matrix, and their interactions. This scale examines crucial factors such as the fiber/matrix interface, fiber distribution, bonding quality, and the presence of voids or defects. Micromechanical modeling at this level, including approaches like the Mori-Tanaka method and Representative Volume Elements (RVEs), helps simulate micro-cracks, fiber pull-out, and void formation [85]. The fiber/matrix interface is especially pivotal, as it plays a key role in load transfer within the composite. Cohesive elements are often used to simulate debonding at this interface, allowing for a more detailed understanding of the material's behavior [84, 90].

In addition to the micro-scale, interactions between layers and components across different structural scales have a substantial impact on the composite's mechanical properties. Important interactions include:

- Interface between Two Layers ($\pm\phi$): Delamination at this interface level significantly influences the composite's resistance to interlaminar stresses.
- Fiber/Matrix Interface: This is central to load transfer within the composite and a major focus in micromechanical modeling [87].

Effective modeling of laminated composites necessitates integrating information across different scales. Methods like homogenization help connect the micro and macro scales by deriving effective properties that can be applied in larger-scale models [89]. Numerical methods, such as Finite Element Analysis (FEA), use material laws that are tailored to the specific characteristics observed at each scale, from micro to macro [88].

This comprehensive multi-scale approach, supplemented by experimental analyses, is crucial for accurately capturing the deformation, damage, and fracture phenomena that define the mechanical response of composite materials [86].

5.5 Multi-Scale Coupling and Integration

Accurate modeling of composite materials requires integrating information across these different scales. Techniques like homogenization bridge the micro to macro scales, allowing for the effective properties derived from the microstructure to inform macro-scale simulations [89]. Nested and concurrent multi-scale modeling approaches provide comprehensive insights into damage evolution [90]. By utilizing a multi-scale approach, engineers can optimize the design of composite structures, as discussed in several studies [84,91]. Software tools like Abaqus and LS-Dyna have been used to incorporate these multi-scale methodologies, with specialized material laws designed for composites [88].

6. Mesoscopic Modeling of Delamination and Fiber Failure in Composite Materials

At the mesoscopic scale, delamination is modeled by fracture mechanics. The most widely used technique in the literature consists of defining interlaminar cohesive elements. This technique is well suited to the study of delamination since the latter can only occur at the interface between two plies. The propagation zone is therefore known in advance and the choice of discretizing at the interlaminar level becomes natural. In addition, the technique makes it possible to limit the dependence on the mesh size as well as stress concentration problems [98]. Indeed, it integrates two intrinsic parameters that define the initiation and drive the propagation of the opening. It is however important to note that the addition of cohesive elements between each fold doubles the number of degrees of freedom of the model compared to a continuous model. The behavior of cohesive zones is governed by the relationship between the initially superimposed node displacement jumps and the nodal forces calculated from a softening law (Fig. 21.). Many formulations of softening laws have been proposed in the literature: bilinear, multilinear, exponential, trapezoidal, etc.

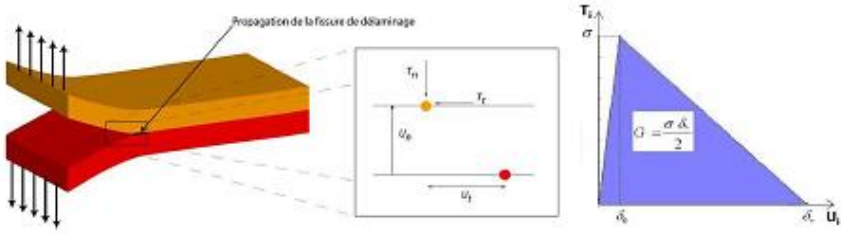

Fig. 21. Principle of a cohesive zone model [92].

Comparing several laws [89-91], Wisnom [89] showed that in the majority of cases, the form of the softening behavior had little influence on the quality (the results. It is the value of the energy restitution rate that plays the main role in the propagation of the crack. For the case of mixed propagation modes, criteria are proposed by different authors. Experimental measurement of the critical energy release rate for the three delamination modes is essential to be able to use these criteria. It is done using tests that are often standardized:

- DCB (Double Cantilever Beam) [96] test for G_{IC} measurement. This is a tensile test on two arms of a pre-cracked specimen (Fig. 22a).
- ENF (End-Notched Flexure) [97] test for G_{IIc}. This is a bending test on a pre-cracked specimen. The shear stresses will cause the crack to propagate (Fig. 22b).
- ECT (Edge Crack Torsion) [98] test for Gill c. This is a torsion test on a pre-cracked flat specimen (Fig. 22c).
- MMF (Mixed Mode Flexure) [99] test for a 1/11 mixed mode. This is a tensile test on the upper arm of a pre-cracked flat specimen. The uncracked end of the specimen is clamped (Fig. 22d).
- CT (Compact Tension) [100, 101]: The Compact Tension test is beneficial for characterizing mode I and mixed-mode toughness in laminates with pre-existing cracks. Although its use in composites is less common compared to metals, it has shown promise for evaluating interfacial toughness in advanced composite materials.
- MMB (Mixed-Mode Bending) [102, 103]: The Mixed-Mode Bending test effectively studies mixed-mode I/II delamination propagation by combining tensile and shear loading. This makes it particularly suited for analyzing delamination growth in composite structures under complex stress states.
- CLS (Cracked Lap Shear) [104, 105]: The Cracked Lap Shear test is widely utilized to determine interlaminar fracture toughness under mode II shear conditions. This method is extensively employed

in the aerospace and automotive industries for evaluating the performance of bonded joints and layered composite systems.

- 4PB (Four-Point Bending) [106]: The Four-Point Bend test, often used as an alternative to the ENF test, is instrumental in assessing mode II fracture toughness. Its design minimizes stress concentrations near loading points, offering enhanced reliability and control over shear loading conditions.
- Arcan Test [107]: The Arcan test setup allows precise control of mixed-mode loading ratios by adjusting the angle of the applied load. This makes it especially useful for simulating real-world stress states in composite structures and examining their failure mechanisms under varied loading conditions.

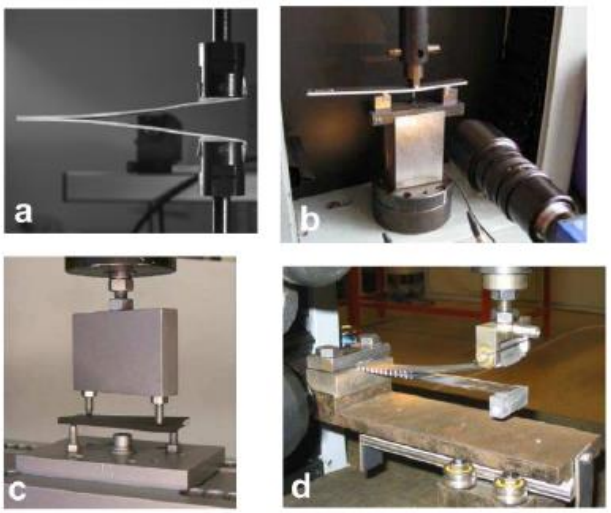

Fig. 22. Test setup for measuring the critical energy release rate, 5A° DCB (mode I) [97] (b) ENF (mode Ⅱ) [97], (c) ECT (mode Ⅲ) [100], (d) MMF (mixed mode I and Ⅱ) [101].

Several authors [111, 112, 113, 114] choose to use cohesive elements to model multiple delamination occurring during impact or quasi-static bending. The technique has the advantage of not requiring a pre-crack and manages both initiation and propagation. Fig. 23. shows some simulation results of delamination during an impact.

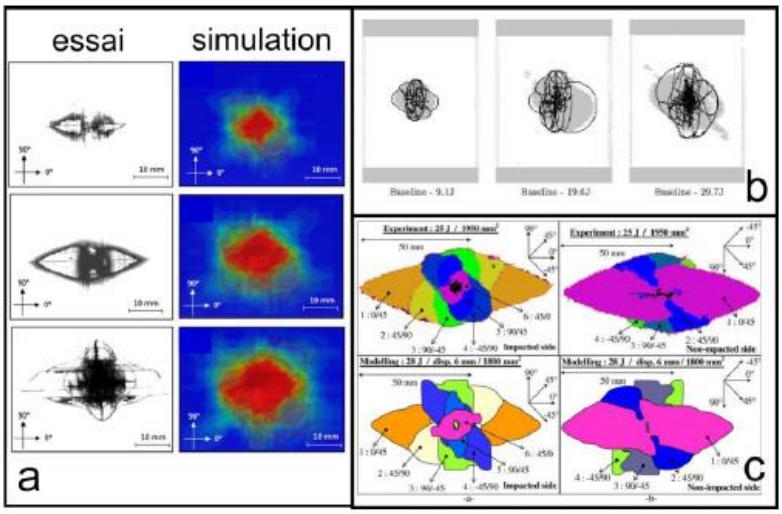

Fig. 23. Modeling of impact delamination. (a) [113], (b) [115], (c) [116]

As illustrated in Fig. 23, the level of delamination correlation varies greatly between models. This difference is largely due to the way matrix cracks are modeled. As described in the experimental section, cracking plays an important role in the initiation and propagation of delamination. There are two modeling approaches: the first, the most widespread, uses continuous damage mechanics. The second, more recent method uses intra-laminar cohesive elements to simulate matrix cracking (Fig. 24).

During impact, cracks initially appear diffusely. Large cracks then appear and can thus be studied in the context of fracture mechanics. This second approach is all the more justified since the failure mode of a laminate involves matrix cracking and delamination. This is the case in particular for a specimen containing folds at ± 45° subjected to tension (Fig. 25).

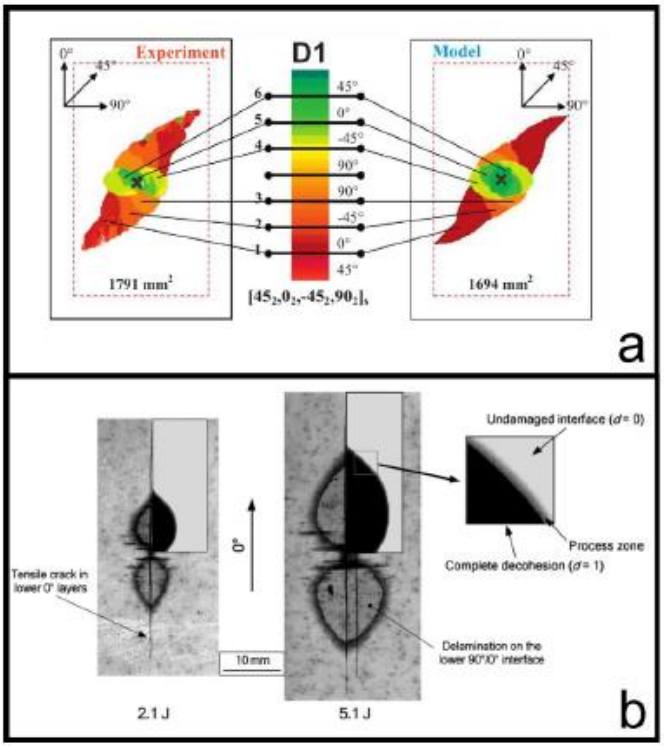

Fig. 24. Modeling of impact delamination in the presence of intra-laminar cohesive elements [118], [119].

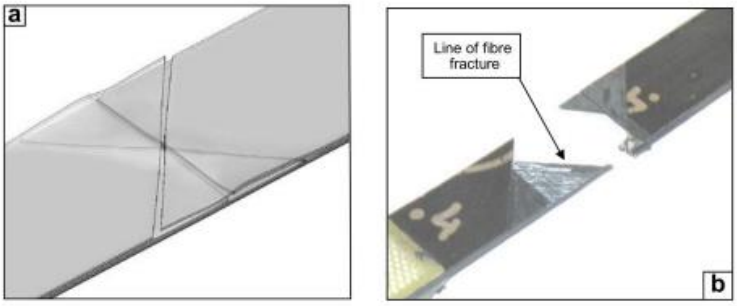

Fig. 25. Modeling of intralaminar cracks with cohesive elements [120].

Several authors [119, 121, 122, 123] have highlighted the importance of taking into account the discrete nature of cracking in the simulation and thus the cracking-delamination coupling. On a quasi-static impact and indentation simulation, Aoki et al. [124] found a better correlation of delamination by adding intra-laminar interface elements. Also, Aymerich et al. [125] and Hongkarnjanakul et al. [126] presented excellent results and managed to predict the elliptical shape of delaminations by using cohesive elements to model matrix cracking. However, the use of intra-laminar cohesive elements has some limitations. First, this technique doubles the number of degrees of freedom of the model compared to the case without intra-laminar cohesive elements. Second, the technique imposes a predetermined discretization of the crack paths. Also, modeling

at the mesoscopic scale means that the crack must necessarily cross the entire thickness of the ply. The reality is more complex, cracks are denser and can be inclined. Consequently, the use of an energy formulation in cohesive elements is not very appropriate because it would lead to limit the amount of energy that can be dissipated by cracking depending on the level of mesh refinement.

As explained in the damage description, fibers exhibit one tensile failure mode and two compressive failure modes. Fiber failure releases a relatively large amount of energy compared to delamination and must be quantified for better simulation fidelity.

At the mesoscopic scale, fiber rupture remains a localized damage relative to the size of the volume elements. It is therefore not possible to model it with continuous fracture mechanics. This would lead to a model whose energy dissipation would vary according to the mesh size. If we wish to rigorously model fiber rupture, it would be necessary to define cohesive elements as for delamination. Thus, the energy dissipated by the rupture could be well quantified. However, this option significantly increases the number of degrees of freedom of the model. In addition, the location of the rupture is not known in advance unlike delamination, which has led several authors [127, 128 ,129 ,130, 113] to model fiber rupture using an internal length propagation law. This approach, initially developed by Bazant [127] for concrete cracking, makes it possible to overcome the dependence of energy dissipation on the mesh size. The formulation (Fig. 26) of the energy balance implies that the energy dissipated in the volume Vo of the element is equal to the energy required to crack its section S.

Fig. 27 represents a typical constitutive law commonly used for fibers. The initiation criterion varies according to the authors. The simplest use maximum deformation criteria. In compression, Pinho [129] uses a stress criterion calculated using Mohr's circle. The propagation in tension or compression is governed by a relation derived from the Bazant relation. In compression, a residual resistance is maintained after rupture to represent the force due to the crushing of the debris.

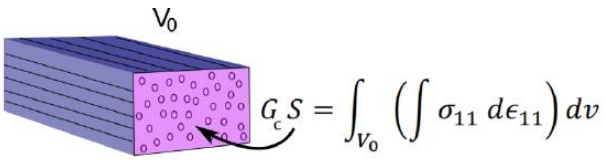

Fig. 26. Principle of formulation of the laws of energy dissipation at internal length.

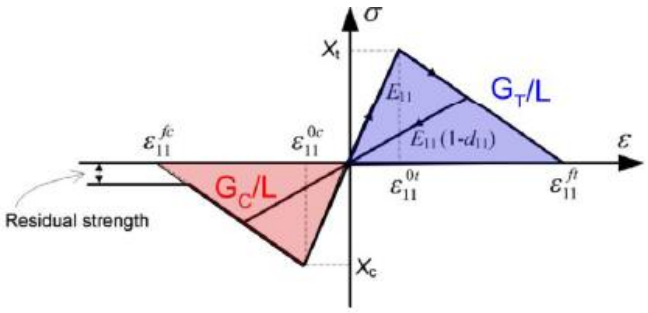

Fig. 27. Typical behavior law for fibers [129].

The value of the critical energy release rate for fiber fracture is difficult to obtain experimentally. Currently, there is no standardized method for measuring these properties. One of the major difficulties in their identification comes from the fact that the laminate has several fracture modes. Consequently, it is not easy to obtain a test with a pure fracture mode. However, some authors have proposed different test configurations. To find the value of the compression-shear toughness, Laffau et al. [133] proposed a four-point bending test on a notched beam. Pinho et al. [129] used CC (Compact Compression) and CT (Compact Tension) tests to measure, respectively, the compression and tension bending band toughness (Fig. 28.a). Lisle [132] proposed to go back to the dissipated energies using a reverse engineering technique coupled with a thermal measurement at the crack front (Fig. 28.b).

Thus, it is possible by coupling the cohesive elements with the approaches mentioned above to describe the intra-laminar damage and the inter-laminar damage (delamination) in a coupled manner.

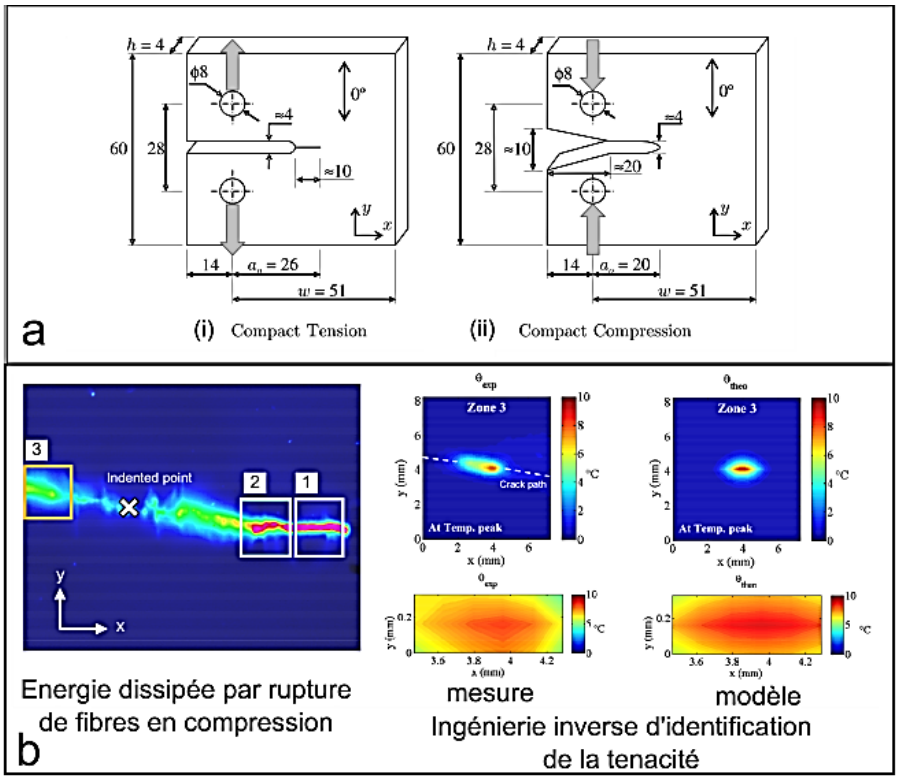

Fig. 28. Techniques for measuring tenacity in the fiber direction [129], [132].

7. Future research in hydrogen storage composite materials

Future research in hydrogen storage composite materials should focus on advancing material design, improving modeling techniques, and addressing commercialization challenges. Developing hybrid composites and multifunctional materials, such as those integrating advanced polymer matrices with nanostructured reinforcements like carbon nanotubes, can significantly enhance resistance to hydrogen embrittlement and thermal damage [134]. Improving multiscale modeling frameworks by coupling machine learning with finite element models can provide better predictions of composite behavior under complex loading conditions [135]. Additionally, addressing cost and scalability issues requires optimizing manufacturing techniques like automated fiber placement and filament winding while implementing standardized testing protocols for safety and reliability [136]. These advancements will pave the way for more efficient, durable, and commercially viable hydrogen storage systems.

8. Conclusion

This comprehensive review provides a detailed examination of the complex mechanical behavior and damage mechanisms of composite materials employed in hydrogen storage tanks, with a particular emphasis on the challenges encountered in the development of Type IV automotive hydrogen tanks. The review begins

with an overview of hydrogen storage techniques and the structure of Type IV tanks, highlighting the importance of composite materials in ensuring the durability and longevity of these high-pressure vessels. The section on mechanical behavior provides an in-depth analysis of the fundamental properties of laminated composites, emphasizing the importance of multiscale characterization under a range of loading conditions. In the context of monotonic loading, both quasi-static and dynamic, the review identifies matrix cracking, fiber breakage and delamination as the primary failure mechanisms. It is vital to consider the impact of loading rates on these mechanisms, particularly in dynamic loading scenarios where sudden impacts can result in rapid damage propagation. Similarly, cyclic loading presents unique challenges, with fatigue-induced damage mechanisms gradually compromising the composite structure over time. A key element of this review is the discussion of methods for characterizing the residual properties of composites following dynamic loading. It outlines a range of experimental techniques, including infrared thermography and X-ray tomography, for detecting and quantifying damage states. These methods provide a foundation for evaluating the material's residual strength, which is essential for assessing the post-impact behavior of hydrogen tanks in real-world applications.

The review also discusses the multi-scale analysis and modeling of composite materials, particularly those produced by filament winding. It emphasizes that composite behavior can be examined at four key scales: the macro scale, meso scale, unidirectional (UD) tape scale, and microstructure scale. This multi-scale approach allows for better optimization of composite designs and more accurate simulations of their mechanical response under various loading conditions. In conclusion, mesoscopic modeling using cohesive elements provides an effective way to simulate delamination and fiber failure in composite materials. Despite the increased computational complexity, these models capture critical damage mechanisms, including matrix cracking and inter-layer interactions.

Looking ahead, advancing composite material design requires a focus on developing higher-performing resins and fibers to enhance durability and reduce costs. Improving multiscale modeling techniques, particularly for capturing damage evolution under complex loading scenarios, is essential to bridge the gap between laboratory findings and real-world applications. Additionally, addressing commercialization challenges, such as scaling up production processes and ensuring long-term reliability under operational conditions, will be key to the broader adoption of hydrogen storage systems. Integrating these research

directions will not only enhance the safety and efficiency of hydrogen storage but also accelerate the transition toward sustainable energy solutions.

Declarations

- Consent to participate: Not applicable.
- Consent to publish: Not applicable.
- Conflict of interest: The authors declare that they have no conflicts of interest.

Authors' contributions

M. Shirinbayan, R. Tie Bi, J-B. Maeso, C. Thomas, J. Fitoussi: construct the idea. I. Feki, M. Shirinbayan, S. Nouira, R. Tie Bi, J-B. Maeso, C. Thomas, J. Fitoussi: prepared the manuscript draft, and wrote the paper. I. Feki, M. Shirinbayan, S. Nouira, J. Fitoussi: corrected the English and the paper format.

Availability of data and materials

The authors declare that the data and the materials of this study are available within the article.

8. References

[1] M. A. Ç. Cevahir Tarhan, «A study on hydrogen, the clean energy of the future: Hydrogen,» Journal of Energy Storage, p. https://doi.org/10.1016/j.est.2021.102676, 2021.

[2] H. T. H. a. A. Varma, «Hydrogen storage for fuel cell vehicles,» Current Opinion in Chemical Engineering, p. http://dx.doi.org/10.1016/j.coche.2014.04.004, 2014.

[3] M. T. a. K. Z. Etienne Rivard, «Hydrogen Storage for Mobility: A Review,» materials, p. doi:10.3390/ma12121973, 2019.

[4] «Study and characterization of a metal hydride container,» INTERNATIONAL JOURNAL OF HYDROGEN ENERGY, p. doi:10.1016/j.ijhydene.2007.12.029, 2008.

[5] L. O. W. a. D. E. SPOND, «A STORAGE TANK FOR VEHICULAR STORAGE OF liquid hydrogen,» Applied Energy, 1980.

[6] Naghdali Choupani,Experimental and numerical investigation of the mixed-mode delamination in Arcan laminated specimens,Materials Science and Engineering: A, Volume 478, Issues 1–2, 2008,Pages 229-242, ISSN 0921-5093,https://doi.org/10.1016/j.msea.2007.05.103.

[7] Avcu, A., Seyedzavvar, M., Boğa, C. et al. Caractérisation des effets de la chemise et de la coque composite en résine renforcée de fibres sur l'énergie de rupture dans les réservoirs composites haute pression de type III. J Braz. Soc. Mech. Sci. Eng. 46 , 13 (2024). https://doi.org/10.1007/s40430-023-04598-9

[8] Avcu, A., Seyedzavvar, M., Boga, C. et al. Évaluation de la sécurité et de la fiabilité des réservoirs composites haute pression de type 3 : une analyse complète des paramètres de défaillance. Sādhanā 49 , 55 (2024). https://doi.org/10.1007/s12046-023-02394-8

[9] M. Nikbakht, N. Choupani, S.R. Hosseini, 2D and 3D interlaminar fracture assessment under mixed-mode loading conditions, Materials Science and Engineering: A, Volume 516, Issues 1–2, 2009, Pages 162-168, ISSN 0921-5093, https://doi.org/10.1016/j.msea.2009.03.011.

[10] Heydari, MH, Choupani, N. et Shameli, M. Étude expérimentale et numérique de la fracture interlaminaire en mode mixte d'un composite tissé stratifié carbone-polyester à l'aide de la méthode Arcan. Appl Compos Mater 18 , 499–511 (2011). https://doi.org/10.1007/s10443-011-9223-x

[11] J. Zheng, J. Guo, J. Yang, Y. Zhao, L. Zhao, X. Pan, J. Ma et L. Zhang, «EXPERIMENTAL AND NUMERICAL STUDY ON TEMPERATURE RISE WITHIN A 70 MPA TYPE III CYLINDER DURING FAST REFUELING.,» 13th China Hydrogen Energy Conference (CHEC) , p. DOI, 2013.

[12] N. M. CebollaB.AcostaP.MorettoF.HarskampC.Bonato, «Compressed hydrogen tanks for on-board application: Thermal behaviour during cycling,» International Journal of Hydrogen Energy, 2015.03.035, 2015.

[13] S. C. K. C. K. H. L. B. Y. B. Yoon, «Thermal characteristics during hydrogen fueling process of type IV cylinder,» International Journal of Hydrogen Energy 35, p. DOI: 10.1016/j.ijhydene.2010.03.130, 2010.

[14] Y. J. Z. Y. P. X. Z. L. Z. L. e. a. Guo J, «Investigations on temperature variation within a type III cylinder during the hydrogen gas cycling test.,» Hydrogen Energy, 2014.03.097, 2014.

[15] T. MORIYA, «DEVELOPMENT OF THE FCX FUEL CELL VEHICLE AT HONDA,» Wako Research Center, Honda R&D, 2003.

[16] M. K. H. M. Y. N. T. T. T. M. a. N. K. Tetsuya Bono, «Development of New TOYOTA FCHV-adv Fuel Cell System,» Journal of Engines, p. https://www.jstor.org/stable/26308444, 2009.

[17] M. K. S. G. a. N. O. Akira Yamashita, «Development of High-Pressure Hydrogen Storage System for the Toyota"Mirai",» SAE Technical Paper, pp. doi:10.4271/2015-01-1169., 2015.

[18] «Faurecia,» 31 mars 2021. [En ligne]. Available: https://www.faurecia.com/newsroom/faurecia-accompagne-stellantis-pour-des-vehicules-utilitaires-hydrogene.

[19] D. chalon, «le journal des flottes,» 18 octobre 2021. [En ligne]. Available: https://journalauto.com/journal-des-flottes/stellantis-vise-2-000-utilitaires-a-hydrogene/.

[20] Park, S. H., & Lee, J. Y. (2020). "Development of advanced polymer liners for hydrogen storage tanks." *International Journal of Hydrogen Energy,* 45(3), 234-245.

[21] Kumar, S., & Singh, R. K. (2021). "Application of carbon nanotubes in improving the thermal and mechanical properties of composite hydrogen tanks." *Materials Today: Proceedings,* 43, 120-130.

[22] Zhang, Y., & Wang, H. (2022). "High-temperature resistant resin systems for composite applications in hydrogen storage." *Composites Science and Technology,* 210, 108846.

[23] Lee, M. H., & Kim, D. (2021). "Filament winding and automated fiber placement techniques in Type IV hydrogen storage tanks." *Composites Part B: Engineering,* 207, 108732.

[24] DoE, Physical Hydrogen Storage, U.S. Department of Energy, America, 2023.

[25] Soutis, C. (2005). Fiber reinforced composites in aircraft construction. Progress in Aerospace Sciences, 41(2), 143-151.

[26] Daniel, I. M., & Ishai, O. (2005). Engineering Mechanics of Composite Materials. Oxford University Press.

[27] Zhang, W., & Richardson, M. O. W. (2007). Interlaminar shear strength of composites exposed to thermal cycling. Composite Structures, 81(1), 101-109.

[28] Harris, B. (2003). Fatigue in Composites: Science and Technology of the Fatigue Response of Fibre-Reinforced Plastics. Woodhead Publishing.

[29] Parvizi, A., & Bailey, J. E. (1978). Multiple transverse cracking in glass fibre epoxy laminates. Journal of Materials Science, 13(9), 2131-2136.

[30] M. B. T.-C. Lafarie-Freno, «Experimental study of the stacking sequence effect on polymer/composite multi-layers submitted to thermomechanical cyclic loadings.,» international journal of hydrogen energy, p. 11397–11404, 2010.

[31] E. a. S. B. (. Gamstedt, «Michromechanisms in tension-compression fatigue of composite laminates containing transverse plies.,» Composites Sciences and Technology, , vol. 59, p. 167–178.

[32] Cox, B. N., & Yang, Q. D. (1999). A continuum model for delamination growth in composites. Composites Science and Technology, 59(7), 951-963.

[33] C. A. U. D. G. M. A. S. B. M. L. a. J. V. L. Jiang, «Recycling carbon fiber composites using microwave irradiation: Reinforcement study of the recycled fiber in new composites,,» J. Appl. Polym, p. 42658–42666, 2015.

[34] Shokrieh, M. M., & Omidi, M. J. (2009). Tension behavior of unidirectional glass/epoxy composites under different strain rates. Composites Part B: Engineering, 40(3), 274-284.

[35] M. G. a. M.-C. L.-F. D. Vu, «The effect of thermo-oxidation on matrix cracking of cross-ply [0/90]s composite laminates,,» Compos. Part A,, pp. 114–121,, 2013.

[36] Emilie Trousset. Prévision des dommages d'impact basse vitesse et basse énergie dans les composites à matrice organique stratifiés. Autre. Ecole nationale supérieure d'arts et métiers - ENSAM, 2013. Français. NNT : 2013ENAM0008. pastel-00942339.

[37] P. PROMBUT, «Caractérisation de la propagation de délaminage des stratifiés composites multidirectionnels,» Université Toulouse, Toulouse, 2007.

[38] Y. D. e. J. QIAN, «Analysis of microdamage evolution histories in composites.,» International Journal of Solids and Structures, p. 1831–1854, 2001.

[39] F. LEBEL, «Contrôle de la fabrication des composites par injection sur renforts.,» Université de Montréal,, Miontréal, 2012.

[40] Li, Y., Mai, Y. W., & Ye, L. (2015). Effects of environmental conditions on the interlaminar shear strength of composite materials. Composite Structures, 132, 132-140.

[41] S.HUGUET, «Application de classification aux données d'émission acoustique :identification de la signature acoustique des mécanismes d'endommagement dans lescomposites à matrice polymère.,» Institut National des SciencesAppliquées de Lyon, lyon, 2002.

[42] R.TALREJA, «Assessment of the fundamentals of failure theories for compositematerials.,» Composites Science and Technology, p. 105:190–201, 2014.

[43] Y. A. B. G. M. J.C.ABRY, «In-situ monitoring of damage in CFRP laminates by means of ACand DC measurements.,» Composites Science and Technology, p. 855–864, 2001.

[44] Feki I , Shirinbayan M , Nouira S , et al. Étude expérimentale multi-échelle des effets de dommages induits par la porosité dans les composites époxy renforcés de fibres de carbone à enroulement filamentaire utilisés dans les réservoirs de stockage d'hydrogène . *Polym Compos* . 2024 ; 1 - 13 . doi: 10.1002/pc.29121

[45] Shirinbayan, M., Nouira, S., Imaddahen, M. A., & Fitoussi, J. (2024). Microstructure-sensitive investigation on the plastic deformation and damage initiation of fiber-reinforced polypropylene composite. *Composites Part B: Engineering*, *286*, 111790.

[46] Nouira, S., Shirinbayan, M., Peixinho, J., Benfriha, K., Hassine, T., & Fitoussi, J. (2024). Effect of processing conditions on morphology and mechanical damage in glass-reinforced polypropylene composite. *Polymer Composites*.

[47] J. PAYAN, «: Etude du comportement de composites stratifiés sous chargement statique et de fatigue,» France, 2004.

[48] H. G. J.BRUNBAUER, «Mechanical properties, fatigue damage and microstructure of carbon/epoxy laminates depending on fibre volumecontent,» International Journal of Fatigue,, p. 85–92, 2015..

[49] Shirinbayan M, Feki I, Nouira S, et al. Multi-scale damage analysis of filament-wound carbon fiber-reinforced epoxy composites for hydrogen storage tanks under high strain rates. *Polym Compos*. 2024; 1-12. doi:10.1002/pc.29273

[50] Jendli Z. Analyse et modelisation multi echelles du comportement mecanique sous sollicitations rapides de composites SMC. 2005.

[51] Shokrieh, M. M., & Omidi, M. J. (2009). Tension behavior of unidirectional glass/epoxy composites under different strain rates. Composites Part B: Engineering, 40(3), 274-284.

[52] Zhu, J., & Choi, I. (2010). Impact behavior and damage tolerance of laminated composites. Journal of Composite Materials, 44(12), 1503-1522.

[53] Zhou, G., Zhao, L., & Adams, R. D. (2015). The influence of matrix cracking on the fatigue life of carbon fiber-reinforced polymer composites. Composite Structures, 123, 345-354.

[54] Shokrieh, M. M., & Lessard, L. B. (2000). Progressive fatigue damage modeling of composite materials. Composite Structures, 48(4), 453-461.

[55] Sendeckyj, G. P. (1990). Life prediction for resin matrix composite materials. International Journal of Fracture, 42(1), 1-31.

[56] K. S. K. R. e. W. S. R.D. JAMISON, «Characterization and analysis of damage mechanisms in tension-tension fatigue of graphite/epoxy laminates.,» Effects of Defects in Composite Materials, p. 21–55, 1984.

[57] Juliette Payan. Etude du comportement de composites stratifiés sous chargement statique et de fatigue. Mécanique [physics.med-ph]. Université de la Méditerranée - Aix-Marseille II, 2004 Français.

[58] Feki, I., Shirinbayan, M., Nouira, S., Bi, R. T., Maeso, J. B., Thomas, C., & Fitoussi, J. (2024). Multi-scale fatigue damage analysis in filament-wound carbon fiber reinforced epoxy composites for hydrogen storage tanks. *Composites Part C: Open Access*, *15*, 100537.

[59] Fitoussi, J., Nouira, S., Benfriha, K., Laribi, M. A., Kallel, A., Bi, R. T., & Shirinbayan, M. (2024). Investigation of manufacturing process effects on microstructure and fatigue prediction in composite automotive tailgate design. *The International Journal of Advanced Manufacturing Technology*, *130*(9), 4295-4310.

[60] J. I. H. H. H. Gerharz, «Impact damage in fatigue loaded composite structure,» 15th Symposium of the international Commitee on Aeronautical Fatigue, pp. 497-516, 1989.

[61] L. G. S. J. N. T. Melin, «Fatigue testing and buckling characteristics of impacted composite specimens,» International Journal of Fatigue., vol. 24, pp. 263-272, 2002.

[62] M. H. H. T. C. G. P. S. P. Mitrovic, «Effect of loading parameters on the fatigue behavior of impact damaged composite laminates,» Composites Science and Technology, vol. 59, pp. 2059-2078, 1999.

[63] J. Aboissiere, «Propagation de dommages d'impact dans un matériau composite stratifié à fibres de carbone et résine époxyde.,» thése de l'université Paul Sabatier, Toulouse, 2003.

[64] W. J. C. P. T. M. J. Cantwell, «An Assessment of the impact performance of CFRP reinforced with high-strain carbon fibres.,» Composites Science and Technology, vol. 25, pp. 133-148, 1986.

[65] ASTM, «Standand Test Method for Compressive Residuel Strength Properties of Damaged Polymer Matrix Composite Plates.,» ASTM Standards, 2006.

[66] A. I. T. Method, «Fiber Reinforced Plastics Determination of Compression Strength after Impact,» AITM-1-0010, 1994.

[67] Hongkarnjanakul, N.: Modélisation numérique pour la tolérance aux dommages d'impact sur stratifié composite: De l'impact à la resistance résiduelle en compression, thèse de l'Université de Toulouse, 2013

[68] Alves, M., et al. (2014). "Infrared Thermography in Monitoring the Fatigue of Carbon Fiber-Reinforced Polymers." Composite Structures 117, 1-9.

[69] S. MAILLARD, J. CADITH, H. WALASZEK et J. L. BODNAR : La thermographie infrarouge active et ses nouvelles applications aux matériaux métalliques. CETIM, 2012. 8, 33, 34

[70] Zhang, Z., et al. (2019). "X-ray Computed Tomography for Damage Characterization in Carbon Fiber Composites." *Materials Today Communications* 21, 100604.

[71] H. HORSIN MOLINARO, F. HILD et S. ROUX : La tomographie en sciences et mécanique des matériaux : voyage aux centres des matériaux. *Sciences et Techniques Industrielles*, 2015. 8, 34.

[72] Lopresto, V., et al. (2010). "Acoustic Emission Monitoring of Damage Evolution in Glass Fiber Reinforced Composites." *Journal of Composite Materials* 44(6), 789-802.

[73] Sikarwar, B. S., et al. (2016). "Surface Strain Mapping of CFRPs Using Digital Image Correlation." *Materials Today: Proceedings* 3(4), 1105-1110.

[74] Garcia, R., et al. (2018). "Ultrasonic Inspection of Delaminations in Impact-Damaged Composite Panels." *Ultrasonics* 87, 1-9.

[75] E. I. L. G. J. DOST, «Sublaminate stability-based modelling of impact damaged composite laminate,» *Conference of American Society of Composites,* pp. 354-363, 1988.

[76] Shivakumar KN, Whitcomb JD. Buckling of a Sublaminate in a Quasi-Isotropic Composite Laminate. Journal of Composite Materials. 1985;19(1):2-18. doi:10.1177/002199838501900101

[77] C. Soutis, P.T. Curtis, Prediction of the post-impact compressive strength of cfrp laminated composites, Composites Science and Technology, Volume 56, Issue 6,1996, https://doi.org/10.1016/0266-3538(96)00050-4.

[78] Soutis C, Fleck NA. Rupture par compression statique d'une plaque composite en fibre de carbone T800/924C avec un seul trou. Journal of Composite Materials . 1990;24(5):536-558. doi: 10.1177/002199839002400505

[79] De Moura MFSF, Gonçalves JPM, Marques AT, De Castro PMST. Modélisation de la rupture par compression après impact à faible vitesse sur des composites stratifiés à l'aide d'éléments d'interface. Journal of Composite Materials . 1997;31(15):1462-1479.

[80] Hao Yan, Caglar Oskay, Arun Krishnan, Luoyu Roy Xu, Compression-after-impact response of woven fiber-reinforced composites, Composites Science and Technology, Volume 70, Issue 14, 2010, https://doi.org/10.1016/j.compscitech.2010.08.012.

[81] Hiroshi Suemasu, Wataru Sasaki, Takashi Ishikawa, Yuichiro Aoki, A numerical study on compressive behavior of composite plates with multiple circular delaminations considering delamination propagation, Composites Science and Technology, Volume 68, Issue 12,2008,Pages 2562-2567,ISSN 0266-3538,https://doi.org/10.1016/j.compscitech.2008.05.014.

[82] E.V. González, P. Maimí, P.P. Camanho, A. Turon, J.A. Mayugo, Simulation of drop-weight impact and compression after impact tests on composite laminates,Composite Structures, Volume 94, Issue 11, 2012, Pages 3364-3378.

[83] Samuel Rivallant, Christophe Bouvet, Natthawat Hongkarnjanakul, Failure analysis of CFRP laminates subjected to compression after impact: FE simulation using discrete interface elements, Composites Part A: Applied Science and Manufacturing, Volume 55, 2013, Pages 83-93, ISSN 1359-835X, https://doi.org/10.1016/j.compositesa.2013.08.003.

[84] Ladevèze, P., & Lubineau, G. (2001). "On a Damage Mechanics Approach to the Multiscale Analysis of Laminated Composites," *Composites Science and Technology*.

[85] Jones, R. M. (1998). *Mechanics of Composite Materials*. CRC Press.

[86] Fish, J., & Yu, Q. (2001). "Computational Mechanics of Multi-Scale Modeling in Composites," *Computational Mechanics*.

[87] Camanho, P. P., et al. (2003). "A Finite Fracture Mechanics Model for the Prediction of the Open Hole Strength of Laminated Composites," *Composites: Part A*.

[88] Ochoa, O. O., & Reddy, J. N. (1992). *Finite Element Analysis of Composite Laminates*, Kluwer Academic Publishers.

[89] Chawla, K. K. (1998). *Composite Materials: Science and Engineering*.

[90] Baran, I., et al. (2015). "Numerical Modelling of Filament Wound Composite Pressure Vessels," *Journal of Composite Materials*.

[91] Hu, N., et al. (2018). "Progressive Failure Analysis of Composite Laminates with Different Orientations," *Composite Structures*. This reference discusses how the stacking sequence and fiber orientation affect the global properties of composite materials, including stiffness and strength.

[92] Thomas Vandellos, Nicolas Carrère, Cédric Huchette. Développement d'une stratégie de modélisation du délaminage dans les structures composites = Development of computational strategy to model delamination in composite structures. JNC 16, Jun 2009, Toulouse, France. 10 p. ffhal-00387376f

[93] M.R. Wisnom, Modelling discrete failures in composites with interface elements, Composites Part A: Applied Science and Manufacturing, Volume 41, Issue 7, 2010, https://doi.org/10.1016/j.compositesa.2010.02.011.

[94] H. L. H. K. ,. W. Z. C. Z. Ming Zhang, «A literature review of failure prediction and analysis methods for composite high-pressure hydrogen storage tanks.,» *international journal of hydrogen energy,* Vols. %1 sur %2Volume 44, Issue 47 , pp. Pages 25777-25799, 2019.

[95] M.L. Benzeggagh, M. Kenane, Measurement of mixed-mode delamination fracture toughness of unidirectional glass/epoxy composites with mixed-mode bending apparatus, Composites Science and Technology, Volume 56, Issue 4,1996, https://doi.org/10.1016/0266-3538(96)00005-X.

[96] NASA: standard tests for toughened resin composites, 1982.

[97] Martin, RH et Davidson, BD (1999). Évaluation de la ténacité à la fracture en mode II à l'aide d'un essai de flexion en quatre points et d'un essai de flexion entaillé en bout. *Plastiques, caoutchouc et composites* , *28* (8), 401–406. https://doi.org/10.1179/146580199101540565

[98] Lee, S. (1er septembre 1993). « Une méthode de torsion des fissures de bord pour les essais de fracture par délaminage de mode III. » ASTM International. *J. Compos. Technol. Res.* . Septembre 1993 ; 15(3) : 193–201. https://doi.org/10.1520/CTR10369J

[99] Russell, A, & Street, K. « Effets de l'humidité et de la température sur la fracture par délaminage en mode mixte du graphite/époxy unidirectionnel. » Délamination et décollement des matériaux. Ed. Johnson, W.100 Barr Harbor Drive, BP C700, West Conshohocken, PA 19428-2959: ASTM International, 1985.

[100] De Moura, M.F.S.F., Gonçalves, J.P.M., Marques, A.T., & De Castro, P.M.S.T. (1997). Modeling of fracture in laminated composites using interface elements. *Journal of Composite Materials, 31(15)*, 1462–1479.

[101] Benzeggagh, M.L., & Kenane, M. (1996). Measurement of mixed-mode delamination fracture toughness of unidirectional glass/epoxy composites. *Composites Science and Technology, 56(4)*, 439–449.

[102] Benzeggagh, M.L., & Kenane, M. (1996). Measurement of mixed-mode delamination fracture toughness of unidirectional glass/epoxy composites. *Composites Science and Technology, 56(4)*, 439–449.

[103] Russell, A., & Street, K. (1985). Effects of moisture and temperature on mixed-mode delamination fracture toughness in graphite/epoxy composites. *Delamination and Debonding of Materials*.

[104] Martin, R.H., & Davidson, B.D. (1999). Evaluation of mode II fracture toughness using a four-point bending test. *Plastics, Rubber, and Composites, 28(8)*, 401–406.

[105] Benzeggagh, M.L., & Kenane, M. (1996). Measurement of mixed-mode delamination fracture toughness of unidirectional glass/epoxy composites. *Composites Science and Technology, 56(4)*, 439–449.

[106] Martin, R.H., & Davidson, B.D. (1999). Evaluation of mode II fracture toughness using a four-point bending test. *Plastics, Rubber, and Composites, 28(8)*, 401–406.

[107] Lee, S. (1993). A method for torsion crack tests of composite laminates for fracture toughness evaluation. *ASTM International*.

[108] Mathieu Hautier. Analyse des réparations des matériaux composites : mise en œuvre d'un procédé par infiltration et étude du comportement mécanique. Mécanique [physics.med-ph]. Université Paul Sabatier - Toulouse III, 2010. Français. ffNNT : ff. fftel-00550139f

[109] A.B. de Morais, A.B. Pereira, M.F.S.F. de Moura, Mode III interlaminar fracture of carbon/epoxy laminates using the Six-Point Edge Crack Torsion (6ECT), Composites Part A: Applied Science and Manufacturing, Volume 42, Issue 11, 2011.

[110] Prombut, Pongtorn (2007). *Caractérisation de la propagation de délaminage des stratifiés composites multidirectionnels.*

[111] GUINARD,S and al: A 3D damage analysis of low-velocity impacts on laminated composites,Composites Science and Technology,62,585-589,2002.

[112] L. Iannucci, M.L. Willows, An energy based damage mechanics approach to modelling impact onto woven composite materials—Part I: Numerical models, Composites Part A: Applied Science and Manufacturing, Volume 37, Issue 11, 2006, compositesa.2005.12.013.

[113] Y. Shi, T. Swait, C. Soutis, Modelling damage evolution in composite laminates subjected to low velocity impact, Composite Structures, 2012, 2902-2913, compstruct.2012.03.039.

[114] M. Wisheart, M.O.W. Richardson, The finite element analysis of impact induced delamination in composite materials using a novel interface element, Composites Part A: Applied Science and Manufacturing, 1998, https://doi.org/10.1016/S1359-835X(97)00080-8.

[115] C.S. Lopes, P.P. Camanho, Z. Gürdal, P. Maimí, E.V. González, Low-velocity impact damage on dispersed stacking sequence laminates. Part II: Numerical simulations, Composites Science and Technology, 2009, Pages 937-947, https://doi.org/10.1016/j.compscitech.2009.02.015.

[116] Christophe Bouvet, Bruno Castanié, Matthieu Bizeul, Jean-Jacques Barrau, Low velocity impact modelling in laminate composite panels with discrete interface elements, International Journal of Solids and Structures, 2009.

[117] F. P. van der Meer∗ and L. J. Sluys Faculty of Civil Engineering and Geosciences, Section of Structural Mechanics Delft University of Technology, P.O. Box 5048, 2600 GA Delft, The Netherlands May 13, 2008.

[118] N. Hongkarnjanakul, C. Bouvet, S. Rivallant, Validation of low velocity impact modelling on different stacking sequences of CFRP laminates and influence of fibre failure, Composite Structures, 2013, https://doi.org/10.1016/j.compstruct.2013.07.008.

[119] F. Aymerich, F. Dore, P. Priolo, Prediction of impact-induced delamination in cross-ply composite laminates using cohesive interface elements, Composites Science and Technology, Volume 68, Issue 12, 2008, https://doi.org/10.1016/j.compscitech.2007.06.015.

[120] Stephen R. Hallett, Wen-Guang Jiang, Bijoysri Khan, Michael R. Wisnom, Modelling the interaction between matrix cracks and delamination damage in scaled quasi-isotropic specimens, Composites Science and Technology, 2008, compscitech.2007.05.038.

[121] M.F.S.F de Moura, J.P.M Gonçalves, Modelling the interaction between matrix cracking and delamination in carbon–epoxy laminates under low velocity impact, Composites Science and Technology, 2004, https://doi.org/10.1016/j.compscitech.2003.08.008.

[122] Nishikawa , Okabe, Takeda, Nobuo: Numerical simulation of interlaminar damage propagation in CFRP cross-ply laminates under transverse loading. International Journal of Solids and Structures 44 (2007) 3101–3113, doi:10.1016/j.ijsolstr.2006.09.007.

[123] Yan Zhang, Ping Zhu, Xinmin Lai, Finite element analysis of low-velocity impact damage in composite laminated plates, Materials & Design, Volume 27, Issue 6, 2006, Pages 513-519, ISSN 0261-3069, https://doi.org/10.1016/j.matdes.2004.11.014

[124] Aoki, Y., Suemasu, H., & Ishikawa, T. (2007). Propagation des dommages dans les stratifiés CFRP soumis à un impact à faible vitesse et à une indentation statique. *Advanced Composite Materials* , *16* (1), 45–61. https://doi.org/10.1163/156855107779755318.

[125] F. Aymerich, F. Dore, P. Priolo, Prediction of impact-induced delamination in cross-ply composite laminates using cohesive interface elements, Composites Science and Technology, Volume 68, Issue 12, 2008, Pages 2383-2390, ISSN 0266-3538, compscitech.2007.06.015.

[126] N. Hongkarnjanakul, C. Bouvet, S. Rivallant, Validation of low velocity impact modelling on different stacking sequences of CFRP laminates and influence of fibre failure, Composite Structures, Volume 106, 2013, Pages 549-559, compstruct.2013.07.008.

[127] C. Bouvet, S. Rivallant, J.J. Barrau, Low velocity impact modeling in composite laminates capturing permanent indentation, Composites Science and Technology, Volume 72, Issue 16, 2012, Pages 1977-1988, ISSN 0266-3538, https://doi.org/10.1016/j.compscitech.2012.08.019.

[128] D. Feng, F. Aymerich, Finite element modelling of damage induced by low-velocity impact on composite laminates, Composite Structures, Volume 108, 2014, Pages 161-171, ISSN 0263-8223, https://doi.org/10.1016/j.compstruct.2013.09.004.

[129] Pinho, ST, Robinson, P. et Iannucci, L. (2006) Résistance à la rupture des modes de rupture des fibres en traction et en compression dans les composites stratifiés. Composites Science and Technology, 66, 2069-2079. https://doi.org/10.1016/j.compscitech.2005.12.023

[130] L. Raimondo, L. Iannucci, P. Robinson, P.T. Curtis, A progressive failure model for mesh-size-independent FE analysis of composite laminates subject to low-velocity impact damage,

Composites Science and Technology, 2012, https://doi.org/10.1016/j.compscitech.2012.01.007.

[131] Bažant, ZP, Oh, BH Théorie des bandes de fissures pour la rupture du béton. *Mat. Constr.* **16** , 155–177 (1983). https://doi.org/10.1007/BF02486267.

[132] Lisle, Teddy (2014). *Analyse par thermographie infrarouge de l'endommagement des structures composites sous sollicitations quasi statiques.*

[133] M.J. Laffan, S.T. Pinho, P. Robinson, L. Iannucci, A.J. McMillan, Measurement of the fracture toughness associated with the longitudinal fibre compressive failure mode of laminated composites, Composites Part A: Applied Science and Manufacturing, Volume 43, Issue 11, 2012, https://doi.org/10.1016/j.compositesa.2012.04.009.

[134] Zhang, Y., & Wang, H. (2022). "High-temperature resistant resin systems for composite applications in hydrogen storage." *Composites Science and Technology,* 210, 108846.

[135] Lee, M. H., & Kim, D. (2021). "Filament winding and automated fiber placement techniques in Type IV hydrogen storage tanks." *Composites Part B: Engineering,* 207, 108732.

[136] Kumar, S., & Singh, R. K. (2021). "Application of carbon nanotubes in improving the thermal and mechanical properties of composite hydrogen tanks." *Materials Today: Proceedings,* 43, 120-130.

Article N°2 :

Feki I, Shirinbayan M,Nouira S, et al. Multi-scale experimental investigation of porosity-induced damage effects in filament-wound carbon fiber reinforced epoxy composites used in hydrogen storage tanks. Polym Compos. 2024;1-13. doi:10.1002/pc.29121

Multi-scale experimental investigation of porosity-induced damage effects in filament-wound carbon fiber reinforced epoxy composites used in hydrogen storage tanks

Imen Feki[1], Mohammadali Shirinbayan[1,*], Samia Nouira[1], Eva Heripre[1], Robert Tie Bi[2], Jean-Baptiste Maeso[2], Cedric Thomas[2], Joseph Fitoussi[1]

[1]Arts et Metiers Institute of Technology, CNAM, CNRS, PIMM, HESAM University, F-75013 Paris, France

[2]Faurecia Hydrogen Solutions, FORVIA Clean Mobility, Bois Sur Prés, 25550 Bavans, France

E-mails: Mohammadali.Shirinbayan@ensam.eu (corresponding author), Imen.Feki@ensam.eu, Samia.Nouira@ensam.eu, Eva.Heripre@ensam.eu, Robert.tbr.tiebi@forvia.com, Jean-Baptiste.Maeso@forvia.com, Cedric.Thomas@forvia.com, Joseph.Fitoussi@ensam.eu.

Abstract

Hydrogen-fueled vehicles, recognized for their environmental benefits as they emit only water vapor, represent a sustainable alternative to traditional cars. This paper investigates the relationship between the microstructure and mechanical properties of carbon fiber-reinforced epoxy composites used to manufacture lightweight hydrogen storage pressure vessels through the filament winding process. This fabrication technique, while common, often results in variable fiber orientations and porosity content that affect the mechanical properties of the composite structures. Our study uses tubes made from carbon fiber reinforced epoxy resin with different angular fiber orientations (±15°, ±30°) and multilayer structures to analyze how these variations impact the mechanical properties and damage behavior of the composites. A series of tests, including physical-chemical characterizations, porosity measurements, and multiscale mechanical assessments such as tensile and loading-unloading analysis have been conducted. The results demonstrate that porosity, measured in the range of 5-7%, significantly impacts mechanical performance. Moreover, a 40% decrease in Young's modulus was observed between the ±15° and ±30° fiber orientations, and a 65% reduction was noted for the multilayer structure. Microscopically, the presence of porosity initiates cracks and leads to fiber/matrix decohesion and fiber breakage. Mesoscopically, these defects can merge to form transverse cracks and micro-delaminations between layers, highlighting the complex behaviors of these composites under loading. This information is critical for improving the design and durability of hydrogen storage systems.

Highlights

- Porosity, measured in the range of 5-7%, significantly affects mechanical performance, reducing Young's modulus by up to 40% between ±15° and ±30° fiber orientations and by 65% in multilayer structures.
- Fiber/matrix decohesion and crack initiation due to porosity lead to the formation of transverse cracks and micro-delaminations between layers, affecting the durability of the composite.
- Optimizing fiber orientation and reducing porosity are critical to improving the mechanical performance and long-term durability of hydrogen storage vessels.

Keywords: Hydrogen; filament winding; porosity; damage; fiber/matrix decohesion.

1. Introduction

The development of plastic materials with specific properties allowing them to replace traditional materials like steel or wood has massively contributed to the growth of consumption of these materials. In fact,

innovations searched are those that preserve the benefits of cost reduction, lightness and ease of processing. Composites can be considered as a superior kind of materials which has a wide range of applications in several industries like aircraft, marine, military, automotive, and medical. One important characteristic of the composites is the possibility to change the stacking sequence of the plies or lamina to obtain structures with the desired mechanical properties [1-3].

It is important to note that hydrogen is a lightweight gas and has the lowest volumetric energy density of any fuel at standard temperature and pressure. With regard to its energy characteristics, the gravimetric energy density of hydrogen is approximately three times higher than that of gasoline and methane [4-10]. The European Integrated Hydrogen Project (EIHP) is spearheading the expansion of global regulatory standards for hydrogen testing and certification of hydrogen refueling infrastructure components and systems, including compressed gas hydrogen storage vessels [11]. These vessels can be divided into five different types, as outlined in Table 1.

Type	Description
Type I	All metallic cylinders (steel/aluminum). Approximate maximum pressure, aluminum/glass 263 bars (26.3 MPa; 3,810 psi), steel/carbon or Aramid 299 bars (29.9 MPa; 4,340 psi).
Type II	Load-bearing metal liner hoop wrapped with resin-impregnated continuous filament. Metal tank (aluminum) with filament windings like glass fiber/aramid or carbon fiber around the metal cylinder. Maximum pressure: Aluminum/glass 263 bars (26.3 MPa; 3,810 psi), steel/carbon 299 bars (29.9 MPa; 4,340 psi).
Type III	Non-load-bearing metal liner axial and hoop wrapped with resin impregnated continuous filament. Maximum pressure: Aluminum/glass 305 bars (30.5 MPa; 4,420 psi), Aluminum/ Carbon 700 bars (70 MPa; 10,000 psi).
Type IV	Non-load-bearing non-metal liner axial and hoop wrapped with resin impregnated continuous filament. Maximum pressure: 700 bars (70 MPa; 10,000 psi).
Type V	Does not have an internal bladder, polyamide, or aluminum. The matrix that forms the gas seal is the only component that poses a significant challenge with hydrogen, as it can migrate even through dense matrices. The density of hydrogen in a type 5 tank is approximately 20 grams per liter. Maximum pressure: 1000 bars

Table. 1. Types of Hydrogen tanks [12,13].

The most innovative lightweight storage system for compressed gas is a vessel comprising an advanced composite tank with a non-load-bearing metallic (Type III) or plastic (Type IV) liner. This research paper

focused on studying the mechanical properties of carbon fiber-reinforced epoxy resin (Type IV) for the manufacturing of lightweight hydrogen storage pressure vessels [14,15].

This is axial and hoop wrapped with resin impregnated continuous filaments. These pressure vessels are attracting high interest from the scientific community. The structure is based on two essential components: the liner part and the composite part. The liner is a barrier for hydrogen permeation, while the composite structure safeguards the mechanical integrity of the tank. This research is focused on the expansion of new methodologies for reliable design and safety qualification of these high-pressure storage systems. Efforts are also being made to extend these techniques to the next generation of compressed hydrogen storage systems, which will include tanks with complex shapes, optimal use of materials and a high safety level [16, 18].

In polymer processing, various treatments can impact the functionality and quality of the final products. The filament winding technique, used to create cylindrical shapes like pipes, tubes, and tanks, is critical for producing large structures in the chemical industry. The effectiveness of this method largely depends on the chosen winding pattern, which directly influences the composite's structural properties. Selecting the right matrix material is crucial in this process, with emphasis on its basic mechanical properties [19,20]. For high-performance composites, essential characteristics include a high tensile modulus, which enhances the compressive strength, and high tensile strength, which helps prevent cracks in composite laminates. Additionally, high fracture toughness is vital as it helps manage the spread of cracks and delamination. These properties are fundamental in designing durable composites that can withstand demanding applications. It is evident that carbon fiber is receiving significant interest in recent times, with its extensive range of applications, especially in the aeronautical and automotive sectors. This is primarily due to the material’s impressive weight-to-strength ratio and superior mechanical properties [21,24].

Several studies indicate that numerous parameters in the filament winding process significantly influence composite quality. Temperature, fiber volume fraction, fiber pattern and angle, winding speed, and tension are some key process parameters in filament winding, significantly impacting the mechanical properties of the composite [25]. Tasdeeq Sofi et al. examined the challenges and potential of the dry fiber winding technique. They employed differential geometry for geodesic and non-geodesic winding paths to achieve accurate fiber orientations on a mandrel. Their study quantified that friction in non-geodesic paths leads to deviations in fiber placement, with errors up to 10%, and proposed new methods for trajectory generation to reduce this error to below 2% [26]. Chang et al. analyzed how filament winding variables impact the interlaminar quality of carbon fiber/polypropylene composites, finding that an increase in tension from 10 N to 50 N improved interlaminar

shear strength by approximately 30%, while changes in temperature from 150°C to 200°C led to a 20% increase in strength. The winding speed, however, had a marginal effect of less than 5% [27]. Madrid et al. evaluated the impact of winding angles on the stiffness and load capacity of filament-wound vessels, noting that stiffness increased by up to 25% as the winding angle varied from 30° to 55°, but beyond this point, stiffness and load capacity began to decrease due to the onset of buckling [28].

The presence of voids has a significant impact on the strength variability of carbon fiber-reinforced epoxy resin. The voids categorized into six types based on location, shape and size: towpreg voids, towpreg-edge voids, crimp voids, overlap gaps, towpreg gaps and interlaminar voids. Each category has a distinct origin. To reduce the number of voids and minimize their impact on tank burst pressure, it is essential to implement effective void-reduction techniques, such as thin towpreg application, compaction roller use, and high-pressure curing [29].

The damage mechanisms in composite pressure vessels are complex and multifaceted, primarily due to the layered structure of these vessels. The typical failure modes in such systems include matrix cracking, delamination, fiber rupture, and interfacial failure between the fibers and the matrix (debonding). These failures often occur due to the combined effects of mechanical loading, environmental factors, voids, and the inherent weaknesses of the composite materials used [30-37].

This paper analyses the interplay between fiber orientations, porosity levels and mechanical properties in carbon fiber-reinforced epoxy resin composites manufactured via the filament winding process. The paper is structured as follows: it begins with an overview of the essential physical-chemical characteristics and microstructure of the composites used. Subsequent sections will explore their thermo-mechanical properties. The paper will place particular emphasis on calculating porosity and examining its impact on mechanical properties across various angular fiber orientations, specifically +/- 15°, +/- 30°, and multilayer tubes with diverse orientations (±15°/±30°/±45°/±86°). The paper will present results from quasi-static tensile tests and loading-unloading tests up to the point of failure. Finally, a multi-scale damage analysis will examine the initiation and progression of damage in composites with different fiber angles.

2. Material preparation and methods

2.1. Epoxy/carbon fiber composite ± θ

Three cylindrical samples of Carbon Fiber Reinforced Epoxy resin were prepared by Forvia, each with different angular orientations of the fibers. These samples included antisymmetric laminates with orientations

of ±15° and ±30°, as well as a multilayer laminate comprising orientations of ±15°/±30°/±45°/±86°. Table 2 presents macroscopic photographs of the various tubes. To analyze the samples, the cylindrical specimens were sliced into curved samples using a cutting machine with a rotational blade.

N° tubes	Orientation	Illustration
1	±15°	
2	±30°	
3	multilayer	

Table. 2. View and illustration of composite of cylindrical carbon fiber reinforced epoxy resin

2.2. Characterization methods

2.2.1. Physico-chemical characterizations

Differential Scanning Calorimetry (DSC) is used not only to determine the specific heat capacity of materials, but also to analyze the curing behavior of epoxy resins. Analysis was performed using a DSC instrument (Q1000 V9.0 Build 275, TA Instruments). Samples were pressed into non-hermetic aluminum pans, sealed and heated at a rate of 10°C/min to 220°C. Samples were then cooled to 30°C at a rate of 10°C/min.

Dynamic Mechanical Analysis (DMA) was used to determine the glass transition temperatures of the epoxy matrix. Experiments were performed using a DMA Q800 TA Instruments instrument on specimens of 25×4 mm². Test conditions included a 3-point flexural loading mode at a frequency of 1 Hz over a temperature range of 25°C to 150°C with a ramp rate of 2°C per minute.

2.2.2. Microscopic observations

The HITACHI S-4800 Scanning Electron Microscope (SEM) was used to qualitatively examine the material microstructure, fracture surfaces of tensile specimens and in particular crack propagation during quasi-static testing. It was also used to quantitatively measure the porosity within the microstructure. Porosity, or void fraction, is the volume of voids in a material compared to its total volume. Following microstructural analysis, the first step in the experimental process is to analyze the porosity of the material, which can be calculated using the following method:

- Determination of the percentage by mass of fiber (M_f %) or epoxy (M_e %): To quantify the fiber content in the composite, all samples were subjected to pyrolysis by heating at 550°C for 5.5 hours. This process resulted in the degradation of the matrix material, leaving behind the carbon fiber. The

formula used to calculate the fiber content is:

(M_0 - M_P) / M_0 * 100, where M_0 is the initial mass and M_P is the mass after pyrolysis. In addition, the density of the carbon fiber (1.8 g/cm³) and the density of the epoxy used (1.2 g/cm³) are used to determine the porosity content.

2.2.3. Quasi-static tensile test

Quasi-static tensile tests were carried out using an Instron 5966 machine at a speed of 10mm/min (~0.001 s^{-1}) and a temperature of 20°C. Measurement of strain in the gauge length was facilitated by a non-contact video extensometer. This advanced instrument uses non-contact optical measurement techniques, using a digital camera and real-time image processing to accurately measure deformation in both the axial and lateral directions during tensile testing. To prevent specimen slippage, self-tightening grips were used to secure the specimens in place. Specimen dimensions are shown in Fig. 1.

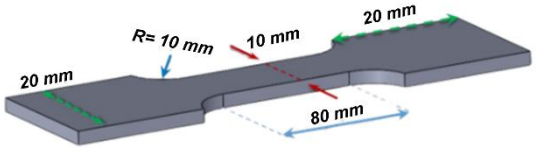

Fig. 1. Dimensions of Carbon Fiber Reinforced Epoxy samples

2.3. Methodology of damage analysis

To demonstrate the specific damage phenomena in CFRP composites, it is necessary to establish a reference state for comparison with different damage states and scenarios in different microstructures. Since damage drives the behavior of CFRP composites, changes in stiffness can be used as an indicator of damage. This approach allows microscopic damage mechanisms and residual stiffness to be tracked over different stress levels. During quasi-static loading-unloading tests, the Young's modulus is measured, and precise SEM scans of the damaged areas are taken at each stress level. This helps to analyze the damage evolution and describe the crack propagation. This process continues until the specimen fails. This method allows a quantitative relationship to be established between changes in macroscopic properties and damage mechanisms.

3. Experimental results and discussion

3.1. Physico-chemical analysis

Three orientations of carbon fiber reinforced epoxy composites, namely ±15°, ±30° and multilayers, were subjected to Differential Scanning Calorimetry (DSC) to evaluate their thermal response to temperature

variations. The DSC results showed a characteristic slope corresponding to the phase change associated with the glass transition temperature (T_g), which was found to be approximately 124°C for all orientations tested. This observation suggests effective cross-linking of the epoxy within the composite structure. Furthermore, no additional peaks or indications of physical ageing were observed throughout the temperature range of 30°C to 220°C, as shown in Fig 2. This absence of peaks indicates that the composites maintained their thermal stability and did not undergo significant changes in molecular structure or thermal properties over the temperature range tested. In conclusion, the DSC analysis confirms that the carbon fiber reinforced epoxy composites with ±15°, ±30° orientations, as well as the multilayers configuration, have stable and well cross-linked resin matrices with consistent thermal behavior and resistance to physical ageing over the specified temperature range.

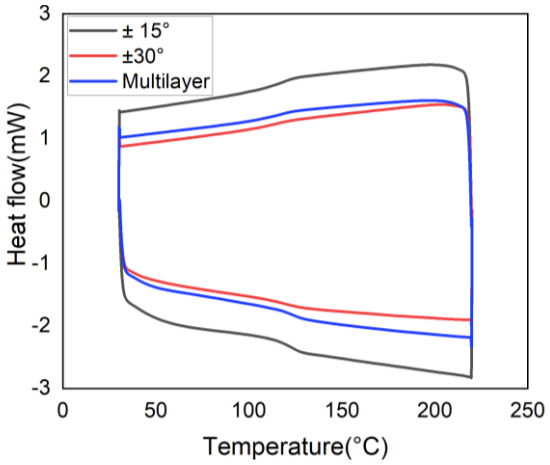

Fig. 2. DSC curve and stability of CFRP composites

The DMA results showed that the storage modulus shows minimal variation with increasing temperature within the glassy zone up to 100°C. However, beyond this temperature there is a significant decrease in the modulus. The glass transition temperature (T_g) values determined by DMA for each sample are consistently around 124°C. This finding corroborates the T_g values obtained from the DSC analysis. These results indicate that the carbon fiber reinforced epoxy composites maintain their structural integrity and stiffness in the glassy state up to about 100°C, after which a significant decrease in modulus occurs. The agreement between the DSC and DMA results further supports the effective cross-linking and thermal stability of the epoxy matrix in the composites.

3.2. Microstructural analysis

Understanding the distribution and impact of these microstructural features, particularly in relation to different fiber orientations, is essential for optimizing manufacturing processes and improving the overall mechanical performance and durability of carbon fiber-reinforced epoxy composites.

Microstructural analysis using optical microscopy (Fig. 3) confirms the laminated composite structure and validates the architecture produced by the industrial process, including different fiber orientations such as ±15°, ±30° and multilayers configurations. Each micrograph shows porosities resulting from the manufacturing process, which can act as crack initiation sites.

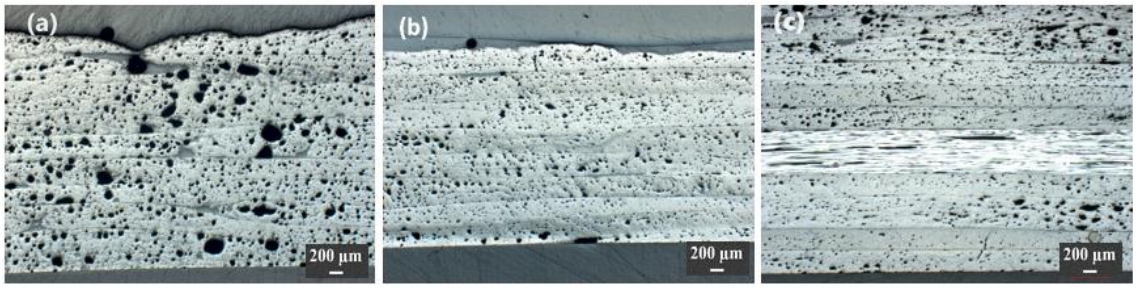

Fig. 3. Optical micrograph: (a) ±15°, (b) ±30° and (c) multilayers configurations

Subsequent SEM observations (Fig. 4) further corroborate the light microscopy findings. These observations not only confirm the layered structure of the composite, but also highlight the heterogeneity and condition of the fiber/matrix interface, particularly in regions adjacent to the observed porosities. Signs of fiber/matrix decohesion are evident, indicating potential weaknesses in the material.

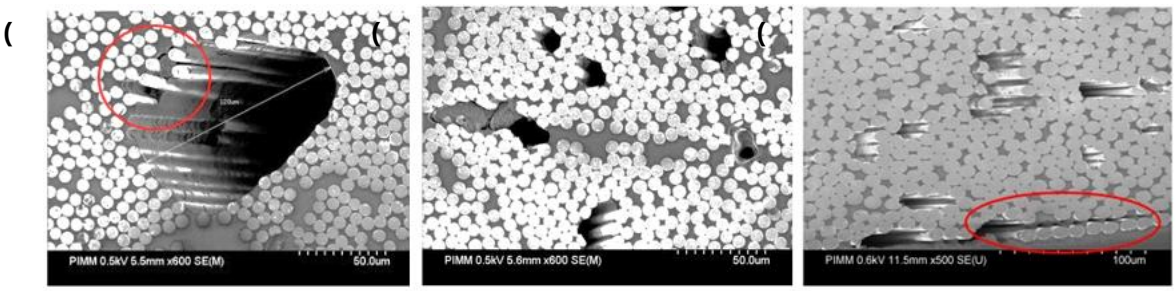

Fig. 4. SEM micrograph: (a) ±15°, (b) ±30° and (c) multilayers configurations

3.3. Impact of fiber orientation on porosity

Table 3 shows the volume percent of porosity in tubes with different fiber orientations and shows significant variations from 4.7% to 7.8%. These results highlight the significant influence of fiber orientation on the porosity levels within the composites.

For the ±15° orientation, the density of the composite is 1.39 g/cm³, with fibers accounting for 69.8% of the mass (54.20% by volume) and epoxy for 30.21% of the mass (37.9% by volume). The porosity is 7.8%. In the ±30° orientation, the density of the composite is 1.45 g/cm³, with fibers making up 70.94% of the mass (57.28% by volume) and epoxy resin 29.06% of the mass (38.00% by volume). The porosity is 4.7%. In the multilayers configuration, the density of the composite is 1.46 g/cm³, with fibers making up 72.92% of the mass (59.17% by volume) and epoxy 27.08% of the mass (35.6% by volume). The porosity is 5.2%.

Overall, across all tubes tested, the average density is 1.44 g/cm³. Fibers constitute 71.1% of the mass (56.9% by volume), while epoxy resin makes up 28.8% of the mass (37.5% by volume). The average porosity for all samples is 5.4%. These findings highlight the critical role of optimizing fiber orientation during composite manufacturing to minimize porosity and enhance overall material integrity and mechanical performance.

Tube	Composite Density	Fiber (mass)	Fiber (vol)	Epoxy (mass)	Epoxy (vol)	% Volume Porosity
±15°	1,39	69,79%	54,20%	30,21%	37,99%	7,8%
±30°	1,45	70,94%	57,28%	29,06%	38,00%	4,7%
Multilayer	1,46	72,92%	59,17%	27,08%	35,65%	5,2%
Average	1,44	71,15%	56,99%	28,85%	37,49%	5,4%

Table. 3. Volume percentage of porosity in tubes with different fiber orientations

3.4. Tensile behavior

The mechanical properties of the carbon fiber reinforced epoxy composites, as shown in Fig. 5 and Table 4, show significant variations influenced by fiber orientation. For each orientation tested ±15°, ±30° and multilayers configurations approximately five specimens were analysed to ensure the reliability and repeatability of the stress-strain curves. These results highlight the consistency of tensile behavior over multiple tests.

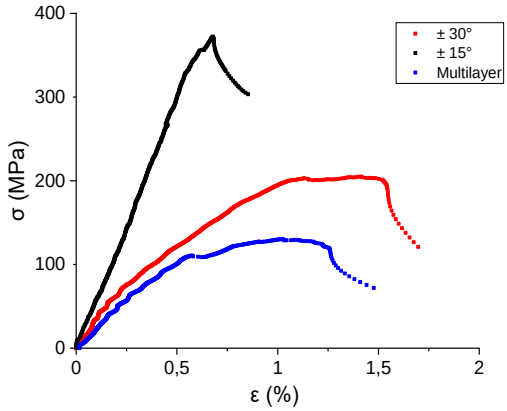

Fig. 5. Representative-curves of quasi-static tensile tests at 20°C ($d\varepsilon/dt = 0.001\ s^{-1}$)

Tube	E (GPa)	$\sigma_{threshold}$ (MPa)	$\varepsilon_{threshold}$ (%)	σ_{max} (MPa)	ε_{max} (%)
±15°	$60^{\pm 2.7}$	$331^{\pm 5.2}$	$0.56^{\pm 0.02}$	$361.4^{\pm 8}$	$0.66^{\pm 0,08}$
±30°	$36.8^{\pm 2.20}$	$55^{\pm 2.3}$	$0.17^{\pm 0.06}$	$206.6^{\pm 4.2}$	$1.3^{\pm 0,10}$
Multilayer	$21.1^{\pm 0.75}$	$111.8^{\pm 3.4}$	$0.538^{\pm 0.10}$	$157.1^{\pm 6.4}$	$0.94^{\pm 0,08}$

Table. 4. Summary of tensile mechanical properties for different tubes

The results show that fiber orientation plays a critical role in determining mechanical behavior. Samples aligned more closely to the applied force, such as those in the ±15° orientation, exhibit higher tensile strength and modulus, reflecting efficient load transfer along the fibers. Conversely, the ±30° and multilayer configurations exhibit greater ductility, characterized by higher elongation at break.

Specifically, the ±15° oriented samples show superior performance due to optimal stress distribution along the fibers, resulting in higher stiffness and resistance to deformation. In contrast, the ±30° oriented specimens and the multilayer configurations, where the fibers are less optimally oriented with respect to the loading direction, experience lower stiffness but show an improved ability to deform before failure. This behavior is attributed to damage and plastic deformation in the epoxy matrix and reflects the influence of fiber-matrix interactions under load.

Samples from different orientations show different fracture characteristics. The ±15° oriented samples exhibit clean and straight fracture surfaces, indicating brittle fracture behavior consistent with their high stiffness and low strain at break. In contrast, the ±30° oriented specimens and multilayers configurations show more irregular and rough fracture surfaces. These observations are consistent with the mechanical properties

summarized in Table 4 and reinforce the critical role of fiber orientation in determining the fracture behavior and overall mechanical performance of carbon fiber reinforced epoxy composites.

The transition from ductile to brittle fracture modes under different loading conditions is investigated by microscopic analysis, as shown in Fig. 6. The ±15° oriented micrographs of the specimens show characteristics indicative of brittle fracture. The fracture surfaces appear flat, smooth and featureless, lacking the typical ductile characteristics. The observed shift from brittle to ductile fracture modes from ±15° to ±30° and multilayers configurations highlights the sensitivity of the fracture behavior of the material to fiber orientation.

Tube	Fractography	
±15°	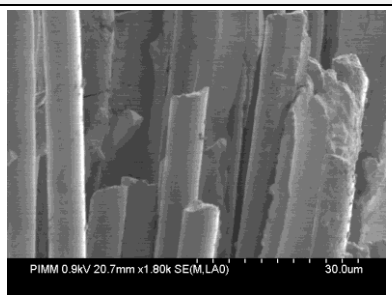	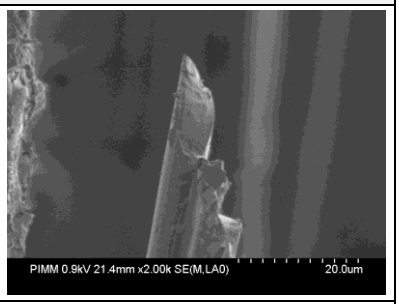
±30°	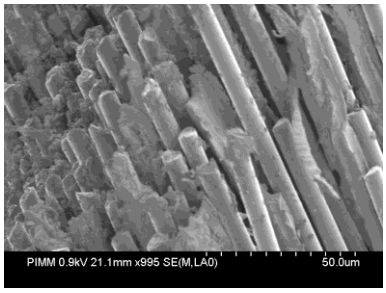	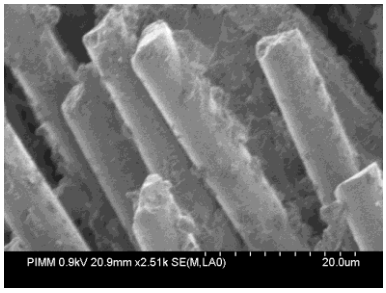
Multilayer	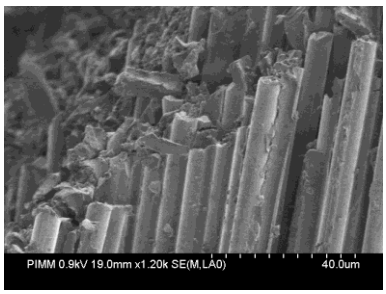	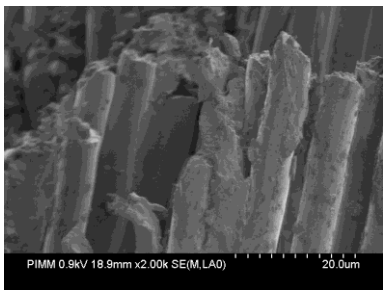

Fig. 6. Microscopic analysis of fracture surfaces

3.5. Damage mechanism analysis

3.5.1. Quantitative macroscopic damage analysis

The evolution of the mechanical behavior of a material, from its initial state to its failure, is described by the following macroscopic damage theory [38-45]:

$$D_{macro} = 1 - \frac{E^D}{E^0}$$

Where $E^0$and E^D are respectively the moduli of the undamaged and damaged material. The analysis of Fig. 5 coupled with Fig. 7 demonstrates the evolution of relative stiffness (E/E_0) for the different tube orientations studied. Regardless of the orientation, two distinct stages are observed:

- In this initial stage, the material exhibits linear behavior without any plasticity or damage.
- In the second stage, the material shows an anelastic response due to the combined effects of damage and matrix plasticity.

Fig. 7 illustrates the macroscopic evolution of damage for the different tube orientations, highlighting how fiber orientation influences the rate and extent of damage and plasticity. The effect of fiber orientation on damage kinetics is significant. The ±30° and mixed tube orientations exhibit faster damage kinetics compared to the ±15° orientation. Specifically, the ±15° tubes demonstrate the lowest levels of damage and plasticity, indicating that this orientation provides greater resistance to damage progression. This visual representation underscores the critical role of fiber orientation in determining the mechanical behavior and durability of CFRP composites under loading.

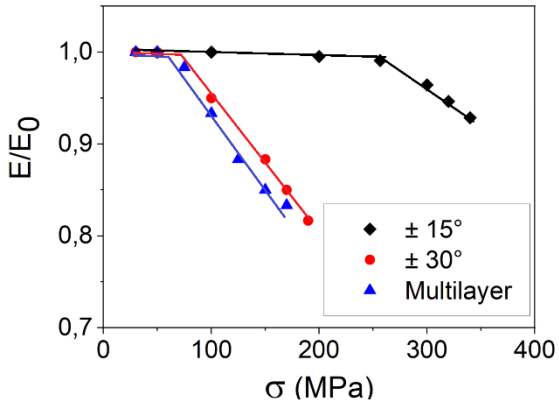

Fig. 7. Macroscopic evolution of damage for different tubes

3.5.2. Qualitative microscopic damage analysis

To identify the damage mechanisms occurring during quasi-static loading, it is necessary to conduct experimental investigations at both macroscopic and microscopic scales. For this purpose, rectangular specimens with polished surfaces enabling microscopic observations using SEM have been prepared. Figure 8 shows the mechanical behavior of the ±15° oriented composite under loading. The material shows no

evidence of damage up to 300 MPa and retains linear elastic behavior. Beyond this point, the material begins to accumulate damage leading to non-linear behavior and eventual failure. The first damage mechanism observed is the decohesion at the fiber-matrix interface, as demonstrated by Nouira et al. [46].

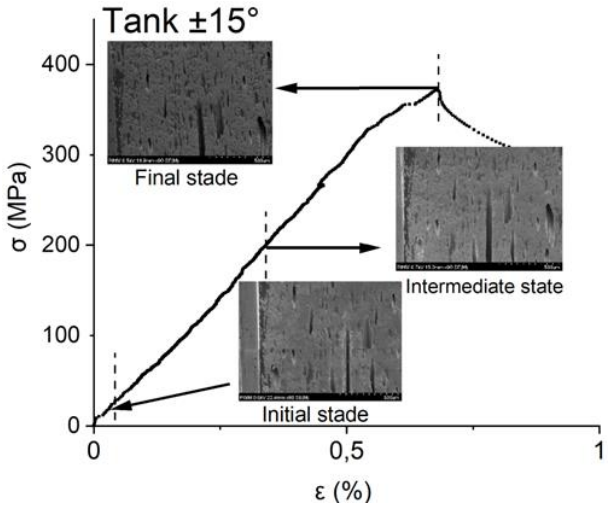

Fig. 8. Microscopic damage mechanisms: ±15° configuration

Figure 9 shows the mechanical behavior of the ±30° oriented multilayer composite under load. Initially the material exhibits linear elastic behavior up to 80 MPa without damage. Again, the first damage mechanism observed is decohesion at the fiber matrix interface.

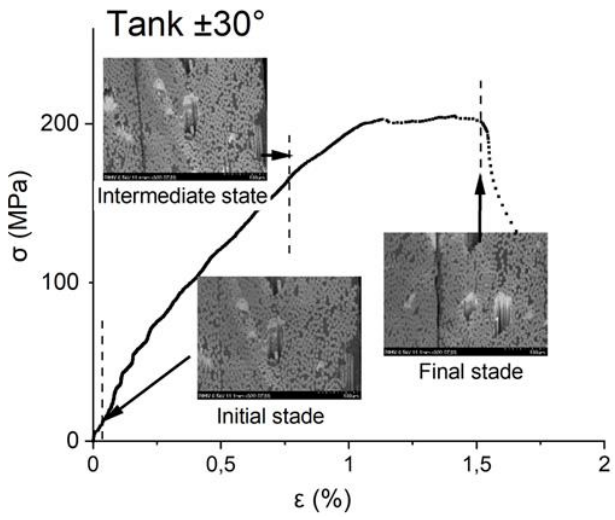

Fig. 9. Microscopic damage mechanisms: ±30° configuration

Fig. 10 shows a stress-strain curve (σ-ε) for a multilayer composite, accompanied by SEM images at different stages of deformation: initial, intermediate and final. At the initial stage, the material exhibits linear elastic behavior with no visible damage or plastic deformation, as shown in the SEM image labelled "Initial

stage". Again, the first damage mechanism observed is decohesion at the fiber matrix interface at around 60 MPa. As the strain increases to around 1.0%, the stress continues to increase but at a decreasing rate, peaking at around 120 MPa. During this intermediate stage, the material begins to show signs of damage and plasticity, as evidenced by the SEM image showing the onset of decohesion at the fiber/matrix interface and micro-cracking, followed by matrix fracture.

Beyond 1.0% strain, after peak stress is reached, the curve shows a decline, indicating failure or significant damage. At this final stage, the material exhibits anelastic behavior due to extensive damage and plastic deformation, with the SEM image labelled 'Final stage' showing large cracks and significant damage leading to delamination specially at ±86° layers and consequently the eventual failure of the material.

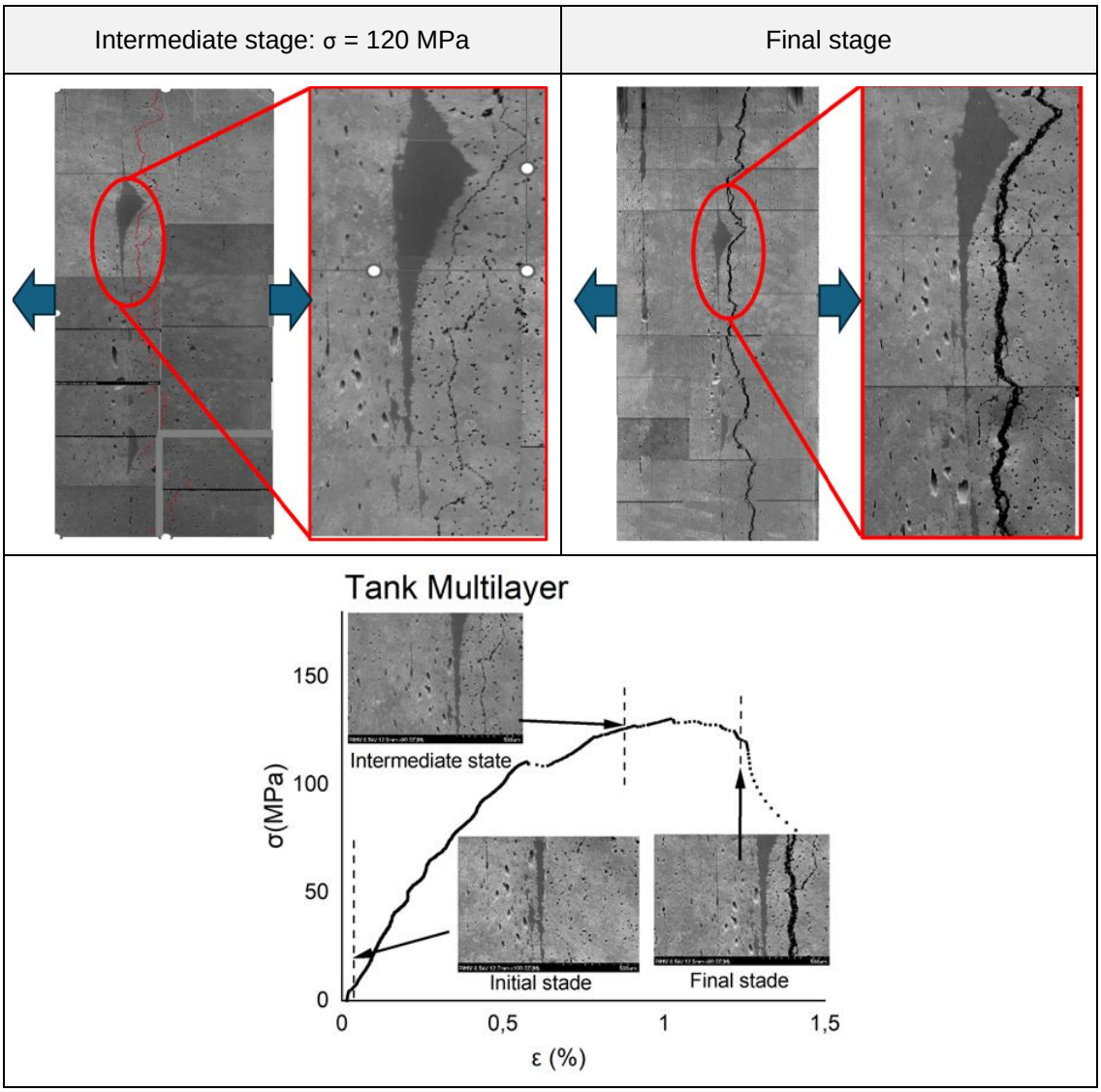

Fig 10. Microscopic damage mechanisms: multilayers configuration

In the microstructure of the ±15°, ±30° and multilayers configurations (Fig. 11), composites in their initial state contain pores or voids resulting from the manufacturing process. These pores may be randomly distributed throughout the material, with fibers often extending to the surface of the pore walls. In tensile testing, due to the different orientation of the fibers in different layers, the stresses are unevenly distributed. Around the pores, the tensile stresses are amplified due to the stiffness mismatch between the matrix and the porous regions, resulting in local stress concentrations (see Fig. 11).

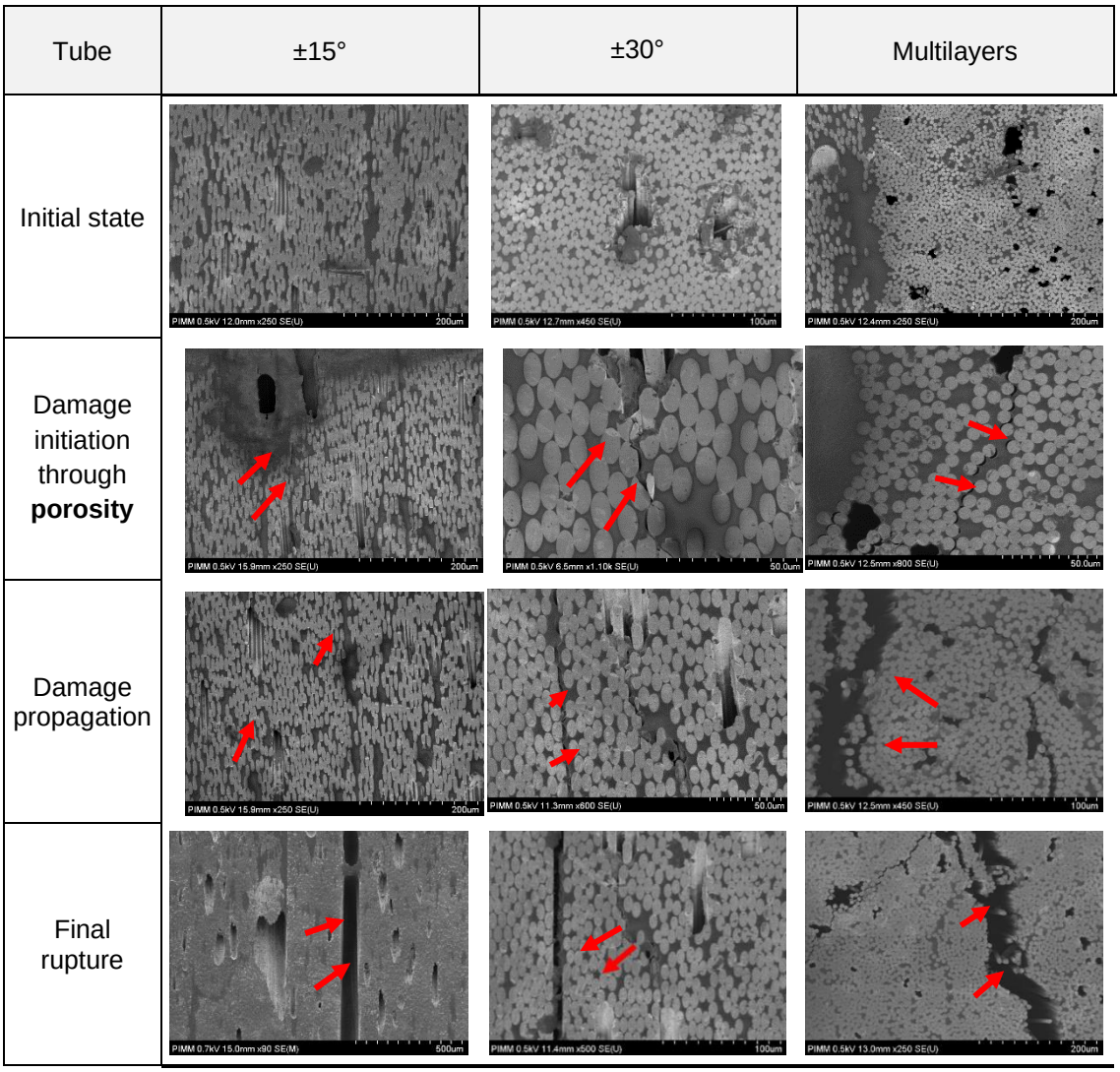

Fig. 11. Microstructural evolution and damage mechanisms for different tubes

These concentrated stresses near the pores can exceed the strength of the material and initiate cracking. These cracks typically originate at the edges of the pores and propagate through the material along paths of least resistance. The initial damage phenomenon is observed to coincide with the first non-linearity in the stress-strain curve, corresponding to fiber/matrix decohesion at the pore interfaces. This results in the

propagation of microcracks between the pores in the direction of the applied stress, this result was confirmed in Shirinbayan et al. for a laminated composite [46].

As the applied stress increases, this damage mechanism spreads diffusely throughout the observation zone, originating at multiple pore locations. At the same time, existing microcracks continue to grow. At the maximum stress level, local deformation by shearing around fiber bundles becomes significant. This leads to fiber deformation around the bundles, resulting in pseudo-delamination near the fracture.

The thresholds and kinetics of damage mechanisms in ±θ composites depend on several factors: the specific orientation of the fibers within each layer, the state of stress experienced by each layer (a function of the stacking sequence and the macroscopic load), the statistical variation in the spatial distribution of pores (which differs with fiber orientation), and the rate at which stress is applied (with threshold stresses increasing with stress rate). During tensile testing, damage in long fiber composite structures is characterized by different behaviors at different scales. At the microscopic scale, crack initiation within porosities contributes significantly to material damage, including fiber/matrix decohesion at interfaces and fiber breakage leading to the formation of new porosities (Fig. 12).

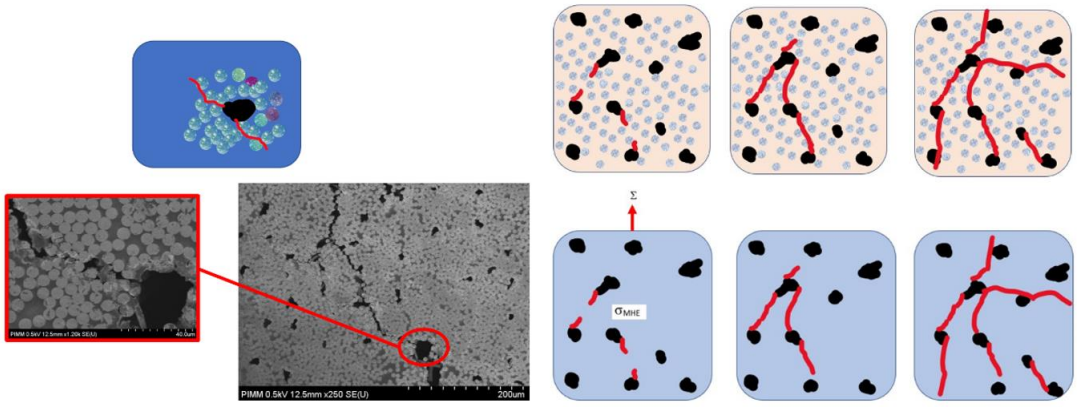

Fig. 12. Schematic of the damage scenario of carbon fiber reinforced epoxy composite

At the mesoscopic scale, the coalescence of these microscopic decohesions forms transverse cracks that extend through the entire ply thickness, with the ends of these cracks acting as sites for micro-delamination, leading to delamination between plies. This complex interaction of multiple damage mechanisms in thick, heterogeneous composites highlights the need for robust models to predict their performance under load.

4. Conclusion

The study investigates composite materials used in hydrogen tanks and examines orientations such as ±15°, ±30°, and multilayers configurations to assess mechanical properties, damage criteria and fracture criteria at the scale of unidirectional layers. Mechanical characterization tests, including tensile tests and loading-unloading tests for damage analysis reveal significant variability in material behavior as a function of orientation. In-situ testing identifies interface decohesion and porosity-induced cracking as the primary mechanisms leading to material failure, with additional factors such as fiber fracture and microcracking contributing in a secondary role. These findings highlight the orientation-dependent complexity of damage mechanisms in composites and provide important insights for model validation in simulations aimed at improving the design and reliability of composite hydrogen tanks. Microstructural analysis of configurations such as ±15°, ±30° and multilayers showed that initial composites may have randomly distributed pores or voids from the manufacturing process, with fibers often extending to the pore surfaces. During tensile testing, uneven stress distribution occurs due to different fiber orientations between the layers. This unevenness causes localized stress concentrations around pores, which are exacerbated by stiffness mismatches between the matrix and porous regions.

5. Declarations

- Consent to participate: Not applicable.
- Consent to publish: Not applicable.
- Conflict of interest: The authors declare that they have no conflicts of interest.

Authors' contributions

M. Shirinbayan, R. Tie Bi, J-B. Maeso, C. Thomas, J. Fitoussi: construct the idea. I. Feki, M. Shirinbayan, S. Nouira, E. Heripre, R. Tie Bi, J-B. Maeso, C. Thomas, J. Fitoussi: analyzed results, drafted manuscript preparation, and wrote the paper. I. Feki, M. Shirinbayan, S. Nouira, J. Fitoussi: corrected the English and the paper format.

Availability of data and materials

The authors declare that the data and the materials of this study are available within the article.

6. References

[1] E. Commission. Further CO2 emission reduction from cars and vans: a win-win for the climate, consumers, innovation and jobs. Brussels, 2012.

[2] Nachtane, M.; Tarfaoui, M.; Goda, I.; Rouway, M. A review on the technologies, design considerations and numerical models of tidal current turbines. Renew. Energy 2020, 157, 1274-1288.
[3] Weger, L.B.; Leitão, J.; Lawrence, M.G. Expected impacts on greenhouse gas and air pollutant emissions due to a possible,transition towards a hydrogen economy in German road transport. Int. J. Hydrogen Energy 2021, 46, 5875-5890.
[4] Foorginezhad, S.; Mohseni-Dargah, M.; Falahati, Z.; Abbassi, R.; Razmjou, A.; Asadnia, M. Sensing advancement towards safety assessment of hydrogen fuel cell vehicles. J. Power Sources 2021, 489, 229450.
[5] IEA. The Future of Hydrogen, Report Prepared by the IEA for the G20, Japan; Seizing Today's Opportunities; IEA: Paris, France, 2019.
[6] M. A. Ç. Cevahir Tarhan, «A study on hydrogen, the clean energy of the future: Hydrogen,» Journal of Energy Storage, p. https://doi.org/10.1016/j.est.2021.102676, 2021.
[7] H. T. H. a. A. Varma, «Hydrogen storage for fuel cell vehicles,» Current Opinion in Chemical Engineering, p. http://dx.doi.org/10.1016/j.coche.2014.04.004, 2014.
[8] M. T. a. K. Z. Etienne Rivard, «Hydrogen Storage for Mobility: A Review,» materials, p. doi:10.3390/ma12121973, 2019.
[9] D. Mori*, K. Hirose. Recent challenges of hydrogen storage technologies for fuel cell vehicles. 2008 International Association for Hydrogen Energy. Published by Elsevier Ltd. doi:10.1016/j.ijhydene.2008.07.115
[10] Rivard, E. ; Trudeau, M. ; Zaghib, K. Stockage d'hydrogène pour la mobilité : une revue. Matériaux 2019 , 12 , 1973. https://doi.org/10.3390/ma12121973
[11] H. LARA, 'Energy revolution,' 21 January 2022.
[12] Zhang, M.; Lv, H.; Kang, H.; Zhou,W.; Zhang, C. A literature review of failure prediction and analysis methods for composite high-pressure hydrogen storage tanks. Int. J. Hydrogen Energy 2019, 44, 25777–25799.
[13] K. H. D. Mori*, «Recent challenges of hydrogen storage technologies for fuel cellvehicles,» international journal of hydrogen energy.
[14] J. Zheng, J. Guo, J. Yang, Y. Zhao, L. Zhao, X. Pan, J. Ma et L. Zhang, «Experimental and numerical study on temperature rise within a 70 mpa type iii cylinder during fast refueling.,» 13th china hydrogen energy conference (CHEC), 2013.
[15] N. M. CebollaB.AcostaP.MorettoF.HarskampC.Bonato, «Compressed hydrogen tanks for on-board application: Thermal behaviour during cycling,» International Journal of Hydrogen Energy, 2015.03.035, 2015.
[16]. Azeem, M.; Ya, H.H.; Alam, M.A.; Kumar, M.; Stabla, P.; Smolnicki, M.; Gemi, L.; Khan, R.; Ahmed, T.; Ma, Q.; et al. Application of FilamentWinding Technology in Composite Pressure Vessels and Challenges: A Review. J. Energy Storage 2022, 49, 103468.
[17] H.S. Roh, T.Q. Hua*, R.K. Ahluwalia. Optimization of carbon fiber usage in Type 4 hydrogen storage tanks for fuel cell automobiles. 2013, Hydrogen Energy Publications, LLC. Published by Elsevier Ltd. 2013.
[18] Damien Halm, B. Magneville, Jacques Renard, Philippe Saffré, Stéphane Villalonga. Optimisation des réservoirs composites de stockage hyperbare de l'hydrogène : bilan du projet Osirhys IV. 22ème Congrès Français de Mécanique, Aug 2015, Lyon, France.

[19]Rosato DV, Grove CS. Filament winding: its development, manufacture, applications, and design. New York: Interscience; 1964.
[20] Peter ST, Humphrey WD, Foral RF. Filament winding: composite structure fabrication. California: SAMPE; 1991.
[21] ISO/DIS 15869/2, Gaseous Hydrogen and Hydrogen blends-land Vehicule Fuel Tanks, September 2005.
[22] NF EN 12245, Bouteilles à gaz transportables-Bouteilles entiérement bobinées en matériaux composites, mars 2009.
[23] Ilyas M. Damage modeling of carbon epoxy laminated composites submitted to impact loading, Thèse de doctorat, Université de Toulouse 2010.
[24] Les matériaux composite dans le secteur ferroviaire, Groupement de la Plasturgie Industrielle et des Composites, 2009.
[25] Aleksander Błachut and al, Influence of fiber tension during filament winding on the mechanical properties of composite pressure vessels,Composite Structures,Volume 304, 2022.
[26] Sofi, T., Neunkirchen, S., & Schledjewski, R. (2018). Path calculation, technology and opportunities in dry fiber winding: a review. Advanced Manufacturing: Polymer & Composites Science, 4(3), 57–72.
[27] C Chang et al. Effect of filament winding process parameters on interlaminar performance for CF/PP thermoplastic composite. 2022. J. Phys.: Conf.
[28] Madrid M, Almeida JHS, Lisbôa TV, Spickenheuer A, Marczak RJ, Amico SC. Test de pression interne de cylindres à extrémité ouverte à enroulement filamentaire utilisant l'expansion radiale d'inserts en élastomère. Journal des plastiques et composites renforcés. 2024;0(0).
[29] M. Ueda and al. Voids in type-IV composite pressure vessels manufactured by a dry filament winding process. International Journal of Pressure Vessels and Piping,Volume 208, 2024.
[30] Han, Geng, Guan, Zhidong, Li, Xing, Ji, Ruipeng and Du, Shanyi. "The failure mechanism of carbon fiber-reinforced composites under longitudinal compression considering the interface" Science and Engineering of Composite Materials, vol. 24, no. 3, 2017, pp. 429-437. 2015.
[31] M. B. T.-C. Lafarie-Freno, «Experimental study of the stacking sequence effect on polymer/composite multi-layers submitted to thermomechanical cyclic loadings», international journal of hydrogen energy, p. 11397-11404, 2010.
[32] E. a. S. B. Gamstedt, «Michromechanisms in tension-compression fatigue of composite laminates containing transverse plies.,» Composites Sciences and Technology, vol. 59, p. 167-178.
[33] M. G. a. M.-C. L.-F. D. Vu, «The effect of thermo-oxidation on matrix cracking of cross-ply [0/90]s composite laminates,,» Compos. Part A, pp. 114–121,, 2013.
[34] C. A. U. D. G. M. A. S. B. M. L. a. J. V. L. Jiang, «Recycling carbon fiber composites using microwave irradiation: Reinforcement study of the recycled fiber in new composites,,» J. Appl. Polym, p. 42658-42666, 2015.
[35] P. PROMBUT, «Caractérisation de la propagation de délaminage des stratifiés composites multidirectionnels,» Université Toulouse, Toulouse, 2007.
[36] Y. D. e. J. QIAN, «Analysis of microdamage evolution histories in composites.,» International Journal of Solids and Structures, p. 1831–1854, 2001.

[37] F. LEBEL, « Contrôle de la fabrication des composites par injection sur renforts.,» Université de Montréal,, Miontréal, 2012.
[38] J. Fitoussi, M. H. Nikooharf, A. Kallel, and M. Shirinbayan, "Mechanical Properties and Damage Behavior of Polypropylene Composite (GF50-PP) Plate Fabricated by Thermocompression Process Under High Strain Rate Loading at Room and Cryogenic Temperatures," Applied Composite Materials, vol. 29, p. 1959–1979, 2022.
[39] M. Shirinbayan, M. Rezaei-Khamseh, M. H. Nikooharf, A. Tcharkhtchi, and J. Fitoussi, "Multi-scale analysis of mechanical properties and damage behavior of polypropylene composite (GF50-PP) plate at room and cryogenic temperatures," Composite Structures, vol. 278, p. 114713, 2021.
[40] M. Shirinbayan, H. B. Rizi, N. Abbasnezhad, A. Tcharkhtchi, J. Fitoussi, "Tension, compression, and shear behavior of advanced sheet molding compound (A-SMC): Multi-scale damage analysis and strain rate effect," Composites Part B: Engineering, vol. 225, p. 109287, 2021.
[41] M. Shirinbayan, "Multi-scale damage analysis of the tension-tension fatigue behavior of a Low-Density Sheet Molding Compound (LD-SMC)", Journal of Applied Polymer Science, 2021.
[42] M. A. Imaddahen, M. Shirinbayan, H. Ayari, M. Foucard, A. Tcharkhtchi, and J. Fitoussi, "Multi-scale analysis of short glass fiber-reinforced polypropylene under monotonic and fatigue loading," Polymer Composites, vol. 41, no. 11, pp. 4649-4662, 2020.
[43] M. Shirinbayan, J. Fitoussi, N. Abbasnezhad, F. Meraghni, B. Surowiec, A. Tcharkhtchi, "Mechanical characterization of a Low-Density Sheet Molding Compound (LD-SMC): Multi-scale damage analysis and strain rate effect". Composites Part B: Engineering, 131: 8-20, 2017.
[44] M. Shirinbayan, J. Fitoussi, M. Bocquet, F. Meraghni, B. Surowiec, A. Tcharkhtchi, "Multi-scale experimental investigation of the viscous nature of damage in Advanced Sheet Molding Compound (A-SMC) submitted to high strain rates". Composites Part B: Engineering, 115: 3-17, 2017.
[45] M. Shirinbayan, J. Fitoussi, F. Meraghni, B. Surowiec, M. Bocquet, A. Tcharkhtchi. "High strain rate visco-damageable behavior of Advanced Sheet Molding Compound (A-SMC) under tension". Composites Part B: Engineering, 82: 30-41, 2015.
[46] Effect of processing conditions on morphology and mechanical damage in glass-reinforced polypropylene composite - Nouira - 2024 - Polymer Composites /doi/10.1002/pc.28338
[47] Shirinbayan M, Nouira S, Imaddahen MA, Fitoussi J. Microstructure-sensitive investigation on the plastic deformation and damage initiation of fiber-reinforced polypropylene composite. Compos Part B Eng. 2024 Nov 1;286:111790.

Article N°3 :

Imen Feki, Mohammadali Shirinbayan, Samia Nouira, Robert Tie Bi, Jean-Baptiste Maeso, Cedric Thomas, Joseph Fitoussi, Multi-scale fatigue damage analysis in filament-wound carbon fiber reinforced epoxy composites for hydrogen storage tanks,Composites Part C: Open Access,Volume 15, 2024,100537,ISSN 2666-6820, https://doi.org/10.1016/j.jcomc.2024.100537.

Multi-scale fatigue damage analysis in filament-wound carbon fiber reinforced epoxy composites for hydrogen storage tanks

Imen Feki[1], Mohammadali Shirinbayan[1,*], Samia Nouira[1], Robert Tie Bi[2], Jean-Baptiste Maeso[2], Cedric Thomas[2], Joseph Fitoussi[1]

[1]Arts et Metiers Institute of Technology, CNAM, CNRS, PIMM, HESAM University, F-75013 Paris, France

[2] Faurecia Hydrogen Solutions, FORVIA Clean Mobility, Bois Sur Prés, 25550 Bavans, France.

E-mails: Mohammadali.Shirinbayan@ensam.eu (corresponding author), Imen.Feki@ensam.eu, Samia.Nouira@ensam.eu, Robert.tbr.tiebi@forvia.com, Jean-Baptiste.Maeso@forvia.com, Cedric.Thomas@forvia.com, Joseph.Fitoussi@ensam.eu.

Abstract

This article presents the findings of a multi-scale experimental study on carbon fiber-reinforced epoxy composites (CFRP) used in lightweight hydrogen storage pressure vessels produced via filament winding. The research employs a combination of tension-tension load-controlled fatigue tests and high-resolution physical-chemical characterization and porosity quantification to assess the impact of porosity on mechanical performance. The findings demonstrate that porosity has a detrimental impact on mechanical properties, acting as nucleation sites for damage mechanisms such as crack initiation, fiber-matrix separation and fiber breakage. At the mesoscopic level, microdefects coalesce into transverse cracks and delamination, resulting in complex failure modes under cyclic loading. The results of the tensile tests demonstrated that the orientation of the fibers has a significant impact on the mechanical behavior of the material. The ±15° configuration demonstrated superior tensile strength and modulus, while the ±30° and multilayer configurations exhibited higher ductility. The results of the fatigue testing confirmed that fiber orientation has a significant impact on fatigue life, with the ±15° configuration proving to be the most resistant. Microscopic analysis indicated that pores act as damage initiation points, accelerating failure through matrix cracking, fiber-matrix debonding, and delamination. This study highlights the need for improved porosity control during manufacturing to enhance the durability of hydrogen storage systems. Additionally, it provides valuable insights for optimizing fiber orientation to improve fatigue performance in practical applications.

Keywords: Hydrogen; CFRP; Porosity; Fatigue; Damage.

1. Introduction

Over the past three decades, the environment has been affected by the combined effects of the depletion of fossil resources (oil, natural gas, and coal) and global warming due to the significant increase in carbon dioxide (CO_2) concentration, which is a greenhouse gas. In order to compensate for the emissions generated by conventional energy systems, it is essential to employ green energy sources that have a minimal carbon footprint. In this context, hydrogen represents a promising candidate for meeting society's demand for sustainable development. This is not only due to its status as an especially promising energy carrier, but also because it is inexhaustible, non-polluting, and can be produced from water [4-6].

The hydrogen sector comprises a number of key stages, including production, distribution, storage and utilization. The storage of this energy carrier represents a significant technological and scientific challenge in the present day. Three main strategies for hydrogen storage have been identified: solid storage (hydrogen atoms stored as simple or complex hydrides, such as borohydrides, alanates, or Li amides in a metallic crystalline network or carbon nanostructures) [7]; liquid or cryogenic storage (hydrogen volume maintained at a temperature of -250°C) [8]; and gaseous storage (compressed storage of the maximum amount of hydrogen in a given volume). Of the aforementioned solutions, compressed gaseous storage appears to be the most developed, offering the optimal compromise in terms of mass density (ratio of stored hydrogen mass to total mass) and volumetric density (ratio of stored hydrogen volume to total volume) [9-10].

Significant advances have been made in the field of storage methods and pressures. In the case of cylinders distributed across the industry, there has been a notable increase from 200 to 350 bars. Presently, research is concentrating on the creation of tanks that can withstand pressures of up to 700 bars. In this context, Type IV tanks comprise a polymer liner that ensures tightness, two metallic end fittings for the introduction and distribution of hydrogen, and a composite deposited around the liner by filament winding to ensure mechanical strength while minimizing the total mass. However, the complex environment and thermomechanical stresses experienced by the structure make it challenging to analyze the damage and failure of the composite, and consequently, to establish predictive models that enable the control of hydrogen tank design. Consequently, the prediction of burst pressure, damage state, and fatigue life in relation to filling and emptying cycles represents a significant and imperative challenge, particularly in terms of safety [11].

Carbon fiber-reinforced polymer (CFRP) composite pressure vessels represent an efficient solution for the storage and transportation of hydrogen. In fuel cell vehicles, the fatigue lifetime of these CFRP hydrogen storage vessels represents a crucial design factor, as it directly impacts the vehicle's overall durability and reliability. However, in practice, the rapid filling of high-pressure hydrogen can result in a significant temperature increase within the vessels due to the heat released during compression and Joule-Thomson heating of the fuel [16, 17]. This situation subjects the composite vessels to cyclic loading involving both high pressure and extreme temperatures, which contributes to intricate failure mechanisms such as fiber breakage, matrix cracking, and fiber/matrix interface debonding [18-20]. Over the course of the vessel's operational lifetime, numerous charging and discharging cycles are repeated, resulting in a complex thermo-mechanical fatigue failure process.

It is therefore of the utmost importance to develop reliable failure theories and fatigue life prediction methodologies that can accurately and effectively forecast the fatigue life of the composite vessel structure. A substantial body of research has demonstrated that the fatigue resistance of carbon fiber-reinforced polymer (CFRP) is significantly influenced by a

multitude of intrinsic factors inherent to the composite system itself, including the types of fibers and matrix resins, the lay-up sequence, residual stresses, and defects at the fiber/matrix interface [21-23]. Each of these factors exerts a considerable influence on the fatigue damage process, including the initiation and propagation of cracks, which in turn affects the final fatigue life and failure mode. The principle forms of fatigue damage include fiber breakage, resin matrix cracking, fiber/resin debonding, and delamination. The presence of high stiffness reinforcing fibers can serve to mitigate the occurrence of matrix cracking. This is attributed to the ability of high-stiffness and strength fibers to withstand higher loads, thus limiting the strain experienced by CFRP and reducing matrix resin cracking. Thermoplastic-based composites [26-28] exhibit a reduced incidence of cracks in the matrix resin compared to thermoset-based composites [29-32]. This difference can be attributed to the high fracture toughness of thermoplastic matrix resins, which decreases the initiation and propagation of cracks at defects and stress concentration zones [33].

The phenomenon of interface debonding may occur when the bond between the fiber and matrix is found to be weak. In composites composed of multiple layers, the ply-delamination failure mode may manifest. Moreover, the fatigue resistance of CFRP is markedly affected by cyclic loads and service environments, which modify the performance of the matrix resin and the fiber/matrix interface. Consequently, fatigue is a complex phenomenon, as the lifetime of composites subjected to cyclic loading is influenced by these factors simultaneously [33].

The term "fatigue" is defined as the gradual deterioration of a material when subjected to repeated cyclic loading [34-36]. The fatigue failure mechanism of CFRP is complex due to the heterogeneous nature of the material [33]. Even when a material is subjected to load below its elastic limit, damage occurs under conditions of continuous cyclic loading. The process of material failure can be delineated into three distinct stages: the initiation of cracks, the propagation of micro-cracks, and the growth of macro-cracks. The accumulation of micro-damage progresses in a steady manner throughout the material, reaching the macro-scale where it results in macro-scale damage and material failure. Moreover, there are significant differences between low-cycle fatigue and high-cycle fatigue in terms of fatigue damage. It should be noted that low-cycle fatigue, which is characterized by high loading levels, results in irreparable damage to CFRP. Conversely, in high-cycle fatigue, the loading levels are sufficiently low for the material to remain within its elastic limit, resulting in progressive fatigue damage to composites. If the loading levels are sufficiently low, it can be assumed that no fatigue damage occurs within CFRP, resulting in an infinite fatigue life [33].

The objective of this study is to conduct an experimental investigation into the influence of fiber orientation and the effect of cyclic loading amplitude on the fatigue behavior of carbon fiber-reinforced epoxy resin composites, manufactured via the filament winding process by Faurecia Hydrogen Solutions. The study is focused on multiscale damage analysis and its impact on the overall behavior of the material under fatigue loading.

Samples of rectangular shape, with different angular orientations of the fibers, were prepared for physical, damage and mechanical characterization. These included antisymmetric laminates with angles of ±15°, ±30°, and a multilayer combination of ±15°/±30°/±45°/±86°. The article is structured as follows. The material description and methods section provides an overview of the main physical characteristics and thermal properties of the carbon fiber-reinforced epoxy composite, which were assessed using differential scanning calorimetry (DSC) and dynamic mechanical analysis (DMA) tests. Tension-tension load-controlled fatigue tests were conducted at varying maximum loadings. The results of these tests, along with a discussion of the findings, are presented in the section on experimental results and discussion. This section also includes a multiscale damage analysis.

2. Material preparation and methods

2.1. Epoxy/carbon fiber composite

Cylindrical samples of carbon fiber-reinforced epoxy resin were initially prepared with different fiber angular orientations, as shown in Figure 1. These included antisymmetric laminates of +/-15°, +/30°, and a multilayer combination of ±15°/±30°/±45°/±86°. To conduct thermochemical, physicochemical analyses and mechanical tests, rectangular samples measuring 130 mm in length, 20 mm in width and 3.3 mm in thickness were cut from the cylindrical samples using a rotational blade cutting machine.

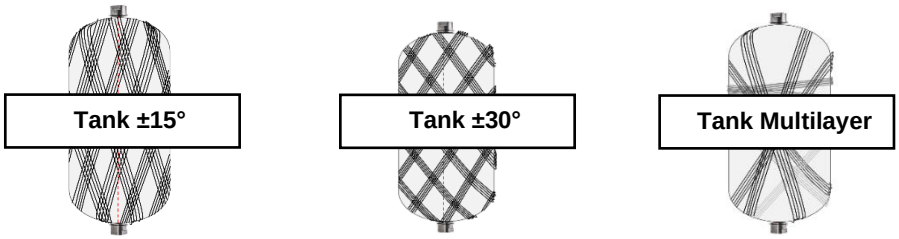

Figure 1. Illustration of composite of cylindrical carbon fiber reinforced epoxy resin

2.2. Methods of characterization and experimental procedure

- Microscopic observations: A Scanning Electron Microscope (HITACHI 4800 SEM) was used to conduct microscopic observations and image analysis, with a particular focus on the composite microstructure, including fiber orientation and damage analysis in the cross-section.

- Porosity measurement: Porosity, or void fraction, represents the volume of void spaces in a material relative to its total volume. Pyrolysis is used to analyze the material's porosity. The fiber mass percentage (M_f%) and epoxy mass percentage (M_e%) were determined by subjecting all samples to pyrolysis at 550°C for 5.5 hours. This process led to the

degradation of the matrix material, leaving only the carbon fiber. The fiber content was calculated using the following formula:

$$\text{Fiber content (\%)} = \left(\frac{M_0 - M_P}{M_0}\right) * 100$$

where M_0 represents the initial mass and M_P represents the mass after pyrolysis. Furthermore, the densities of the carbon fiber (1.1 g/cm³) and the epoxy resin (0.8 g/cm³) were employed to ascertain the porosity content of the composite material.

- **Thermo-mechanical properties:** The main transition temperatures were initially measured using Differential Scanning Calorimetry (DSC), which was also employed to determine the specific heat capacity and analyze the curing behavior of the epoxy resins. The analysis was conducted using a DSC instrument (Q1000 V9.0 Build 275, TA Instruments). The samples were pressed into non-hermetic aluminum trays, sealed and heated to 220°C at a rate of 10°C/min, then cooled to 30°C at the same rate.

- **Quasistatic tensile test:** Quasistatic tensile experiments were achieved using the Instron 5966 machine with a loading cell of 10 kN under a loading velocity of 10 mm/min and a temperature of 20°C.

- **Fatigue test:** Tension-tension load-controlled fatigue tests have been conducted on the MTS 830 hydraulic fatigue machine at varying maximum loading levels (F_{max}). The minimum applied force (F_{min}) is always set at 10% of the maximum applied force. The selected stress ratio is therefore (R_σ = 0.1), resulting in a mean loading level of 0.55 F_{max}. The experiments are conducted at a frequency of 10 Hz. To ensure accurate measurement of the reduction in stiffness due to the initial loading phase, each fatigue test is preceded by a quasi-static tensile loading-unloading-reloading phase. Tensile and fatigue tests were performed on the samples after a few rounds of polishing, with the geometry shown in Figure 2.

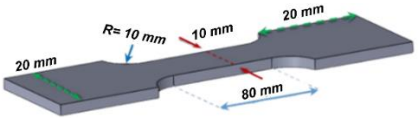

Figure 2. Dimensions of Carbon Fiber Reinforced Epoxy samples

2.3. Methodology of damage analysis in fatigue

To demonstrate the particular damage phenomena in CFRP composites, it is vital to create a benchmark for comparing different damage states and scenarios in various microstructures. This baseline provides a comprehensive understanding of how damage affects the behavior of CFRP composites. Changes in stiffness are an important indicator

of damage progression. Monitoring stiffness changes enables the tracking of microscopic damage mechanisms and residual stiffness across varying loading levels, providing a comprehensive and detailed overview of damage evolution.

The methodology involves conducting quasi-static loading and unloading tests, during which Young's modulus is quantified at each loading level. At each stage of the test, high-resolution SEM scans of the damaged areas are conducted to capture the microstructural changes and crack propagation. These detailed scans are essential for understanding the origin and progression of damage within the composite material. The process continues with repeated measurements and scans until the specimen fails. This approach allows for comprehensive monitoring of damage progression from initial crack formation to complete failure. By correlating the measured changes in Young's modulus with the observed microscopic damage mechanisms, it is possible to establish a quantitative relationship between macroscopic properties and the underlying damage phenomena. This relationship is of critical importance for understanding how different loading levels and microstructural configurations affect the overall integrity and functionality of carbon fiber-reinforced polymer (CFRP) composites. The value of this methodology lies in its ability to provide a clear and quantifiable link between damage at the microscopic level and the resulting changes in the material's mechanical properties. This information is crucial for the development of more durable and reliable composite materials, as it offers insights into damage mitigation and the enhancement of the material's resistance to failure. Figure 3 illustrates the detailed methodology used to identify and understand the specific damage mechanisms in carbon fiber-reinforced polymer (CFRP) composites.

The figure provides a visual representation of the step-by-step process, beginning with the establishment of the baseline and concluding with the capture of SEM images and the analysis of the evolution of damage. This comprehensive approach ensures a comprehensive understanding of the intricate relationship between microstructural damage and macroscopic mechanical behavior in CFRP composites.

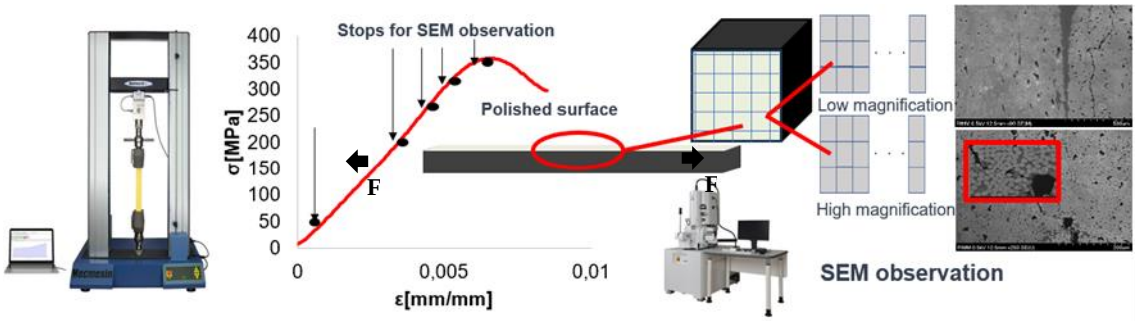

Figure 3. Methodology used to demonstrate the specific damage phenomena

3. Experimental results and discussion

3.1. Microstructure analysis

The observations made under a scanning electron microscope (SEM) are presented in Figure 4. The SEM micrographs confirm the structure of a laminated composite and validate the architecture manufactured by the industrial process. They also highlight the heterogeneity and state of the fiber/matrix interface. In each micrograph, porosities resulting from the manufacturing process can be observed, which may promote crack initiation.

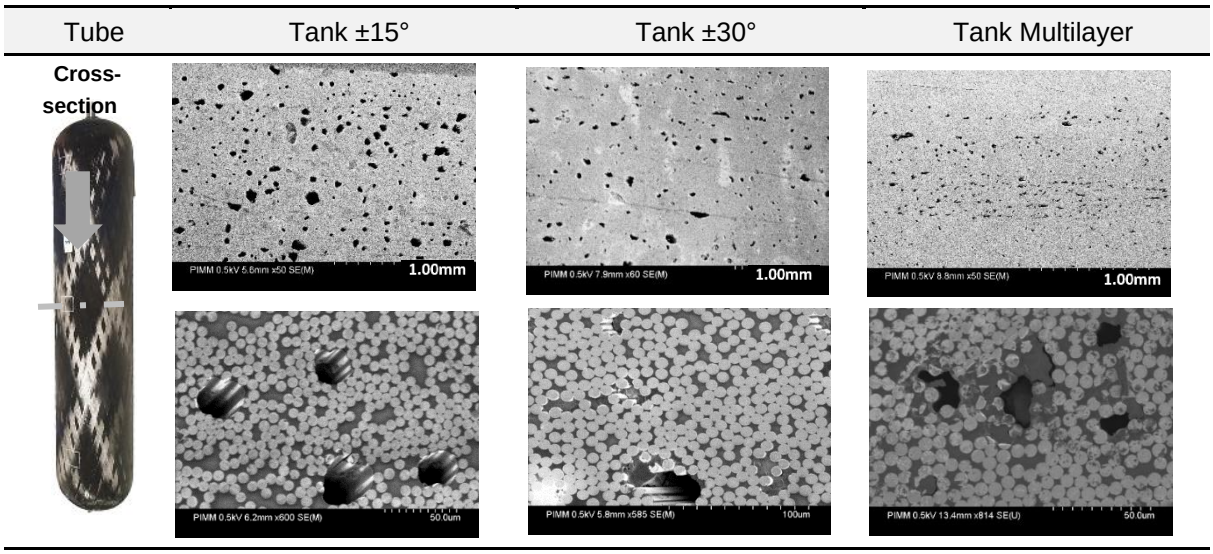

Figure 4. SEM micrograph of Carbon Fiber Reinforced Epoxy resin samples at different orientation

3.2. Porosity measurement

Table 3 highlights the significant variations in porosity levels, ranging from 4.7% to 7.8%, in composite tubes with different fiber orientations. These findings emphasize the critical influence of fiber orientation on porosity within the composites. For the ±15° orientation, the composite density is 1.39 g/cm³, with fibers accounting for 69.8% of the mass (54.2% by volume) and epoxy for 30.2% of the mass (38.0% by volume), resulting in a porosity level of 7.8%. In the ±30° orientation, the composite density is 1.45 g/cm³, with fibers making up 70.9% of the mass (57.3% by volume) and epoxy 29.1% of the mass (38.0% by volume), leading to a porosity of 4.7%. In the multilayer configuration, the density is 1.46 g/cm³, with fibers constituting 72.9% of the mass (59.2% by volume) and epoxy resin 27.1% of the mass (35.6% by volume), with a porosity of 5.2%. Overall, the average density across all tested tubes is 1.44 g/cm³, with fibers representing 71.1% of the mass (56.9% by volume) and epoxy 28.8% of the mass (37.5% by volume). The average porosity for all samples is 5.4%. These results underscore the importance of optimizing fiber orientation during the manufacturing process to minimize porosity, thereby improving the integrity and mechanical performance of the material.

Tube	Composite Density	Fiber (mass)	Fiber (vol)	Epoxy (mass)	Epoxy (vol)	% Volume Porosity
±15°	1,39	69,79%	54,20%	30,21%	37,99%	7,8%
±30°	1,45	70,94%	57,28%	29,06%	38,00%	4,7%
Multilayer	1,46	72,92%	59,17%	27,08%	35,65%	5,2%
Average	1,44	71,15%	56,99%	28,85%	37,49%	5,4%

Table 1. Volume percentage of porosity in tubes with different fiber orientations

3.3. Physico-chemical characterizations

Three orientations of carbon fiber-reinforced epoxy composites, namely ±15°, ±30°, and multilayers, were subjected to differential scanning calorimetry (DSC) to evaluate their thermal response to temperature variations. The DSC results for each orientation displayed a distinctive slope indicative of the phase change associated with the glass transition temperature (T_g), which was determined to be approximately 124°C across all orientations tested. This indicates that the epoxy has been effectively cross-linked within the composite structure. Furthermore, no additional peaks or indications of physical ageing were observed throughout the temperature range of 30°C to 220°C. This indicates that the composites maintained their thermal stability and did not undergo significant changes in molecular structure or thermal properties over the tested temperature range. In conclusion, the DSC analysis confirms that the carbon fiber reinforced epoxy composites with ±15°, ±30° orientations, and the multilayer configuration, have stable and well cross-linked resin matrices with consistent thermal behavior and resistance to physical ageing over the specified temperature range (Table 2).

Orientation	T_g	Observations
Tank ±15° Tank ±30° Tank Multilayer	~124°C	Effective cross-linking, no additional peaks, no physical aging observed

Table 2. Glass transition temperature of epoxy matrix obtained from DSC

3.4. Quasistatic tensile behavior

The mechanical properties of carbon fiber-reinforced epoxy composites, as illustrated in Figure 5 and detailed in Table 3, exhibit significant variations influenced by fiber orientation. To ensure the reliability and repeatability of the stress-strain curves, approximately five specimens were analysed for each tested orientation ±15°, ±30°, and multilayer configurations. These results demonstrate the consistency of the tensile behavior observed across multiple tests, providing

a robust basis for further analysis. The results demonstrate that the orientation of the fibers has a significant impact on the mechanical behavior of carbon fiber-reinforced epoxy composites. Samples with fibers oriented in a direction parallel to the applied force, such as those in the ±15° orientation, exhibited higher tensile strength and modulus, indicating efficient load transfer along the fibers. Conversely, the ±30° and multilayer configurations exhibited greater ductility, as evidenced by their higher elongation at break.

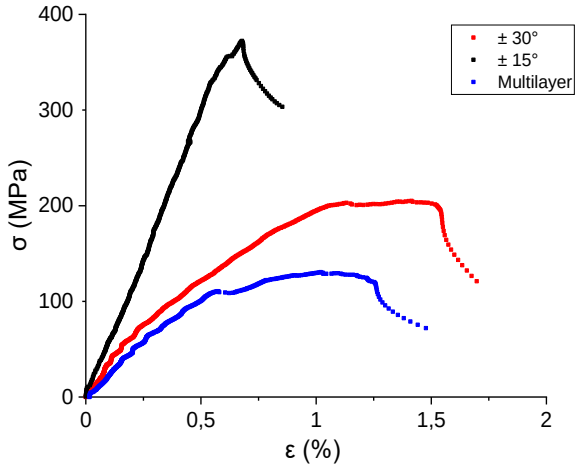

Figure 5. Representative-curves of quasi-static tensile tests.

Tube	E (GPa)	$\sigma_{threshold}$ (MPa)	$\varepsilon_{threshold}$ (%)	σ_{max} (MPa)	ε_{max} (%)
Tube ± 15°	$60^{\pm 2.7}$	$331^{\pm 5.2}$	$0.56^{\pm 0.02}$	$361.4^{\pm 8}$	$0.66^{\pm 0,08}$
Tube ± 30°	$36.8^{\pm 2.20}$	$55^{\pm 2.3}$	$0.17^{\pm 0.06}$	$206.6^{\pm 4.2}$	$1.3^{\pm 0,10}$
Tube Mixte	$21.1^{\pm 0.75}$	$111.8^{\pm 3.4}$	$0.538^{\pm 0.10}$	$157.1^{\pm 6.4}$	$0.94^{\pm 0,08}$

Table 3. Summary of tensile mechanical properties for different tubes

The results demonstrate that the orientation of the fibers has a significant impact on the mechanical behavior of carbon fiber-reinforced epoxy composites. Samples with fibers oriented in a direction parallel to the applied force, such as those in the ±15° orientation, demonstrated enhanced tensile strength and modulus, indicating optimal load transfer along the fibers. In contrast, the ±30° and multilayer configurations demonstrate superior ductility, as evidenced by their higher elongation at break. In particular, the ±15° oriented samples exhibit superior performance due to optimal stress distribution along the fibers, resulting in higher stiffness and resistance to deformation. In contrast, the ±30° oriented specimens and multilayer configurations, where the fibers are less optimally aligned with respect to the loading direction,

experience lower stiffness but demonstrate an enhanced ability to deform before failure. This behavior is attributed to damage and plastic deformation in the epoxy matrix, which reflects the influence of fiber-matrix interactions under load.

The transition from ductile to brittle fracture modes under varying loading conditions was investigated through microscopic analysis, as illustrated in Figure 6. The micrographs of the specimens oriented at ±15° show features typical of brittle fracture, with flat, smooth, and featureless fracture surfaces. These lack the typical ductile characteristics observed in specimens oriented at ±30°. The observed shift from brittle to ductile fracture modes as fiber orientation changes from ±15° to ±30° and multilayer configurations highlights the sensitivity of the material's fracture behavior to fiber orientation.

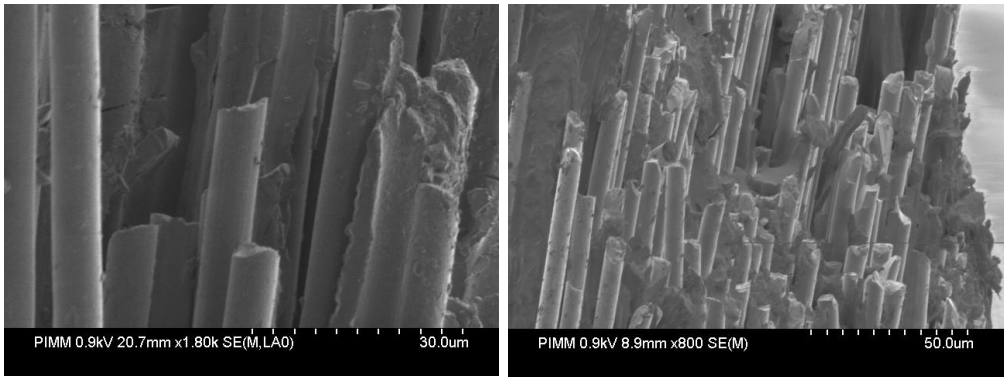

Figure 6. Fractured surfaces of the samples after the quasi-static tensile test ±15°

3.5. Fatigue behavior analysis: effect of the fiber orientation distribution

Figure 7 shows the Wöhler curves derived from tension-tension fatigue tests at a frequency of 10 Hz for samples with fiber orientations of ±15°, ±30° and multi-layer configurations. These curves show the significant influence of the fiber orientation distribution on the fatigue behavior.

The ±15° configuration shows the superior fatigue resistance compared to the other configurations. Both the ±30° and Multilayer configurations show overlapping data points, indicating similar fatigue behavior.

The data show that an applied stress of approximately 120 MPa results in a fatigue life of approximately 10^3 cycles for the ±30° and mixed orientation samples. Conversely, an applied stress of approximately 90 MPa extends the fatigue life to approximately 10^5 cycles. This indicates that a 33% reduction in applied stress can result in 100 times the fatigue life.

The results highlight the critical role of fiber orientation in determining fatigue life. In particular, fiber orientation can be optimized to improve the fatigue resistance of the material. For practical applications such as hydrogen tanks, this means that adjusting the fiber orientation can significantly improve the fatigue performance without significantly

compromising the transverse properties of the material. In conclusion, the fatigue life of fiber reinforced composites is highly sensitive to the fiber orientation distribution. By strategically modifying the fiber orientation, it is possible to optimize the fatigue design and improve the durability of structures subjected to cyclic loading.

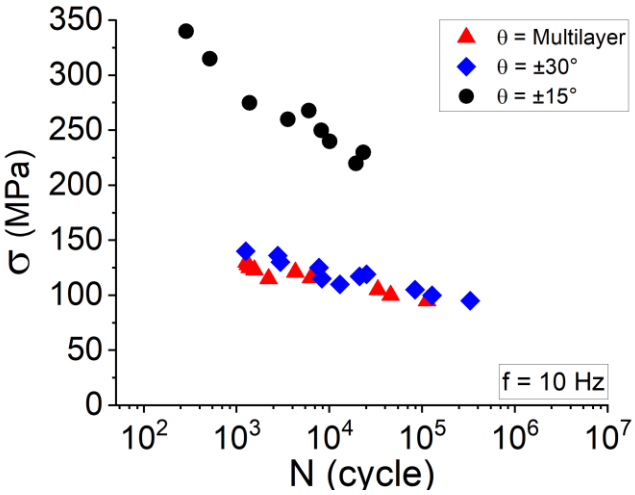

Figure 7. Wöhler curves for samples loaded at 10 Hz

3.6. Multiscale analysis of fatigue damage

3.6.1. Macroscopic damage evolution

The damage mechanisms in specimens with different angular fiber orientations are shown in Figure 8. The curves show the existence of different damage kinetics for different fiber orientations. Although the macroscopic damage patterns remain consistent for a given fiber orientation across different stress levels, the number of cycles to failure decreases as the stress amplitude increases. This observation is significant in the context of understanding the fatigue behavior of composites.

For all orientations tested, the curves show three distinct stages of damage evolution. The first stage is characterized by a linear constancy in damage. The second stage is characterized by a slow increase in damage. The third stage is characterized by a rapid increase in damage. A sharp decrease in stiffness finally leads to failure. These stages serve to elucidate the kinetics of damage progression, thereby enabling the refinement of micromechanical models for the purpose of predicting fatigue life and behavior in composite materials. Figure 8 further illustrates the evolution of the relative modulus of elasticity (E/E_0) during tensile-tension fatigue testing at 10 Hz. In the case of high amplitude loading, the E/E_0 decreases rapidly in a linear logarithmic regime up to the point of failure. This process is accompanied by a significant amount of early damage within the laminate, particularly at the interfaces between different layers. These failures are predominantly interfacial in nature and manifest as delamination and fiber-matrix debonding. In contrast, the modulus

decreases more gradually at lower amplitude loading. This is characterized by an initial rapid decrease due to early damage accumulation, a slower progressive decrease and a final sharp decrease prior to catastrophic failure. This gradual decrease is primarily controlled by matrix-fiber interactions, including matrix cracking.

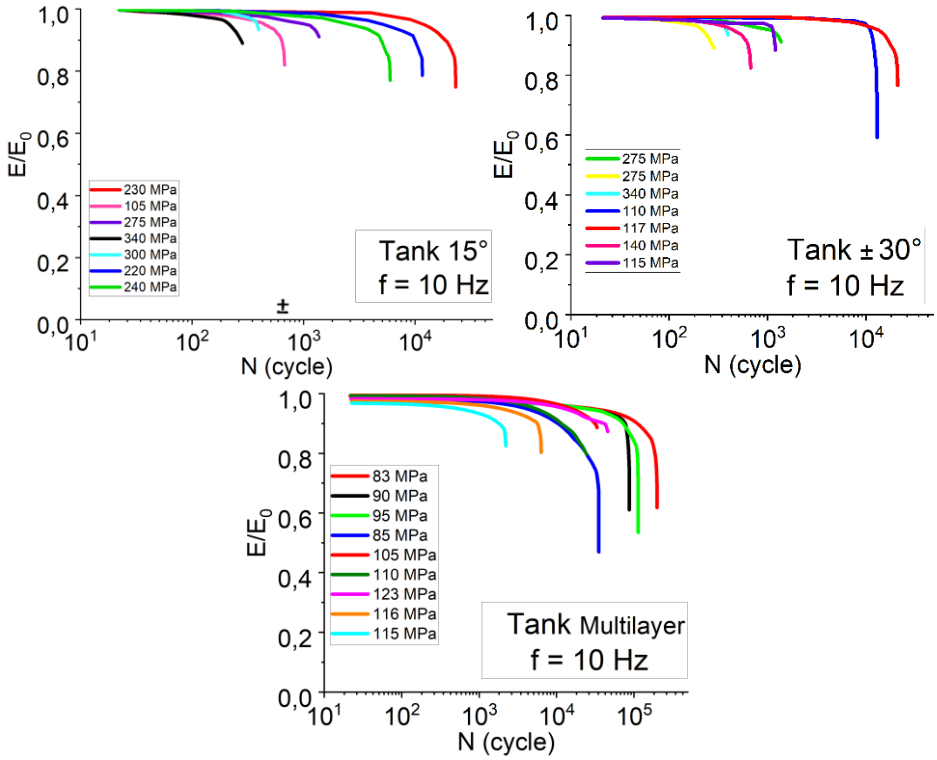

Figure 8. Evolutions of the relative Young's modulus (E/E_0) during fatigue tests:

(a) Tank ±15°, (b) Tank ±30° and (c) Tank Multilayer

The orientation of the fibers within the laminate has a significant effect on the fatigue behavior, with the ±15° orientation leading to a significant amount of early damage and a rapid decrease in modulus, whereas the ±30° and multi-layered orientations show a slower rate of degradation and a range of fracture behaviors (Figure 9). It is therefore of great importance to gain an understanding of these evolutions if we are to develop and validate micromechanical models that will enable us to predict fatigue life and damage evolution in laminated composites. This knowledge will allow the optimization of laminate design by adjusting fiber orientations and improving interfacial properties, thereby improving the fatigue strength, mechanical performance, durability and reliability of composite structures in high load applications.

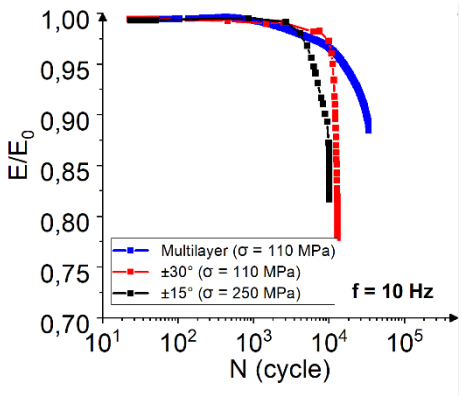

Figure 9. Evolution of the relative Young's modulus (E/E_0) during fatigue tests

3.6.2. Microscopic damage evolution

To monitor the damage progression at the microstructural level during fatigue testing, interrupted fatigue tests were conducted in conjunction with microstructure observations for different angular orientations. Microscopic analysis was conducted on a 5×10 mm² observation zone, with each cycle examined individually as the number of cycles increased. Figure 10 shows the outcomes for samples subjected to an applied stress amplitude of 250 MPa for the ±15° orientation at a frequency of 10 Hz.

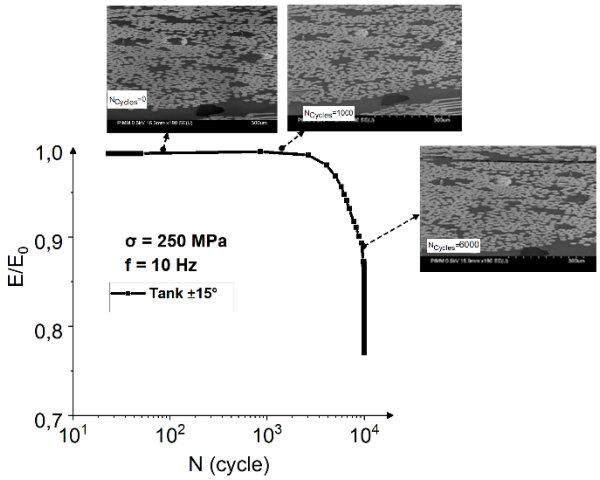

Figure 10. Interrupted fatigue test coupled to microstructure observations for ±15°

Figure 10 demonstrates the microscopic fatigue damage evolution of the ±15° oriented composite under loading. The ±15° configuration displays linear elastic behavior without any indication of damage up to 300 MPa (please refer to Figure 5). Once this threshold is exceeded, damage accumulation begins, resulting in non-linear behavior and eventual failure. The initial stage is defined by a linear increase in damage. It is worth noting that the initial formation of damage, which manifested as matrix cracking and fiber-matrix debonding,

was evident in samples oriented at ±15°. This damage exhibited an early onset, particularly in these samples. As the number of cycles increased, damage to the matrix and at the fiber-matrix interface worsened, leading to delamination (see Figure 11).

In the microstructures of ±15°, ±30°, and multilayer configurations, the composites initially exhibit the presence of pores or voids, which can be attributed to the manufacturing process. The aforementioned pores are randomly distributed throughout the material and frequently exhibit fibers extending to their surfaces. The heterogeneous distribution of fiber orientations across the layers gives rise to an uneven stress distribution during fatigue testing. The presence of pores in the material results in an amplification of fatigue stresses due to the disparity in stiffness between the matrix and the porous regions, which in turn gives rise to localized stress concentrations. As the applied loading increases, damage mechanisms propagate throughout the observation zone, originating at multiple pore locations. Concurrently, existing microcracks continue to expand. At the peak stress levels, a significant local deformation occurs via shearing around the fiber bundles, which results in pseudo-delamination near the fracture zones.

<table>
<tr><th colspan="2">Tank ±15°</th></tr>
<tr><td>Initial stage: N_{Cycle} = 0, σ = 250 MPa</td><td>Damage mechanism</td></tr>
<tr><td> 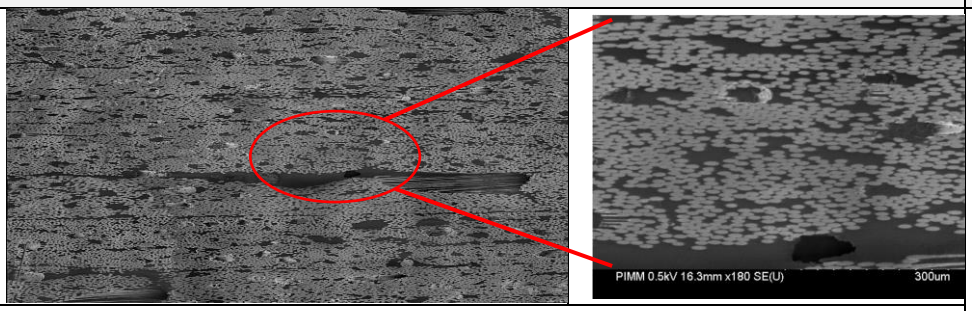
</td><td rowspan="3">No damage</td></tr>
<tr><td>Intermediate stage: N_{Cycle} = 1000, σ = 250 MPa</td></tr>
<tr><td> 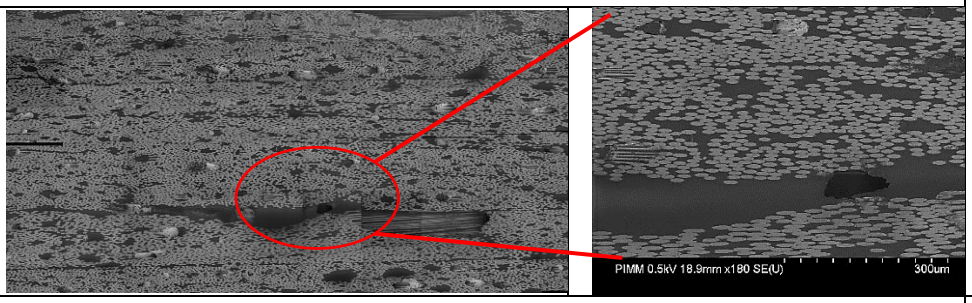
</td></tr>
<tr><td>Advanced stage, N_{Cycle} = 6000, σ = 250 MPa</td><td></td></tr>
</table>

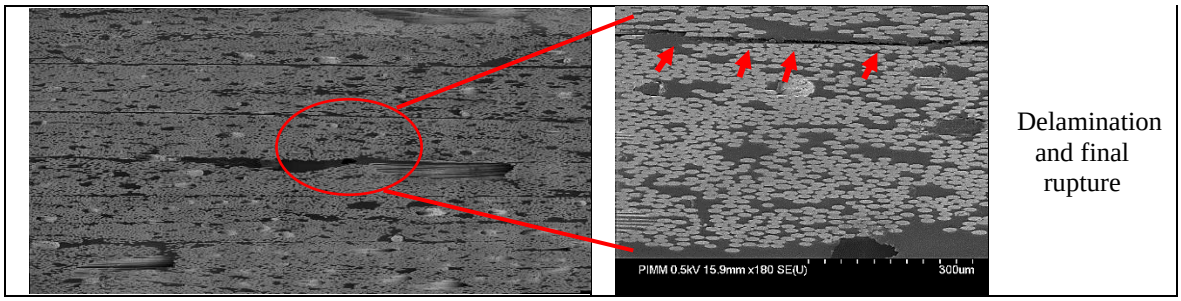

Figure 11. Interrupted fatigue test and damage mechanisms: ±15°configuration

Figures 12 and 13 present experimental fatigue tests coupled with microstructure observations for ±30° configuration, analyzed at different cycle stages: initial, intermediate, and final. In the initial stage, the material exhibits linear elastic behavior with no visible damage, as evidenced by the SEM image labeled "Initial stage" (Figure 13).

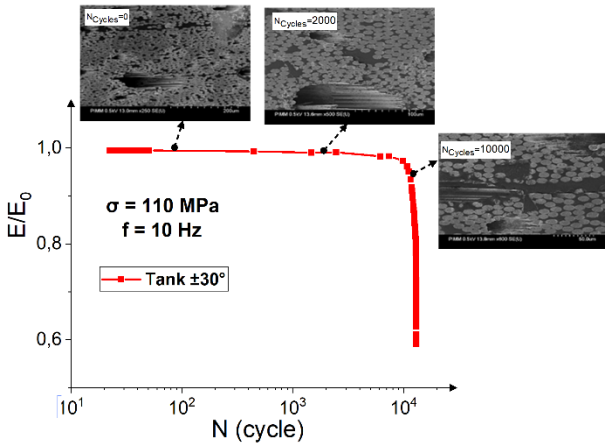

Figure 12. Interrupted fatigue test coupled to microstructure observations for ±30°

The initial observed damage mechanism is decohesion at the fiber-matrix interface. As the number of cycles increases to approximately 2×10^3 cycles, damage continues to accumulate at a moderate rate. During this intermediate stage, the material exhibits signs of damage, as evidenced by the SEM image displaying the onset of decohesion at the fiber-matrix interface, micro-cracking, and subsequent matrix fracture. The SEM image designated "Final Stage" (approximately 10^4 cycles) illustrates the presence of extensive cracks and significant damage, which ultimately leads to delamination and the complete failure of the material. The phenomena responsible for this damage include initial decohesion at the fiber-matrix interface, microcracking in the matrix, progression to matrix fracture, and development of large cracks resulting in delamination. This damage progression serves to highlight the critical stages of fatigue failure in fiber-reinforced composites and

to underscore the importance of understanding these mechanisms for the purpose of improving material design and fatigue resistance.

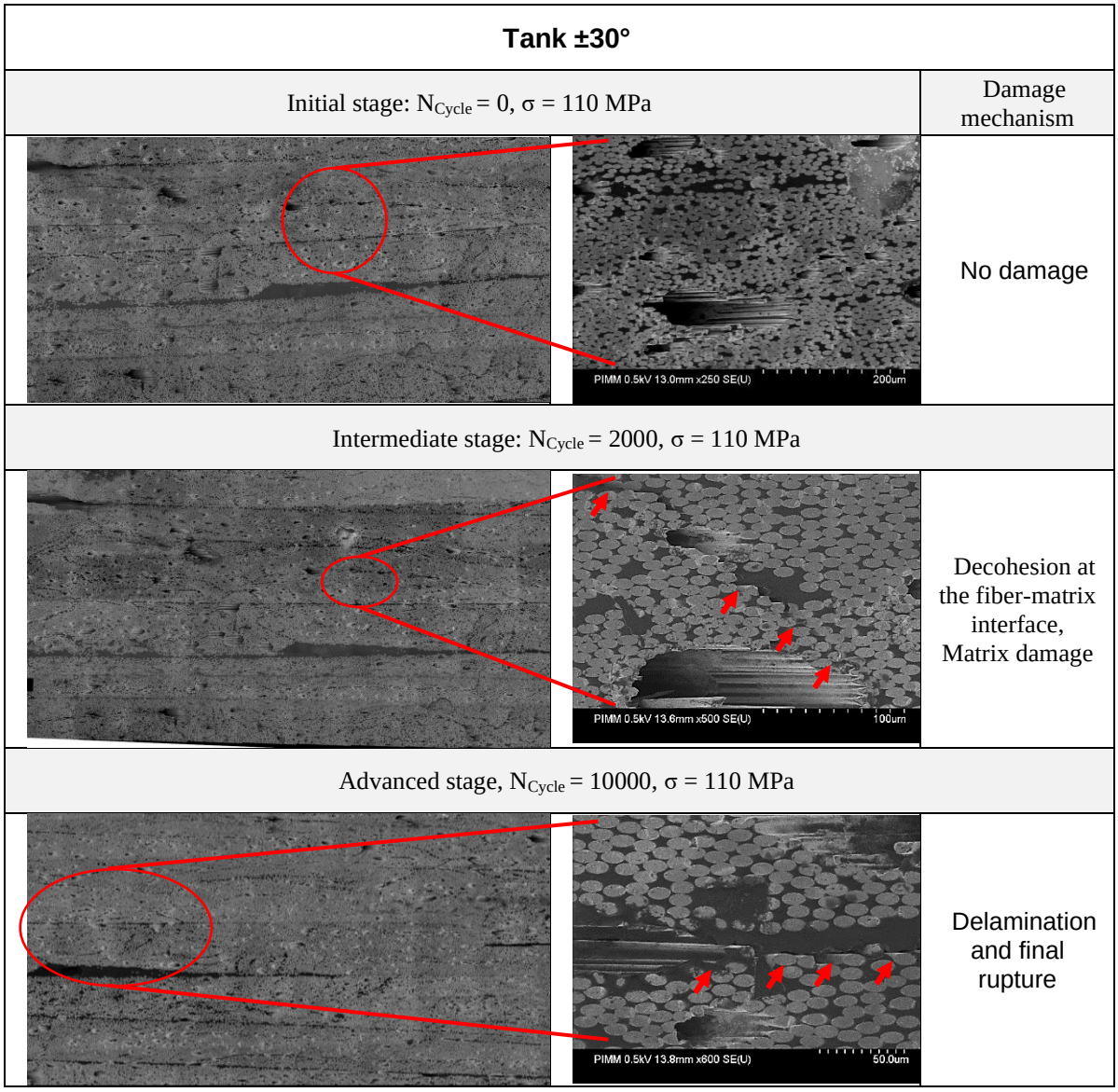

Figure 13. Microscopic damage mechanisms: ±30°configuration

Figures 14 and 15 present the results for a multilayer configuration. The same damage scenario is observed for this composite configuration, namely that damage mechanisms propagate from multiple pore locations. It can be noted that damage propagation occurs at the ±86° layers of the multilayer composite (Figure 15).

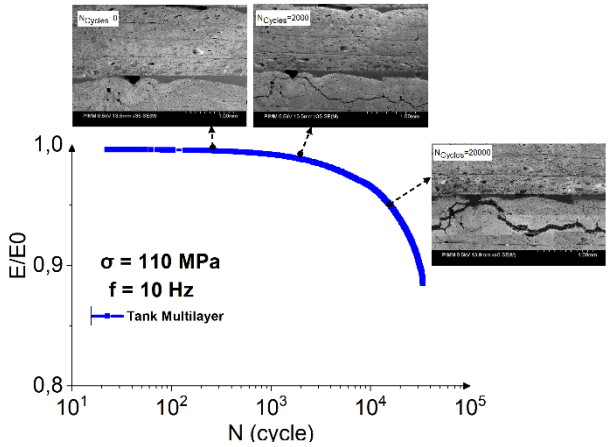

Figure 14. Interrupted fatigue test coupled to microstructure observations for multilayer configuration

Indeed, the thresholds and kinetics of damage mechanisms in ±θ composites are contingent upon a number of factors, including the specific orientation of fibers in each layer, the stress state experienced by each layer (which is influenced by the stacking sequence and macroscopic load), the statistical variation in pore spatial distribution (which varies with fiber orientation), and the rate at which load is applied. During fatigue testing, damage in long fiber composite structures manifests in a manner that varies according to the scale under consideration. At the microscopic level, the initiation of cracks within porosities plays a significant role in the damage of the material, including the separation of fibers and matrices at interfaces and the breaking of fibers, which in turn leads to the formation of new porosities.

It is crucial to understand the significance of these microscopic damage events in order to gain insight into the initial stages of composite failure. They serve to establish the conditions that facilitate further damage propagation, which is a key factor in the overall assessment of the material's resilience. At the mesoscopic scale, the coalescence of these microscopic decohesions results in the formation of transverse cracks that extend through the entire ply thickness (see Figures 11, 13 and 15).

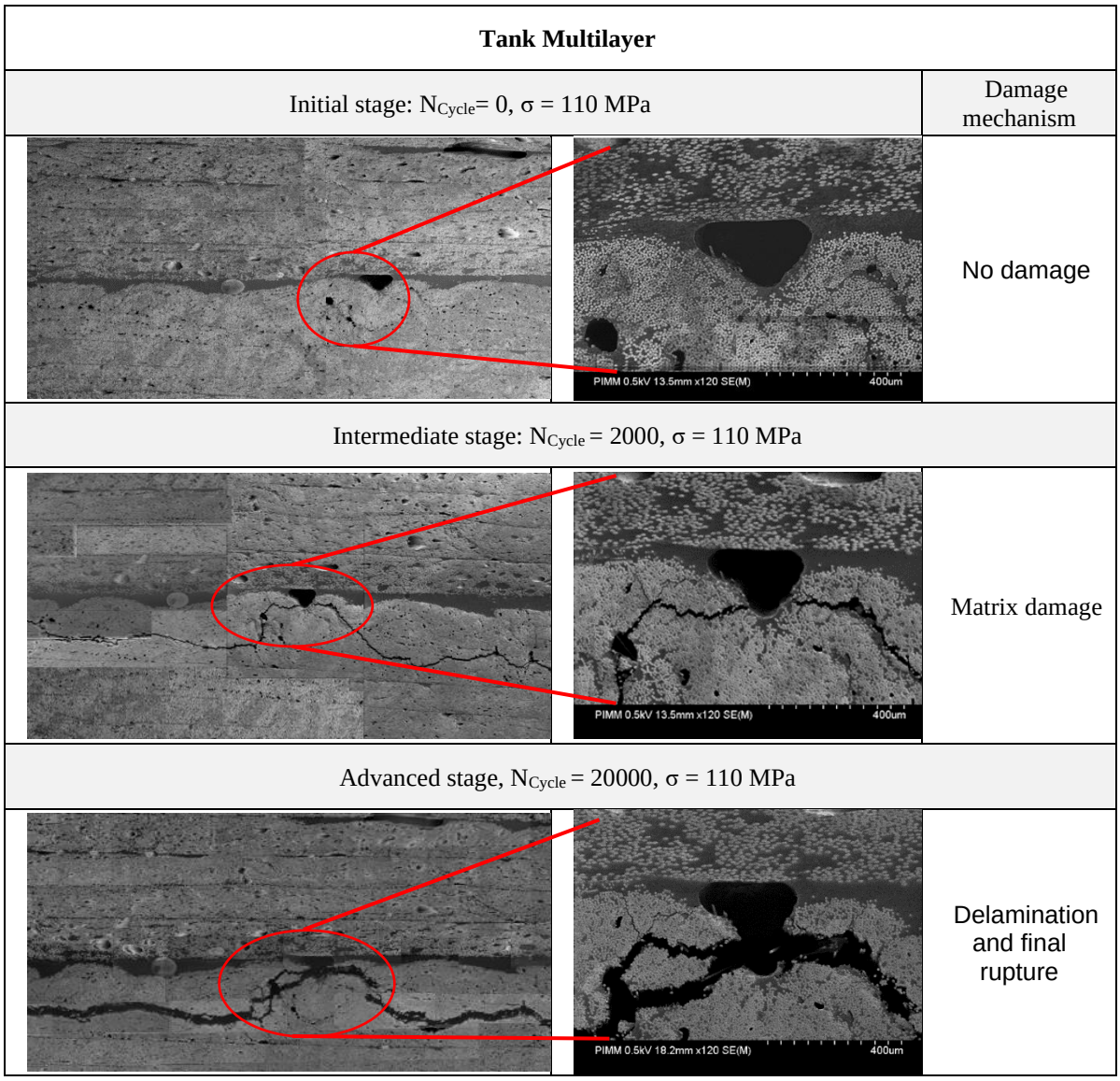

Figure 15. Microscopic damage mechanisms: multilayers configuration

The ends of these transverse cracks become sites for micro-delamination, which can further evolve into delamination between plies. It is therefore clear that this mesoscopic damage represents a critical factor in the overall structural integrity of the composite, as it directly impacts the load-bearing capacity and durability of the material. The complex interaction of multiple damage mechanisms in thick, heterogeneous composites requires the development of robust models to accurately predict their performance under load. It is essential that these models account for the various scales of damage, from microscopic crack initiation to mesoscopic crack propagation and delamination. It is crucial to gain insight into these interactions to enable the design of composites with enhanced durability and resistance to failure under cyclic loading conditions. To conclude, the specific fiber orientation, stress state, pore distribution and stress rate all have a significant impact on the

damage mechanisms of ±θ composites. At the microscopic level, the primary damage mechanisms are crack initiation within porosities and fiber/matrix decohesion. At the mesoscopic level, the coalescence of microscopic damage leads to transverse cracking and delamination. These findings highlight the importance of multiscale analysis in understanding and anticipating the behavior of carbon fiber-reinforced epoxy composites under cyclic loading.

3.7. Fatigue fracture surface

Figure 16 presents the fractographic analysis of tube samples that have undergone fatigue testing. As previously outlined, the initial damage observed in these samples is the separation of fibers from the matrix. As the fatigue process continues, this can result in fiber breakage. The fractography of the multilayer carbon fiber epoxy composite reveals typical failure features, including fiber fracture, matrix cracking, fiber pull-out and potential delamination. These characteristics demonstrate the critical importance of fiber-matrix adhesion and the role of voids in the structural integrity of the composite material.

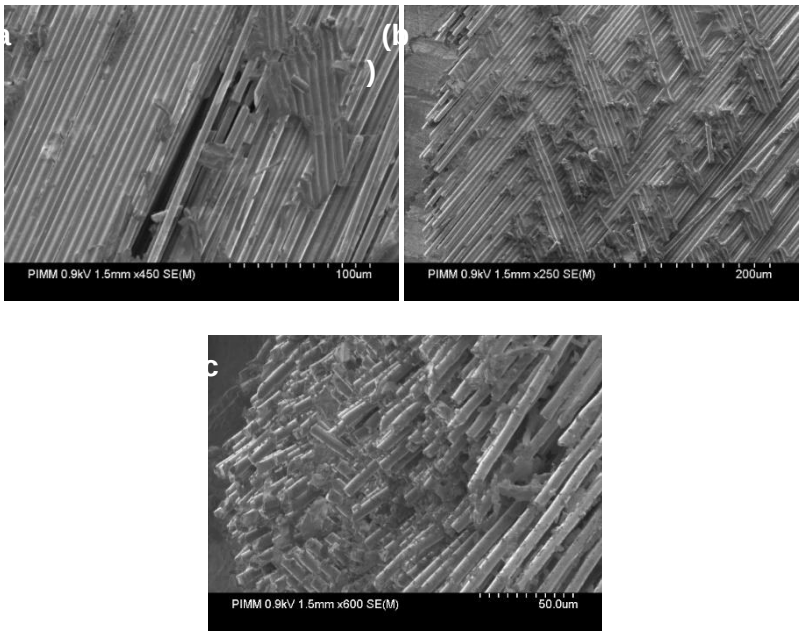

Figure 16. Micrograph of fatigue fracture surface:

(a)Tank ±15°, (b), Tank ±30° and (c) Tank Multilayer

4. Conclusion

This study presents a comprehensive multi-scale analysis of fatigue and damage mechanisms in filament-wound carbon fiber-reinforced epoxy composites used for hydrogen storage tanks, with a particular focus on the effects of

porosity. Three configurations were investigated: ±15°, ±30°, and multilayers. The results of the Differential Scanning Calorimetry (DSC) tests showed a stable thermal response across all orientations, with a consistent glass transition temperature (T_g) of around 124°C. This confirms that the epoxy matrix has been effectively cross-linked, and that the material has demonstrated resistance to physical ageing.

The results of the quasi-static tensile tests demonstrated that the orientation of the fibers has a significant impact on the mechanical behavior. The ±15° configuration demonstrated superior tensile strength and modulus, ideal for load transfer, while the ±30° and multilayer configurations exhibited enhanced ductility. Microscopic analysis revealed a transition from brittle to ductile fracture modes with varying fiber orientations, emphasizing the role of fiber alignment in fracture behavior.

The analysis of fatigue behavior demonstrated the critical impact of fiber orientation on fatigue life. The ±15° configuration demonstrated superior fatigue resistance, while the ±30° and multilayer configurations exhibited fatigue performance that was similar to one another. The study demonstrated that a reduction in applied loading significantly extends fatigue life, emphasizing the importance of optimizing fiber orientation for enhanced fatigue performance in practical applications.

The macroscopic damage evolution was characterized by distinct stages: initial linear damage, slow progressive damage, and rapid damage leading to failure. The progression was influenced by fiber orientation, with different orientations exhibiting varying rates of damage accumulation. Microscopic analysis revealed that damage initiates at pores and evolves through matrix cracking and fiber-matrix debonding, leading to delamination and failure. The multiscale analysis revealed that damage mechanisms at the microscopic level, such as crack initiation and fiber/matrix decohesion, merge at the mesoscopic level to form transverse cracks and delamination. Gaining an understanding of these mechanisms is vital for accurately predicting the fatigue life and performance of composites. The study highlighted the need for robust models that account for multiscale damage interactions to improve composite design and durability under cyclic loading.

The fractographic analysis of fatigue-tested samples revealed typical failure features, including fiber fracture, matrix cracking, fiber pull-out and delamination. This highlights the critical importance of fiber-matrix adhesion and voids in the structural integrity of the composite material.

In conclusion, this research highlights the importance of fiber orientation, pore distribution and load state on the fatigue and damage behavior of carbon fiber-reinforced epoxy composites. The findings provide valuable insights for optimizing the design and durability of hydrogen storage tanks and similar applications, demonstrating the efficacy of a multiscale approach in understanding and predicting composite performance under cyclic loading.

5. Declarations

- Consent to participate: Not applicable.
- Consent to publish: Not applicable.
- Conflict of interest: The authors declare that they have no conflicts of interest.

Authors' contributions

M. Shirinbayan, R. Tie Bi, J-B. Maeso, C. Thomas, J. Fitoussi: construct the idea. I. Feki, M. Shirinbayan, S. Nouira, R. Tie Bi, J-B. Maeso, C. Thomas, J. Fitoussi: analyzed results, prepared the manuscript draft, and wrote the paper. I. Feki, M. Shirinbayan, S. Nouira, J. Fitoussi: corrected the English and the paper format.

Availability of data and materials

The authors declare that the data and the materials of this study are available within the article.

6. References

1. Nachtane, M.; Tarfaoui, M.; Goda, I.; Rouway, M. A review on the technologies, design considerations and numerical models of tidal current turbines. *Renew. Energy* **2020**, *157*, 1274–1288.
2. Nachtane, M.; Tarfaoui, M.; Saifaoui, D.; El Moumen, A.; Hassoon, O.; Benyahia, H. Evaluation of durability of composite materials applied to renewable marine energy: Case of ducted tidal turbine. *Energy Rep.* **2018**, *4*, 31–40.
3. Nachtane, M.; Tarfaoui, M.; Mohammed, M.A.; Saifaoui, D.; El Moumen, A. Effects of environmental exposure on the mechanical properties of composite tidal current turbine. *Renew. Energy* **2020**, *156*, 1132–1145.
4. Cevahir Tarhan, M. A. Ç. A study on hydrogen, the clean energy of the future: Hydrogen. *Journal of Energy Storage* **2021**.
5. H.T.H., Varma, A. Hydrogen storage for fuel cell vehicles. *Current Opinion in Chemical Engineering* **2014**.
6. Rivard, E.; Trudeau, M.; Zaghib, K. Hydrogen storage for mobility: A review. *Materials* **2019**,
7. Melnichuk, M.; Andreasen, G.; Corso, H.L.; Visintin, A.; Peretti, H.A. Study and characterization of a metal hydride container, *International Journal of Hydrogen Energy* **2008**, 33, 13.
8. Spond, L.O.; White, D.E. A storage tank for vehicular storage of liquid hydrogen. *Applied Energy* **1980**.
9. Gondor, G. Pour le stockage de l'hydrogène : Analyse thermodynamique de la formation d'hydrures métalliques et optimisation du remplissage d'un réservoir. *HAL Id* **2013**, *tel-00782271*.
10. Mori, K. H. Recent challenges of hydrogen storage technologies for fuel cell vehicles. *International Journal of Hydrogen Energy* **2009**.
11. Lara, H. Energy revolution. *January 21, 2022*.
12. Zhang, M.; Lv, H.; Kang, H.; Zhou, W.; Zhang, C. A literature review of failure prediction and analysis methods for composite high-pressure hydrogen storage tanks. *International Journal of Hydrogen Energy* **2019**, *44*, 25777–25799.
13. Mori, K. H. Recent challenges of hydrogen storage technologies for fuel cell vehicles. *International Journal of Hydrogen Energy* **2009**, doi:10.1016/j.ijhydene.2008.07.115.
14. Vasiliev, V.V.; Krikanov, A.A.; Razin, A.F. New generation of filament-wound composite pressure vessels for commercial applications. *Composite Structures* **2003**, *62*(3), 449–459.
15. Liu, P.; Chu, J.; Hou, S.; Xu, P.; Zheng, J. Numerical simulation and optimal design for composite high-pressure hydrogen storage vessels: A review. *Renewable and Sustainable Energy Reviews* **2012**, *16*(4), 1817–1827.
16. Wang, L.; Zheng, C.; Wei, S.; Wang, B.; Wei, Z. Thermo-mechanical investigation of composite high-pressure hydrogen storage cylinders during fast filling. *International Journal of Hydrogen Energy* **2015**, *40*(21), 6853–6859.
17. Galassi, M.C.; Baraldi, D.; Iborra, B.A.; Moretto, P. CFD analysis of fast filling scenarios for 70 MPa hydrogen type IV tanks. *International Journal of Hydrogen Energy* **2012**, *37*(8), 6886–6892.
18. Bie, H.; Li, X.; Liu, P.; Liu, Y.; Xu, P. Fatigue life evaluation of high-pressure hydrogen storage vessels. *International Journal of Hydrogen Energy* **2010**, *35*(7), 2633–2636.

19. Tomioka, J.; Kiguchi, K.; Tamura, Y.; Mitsuishi, H. Influence of temperature on the fatigue strength of compressed-hydrogen tanks for vehicles. *International Journal of Hydrogen Energy* **2011**, *36*(3), 2513–2519.
20. Wang, L.; Zheng, C.; Luo, H.; Wei, S.; Wei, Z. Continuum damage modeling and progressive failure analysis of carbon fiber/epoxy composite pressure vessels. *Composite Structures* **2015**, *134*, 475–482.
21. Gamstedt, E.K.; Talreja, R. Fatigue damage mechanisms in unidirectional carbon-fibre-reinforced plastics. *Journal of Materials Science* **1999**, *34*, 2535–2546.
22. Dong, H.; Li, Z.; Wang, J.; Karihaloo, B.L. A new fatigue failure theory for multidirectional fiber-reinforced composite laminates with arbitrary stacking sequence. *International Journal of Fatigue* **2016**, *87*, 294–300.
23. Lasri, L.; Nouari, M.; EI Mansori, M. Wear resistance and induced cutting damage of aeronautical FRP components obtained by machining. *Wear* **2011**, *271*, 2542–2548.
24. Shao, Y.; Okubo, K.; Fujii, T.; Ou, S.; Fujita, Y. Effect of matrix properties on the fatigue damage initiation and its growth in plain woven carbon fabric vinylester composites. *Composites Science and Technology* **2014**, *104*, 125–135.
25. Jones, C.J.; Dickson, R.F.; Adam, T.; Reiter, H.; Harris, B. The environmental fatigue behaviour of reinforced plastics. *Proceedings of the Mathematical and Physical Sciences* **1984**, *396*, 315–338.
26. Fitoussi, J.; Nikooharf, M.H.; Kallel, A.; Shirinbayan, M. Mechanical properties and damage behavior of polypropylene composite (GF50-PP) plate fabricated by thermocompression process under high strain rate loading at room and cryogenic temperatures. *Applied Composite Materials* **2022**, *29*, 1959–1979.
27. Shirinbayan, M.; Rezaei-Khamseh, M.; Nikooharf, M.H.; Tcharkhtchi, A.; Fitoussi, J. Multi-scale analysis of mechanical properties and damage behavior of polypropylene composite (GF50-PP) plate at room and cryogenic temperatures. *Composite Structures* **2021**, *278*, 114713.
28. Imaddahen, M.A.; Shirinbayan, M.; Ayari, H.; Foucard, M.; Tcharkhtchi, A.; Fitoussi, J. Multi-scale analysis of short glass fiber-reinforced polypropylene under monotonic and fatigue loading. *Polymer Composites* **2020**, *41*(11), 4649–4662.
29. Shirinbayan, M.; Fitoussi, J.; Abbasnezhad, N.; Meraghni, F.; Surowiec, B.; Tcharkhtchi, A. Mechanical characterization of a low-density sheet molding compound (LD-SMC): Multi-scale damage analysis and strain rate effect. *Composites Part B: Engineering* **2017**, *131*, 8–20.
30. Shirinbayan, M.; Fitoussi, J.; Bocquet, M.; Meraghni, F.; Surowiec, B.; Tcharkhtchi, A. Multi-scale experimental investigation of the viscous nature of damage in advanced sheet molding compound (A-SMC) submitted to high strain rates. *Composites Part B: Engineering* **2017**, *115*, 3–17.
31. Shirinbayan, M.; Fitoussi, J.; Meraghni, F.; Surowiec, B.; Bocquet, M.; Tcharkhtchi, A. High strain rate visco-damageable behavior of advanced sheet molding compound (A-SMC) under tension. *Composites Part B: Engineering* **2015**, *82*, 30–41.
32. Shirinbayan, M.; Rizi, H.B.; Abbasnezhad, N.; Tcharkhtchi, A.; Fitoussi, J. Tension, compression, and shear behavior of advanced sheet molding compound (A-SMC): Multi-scale damage analysis and strain rate effect. *Composites Part B: Engineering* **2021**, *225*, 109287.
33. Masaki, H.; Shojiro, O.; Gustafson, C.G.; Keisuke, T. Effect of matrix resin on delamination fatigue crack growth in CFRP laminates. *Engineering Fracture Mechanics* **1994**, *49*, 35–47.
34. Shirinbayan, M. Multi-scale damage analysis of the tension-tension fatigue behavior of a low-density sheet molding compound (LD-SMC). *Journal of Applied Polymer Science* **2021**.
35. Shirinbayan, M.; Fitoussi, J.; Meraghni, F.; Farzaneh, S.; Surowiec, B.; Tcharkhtchi, A. Effect of a post-fatigue damage on the residual dynamic behavior of advanced-SMC composites. *Applied Composite Materials* **2019**, *26*, 1313–1331.
36. Shirinbayan, M.; Fitoussi, J.; Meraghni, F.; Laribi, M.; Surowiec, B.; Tcharkhtchi, A. Coupled effect of loading frequency and amplitude on the fatigue behavior of advanced sheet molding compound (A-SMC). *Journal of Reinforced Plastics and Composites* **2017**, *36*(4), 271–282.

Article N°4 :

Shirinbayan M, Feki I, Nouira S, et al. Multi-scale damage analysis of filament-wound carbon fiber-reinforced epoxy composites for hydrogen storage tanks under high strain rates. Polym Compos. 2024;1-12. doi:10.1002/pc.29273.

Multi-scale damage analysis of filament-wound carbon fiber-reinforced epoxy composites for hydrogen storage tanks under high strain rates

Mohammadali Shirinbayan[1,*], Imen Feki[1], Samia Nouira[1], Robert Tie Bi[2], Jean-Baptiste Maeso[2], Cedric Thomas[2], Joseph Fitoussi[1]

[1]Arts et Metiers Institute of Technology, CNAM, CNRS, PIMM, HESAM University, F-75013 Paris, France
[2]Zero Emission, FORVIA Clean Mobility, Bois Sur Prés, 25550 Bavans, France

E-mails: Mohammadali.Shirinbayan@ensam.eu (corresponding author), Imen.Feki@ensam.eu, Samia.Nouira@ensam.eu, Robert.tbr.tiebi@forvia.com, Jean-Baptiste.Maeso@forvia.com, Cedric.Thomas@forvia.com, Joseph.Fitoussi@ensam.eu.

Abstract

This study investigates the relationship between microstructure and mechanical properties of carbon fiber reinforced epoxy composites, specifically in the context of lightweight hydrogen storage pressure vessels manufactured by the filament winding process. The filament winding technique often introduces variability in fiber orientation and porosity which can lead to inconsistencies in mechanical properties. By investigating the influence of dynamic loading over a range of strain rates, from quasi-static to 100s^{-1}, this research aims to understand the effects of different fiber orientations (±15° and ±30°) and multilayer structures on the performance of these composites. Using a custom-designed Interrupted Dynamic Tensile Test (IDTT) apparatus, we investigated how damage mechanisms evolve during rapid tensile deformation. The results showed that porosity has a significant impact on mechanical performance, particularly at high strain rates, where cracks initiate at pores and propagate via fiber/matrix decohesion and fibre breakage. These microstructural defects contribute to mesoscopic failure mechanisms such as transverse cracking and micro-delamination between composite layers. The mechanical properties were found to be strain rate sensitive, with visco-damage phenomena playing a critical role in determining the damage evolution under dynamic loading. These findings provide important insights into the design and optimization of hydrogen storage vessels, highlighting the importance of controlling porosity and understanding the response of the composite to varying strain rates for improved durability and performance.

Highlights

- Comprehensive analysis of dynamic loading,
- Influence of fiber orientation and porosity on mechanical integrity,
- Visco-damage and failure mechanisms under high strain rates.

Keywords: Hydrogen; porosity; strain rate; damage; fiber/matrix decohesion.

1. Introduction

Hydrogen is increasingly recognized as a transformative energy carrier with the potential to reduce harmful greenhouse gas emissions and reduce global dependence on fossil fuels. Its high energy content per unit mass, combined with water as the only by-product of combustion, makes it an attractive choice for many

applications. These include fuel cell vehicles, where hydrogen offers a clean alternative to petrol and diesel, and industrial processes such as ammonia production and metal refining. Hydrogen also plays an important role in power generation, enabling zero-emissions electricity production through turbines and fuel cells [1-5].

Notwithstanding the numerous advantages of hydrogen, the effective storage and transportation of this substance remain significant challenges. The low volumetric energy density of hydrogen necessitates the storage of the gas at exceedingly high pressures to achieve practical energy densities [6-7]. In the context of automotive applications, this typically entails the compression of hydrogen to pressures reaching 700 bar (70 MPa). This high-pressure storage is indispensable for ensuring that a sufficient quantity of hydrogen can be stored in a vehicle to provide a reasonable range between refuelling stops, which is a pivotal factor in the widespread adoption of hydrogen fuel cell vehicles. The necessity for high-pressure storage places considerable demands on the materials and design of hydrogen storage systems.

Fiber-reinforced polymers are highly favored for the construction of high-pressure hydrogen tanks due to their excellent strength-to-weight ratio and corrosion resistance. However, the design and testing of these composite tanks requires careful attention to ensure long-term durability and reliability. Understanding the material behavior under different loading conditions, such as impact and cyclic loading, is critical to the development of safe and efficient hydrogen storage systems [13-16].

Composite hydrogen tanks offer several advantages, but they are susceptible to various forms of mechanical damage under different loading conditions. Understanding their behavior under both quasi-static and dynamic impacts is essential to ensure safety and reliability. These loading scenarios are critical as they can result in significant damage despite the high strength and low weight of composites. Due to their heterogeneous composition, composites exhibit complex failure mechanisms and the energy absorption and damage distribution within the material can vary significantly during mechanical loading such as impact. This variability highlights the need for comprehensive studies to evaluate the response of composite hydrogen tanks under different loading conditions. In quasi-static impacts, the load is applied gradually, allowing detailed observation of the progressive damage and failure mechanisms of the material. Quasi-static loading can result in several types of damage, including matrix cracking, fiber fracture and interlaminar delamination. Matrix cracking occurs when the resin matrix within the composite fractures, typically due to tensile or shear stresses. Fiber fracture, caused by excessive loading, compromises the load carrying capacity of the material. Interlaminar delamination, the separation between composite layers, is of particular concern as it can propagate under continued loading and potentially lead to catastrophic failure. [20-24].

The effects of quasi-static impacts on composite structures have been demonstrated by research. For example, a study by Berthelot [20] showed that quasi-static indentation tests on composite laminates can effectively detect the onset of matrix cracking and subsequent delamination. These findings highlight the importance of considering such damage modes in the design and evaluation of composite hydrogen tanks.

Dynamic impacts, characterized by rapid loading events, present a unique set of challenges for composite materials. The high strain rates associated with dynamic impacts can result in more severe damage compared to quasi-static loading. Dynamic loading often results in higher energy absorption, which can lead to extensive fiber breakage, matrix cracking and even complete penetration of the impactor. The significant energy involved in these impacts can cause localized damage that may not be immediately visible but can critically weaken the structure over time [25-30]. The influence of dynamic impacts on composite materials has been the subject of extensive study. For example, Gower and Shaw [25] investigated the impact resistance of fiber-reinforced composites and found that high-velocity impacts can cause significant internal damage, including fiber breakage and extensive matrix cracking. The study emphasized that the rate of loading significantly affects the damage patterns and failure modes, which are critical to assessing the structural integrity of composite hydrogen tanks.

Experimental techniques such as drop-weight tests and high-velocity projectile impacts are commonly used to simulate real-world impact scenarios. In drop-weight tests, a known mass is dropped onto the specimen from a specified height to simulate low-velocity impacts. These tests provide valuable insight into the initial damage mechanisms and residual strength of the material [31]. High-velocity impacts, often studied using gas guns or other projectile launchers, simulate conditions such as automobile crashes or debris impacts and reveal the behavior of the material under extreme loading conditions.

Several studies have focused on the development of models to describe the damage behavior of composite materials, together with specific techniques for numerical simulations [32-33]. These models can be broadly categorized into two main types: phenomenological and micromechanical. The micromechanical approach uses damage variables to monitor the evolution of microcracks during loading [34-35]. This method provides a physical interpretation of the damage, as the variables represent parameters such as the volume fraction of cracks or the energy dissipation rate associated with fracture.

In contrast, the phenomenological approach is concerned with the macroscopic effects of local damage, such as stiffness loss, and typically employs the representative volume element (RVE) of the composite for calculations [34-36]. Mixed models frequently integrate elements of both approaches to account for both local

and macroscopic damage behavior. Micromechanical models are particularly useful for predicting the behavior of laminated composites, which exhibit significant anisotropy due to damage. These models consider local damage criteria and the competitive introduction of microcracks at the local scale [38]. Regardless of the approach, understanding the local damage mechanisms and their kinetics is crucial for selecting an appropriate damage behavior law and identifying its variables [39].

This study focuses on the recently developed carbon fiber reinforced epoxy composites used in the construction of hydrogen storage tanks. The composites, supplied by Faurecia Hydrogen Solutions, are processed using the filament winding technique. The primary objective is to investigate the damage mechanisms and their impact on the macroscopic and microscopic response of these composites when subjected to high strain rates. A range of experimental techniques, including load-unload tests in different directions, are used to characterize damage at the microscopic scale.

In summary, both quasi-static and dynamic impacts have a significant impact on the integrity of composite hydrogen tanks. Quasi-static tests typically result in progressive damage that can propagate under continued loading, while dynamic impacts result in severe localized damage due to high energy absorption. Understanding these damage mechanisms is essential for the design and safety assessment of composite hydrogen storage tanks.

2. Material specification and methods

2.1. Carbon fiber-reinforced epoxy resin composites ± θ

In this study, cylindrical tank specimens (Table 1) manufactured by Faurecia from carbon fiber-reinforced epoxy resin composites were employed to assess their mechanical performance and damage behavior under a range of loading conditions. These composites, renowned for their exceptional strength-to-weight ratio and remarkable resilience to external influences, were chosen for their potential suitability in high-pressure hydrogen storage applications. The manufacturing process entailed the precise alignment of carbon fibers at specific angles (±θ) within the epoxy matrix, thereby ensuring optimal reinforcement and load distribution.

N° tubes	Orientation	Illustration
1	±15°	
2	±30°	
3	multilayer	

Table. 1. View and illustration of composite of cylindrical carbon fiber reinforced epoxy resin

The advanced manufacturing techniques employed by Faurecia enabled the production of high-quality composite tanks that met the exacting standards set by the industry. The specimens with orientations of ±15° and ±30°, as detailed in Table 1, as well as a multilayer laminate comprising orientations of ±30°/±45°/±88°/±30°/±45°/±45°/±30°, were subjected to testing protocols to investigate their response to quasi-static and dynamic impacts.

2.2. Microscopic observations

The HITACHI 4800 SEM scanning electron microscope was employed for qualitative examination of the material microstructure, fracture surfaces of tensile specimens, and particularly for investigation of crack propagation during testing. Additionally, it was utilized for quantitative measurement of porosity within the microstructure. Porosity, or void fraction, is defined as the volume of voids in a material relative to its total volume.

2.3. Low and high-speed tensile tests

Low-speed tensile tests were performed at various pre-defined maximum stress levels using an Instron 5966 machine at a speed of 10 mm/min and a temperature of 20°C.

In addition, a servo-hydraulic machine (Schenk Hydropuls VHS 5020) was used to perform tensile tests at various strain rates ranging from quasi-static to $100s^{-1}$. The composite specimen was positioned between the load cell (upper extremity) and the moving device (lower extremity) as shown in Figure 1(a). To ensure a constant strain rate from the start of the high-speed tensile test, a tube-piston device was used to apply displacement to the moving device without loading during the acceleration phase.

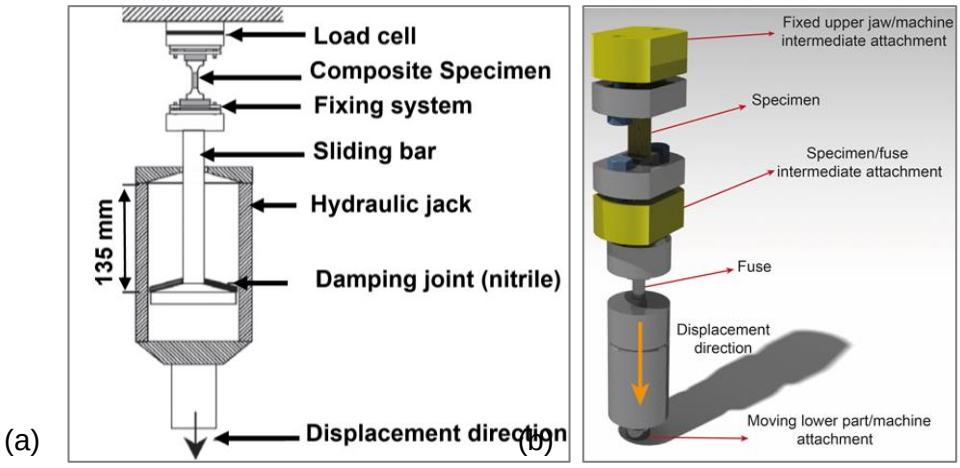

Figure 1. (a) High-strain rate tensile apparatus; Interrupted dynamic tensile test setup, and (b) interrupted high-speed tensile tests

2.4. Interrupted Dynamic Tensile Test (IDTT)

The concept of interrupted high strain rate tensile testing was first proposed by Lataillade et al [40] for glass-epoxy laminates and subsequently applied by Fitoussi et al to standard SMC composites, carbon-epoxy laminates [41] and short glass fibre reinforced polypropylene [42]. The Interrupted Dynamic Tensile Test (IDTT) serves two distinct purposes: first, to identify the progressive damage mechanisms that occur at the microscopic level, and second, to determine the progressive loss of stiffness due to damage. By analysing both the threshold and the kinetics of damage, these tests allow correlation of findings at both microscopic and macroscopic levels. In this study, the IDTT has been adapted for use with carbon fibre reinforced epoxy resin composites. The IDTT is a dynamic load-unload test that produces successive damage states in the specimen at different force levels during high speed loading. The same specimen is subjected to repeated loading cycles at progressively increasing levels of applied force. Prior to each reloading stage, SEM observations were made on the polished surfaces to quantify the effects of strain rate on microscopic damage mechanisms. This approach provided a comprehensive assessment of damage in carbon fibre reinforced epoxy composites at both micro and macro levels.

The IDTT device, illustrated in Figure 1(b), encounters a significant challenge during dynamic loading due to the inertia of the hydraulic cylinder. Once the test has commenced, this inertia impedes the ability to halt the test at pre-determined stress levels, in contrast to quasi-static load/unload tests. Consequently, the loading continues until the specimen experiences macroscopic failure. To address this issue, an elastic brittle fuse is integrated in series with the composite specimen. In this study, a custom fixture was developed and tailored

to accommodate cylindrical notched steel fuses. The ligament length of the fuse is precisely calibrated to match the maximum force requirement.

2.4.1. Fuse characterization

Tensile tests have been carried out on the steel fuse to determine the magnitude of the ultimate stress for different ligament lengths. Figure 2 shows the ultimate load as a function of the length of the ligament. It can be seen that by varying the ligament length, the defined force can be achieved during the intermittent high strain rate. It is noteworthy that the ultimate stress can vary at high strain rates. However, no significant variation was observed during IDTT.

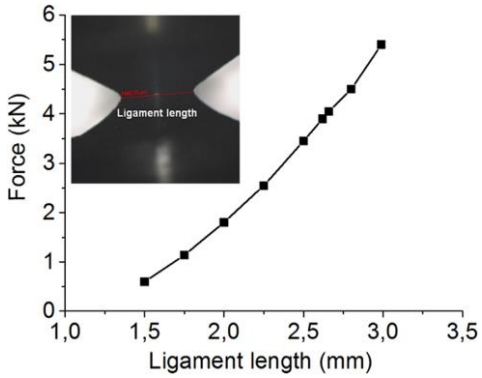

Figure 2. Required ultimate force as a function of fuse diameter

2.4.2. Strain and strain rate measurements

A contactless technique is employed to quantify the local deformation via a high-speed camera (FASTCAM-APX RS). The methodology for measuring strain rates has been previously outlined in a separate publication [7]. This involves the analysis of images captured during the deformation of the filmed surface.

To gain insight into the damage mechanisms that occur during dynamic loading, it is essential to carry out experimental investigations at both the macroscopic and microscopic levels. To this end, rectangular specimens with polished surfaces were used, which are ideal for SEM observations (Figure 3).

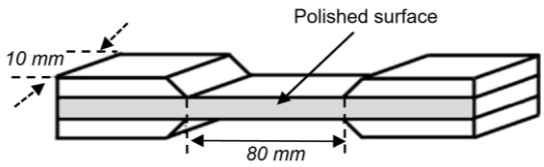

Figure 3. Dimensions of Carbon Fiber Reinforced Epoxy samples

3. Experimental results and discussion

3.1. Microstructural analysis

It is crucial to comprehend the distribution and influence of these microstructural characteristics, particularly in relation to diverse fiber orientations, in order to optimize manufacturing processes and enhance the overall mechanical performance and durability of carbon fiber-reinforced epoxy composites. The microstructural analysis, conducted using optical microscopy (Figure 4), corroborates the laminated composite structure and corroborates the architectural configuration produced by the industrial process, including different fiber orientations such as ±15°, ±30° and multilayer configurations. The micrographs display porosities resulting from the manufacturing process, which have the potential to act as sites of crack initiation.

Further analysis using a scanning electron microscope (SEM) (Figure 5) supports the findings from the initial light microscopy assessment. These observations not only confirm the layered structure of the composite, but also highlight the heterogeneity and condition of the fibre/matrix interface, particularly in regions adjacent to the observed porosities. The presence of signs of fibre/matrix decohesion indicates the potential for weaknesses in the material.

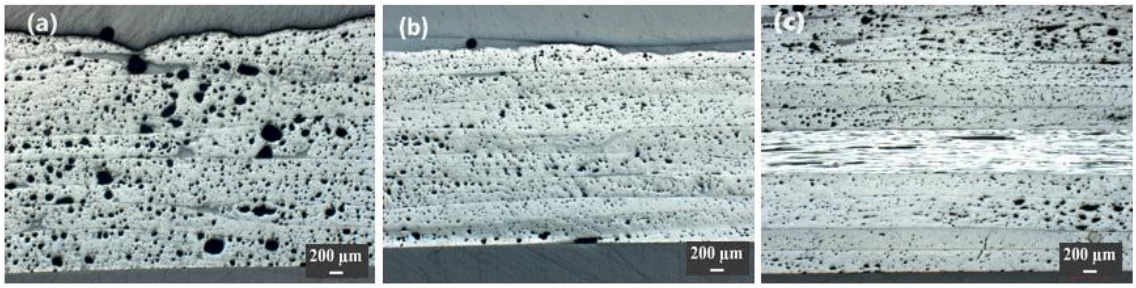

Figure. 4. Optical micrograph: (a) ±15°, (b) ±30° and (c) multilayers configurations

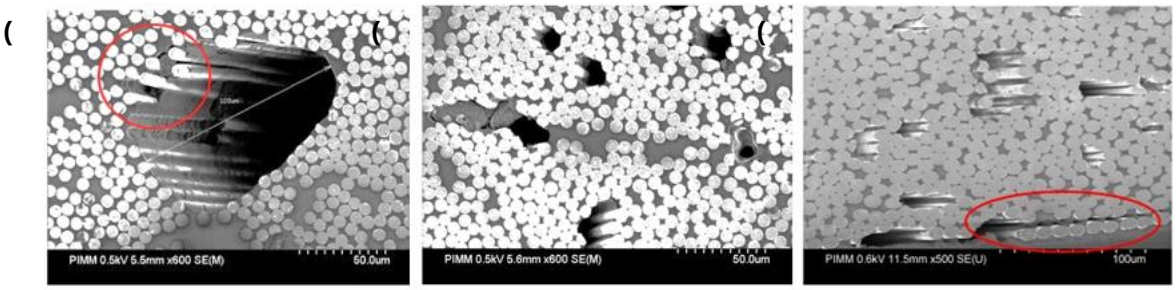

Figure. 5. SEM micrograph: (a) ±15°, (b) ±30° and (c) multilayers configurations

3.2. Quasistatic tensile behavior

Figure 6 illustrates the stress-strain curves for carbon fiber-reinforced epoxy composites with varying fiber orientations (i.e. ±15°, ±30°, and multilayer) under quasi-static loading conditions. The ±15° orientation demonstrates a gradual increase in stress with strain, reaching a peak stress of approximately 350 MPa,

followed by a notable decline indicative of failure, with relatively high stiffness and significant ductility. The ±30° orientation exhibits the highest peak stress of approximately 200 MPa, with a comparable abrupt decline following the peak. This demonstrates a balance between stiffness and ductility, although the initial stiffness is slightly reduced in comparison to the ±15° orientation. The multilayer orientation demonstrates the lowest peak stress of approximately 130 MPa, with a gradual increase and an extended plateau before failure, indicating a reduction in stiffness but an enhancement in ductility. These observations demonstrate that the ±15° and ±30° orientations exhibit higher stiffness and strength, while the multilayer configuration offers greater ductility. The results demonstrate that all orientations exhibit brittle failure modes, characterized by a sharp decline in stress after peak values. The ±30° orientation shows the best load transfer and resistance to deformation, while the multilayer configuration demonstrates superior energy absorption through deformation prior to failure. These findings highlight the significant influence of fiber orientation on the mechanical behavior of composites, which is crucial for the design of materials tailored for specific strength and ductility requirements under quasi-static loading conditions.

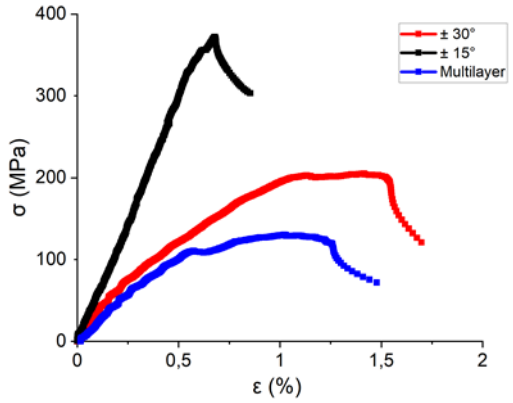

Figure 6. Representative-curves of quasi-static tensile tests

3.3. High strain rate tensile behavior

Figure 7 illustrates the stress-strain curves for carbon fiber-reinforced epoxy specimens subjected to high strain rate tensile tests until failure. The specimens were oriented at varying angles, including ±15°, ±30°, and multilayer configurations. Tests were conducted at different strain rates, namely $100s^{-1}$, $1s^{-1}$, $0.1s^{-1}$, and quasi-static. The high strain rate tensile tests on carbon fiber-reinforced epoxy specimens oriented at ±15°, ±30°, and multilayer configurations provide crucial insight into the behavior of the material under dynamic loading conditions. The tests, conducted at varying strain rates ($100s^{-1}$, $1s^{-1}$, $0.1s^{-1}$, and quasi-static), demonstrate notable strain rate sensitivity. It was observed that higher strain rates consistently resulted in increased stress

levels and reduced ductility in all orientations. For instance, the ±15° samples demonstrate the highest stress levels, reaching approximately 480 MPa at $100s^{-1}$, with notable stress levels at lower rates (approximately 430 MPa at $1s^{-1}$ and 400 MPa at $0.1s^{-1}$), while the quasi-static tests reach approximately 350 MPa. Similarly, the ±30° orientation exhibits peak stress values of approximately 300 MPa at $100s^{-1}$, which decrease to 235 MPa and 225 MPa at $1s^{-1}$ and $0.1s^{-1}$, respectively. The quasi-static tests reach a peak of approximately 200 MPa. The multilayer configuration, although exhibiting lower overall stress values, demonstrates a similar trend, with stress peaks of 210 MPa for $100s^{-1}$, 175 MPa for $1s^{-1}$ and 140 MPa for $0.1s^{-1}$, with quasi-static tests reaching approximately 130 MPa.

These findings demonstrate that the material displays enhanced resilience in response to rapid loading. This can be attributed to the viscoelastic characteristics of the epoxy matrix, which offers heightened resistance at higher strain rates. However, it should be noted that the ductility decreases with increasing strain rate, as indicated by the shorter strain to failure. The discrepancy in stress-strain behavior across different orientations suggests the presence of disparate damage mechanisms. At elevated strain rates, there is a greater likelihood of matrix and fiber-matrix interface failures, whereas at lower rates, fiber breakage and matrix cracking are more probable. The orientation of the fibers also has a significant impact on performance. The ±15° and ±30° orientations demonstrate superior performance compared to the multilayer structure, due to the enhanced transfer of loads and the reduction of interlayer weaknesses. These findings are crucial for optimizing composite designs for applications that require high performance under dynamic conditions. They also emphasize the importance of considering strain rate effects and fiber orientation in engineering applications. Figure 7 presents a comprehensive analysis of the tensile behavior and fracture surfaces of carbon fiber-reinforced epoxy composites with varying fiber orientations (i.e., ±15°, ±30°, and multilayer) under quasi-static (QS) and high strain rate (100 s^{-1}) loading conditions. The stress-strain curves demonstrate that the highest stress values are observed at the highest strain rate (100 s^{-1}), with increases of 37%, 50%, and 62% for the ±15°, ±30°, and multilayer configurations, respectively, compared to quasi-static loading. The high strain-rate curves display a precipitous decline following the peak, indicative of brittle fracture behavior. A microscopic analysis of the fracture surfaces indicates that under quasi-static loading, the fracture surfaces for all orientations exhibit a combination of fiber pull-out and matrix cracking, suggesting a mixed-mode failure. At $100s^{-1}$, the fracture surfaces are characterized by extensive fiber breakage and less fiber pull-out, indicating a more brittle failure mode. The ±15° orientation exhibits the highest strength, followed by ±30°, with the multilayer configuration displaying the lowest strength but higher ductility under QS loading. The transition from

ductile to brittle failure modes is more pronounced at higher strain rates across all orientations, driven by the rapid loading conditions. These observations highlight the significant strain-rate sensitivity and the influence of fiber orientation on the tensile properties and fracture mechanisms, with higher strain rates leading to increased strength but reduced ductility.

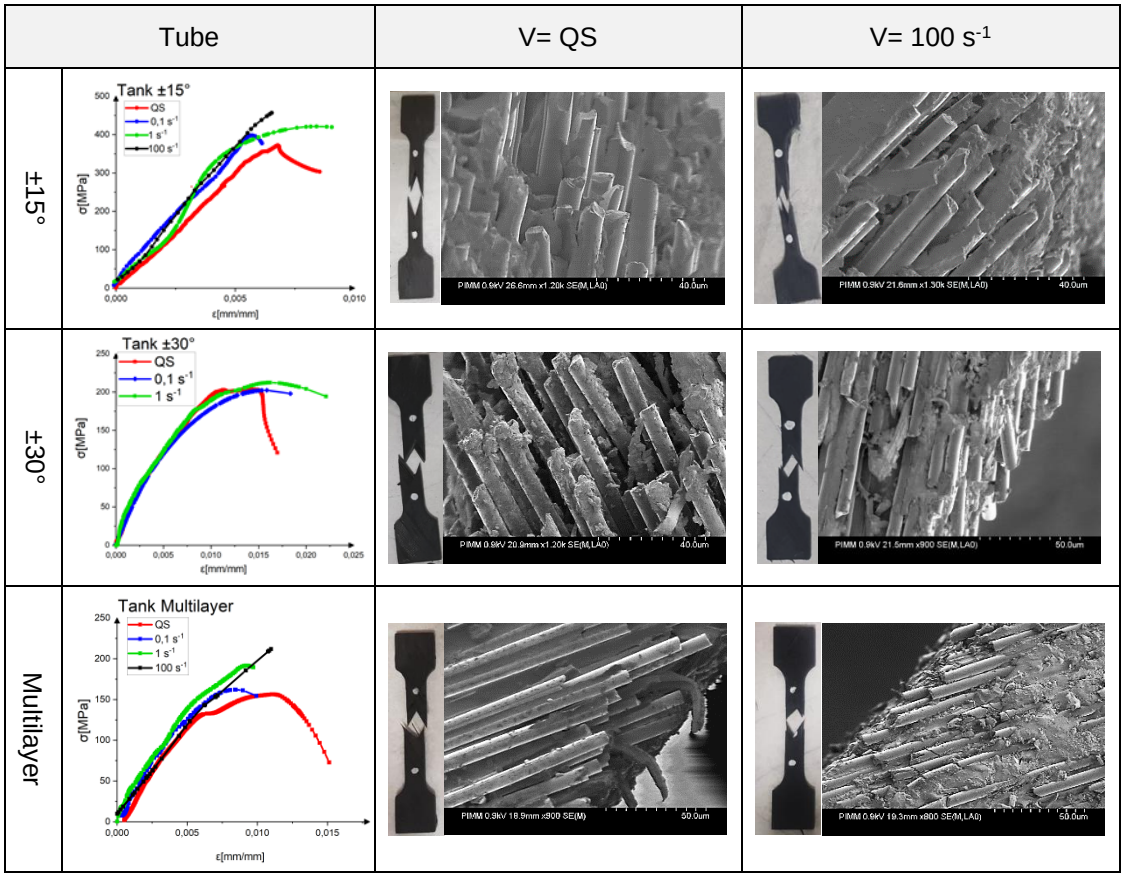

Figure 7. High strain rate tensile curves: impact of orientation and strain rate on fracture surfaces

This analysis is crucial for the design and optimization of composite materials for dynamic loading applications, ensuring a balance between strength, stiffness, and fracture toughness based on specific performance requirements.

3.4. Effects of strain-rate on the overall tensile response

Figures 8 and 9 demonstrate the impact of strain rate on the tensile response of carbon fiber-reinforced epoxy composites with varying fiber orientations, namely ±15°, ±30°, and multilayer. The data, presented through a variety of metrics, including Young's modulus, threshold stress, ultimate stress, threshold strain, and ultimate strain, offer significant insights. The variation in Young's modulus with strain rate is dependent on the fiber orientation. The ±15° orientation generally exhibits the highest values, indicating greater stiffness, while

the multilayer configuration shows lower modulus values, suggesting less stiffness. At higher strain rates (≥0.1s^{-1}), an increase in modulus is observed for all orientations, indicative of strain-rate dependent stiffening. Threshold stress demonstrates an increase with strain rate for all orientations, with the ±15° and ±30° orientations exhibiting higher values than the multilayer configuration. Additionally, ultimate stress demonstrates an increase with strain rate, with the ±15° orientation exhibiting the highest values, followed by the ±30° orientation, and the multilayer configuration showing the lowest. Threshold strain exhibits less significant variation with strain rate, with ±30° displaying slightly elevated values at lower rates, indicative of an earlier onset of damage. The ultimate strain rate demonstrates a decrease with increasing strain rate for all orientations, with the multilayer configuration displaying the highest values, indicating greater ductility in comparison to the ±15° and ±30° orientations. The reduction in ultimate strain at higher rates indicates an increase in brittleness, which is a cause for concern. These findings highlight the significant strain-rate sensitivity of the tensile properties, with elevated rates resulting in enhanced stiffness and strength but reduced ductility. The ±15° orientation consistently demonstrates superior properties in comparison to ±30° and multilayer configurations, which, despite exhibiting diminished strength and stiffness, demonstrate augmented ductility. The variation in threshold and ultimate strains suggests disparate damage mechanisms across orientations and strain rates, with elevated rates likely leading to matrix cracking and fibre-matrix debonding.

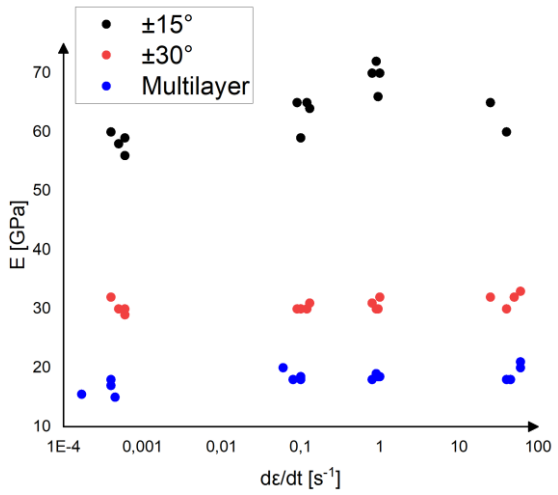

Figure 8. Evolution of the Young's modulus vs. strain rate

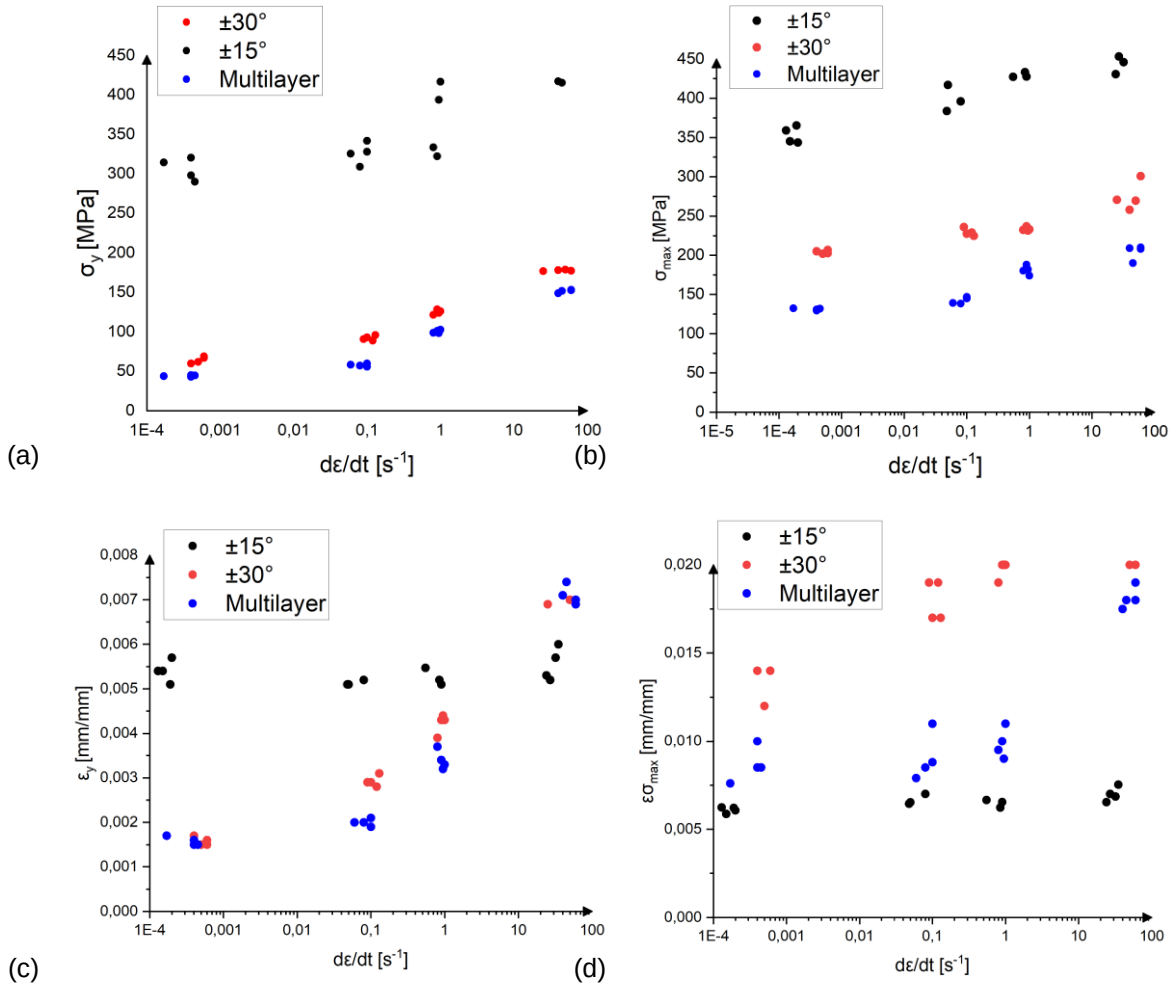

Figure 9. Influence of strain rate on: (a) threshold stress, (b) ultimate stress, (c) threshold strain and (d) ultimate strain

3.6. Qualitative damage mechanisms investigation

Figure 10 illustrates the results of an Interrupted Dynamic Tensile Test (IDTT) on a multilayer carbon fiber reinforced epoxy composite, demonstrating the progressive damage mechanisms at a microscopic level and the corresponding loss of stiffness due to damage, with a strain rate of $1s^{-1}$. The stress-strain curve initially exhibits a linear elastic region, indicating a consistent increase in stress with strain. However, as the strain progresses, the curve deviates from linearity, thereby highlighting the onset of damage mechanisms. The initial stage micrograph demonstrates the emergence of early matrix damage, characterized by the formation of micro-cracks and voids. However, the curve remains linear, indicating that the impact on stiffness is minimal. At the intermediate stage (σ = 90 MPa), the micrograph illustrates a progression in matrix damage and the advent of delamination, leading to a deviation in the stress-strain curve and indicating a reduction in stiffness.

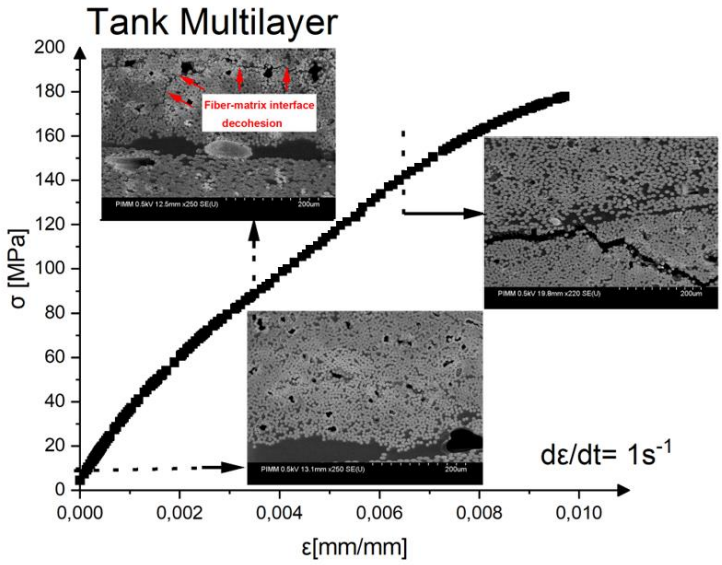

Figure 10. Microscopic damage mechanisms: multilayers configuration

At the advanced damage stage (σ = 140 MPa), the micrograph clearly shows extensive damage to the matrix and notable delamination, with larger cracks compromising the fiber/matrix interface. This results in a notable reduction in the slope of the stress-strain curve and a considerable loss of stiffness. The primary damage mechanisms include matrix cracking, delamination and fiber/matrix debonding. These initiate at lower strains and progressively worsen, leading to cumulative stiffness degradation and structural integrity loss. As damage accumulates, the composite's initial elastic behavior transitions to a nonlinear response, which highlights the strain-rate sensitivity of these mechanisms. This IDTT effectively demonstrates how initial matrix damage leads to delamination and further cracking, which significantly reduces the composite's load-bearing capacity. This emphasizes the importance of understanding damage kinetics for predicting composite performance and failure under dynamic loading conditions.

The images provided (Figure 11) illustrate the progression of damage in a multilayer carbon fiber-reinforced epoxy composite tank under varying stages of tensile loading. The images are used to identify and analyze the qualitative damage mechanisms at different stages: initial, intermediate, and final.

In the initial stage (F = 0 N, $d\varepsilon/dt = 1s^{-1}$), the composite exhibits its pristine condition in the absence of applied force, displaying a largely intact surface with a few minor surface defects or porosities that are typical of the manufacturing process. These minor porosities indicate potential sites for crack initiation when the material is subjected to loading, though the overall structure remains undamaged, thus providing a baseline for comparison with later stages.

At the intermediate stage (F = 4000 N or σ = 90 MPa), initial cracks (decohesion at fiber/matrix interface) emerge and propagate from the surface porosities through the matrix material, indicating the presence of internal stress concentrations around the porosities and marking the onset of damage accumulation in the composite structure. The linear and branching patterns of the cracks indicate the presence of both tensile and shear stress components, thereby highlighting the existence of weaker matrix-fiber bonding areas. This propagation results in a degradation of stiffness, which is observable in the stress-strain curve as a deviation from linearity. Furthermore, it impairs the load transfer efficiency between fibers and the matrix, creating localized stress concentrations that accelerate damage. In the final stage (F = 6000 N or σ = 140 MPa), extensive cracking is visible throughout the composite, with cracks growing significantly, intersecting, and forming a network that compromises the material's integrity, indicating a high degree of internal damage. The interconnected cracks indicate a reduction in load-bearing capacity, resulting in macroscopic failure. The observed damage mechanisms, including matrix cracking, fiber/matrix debonding and potential fiber breakage, collectively contribute to the material's ultimate failure under high stress.

Tank Multilayer
Initial stage: F = 0 N , $d\varepsilon/dt = 1s^{-1}$
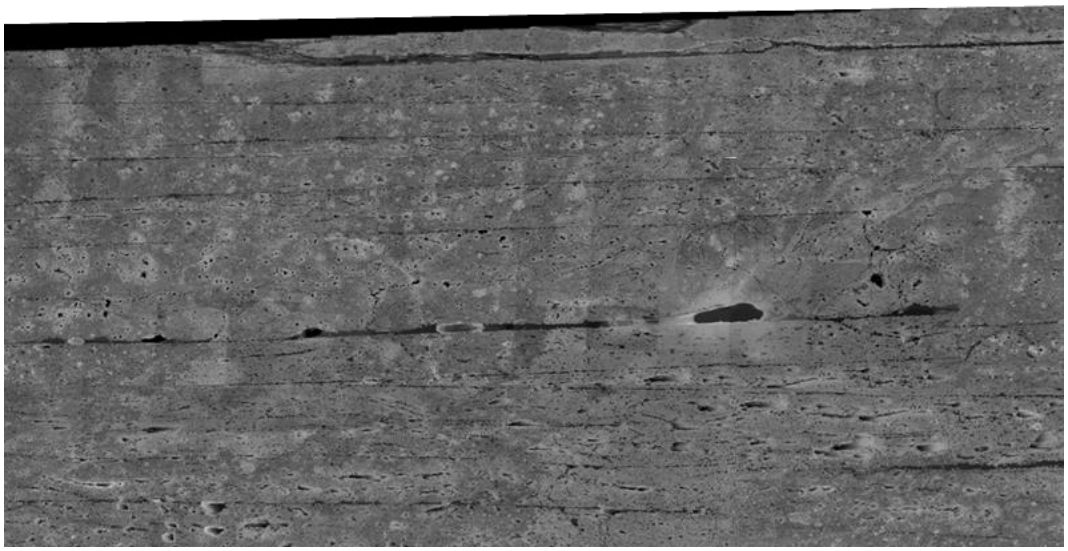
Intermediate stage: F = 4000 N , $d\varepsilon/dt = 1s^{-1}$

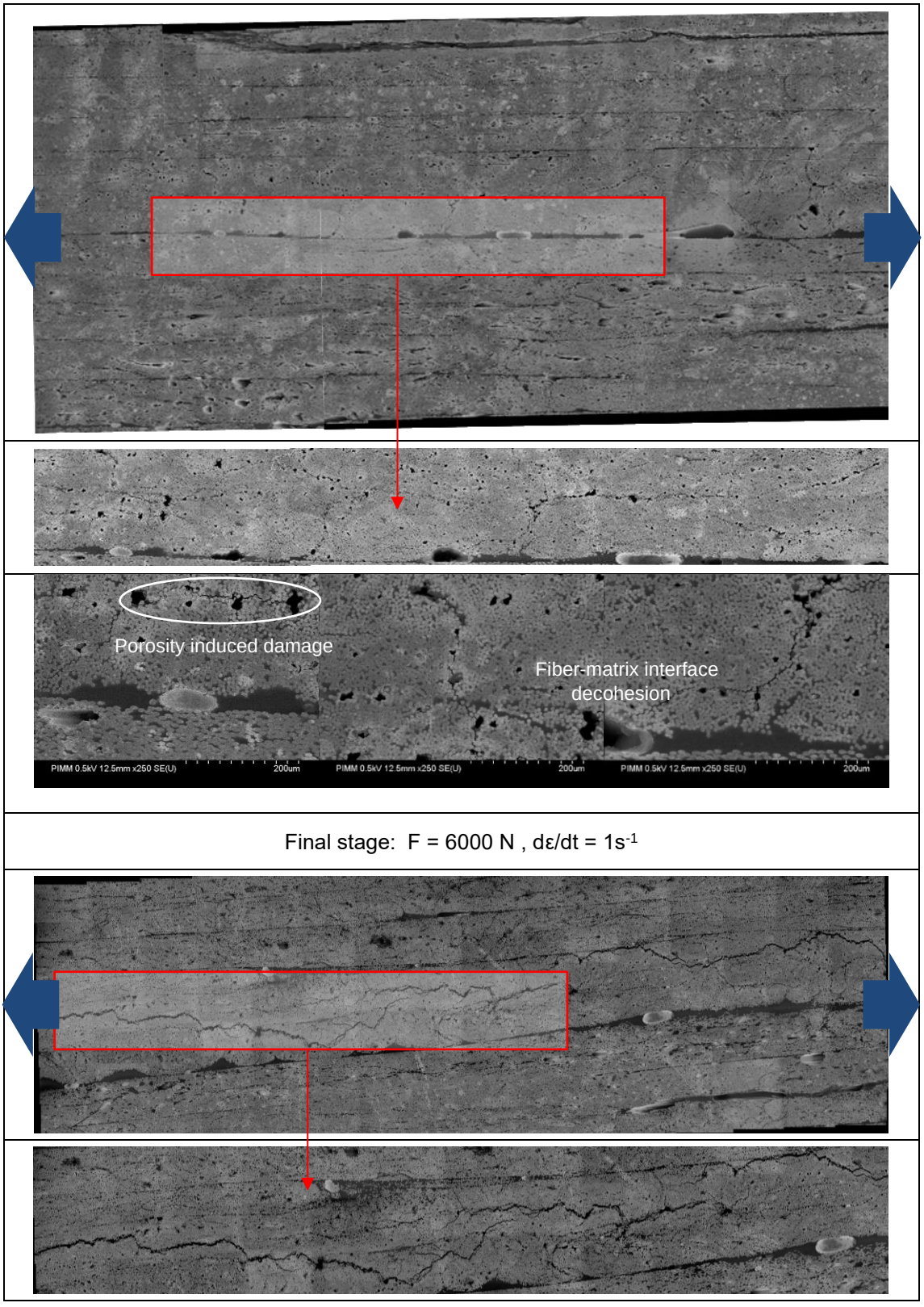

Final stage: F = 6000 N , $d\varepsilon/dt = 1s^{-1}$

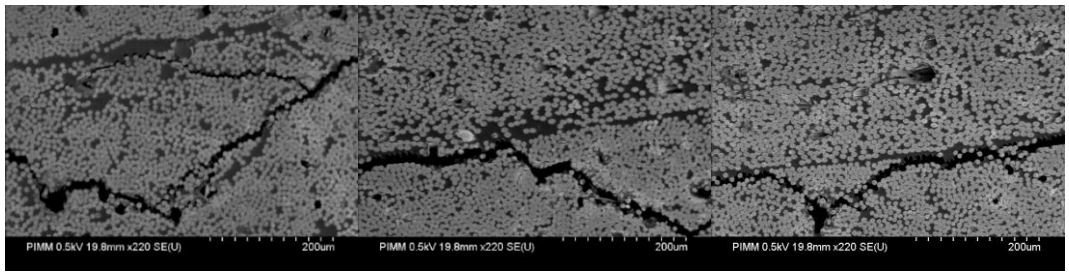

Figure 11. Microstructural evolution and damage mechanisms for multilayers configuration

The investigation findings indicate that damage originates at pre-existing defects or porosities and progresses through the matrix. Porosities act as stress concentrators, facilitating the initiation of cracks. The primary failure mechanisms observed include fiber/matrix debonding and matrix cracking, which impair the efficiency with which loads are transferred between fibers and the matrix, thereby reducing the overall strength of the material and ultimately leading to its failure. The consistent strain rate ($d\varepsilon/dt = 1s^{-1}$) across all stages provides insights into the material's response to dynamic loading, thereby highlighting the importance of strain rate in determining the mechanical properties of composites. The qualitative damage mechanisms investigation of the multilayer carbon fiber reinforced epoxy composite tank under tensile loading reveals critical insights into the material's behavior, emphasizing the importance of understanding these mechanisms for improving composite manufacturing processes and enhancing the material's performance and durability in practical applications.

4. Conclusion

This research provides a detailed investigation of the mechanical behavior and damage mechanisms of carbon fiber reinforced epoxy composites used in the manufacture of hydrogen storage tanks. The study focused on dynamic loading scenarios with strain rates ranging from quasi-static to $100s^{-1}$ and considered fiber orientations of ±15° and ±30°, as well as multi-layer structures. The mechanical tests showed that the mechanical properties of the composite varied significantly with the strain rate, with higher strain rates resulting in increased stiffness and strength, indicating the sensitivity of the material to dynamic loading conditions. The interrupted dynamic tensile tests (IDTT) allowed the identification of key damage mechanisms, including porosity-induced cracking, fiber/matrix interface decohesion, fiber fracture and microcracking. These primary damage mechanisms were exacerbated by the presence of manufacturing defects, such as porosity, which acted as stress concentrators and significantly influenced damage initiation and crack propagation. At the

mesoscopic level, porosity and fiber orientation resulted in localized stiffness mismatches, leading to complex failure patterns such as transverse cracking and micro-delamination between composite layers.

Furthermore, this study highlighted the role of visco-damage mechanisms, where time-dependent damage processes become critical under dynamic loading conditions. The interaction between strain rate, fiber orientation and porosity was found to be critical in determining the overall performance and failure modes of the composites. The results emphasize the need to consider these factors during the design phase to improve the safety, reliability and durability of hydrogen storage systems. The results of this research provide valuable insights into optimizing the design of composite materials for dynamic applications and provide a basis for future efforts to improve the performance of composite pressure vessels through better control of microstructural features and loading conditions.

5. Declarations

- Consent to participate: Not applicable.
- Consent to publish: Not applicable.
- Conflict of interest: The authors declare that they have no conflicts of interest.

Authors' contributions

M. Shirinbayan, R. Tie Bi, J-B. Maeso, C. Thomas, J. Fitoussi: construct the idea. I. Feki, M. Shirinbayan, S. Nouira, R. Tie Bi, J-B. Maeso, C. Thomas, J. Fitoussi: analyzed results, drafted manuscript preparation, and wrote the paper. I. Feki, M. Shirinbayan, S. Nouira, J. Fitoussi: corrected the English and the paper format.

Availability of data and materials

The authors declare that the data and the materials of this study are available within the article.

6. References

[1] M. A. Ç. Cevahir Tarhan, «A study on hydrogen, the clean energy of the future: Hydrogen,» Journal of Energy Storage, p. https://doi.org/10.1016/j.est.2021.102676, 2021.

[2] H. T. H. a. A. Varma, «Hydrogen storage for fuel cell vehicles,» Current Opinion in Chemical Engineering, p. http://dx.doi.org/10.1016/j.coche.2014.04.004, 2014.

[3] M. T. a. K. Z. Etienne Rivard, «Hydrogen Storage for Mobility: A Review,» materials, p. doi:10.3390/ma12121973, 2019.

[4] E. Commission. Further CO2 emission reduction from cars and vans: a win-win for the climate, consumers, innovation and jobs. Brussels, 2012.

[5] Weger, L.B.; Leitão, J.; Lawrence, M.G. Expected impacts on greenhouse gas and air pollutant emissions due to a possible,transition towards a hydrogen economy in German road transport. Int. J. Hydrogen Energy 2021, 46, 5875-5890.

[6] «Study and characterization of a metal hydride container,» INTERNATIONAL JOURNAL OF HYDROGEN ENERGY, p. doi:10.1016/j.ijhydene.2007.12.029, 2008.
[7] R.K. Ahluwalia, J.-K. Peng, H.-S. Roh, D. Papadias, X. Wang, S.M. Aceves, Liquid hydrogen storage system for heavy duty trucks: Capacity, dormancy, refueling, and discharge, International Journal of Hydrogen Energy, Volume 48, Issue 87, Pages 34120-34131, 2023,
[8] G. AlZohbi, A. Almoaikel, L. AlShuhail, An overview on the technologies used to store hydrogen, Energy Reports, Volume 9, Supplement 11, Pages 28-34, 2023.
[9] Pobitra Halder, Meisam Babaie, Farhad Salek, Nawshad Haque, Russell Savage, Svetlana Stevanovic, Timothy A. Bodisco, Ali Zare, Advancements in hydrogen production, storage, distribution and refuelling for a sustainable transport sector: Hydrogen fuel cell vehicles, International Journal of Hydrogen Energy, Volume 52, Part D, Pages 973-1004, 2024.
[10] Lei Ge, Jikang Zhao, Hefeng Li, Jingxuan Dong, Hongbo Geng, Lei Zu, Song Lin, Xiaolong Jia, Xiaoping Yang, A three-dimensional progressive failure analysis of filament-wound composite pressure vessels with void defects, Thin-Walled Structures, Volume 199, 2024.
[11] Liu P, Chu J, Hou S, Xu P, Zheng J. Numerical simulation and optimal design for composite high-pressure hydrogen storage vessel: a review. Renew Sustain Energy Rev 2012;16(4):1817e27.
[12] Schmidt, W. (2012). Hydrogen storage in carbon fiber composite pressure vessels. *Carbon*, 50(5), 1813-1823.
[13] Gandhi, U. N., & Thompson, A. (2010). Polymer-based hydrogen storage: Material properties and structural integrity. *International Journal of Hydrogen Energy*, 35
[14] G. Gondor, «Pour le stockage de l'hydrogène : Analyse thermodynamique de la formation d'hydrures métalliques et optimisation du remplissage d'un réservoir.,» HAL Id: tel-00782271, Besançon, 29 jan 2013.
[15] K. H. D. Mori*, «Recent challenges of hydrogen storage technologies for fuel cell vehicles,» international journal of hydrogen energy 3 4, p. doi:10.1016/j.ijhydene.2008.07.115, 2009.
[16] H. LARA, 'Energy revolution,' 21 January 2022. [Online]. Available: https://www.revolution-energetique.com/cette-giga-usine-dhydrogene-consommera-autant-delectricite-quune-grande-ville/
[17] Han, Geng, Guan, Zhidong, Li, Xing, Ji, Ruipeng and Du, Shanyi. "The failure mechanism of carbon fiber-reinforced composites under longitudinal compression considering the interface" Science and Engineering of Composite Materials, vol. 24, no. 3, 2017, pp. 429-437. 2015.
[18] P. PROMBUT, «Caractérisation de la propagation de délaminage des stratifiés composites multidirectionnels,» Université Toulouse, Toulouse, 2007.
[19] Y. D. e. J. QIAN, «Analysis of microdamage evolution histories in composites.,» International Journal of Solids and Structures, p. 1831–1854, 2001.
[20] Rahmani, H., Najafi, S.H.M., Saffarzadeh-Matin, S. and Ashori, A. (2014), Mechanical properties of carbon fiber/epoxy composites: Effects of number of plies, fiber contents, and angle-ply layers. Polym Eng Sci, 54: 2676-2682.
[21] M. Shirinbayan, M. Rezaei-Khamseh, M. H. Nikooharf, A. Tcharkhtchi, and J. Fitoussi, "Multi-scale analysis of mechanical properties and damage behavior of polypropylene composite (GF50-PP) plate at room and cryogenic temperatures," Composite Structures, vol. 278, p. 114713, 2021.

[22] M. Shirinbayan, "Multi-scale damage analysis of the tension-tension fatigue behavior of a Low-Density Sheet Molding Compound (LD-SMC)", Journal of Applied Polymer Science, 2021.
[23] M. A. Imaddahen, M. Shirinbayan, H. Ayari, M. Foucard, A. Tcharkhtchi, and J. Fitoussi, "Multi-scale analysis of short glass fiber-reinforced polypropylene under monotonic and fatigue loading," Polymer Composites, vol. 41, no. 11, pp. 4649-4662, 2020.
[24] I. Feki, M. Shirinbayan, S. Nouira, R. Tie Bi, J. Maeso, C. Thomas, J. Fitoussi, "Multi-scale experimental investigation of porosity-induced damage effects in filament-wound carbon fiber reinforced epoxy composites used in hydrogen storage tanks." Polymer Composites, 2024.
[25] M.A.Shadab Siddiqui, M.S. Rabbi, Shapla Dewanjee, Low-velocity impact response of natural fiber reinforced composites: A comprehensive review on influential parameters, Composites Part C: Open Access, Volume 12, 2023.
[26] M. Shirinbayan, J. Fitoussi, N. Abbasnezhad, F. Meraghni, B. Surowiec, A. Tcharkhtchi, "Mechanical characterization of a Low-Density Sheet Molding Compound (LD-SMC): Multi-scale damage analysis and strain rate effect". Composites Part B: Engineering, 131: 8-20, 2017.
[27] M. Shirinbayan, J. Fitoussi, M. Bocquet, F. Meraghni, B. Surowiec, A. Tcharkhtchi, "Multi-scale experimental investigation of the viscous nature of damage in Advanced Sheet Molding Compound (A-SMC) submitted to high strain rates". Composites Part B: Engineering, 115: 3-17, 2017.
[28] M. Shirinbayan, J. Fitoussi, F. Meraghni, B. Surowiec, M. Bocquet, A. Tcharkhtchi. "High strain rate visco-damageable behavior of Advanced Sheet Molding Compound (A-SMC) under tension". Composites Part B: Engineering, 82: 30-41, 2015.
[29] J. Fitoussi, M. H. Nikooharf, A. Kallel, and M. Shirinbayan, "Mechanical Properties and Damage Behavior of Polypropylene Composite (GF50-PP) Plate Fabricated by Thermocompression Process Under High Strain Rate Loading at Room and Cryogenic Temperatures," Applied Composite Materials, vol. 29, p. 1959–1979, 2022.
[30] M. Shirinbayan, H. B. Rizi, N. Abbasnezhad, A. Tcharkhtchi, J. Fitoussi, "Tension, compression, and shear behavior of advanced sheet molding compound (A-SMC): Multi-scale damage analysis and strain rate effect," Composites Part B: Engineering, vol. 225, p. 109287, 2021.
[31] Cantwell, W. J., & Morton, J. (1991). The impact resistance of composite materials – a review. *Composites*, 22.
[32] Kastner M, Obst M, Brummund J, Thielsch K, Ulbricht V. Inelastic material behavior of polymers-experimental characterization, formulation and implementation of a material model. Mech Mater 2012;52:40e57.
[33] Kweon S, Benzerga A. Finite element implementation of a macromolecular viscoplastic polymer model. Int J Numer Methods Eng 2013;94(10):895e919.
[34] Patel BP, Gupta AK. An investigation on nonlocal continuum damage models for composite laminated panels. Compos Part B Eng 2014;60:485e94.
[35] Bere P, Berce P, Nemes O. Phenomenological fracture model for biaxial fibrenreinforced composites. Compos Part B Eng 2012;43(5):2237e43.

[36] Lacy TE, MacDowell DL, Talreja R. Gradient concepts for evolution of damage. Mech Mater 1999;31(12):831e60.
[37] Shao JF, Rudnicki JW. A microcrack-based continuous damage model for brittle geomaterials. Mech Mater 2000;32:607e19.
[38] Jendli Z, Meraghni F, Fitoussi J, Baptiste D. Multi-scales modeling of dynamic behaviour for discontinuous fibre SMC composites. Compos Sci Technol 2009;69(1):97e103.
[39] Jendli Z, Meraghni F, Fitoussi J, Baptiste D. Micromechanical analysis of strain rate effect on damage evolution in sheet molding compound composites. Compos Part A Appl Sci Manuf 2004;35(7e8):779e85.
[40] Lataillade JL, Delaet M, Collombet F, Wolff C. Effects of the intralaminar shear loading rate on the damage of multi-ply composites. Int J Impact Eng 1996;18(6):679e99.
[41] Fitoussi J, Bocquet M, Meraghni F. Effect of the matrix behavior on the damage of ethylene-propylene glass fiber reinforced composite subjected to high strain rate tension. Compos Part B Eng 2013;45(1):1181e91.

Imen FEKI

Étude et modélisation de l'effet des séquences de sollicitations thermomécanique sur le comportement, l'endommagement et la rupture des matériaux composites des réservoirs à hydrogène

Résumé : La préservation de l'environnement et la promotion du développement durable représentent des enjeux cruciaux à l'échelle mondiale. Dans ce contexte, l'hydrogène émerge comme un vecteur énergétique prometteur pour la génération d'électricité et de chaleur. Parmi les différentes technologies de stockage, le stockage gazeux comprimé dans des réservoirs de type IV s'affirme comme la solution la plus aboutie en termes de densité de masse et de volume. Forvia conçoit des systèmes de stockage d'hydrogène légers et concurrentiels, capables de supporter des pressions atteignant 700 bars, ainsi que des contraintes thermomécaniques complexes telles que les cycles de fatigue, les chocs, le fluage et les variations de température. Dans de telles conditions extrêmes, les matériaux composites époxy renforcés de fibres de carbone sont particulièrement sujets à divers mécanismes de détérioration. Cette recherche expérimentale vise à établir les fondements pour la conception des structures en composites CFRP (polymère renforcé de fibres de carbone) dédiées aux réservoirs d'hydrogène de type IV. Une approche multi-échelle est utilisée pour analyser l'impact de la microstructure sur les mécanismes de détérioration sous sollicitations quasi-statiques, dynamiques et en fatigue. Des méthodes expérimentales novatrices sont développées afin d'établir des corrélations entre ces mécanismes de détérioration et les comportements macroscopiques observés. L'étude commence par une caractérisation physico-chimique et microstructurale des composites, suivie d'une analyse thermomécanique approfondie. L'accent est mis sur l'influence de la porosité et des orientations des fibres (±15°, ±30°, et configurations multicouches) sur les performances mécaniques. Les résultats expérimentaux révèlent que la porosité, située entre 5 % et 7 %, diminue considérablement les performances mécaniques, avec une diminution de 40 % du module de Young entre les orientations de fibres ±15° et ±30°, et une réduction de 65 % pour les structures multicouches. À l'échelle microscopique, la porosité entraîne la fissuration et la rupture des fibres, tandis qu'à l'échelle mésoscopique, elle favorise l'apparition de fissures transversales et de délaminations. Les analyses multi-échelles, réalisées dans des conditions quasi-statiques, dynamiques et de fatigue, mettent en évidence l'impact significatif de la porosité sur la durabilité des réservoirs d'hydrogène. Les résultats obtenus permettent de mieux comprendre les effets de l'endommagement causé par la porosité, et ils servent de base expérimentale robuste pour améliorer la conception des réservoirs d'hydrogène en prenant en compte le contrôle de la porosité et de l'orientation des fibres.

Mots clés : Hydrogène, Composite CFRP, Porosité, Comportement mécanique, Endommagement, Fatigue, Dynamique.

Abstract: Preserving the environment and promoting sustainable development are crucial global challenges. In this context, hydrogen is emerging as a promising energy vector for generating electricity and heat. Among the various storage technologies, compressed gas storage in type IV tanks is emerging as the most successful solution in terms of mass density and volume. Forvia designs lightweight, competitive hydrogen storage systems capable of withstanding pressures of up to 700 bar, as well as complex thermomechanical stresses such as fatigue cycles, impact, creep and temperature variations. Under such extreme conditions, carbon fibre-reinforced epoxy composites are particularly prone to various deterioration mechanisms. This experimental research aims to establish the basis for the design of CFRP (carbon fibre reinforced polymer) composite structures dedicated to type IV hydrogen tanks. A multi-scale approach is used to analyse the impact of microstructure on deterioration mechanisms under quasi-static, dynamic and fatigue loading. Innovative experimental methods are developed to establish correlations between these deterioration mechanisms and the macroscopic behaviours observed. The study begins with a physico-chemical and microstructural characterisation of the composites, followed by an in-depth thermomechanical analysis. The focus is on the influence of porosity and fibre orientations (±15°, ±30°, and multilayer configurations) on mechanical performance. Experimental results show that porosity, between 5% and 7%, significantly reduces mechanical performance, with a 40% reduction in Young's modulus between ±15° and ±30° fibre orientations, and a 65% reduction for multilayer structures. On a microscopic scale, porosity leads to fibre cracking and breakage, while on a mesoscopic scale, it favours the appearance of transverse cracks and delamination. The multi-scale analyses, carried out under quasi-static, dynamic and fatigue conditions, highlight the significant impact of porosity on the durability of hydrogen tanks. The results provide a better understanding of the effects of porosity-induced damage, and serve as a robust experimental basis for improving the design of hydrogen storage tanks by taking into account the control of porosity and fibre orientation.

Keywords : Hydrogen, CFRP composite, Porosity, Mechanical behaviour, Damage, Fatigue, Dynamics.